ADVANCES IN THE THEORY AND PRACTICE

OF HARD CHROMIUM PLATING

by

Mark Fraser Singleton, B.Sc.

86

This thesis is submitted

in fulfilment of the

requirements for the degree

of Doctor of Philosophy,

University of Sheffield.

ADVANCES IN THE THEORY AND PRACTICE OF HARD CHROMIUM PLATING

Most of the change we think we see in life

Is due to truths being in and out of favour.

Robert Frost.

INDEX

SUMMARY

A consideration of pertinent aspects of general electrochemistry and electrodeposition was followed by a review of the relevant literature relating to hard chromium plating technique and understanding (and problems and proposed improvements therein).

Following the establishment and evaluation (using a Standard Solution at 55°C) of a reproducible technique for the measurement of (low current density) partial cathodic polarization data during plating, the Tafel regions of the resulting curves were analysed using the relationship -

$$\frac{d\eta_{CT}}{d\log i} = \frac{-2.303\ RT}{\alpha_{term}\ \lambda F}$$

to provide an indication as to the nature of the rate-determining step in the plating and hydrogen evolution (cathodic) reactions.

Information thus generated was used with a modified Arrhenius-type expression -

$$\frac{d\log i}{d(1/T)} = \frac{-0.43T}{R} \cdot \frac{0.43\ \Delta H_A}{R} + \frac{0.43\alpha_{term}\ \eta\lambda F}{R}$$

and further (experimentally determined) data to provide values of the thermodynamic constants of activation for the plating reaction.

A series of experiments were undertaken to determine the effects upon various (physical) plate and plating parameters of three new inorganic additions (at selected concentrations) to a Standard Solution at 55°C. The results of these tests were commented upon with regard to potential industrial applications.

The electrochemical investigative techniques referred to earlier were then employed with each new solution tested to determine the effect (if any) of the new additions upon those aspects of the deposition mechanism yielded, and to relate these effects to the observed (corresponding) changes in plate and plating parameters. The new additions were found to have profound effects upon a number of (physical) plate and plating parameters, and upon experimentally determined theoretical aspects of the deposition mechanism (the relationship between the two is discussed).

Whilst no definite conclusion has been reached with regard to the precise mechanism of chromium plating, the techniques employed and the data generated have been used to provide significant pointers with regard to the direction future investigations might take.

ACKNOWLEDGEMENTS

I am indebted to Professors G. J. Davies, G. W. Greenwood and B. B. Argent for the opportunity to undertake research in the Department of Metallurgy and for the provision of excellent laboratory facilities. Sincere thanks are due to Dr. J. M. West for his help and patient guidance throughout his supervision of this work.

I would also like to express my gratitude to the academic, technical and clerical staff of the department for the friendly and cooperative atmosphere in which the research was carried out. In particular, I wish to thank Dr. J. A. Naismith for his encouragement and Mike Dobby for his assistantance in the laboratory.

The award of a Departmental research grant for the first year and an S.E.R.C. Research Studentship for the two subsequent years is also gratefully acknowledged.

Finally, I would like to record my sincere appreciation of the active support given by my mother during the period in which this work was undertaken.

INTRODUCTION

Hard chromium plating as a means of conferring an intensely hard, smooth and wear-resistant engineering coating to a substrate material has been practised industrially from chromic acid-based solutions for more than half a century. Throughout that period efforts have been made to provide answers to the many problems (practical and theoretical) which dog the process but, although some advances have been made, the problems remain.

Chromium deposition from a chromic acid solution containing an essential 'catalyst' is a highly complex, multi-dimensional electrochemical process during which three competing cathode reactions and two competing anode reactions take place. The presence of a 'catalyst' (usually the sulphate anion) at a precise concentration ratio with regard to the chromic acid is a pre-requisite to successful plating practice which has been investigated by many researchers but with little success in terms of an incontrovertible explanation.

The disagreement which exists with regard to the deposition mechanism is considered to be largely as a consequence of inaccuracy in the techniques employed by earlier workers. To this end, the first aim of this project is to develop a technique which ensures a high relative reproducibility of data in the measurement of cathode polarization during chromium plating, a primary means of investigating electrode processes.

Polarization (and subsequently derived) data thus recorded in a conventional industrial plating solution (under practical plating conditions) is used with experimentally determined Arrhenius-

type data to yield results which provide a better insight into the mechanisms of chromium deposition.

Numerous investigations have been carried out into the effects (if any) of specific new additives to plating solutions, mainly as alternatives to the sulphate and silicofluoride 'catalysts' conventionally used. In most cases these attempts have been unsuccessful, in that where some aspect of the process or product is improved, another aspect is impaired. In this thesis a thorough investigation into the effects of three novel inorganic additions to a Standard Solution is described. Whilst each has a profound influence upon both process and product, one in particular is considered to demonstrate considerable commercial potential through its apparent ability to improve solution throwing power (a major drawback in conventional hard chromium plating) and related problems.

The techniques initially developed to investigate the cathode reaction mechanism in a Standard Solution (conventionally catalysed) are subsequently used with each of the new solutions tested (i.e. containing the three novel additives) in an attempt to relate the effects of the additives upon practical aspects of the process with their corresponding effects upon theoretical aspects. Mechanisms are proposed by which the observed consequences of specific additive presence are explained.

This thesis is therefore intended to provide an insight into both practical and theoretical aspects of hard chromium plating, and suggest answers to certain problems inherent in each area.

GLOSSARY

Symbol	Description
α	Raoultian activity
a	Tafel curve intercept
b	Tafel slope
C	Concentration
D	Diffusion coefficient
E	Electrode potential (vs S.H.E)
e	Electron
F	Faraday's constant (96485 C/mol)
G	Gibbs free energy (kJ/mol)
H	Enthalpy (kJ/mol)
h	Henrian activity
h'	Planck's constant (6.63×10^{-34} Js)
I	Current
i	Current density
i_o	Exchange current density
i_L	Limiting current density
i_r	Reaction limiting current density
K	Equilibrium constant
k	Rate constant
k'	Boltzmann's constant (1.38×10^{-23} J/K)
l	Current (liquid) flow coordinate
M	Metal
P	Partial pressure
p'	Reaction layer thickness
Pr	Prandtl's number
R	Gas constant (8.3143 J/mol K)
Re	Reynold's number
r	Number of electrons participating in the R.D.S.

S	Entropy (J/mol.K)
T	Temperature in kelvins (K), absolute temperature
t	Transport number, time in seconds.
U	Fluid velocity
V	Potential difference
v_o	Equilibrium exchange reaction rate
z	Number of unit (proton) charges on an ion, Valence change involved in reaction.
α	Symmetry factor
δ	Diffusion layer thickness
ε^o	Standard single electrode potential
ε	Single electrode potential
ϵ	Elementary charge (1.602×10^{-19} C)
ζ	Surface potential
η	Overpotential
Λ	Solution conductivity
λ	Number of unit charges transferred across double layer (and film) for each occurrence of overall reaction.
μ	Chemical potential
μ_*	Electrochemical potential
μ^*	Fluid viscosity
ν	Stoichiometric number (number of times the R.D.S. takes place for each occurrence of the overall reaction).
ρ	Fluid density
ϕ	Inner potential
ψ	Electrical potential (external)
ω	Chemical reaction order
$\vec{\gamma}, \overleftarrow{\gamma}$	Number of electrons participating in steps preceding and following the R.D.S.

H.E.R.	Hydrogen evolution reaction
O.E.R.	Oxygen evolution reaction
R.D.S	Rate-determining step
S.H.E; S.C.E	Standard hydrogen electrode; Standard calomel electrode.

LITERATURE REVIEW

SECTION 1

Electroplating
Fundamentals

1.1. Principles

A metal electrodeposition reaction may be represented simply as -

$$M^{z+}_{(aq)} + ze^- \rightarrow M^o$$

whereby a metal ion is discharged at a cathode surface.

The nature of the individual steps in the overall process is largely dependent upon the particular circumstances. However, certain general principles pertinent to electrodeposition may be outlined.

1.1.1. Faraday's Laws

Faraday's Laws of electrolysis may be summarised thus -

(a) The amount of chemical change involved in an electrolytic reaction is directly proportional to the number of unit electrical charges passing.

(b) The amounts of different substances liberated by the passage of a fixed number of unit electrical charges are proportional to their chemical equivalent weights.

Where

$$\text{Chemical equivalent weight} = \frac{\text{Relative atomic mass}}{\text{Valence change}} = \frac{A}{z}$$

Expressing the first law as an equation, it becomes

$$g = \frac{I\ A\ t}{Z\ F} \qquad (1.1.1,1)$$

Where

g = grams of material reacting (depositing),

I = current in Amperes,

t = time in seconds,

A = relative atomic mass of reacting material,

z = valence change involved in reaction,

F = Faraday's number = 96,485 Coulombs. mol^{-1}.

There are no exceptions to these laws. Apparent anomalies may usually be explained by a failure to take into account all of the electrode reactions. In other words, where a number of electrolytic reactions take place simultaneously at an electrode, each reaction uses up a particular fraction of the total electrical current. This fraction, when expressed as a percentage, is termed the current efficiency of the reaction.

The current efficiency of the electrode reaction 'n' is, therefore, given by -

$$C.E. = \frac{I_n}{I_{total}} \times 100\% \qquad (1.1.1,2)$$

where I_n is calculated from equation (1.1.1,1).

The current efficiency of a metal electrodeposition reaction may be combined with the overall cathode current to reflect the actual rate of deposition. However, in electroplating (as opposed to certain other electrodeposition processes) the deposition rate is not generally considered as important as the nature of the deposit produced, although (from an energy utilization standpoint) the highest deposition rate consistent with 'good' plate is clearly always aimed for.

1.1.2 Deposition criteria

In electroplating, a uniform, coherent and adherent layer of metal is deposited onto a substrade metal cathode in order to confer the beneficial properties of the plating metal onto the substrate.

The specific deposition criteria applicable to electroplating depend to a great extent upon the metal being deposited because, although many metals may be electrodeposited from (various types of) aqueous solutions, the ease with which plating may be carried out is a function of the thermodynamic and kinetic conditions pertinent to the particular process.

Once the composition, thickness, morphology and physical properties of the plate required have been specified, a plating bath (and conditions) may be selected which best allows for easy deposition of the coating.

1.1.3 Plating baths

Aqueous electroplating baths may, in general, be split into two simple categories; acid and alkaline.

Acid baths are usually solutions of relatively simple salts with little complex formation, whereas alkaline baths are, by their very nature, complex, because the metal is contained in an anion. Neutral baths (pH 5 to 8) may be simple salt solutions (as in certain nickel plating baths) or complexed ion solutions (as in copper plating from pyrophosphate baths).

Conventional chromium plating baths, whilst highly acidic, are unusual in that the metal is contained in an anion (a point covered more fully in Section 1.7.1).

1.1.4. Bath additions in electroplating

Bath additions may be classified in terms of their effect on particular properties of the solution and/or the deposit :-

(i) To provide or supplement solution conductivity, as in the acidification of sulphate plating baths.

(ii) To stabilize certain ionic species in solution, and hence prevent their decomposition, as in the addition of hydroxides to cyanide solutions.

(iii) To act as a 'buffer' and stabilize solution pH which, if not controlled (in certain baths), can lead to the precipitation of insoluble metal hydroxides.

(iv) To modify the physical nature of the metal deposit.

1.1.4.1. Levellers and brighteners

These are usually organic compounds and are, therefore, not generally used in highly acidic plating solutions where they tend to be unstable. For this reason, they are not employed in chromic acid-based chromium plating solutions.

1.1.5 Plating control variables

Once the chemical composition of the plating solution (a means of control in itself) and the nature of the electrodes have been established, it is necessary to define precisely the optimum plating conditions for the particular process (those which permit the shortest process time consistent with the production of an acceptable deposit).

The principal means of control available in electroplating are the nature and magnitude of the current density employed, the plating temperature and the nature and extent of solution agitation. Optimum plating conditions in terms of these control variables depend very much upon the individual plating process, but certain general observations may be made.

1.1.5.1. Plating current

When referring to the rate of charge transfer through a plating circuit, it is conventional and more convenient to talk in terms of current density than current as this does not require immediate consideration of electrode surface areas. The S.I. unit of current density is the Ampere/m^2, but this is not universally adhered to, and care is necessary when establishing units of current density.

For obvious reasons, unidirectional current (direct current) is the only type of current of use to the electroplater, as alternating current has no net effect in either direction. Sometimes, however, deliberate deviations from straight direct current are employed in electroplating. These take numerous forms, the presumed benefits of which are still, to some extent, controversial.

Such current modifications promise certain advantages under certain circumstances. However, for most electroplating processes a straightforward direct current supply is perfectly adequate.

The actual level of control of cathode current density required in electroplating is a function of the characteristics of the particular process. However, for most electroplating processes, there exists a recommended range of cathode current densities within which an acceptable (in terms of appearance and physical properties) deposit may be produced. The extent of the 'safe' current density range is, therefore a measure of the controllability of a particular system, although it is often highly dependent on other control variables such as bath temperature and agitation. Deposits produced outside the so-called 'bright' range may exhibit any of a number of

properties which make the resultant plate unacceptable (see Section 1.6).

In industrial plating, current flow in the plating circuit and and potential drop across the plating 'cell' are monitored by straightforward (if robust) ammeters and voltmeters. However, laboratory research into electroplating often demands a higher degree of accuracy in measurement, and in these circumstances special instrumentation is employed (see Section 1.10.4).

1.1.5.2. Plating temperature

Increasing bath temperature causes an increase in diffusion rates and ionic mobilities, and therefore results in higher conductivities which permit 'easier' plating. However, high bath temperatures also result in high evaporation rates, hydrolysis of bath constituents and decomposition of organic additives. These opposing effects often define an optimum plating temperature peculiar to the particular process. Once defined, control of bath temperature to within a few degrees of the optimum is not usually difficult. The passage of current through the cell itself has a (I^2 R) heating effect however, and although this may be offset to an extent by cooling through evaporation, it is generally necessary to employ some means of temperature control such as a thermostat.

1.1.5.3. Agitation

Agitation during electroplating simply involves an enhanced movement of the cathode and solution relative to one another, and is achieved in a number of ways, from the use of stirring rods or propellors to the movement (sometimes vibration) of the cathode itself.

During electrodeposition, the reduction of aqueous metal ions to the metallic state results in the solution adjacent to the cathode becoming depleted in the aforementioned ions. In order for deposition to continue therefore, this region must be replenished from the bulk solution via some mass transport process. Three modes of mass transport predominate in electrodeposition processes.

(i) Convection

This is the major mode of bulk mass transport in electroplating, and involves the movement of substantial volumes of solution relative to the electrodes. Natural (as opposed to 'forced') convection in electroplating may be due to one or more of a number of phenomena;

(a) The fall in solution density adjacent to the cathode, due to depletion in metal ions, causes a tendency for the solution to rise in this region, pulling in fresh solution as it does so. This can lead to bath stratification (when combined with the opposite effect at the anode) and possible non-uniform deposition across the cathode (3).

(b) The passage of current through electrodes causes a degree of resistance heating which can lead to the establishment of temperature gradients in the solution. These aid convective mass transport and oppose bath stratification.

(c) Concomitant gas evolution during electroplating can greatly enhance convection as it tends to pull in fresh solution as the reaction proceeds.

In electroplating processes where natural convection is

insufficient to provide the required bulk solution movement, forced convection (through agitation) is often employed to good effect.

(ii) Diffusion

Immediately adjacent to the cathode surface there exists a thin layer of solution in which convection, as a mode of mass transport, is negligible. In this region the concentration of any reacting species differs from its bulk concentration, and the predominant mass transport mode is diffusion (assuming poor ionic migration conditions). The thickness of the diffusion layer is dependent (via certain solution variables) upon deposition rate, with higher rates corresponding to thicker diffusion layers. At a maximum (or 'limiting') current density (and, therefore, deposition rate), a point is reached at which the rate of metal deposition is limited by the rate of diffusion of the metal-bearing species across the diffusion layer.

Bath agitation has been shown to cause a reduction in diffusion layer thickness and a corresponding increase in limiting current density. Indeed, assuming no natural convection, it has been proposed (4.5) that the relationship between diffusion layer thickness and the rate of stirring of a solution could be described by -

$$\delta \propto U^{-m} \qquad (1.1.5.3,1)$$

Where,

U = rate of stirring of the solution (volume/second),

δ = diffusion layer thickness,

m = constant of value between 0.5 and 1, depending on the system.

On this basis, δ was observed to vary from 5×10^{-4}m for a stagnant solution, to 10^{-7}m in highly agitated solutions.

(iii) Ionic migration

As ionic migration depends on the movement of a charged species in an electrical field, it is clear that solution agitation should have no effect on this mode of mass transport.

1.1.6. Plate categories

The physical nature of the deposit produced in electroplating is largely dependent upon the characteristics of the particular process and the way in which the available control variables are manipulated. It is, therefore possible to control deposit nature in such a way as to meet the property requirements for a particular application. Indeed, deposit types are often classified in terms of their intended application :

(i) Decorative, in which deposit appearance (reflectivity, colour) is of prime importance and physical properties take a secondary role.

(ii) Sacrificial, which provide corrosion resistance by virtue of their anodic nature with respect to the substrate.

(iii) Engineering, in which the conferment of specific advantageous physical properties of the deposit to the substrate is the aim.

Clearly, the category into which a particular deposit fits depends upon the metal being deposited. However, plating conditions may also have a significant effect on the deposit properties, and whilst no two systems are the same, certain generalisations may be made.

1.1.6.1. The relationship of deposit type to plating conditions

The high reflectivity demanded of decorative plate translates to a generally even morphology (microscopic, i.e., on a scale of microns) with few outgrowths or discontinuities which scatter incident light. In general, such a (bright) deposit is produced under conditions where deposition occurs randomly and non-crystallographically, conditions which prevail at relatively high current densities and (or) in the presence of brightening addition agents. Under these conditions the nucleation process is favoured at the expense of growth (the diameter of the critical nucleus is inversely related to overpotential (6)) and a fine-grained (diameters of the order of 10^{-8}m), smooth deposit results.

While a morphologically smooth deposit demonstrates a high reflectivity, it is generally true that such a deposit tends to exhibit 'good' physical properties as well. This is partially due to the low porosity (providing good corrosion and wear resistance) which generally accompanies a smooth morphology, and partially due to the fine grain size which translates (via the Petch analysis) to high hardness. In most electroplating (decorative and engineering) applications, therefore, a fine-grained, smooth deposit is the aim.

As well as being important on a morphological scale, evenness of deposit distribution is obviously desired on a macro-scale across the cathode (e.g., on a scale of centimetres). Large variations in plate thickness across the cathode can lead to the necessity of lengthy post-plating (grinding) treatment in order to satisfy industrial user-specifications, an unwelcome addition to the electroplater's costs. Deposit distribution is a function of the

'throwing power' of the plating solution, a property highly dependent upon the particular solution and the conditions under which it is operated.

1.1.7 Throwing power

The throwing power of an electroplating solution may be (arbitrarily) defined as the 'ability' of the solution to deposit metal in such a way as not to amplify any surface irregularities (macro and micro) on the pre-plated substrate. Such an even deposit distribution, regardless of substrate profile,depends upon a regular 'current distribution' with no regions of the cathode demonstrating a locally high plating current density.

The 'primary' current distribution depends only upon Ohm's law and is exclusive of any polarization effects, so that system geometry is an important factor in its determination. However, during metal deposition the cathode is polarized and the current distribution is changed to the actual or 'secondary' current distribution. Under this regime activation (charge-transfer) and concentration polarization (increasing with increasing current density) act as barriers to deposition and, in this way, oppose irregular current distribution. Hence, secondary current distribution is always more uniform than primary.

The situation is complicated where the plating reaction is not the sole cathodic process, and plating efficiency varies with cathode current density. In baths where plating efficiency rapidly decreases with increasing cathode current density, the excess deposit in regions of locally high current density (edges, projections, discontinuities) is not as great as might be expected from current

distribution alone. Such baths (many cyanide baths, for example) accordingly exhibit better throwing power.

Conversely, some plating solutions operate at higher efficiencies with increasing current densities, and thereby exaggerate non-uniform metal distribution as plating proceeds. These solutions tend to demonstrate 'negative throwing power', a characteristic which presents considerable problems in certain plating processes (chromium plating from chromic acid baths, for example).

The macro and micro throwing power of a plating solution affect different aspects of the deposition process. Macro throwing power of a plating bath determines the magnitude of the deviation from mean deposit thickness in cathode regions which receive locally high current densities, whereas micro throwing power (or 'levelling' power) has a direct effect on deposit morphology.

1.1.8. Morphology in electroplating

A solution with good micro throwing power tends to deposit onto the 'valleys' rather than the 'peaks' of the growing morphology, resulting in a smooth deposit with no outgrowths. Poor micro throw has the reverse effect on deposition and hence tends to result in a nodular morphology which is rough to the touch and fairly porous.

Deposit morphology is generally sensitive to the nature and degree of cathode polarization during deposition, as highly polarized reactions give a more even secondary current distribution and, therefore improved throwing power.

1.1.8.1. Polarization and morphology

Most metal electrodeposition takes place under conditions of mixed charge-transfer and concentration overpotential control (see

section 1.3.6). Where concentration overpotential is the predominant mode, deposits tend to exhibit a nodular morphology and no epitaxial relationship with the substrate. However, at lower current densities, where charge-transfer overpotential predominates, deposition tends to occur along growth edges (7, 8) which bear a definite crystallographic relationship to the basis metal (usually along close-packed directions).

Charge-transfer control therefore tends to favour relatively large epitaxial grains (9) which grow via the movement of surface steps across the deposit, whereas under diffusion control, growth is governed by the transport of metal ions to the cathodesurface with the favoured deposition sites being those 'closest' to the bulk solution (i.e, the 'peaks' of the growing deposit).

Clearly, neither control regime is entirely conducive to the production of a fine-grained level deposit, and in practice optimum structure and morphology are obtained by plating under mixed conditions of charge-transfer and diffusion control, and through the use (where possible) of surface-active agents.

The action of such addition agents (see Section 1.1.4.1) is considered to depend upon the predominant mode of overpotential prevailing during deposition and the nature of the solution (organic additions are not used in highly acidic plating solutions where they would break down) (10, 11, 12).

The micro-throwing power of a plating solution, and therefore deposit morphology, is not only dependent upon the extent (and therefore, by inference, nature) of cathode polarization during deposition, but also by the manner in which it varies with current density.

Solutions which demonstrate a small variation in current density for a large variation in overpotential exhibit better micro-throwing power (see section 1.6.1).

The overpotential regime under which chromium deposits from a catalyzed chromic acid solution is more difficult to define because of the effects of the concomitant hydrogen evolution reaction in breaking up the diffusion layers.

1.1.8.2. Dendritic and 'burnt' deposits

At very high current densities (under concentration over-potential control and approaching the limiting current density), deposit morphology in most plating processes becomes highly nodular and even dendritic in places. This is because 'peaks' in the growing deposit are closer to the anode and, therefore received higher current densities, and assuming the presence of a diffusion layer, are in more metal-rich solution than the 'valleys'. In solutions which exhibit poor throwing power therefore, the 'peaks' grow (progress-ively faster) at the expense of the 'valleys' until a point is reached where control is lost and dendrites form.

A dendritic deposit is porous and rough, and therefore to be avoided if possible. This is usually achieved by ensuring that no part of the cathode receives a locally high current density, through the careful positioning of anodes (and current deflectors, shields, etc.) with respect to the cathode.

Another type of unsatisfactory deposit sometimes produced is the 'burnt' deposit obtained in regions of locally high current density in processes where hydrogen evolution is a concomitant cathode reaction. Such deposits are generally powdery and of a dark appearance.

The cause of 'burnt' deposits is not yet unequivocally explained. However, they have been attributed to the co-precipitation of metal hydroxides or basic salts at the high cathode pH values which inevitably accompany high rates of hydrogen discharge.

SECTION 2

Electrochemistry

1.2. Principles

Electroplating is a cathodic process, and whilst anodic reactions are an essential (and important) part of the overall picture, it is inevitable that most attention should focus on the cathode and the reactions which take place there.

Most metal electrodeposition reactions require energy input before reduction can take place, energy which may be provided as electrical work. The electrical potential required to cause an electrode reaction to commence (under ideal conditions) is the standard single electrode potential, ϵ^{o}.

1.2.1 Electrode potentials

Consider an electrically isolated solid phase whose surface holds an excess of electrical charge in the form of ions or electrons (12). In order to bring a unit charge from an infinite distance up to the surface of the phase, work has to be done equivalent to an electrical potential ψ, which is termed the external electrical potential and which is entirely dependent upon the quantity and sign of the excess charge. The surface of the phase also usually contains an electrical double layer of orientated dipoles which give rise to a surface potential ζ which is independent of the excess charge.

So, the total work required to move a unit charge from infinity into the interior of the phase may be expressed as the inner potential

$$\phi = \psi + \zeta \qquad (1.2.1,1)$$

Now if an ionic species i, having a charge (protonic) of z_i, is present

in the aforementioned phase, its electrochemical potential may be defined as -

$$\mu_i^* = \mu_i + z_i F \phi \qquad (1.2.1,2)$$

Where μ_i is the chemical potential of (neutral) species i, and may be defined as -

$$\mu_i = \mu_i^o + RT \ln a_i \qquad (1.2.1,3)$$

Where a_i is the activity of i in the phase, and μ_i^o is the standard chemical potential of species i (equivalent to the standard molar free energy). μ_i, μ_i^o, and μ_i^* are expressed in J/mol, and ϕ is expressed in V.

If the distribution of ion i is now considered between two phases, it is governed by the equilibrium condition that the electrochemical potentials must be equal on both sides of the phase boundary.

$$\mathrm{I}\ \mu_i^* = \mathrm{II}\ \mu_i^* \qquad (1.2.1,4)$$

This two phase system involving a single charge carrier i, crossing the phase boundary is a simple electrode, and describes the equilibrium set up when a metal (phase I) is immersed in a solution of its ions (phase II).

$$\mathrm{I}_M \rightleftharpoons \mathrm{II}_{M^{z+}(aq)}$$

If equations (1.2.1,2) and (1.2.1,4) are combined,

$$(\mu_i + zF\phi)^{I} = (\mu_i + zF\phi)^{II}$$

which leads to

$$\Delta\phi = \phi^{II} - \phi^{I} = -\frac{^{II}\mu_i - {}^{I}\mu_i}{z_i F} = \epsilon \quad (1.2.1,5)$$

Where ϵ is usually termed the single electrode potential.

1.2.1.1. Standard electrode potentials

If a_i in equation (1.2.1,3) is considered to be unity for a solid metal, equation (1.2.1,5) may be rewritten for the reaction

$$M \rightleftharpoons M^{z+}_{(aq)} ,$$

$$\epsilon_M = -(\mu^{o}_{M^{z+}} + RT \ln a_{M^{z+}}) - \mu^{o}_{M}) \quad (1.2.1,6)$$

$$\epsilon_M = -\frac{(\mu^{o}_{M^{z+}} - \mu^{o}_{M})}{zF} + \frac{RT \ln a_{M^{z+}}}{zF} \quad (1.2.1,7)$$

Under standard conditions, $a_{M^{z+}} = 1$ and $\epsilon_M = \epsilon^{o}_M$, where ϵ^{o}_M = standard single electrode potential.

Hence, $$\epsilon^{o}_M = -(\mu^{o}_{M^{z+}} - \mu^{o}_{M}) \quad (1.2.1,8)$$
$$zF$$

and therefore

$$\epsilon_M = \epsilon^{o}_M + \frac{RT}{zF} \ln a_{M^{z+}} \quad (1.2.1,9)$$

This is the Nernst equation which describes the variation of single electrode potential with activity (concentration) and valency of reacting species.

The single electrode potential cannot be measured directly. However, an absolute value may be obtained using the relationship,

$$\Delta G = -zF \ (\epsilon_{M_1} - \epsilon_{M_2}) \qquad (1.2.1,10)$$

M_1 refers to electrode 1
M_2 refers to electrode 2

which relates chemical free energy change to potential difference. If a suitable energy cycle is constructed, the total ΔG for the electrode process may be determined, thereby allowing the calculation of the (theoretical) single electrode potential (13, 14). Alternatively, relative values of single potentials may be determined experimentally with respect to a suitable reference half-cell (single electrode).

1.2.2. Reference electrodes

1.2.2.1. Standard hydrogen electrode

Single electrode potentials are usually quoted with respect to the standard hydrogen electrode (or S.H.E.), although it is not widely used in experimentation.

The S.H.E. half-cell consists of a platinum sheet of large specific surface area in contact with hydrogen ions at unit activity, and in equilibrium with hydrogen gas at 1 atmosphere pressure. It may be written -

$$Pt_{(s)}, H_2 (g;\ p = 1 \text{ atm.}) \ | \ H^+ (aq; a = 1)$$

and represents the reaction $2H^+_{(aq)} + 2e^- \rightarrow H_{2(g)}$

It is arbitrarily assumed that the single potential for this half-cell is zero volts at all temperatures. When a different half-cell is connected in circuit, the overall cell may be written as -

$$Pt_{(s)},\ H_{2(g;\ p\ =\ 1\ atm)}\ |\ H^{+}_{(aq;\ a\ =\ 1)}\ \|\ M^{z+}_{(aq;\ a\ =\ a_{M}z+)}\ |\ M_{(s)}$$

where the half cell under investigation involves the reaction,

$$M^{z+}_{(aq)} \rightleftarrows M_{(s)}$$

Under these circumstances the overall cell potential difference is measurable and is equal to -

$$E = \varepsilon_{(M,M^{z+})} - \varepsilon_{S.H.E.}$$

But, as $\varepsilon_{S.H.E.}$ is zero, the single potential of the half-cell under investigation is given directly, and on the S.H.E. scale.

In order to avoid confusion, electrode reactions are all considered as reduction reactions under I.U.P.A.C. convention (13), so that the single (half-cell) potential given on the S.H.E. scale is, strictly, the reduction potential.

On this basis, a table of standard single electrode potentials (ε^{o}_{M}) with respect to the S.H.E. may be drawn up. This is the familiar 'electrochemical series'.

1.2.2.2. Standard calomel electrode

It is not always convenient to use a S.H.E. as a reference half-cell, especially when (as during investigation of an electrochemical process) interest is centred on only one electrode at a particular time. Potential measurements of this kind are made by using a reference electrode which has a (relatively) fixed value of potential regardless of the environment in which it is used. Such

an electrode ensures that any change in system e.m.f. is the result of a potential change at the electrode under observation, and not at the reference. The standard calomel electrode (or S.C.E.) fulfils these conditions.

It consists of mercury in equilibrium with Hg_2^{2+}, the activity of which is determined by the solubility of Hg_2Cl_2 (mercurous chloride or 'calomel'). The half-cell reaction is -

$$2Hg_{(l)} + 2Cl^-_{(aq)} \rightleftharpoons Hg_2Cl_{2(s)} + 2e^-$$

and may be written as -

$$Hg, Hg_2Cl_{2(s)} \mid Cl^-_{(aq,\ KCl)}$$

The electrode potential varies with the concentration of the supporting electrolyte, KCl, which must therefore be specified. The saturated KCl calomel electrode has a potential of +0.2415V with respect to the S.H.E, and being the easiest to prepare, is the most widely used.

SECTION 3

Overpotential

1.3 Principles

In an operating electrolytic cell through which a current is passing, the potential will differ from the equilibrium potential by an amount η which is termed the overpotential, so that,

$$\eta = E_i - E_{eq} \qquad (1.3,1)$$

The overpotential at an electrode surface may have several causes, depending upon the nature of the system and the conditions of operation.

1.3.1 Charge-transfer overpotential, η CT.

The Nernst equation (1.2.1,9) defines an electrode reduction potential at which, under certain conditions, an electrode reaction may commence. At this potential, a dynamic equilibrium exists

$$M^{z+}_{(aq)} + ze^- \rightleftharpoons M^{o}_{(s)}$$

in which the deposition reaction (reduction) takes place at the same rate as the dissolution reaction (oxidation), so that the current density flowing across the interface is the same in both directions, the exchange current density, i_o.

The exchange current density is a function of the system and is an indication of the ease with which electronic charge is transferred across the interface. At equilibrium therefore,

$$i_{red} = i_{ox} = i_o \qquad (1.3.1,1)$$

Increasing the cathode (electrode) potential in a negative direction causes an increase in the driving force for reduction, so that a net current density flows in the reduction direction,

$$i = i_{red} - i_{ox}$$

The increase in potential required to drive the reaction at current density i is the overpotential defined in equation (1.3,1), and is equal to the potential drop across the electrical double layer which exists at the electrode/solution interface.

1.3.1.1 The electrical double layer

The surface of a cathode in an aqueous solution is negatively charged. Water molecules, polarized as a result of their free electron pairs, therefore align themselves accordingly against the cathode surface. Metal cations bound up in aquo-complexes are hence held away from the cathode surface by their ligand groups, with a distance of closest approach for the cation dependent to a degree upon cation size.

The alignment of opposing charges across the distance of closest approach for the solvated cation is equivalent to an electrical capacitor, and is referred to as the Helmholtz double layer, the innermost plane of which virtually coincides with the average surface plane and passes through adsorbed orientated water molecules, metal ad-atoms and any unsolvated adsorbed anions. The outer Helmholtz plane passes through the centre of the solvated metal cations.

Beyond the Helmholtz double layer exists the diffuse Gouy-Chapman layer in which charge distribution differs from that in the bulk solution. The thickness of the Gouy-Chapman layer is a function of a number of solution and process variables (including agitation), but is generally of the order of 100 nm (15).

The Helmholtz double layer may be seen as a barrier to reaction (charge transfer), and at equilibrium, although an equal and opposite

(exchange) current density flows, an electrochemical free energy of activation must be overcome for charge-transfer to take place.

1.3.1.2 Charge-transfer

The equilibrium activation energy, ΔG_A, may be regarded as the difference between the free energies (equal at equilibrium) of the ionic species (in the outer Helmholtz plane) and the cathode metal atoms (in the inner Helmholtz plane), and the free energy of the 'activated' species. The overall reduction step may thus be written;

$$\underset{\text{O.H.P.}}{M^{z+}} \longrightarrow \underset{\alpha}{M^{z+}_{\text{activated}}} + ze^- \longrightarrow \underset{\text{I.H.P.}}{M^{o}_{\text{ads}}} \longrightarrow M^{o}_{\text{lattice}}$$

in which the point of activation is deemed to be situated a fraction α of the Helmholtz double-layer thickness from the metal surface ($\alpha \simeq 0.5$). However, at equilibrium the rate of reduction ($M^{z+} + ze^- \longrightarrow M^o$) and oxidation ($M^o \longrightarrow M^{z+} + ze^-$) across the double-layer are equal, a rate which may be represented in terms of an 'exchange current density', i_o.So, at equilibrium,

$$\frac{i_{red}}{zF} = \frac{i_{ox}}{zF} = \frac{i_o}{zF} \qquad (1.3.1.2,1)$$

As an activation energy barrier is involved (ΔG_A at equilibrium) an Arrhenius-type expression may be written;

$$\text{Rate} = \frac{i_o}{zF} = \text{Constant x exp.}(-\Delta G_A/RT)$$

$$\text{or} \quad i_o = zF.\text{Constant x exp.}(-\Delta G_A/RT) \qquad (1.3.1.2,2)$$

where the Constant incorporates certain concentration terms.

If the electrochemical free energy of the atoms in the metal surface is raised by $zF\eta$ J/mol (η is measured in Volts) relative to

the equilibrium value, then that of ions in the activated state is raised by $(1-\alpha)zF\eta$ (assuming a uniform potential gradient in the double-layer). This means that the activation energy for the anodic oxidation reaction becomes

$$\Delta G_A + (1-\alpha)zF\eta - zF\eta = \Delta G_A - \alpha zF\eta$$

so that the anodic oxidation current density i_{ox} becomes

$$i_{ox} = zF.\text{Const.}\exp\{-(\Delta G_A - \alpha zF\eta)/RT\}$$

substituting Equation (1.3.1.2,2), this becomes

$$i_{ox} = i_o.\exp(\alpha zF\eta/RT) \qquad (1.3.1.2,3)$$

taking logs to the base ten and rearranging;

$$\eta = \frac{2.303RT}{\alpha zF}.\log(i_{ox}/i_o) \qquad (1.3.1.2,4)$$

Equation (1.3.1.2,4) is the Tafel equation for an anodic process.

Using a similar argument, it is evident that the increase of $zF\eta$ to the free energy of atoms in the metal surface raises the activation energy for deposition (reduction) to

$\Delta G_A + (1-\alpha)zF\eta$ giving a reduction current density of

$$i_{red} = i_o.\exp\{-(1-\alpha)zF\eta/RT\} \qquad (1.3.1.2,5)$$

As the actual current density that passes due to the application of the overpotential η is the difference between the oxidation and reduction current densities (i.e., $i_a = i_{ox} - i_{red}$), at values of η greater than 0.03V the minor component becomes relatively insignificant and can be ignored.

There is therefore a log-linear relationship between nett anodic current density and electrode overpotential. This may be simplified to the form;

$$\eta_{CT} = b_a.\log\ (i_a/i_o) \qquad (1.3.1.2,6)$$

where b_a is the anodic Tafel coefficient and represents the slope of a η vs $\log i_a$ plot:- $b_a = \frac{2.303RT}{\alpha zF}$

b_a has the units of Volts per tenfold change in current density, or Volts/decade.

Overpotential for anodic oxidation is positive. However, if a negative overpotential is applied to the metal electrode ($\eta<0$) the oxidation reaction is suppressed and the reduction reaction ($M^{z+} + ze^- \rightarrow M^o$) is favoured, as the free energy of activation is increased for the former and decreased for the latter. So, the nett current density across the double-layer at η more negative than 0.03V becomes i_c. The cathode polarization curve thus generated is represented by

$$\eta_{CT} = b_c.\log\ (i_c/i_o)$$

in which $b_c = \frac{-2.303RT}{(1-\alpha)zF}$ = slope of a plot of η vs $\log i_c$.

The relevant Tafel expression for electrodeposition is therefore

$$\eta_{CT} = \frac{-2.303RT}{(1-\alpha)zF}.\log\ (i_c/i_o) \qquad (1.3.1.2,7)$$

1.3.2 Crystallization overpotential, η_X

Although a model has been presented for charge-transfer, uncertainty exists with regard to the precise mechanisms involved in discharge and subsequent lattice incorporation.

Two alternative routes are available:

(a) Assuming that activation and charge-transfer can only occur at specific growth centres on the surface (edges, kinks, vacancies), the ions in the outer Helmholtz plane must migrate to positions opposite these growth sites prior to discharge. The extra overpotential (energy) required to deform the electric field during this proposed migration is considerably less than that which is observed (17), and suggests a different mechanism.

(b) If it is assumed that complexed cations may be activated and discharged at any point in the outer Helmholtz plane, they may then adsorb onto any site on the cathode surface as 'ad-atoms', before moving to active growth centres by surface diffusion. The extra observed 'crystallization' overpotential may now be interpreted as a form of diffusion-controlled or 'concentration' overpotential (18,19).

The discharge of the 'ad-atom' from its solvation sheath at various surface sites was considered (20). It was concluded that, as distortion and displacement of the solvation sheath is necessary prior to discharge and that this would be least at a planar site (compared with an edge, kink or vacancy), planar discharge is the most energetically favoured first step. It was also proposed (19) that the adsorbed particles retain a dipolar character with respect to an electron in the metal surface, making them (while not conventionally charged) 'ad-ions' rather than 'ad-atoms'. If this was the case, some solvating ligand is likely to remain attached to the adsorbed particle, only to be removed on arrival (through surface diffusion) at a growth site. Any post-charge-transfer ligand retention (dependent upon the cation-ligand bond strength) would hinder surface diffusion, but would also lower the activation energy for charge-transfer, and hence η_{CT}. Under this regime, an excess of free

(polarised) ligand groups might be expected in the region of growth sites. This again would tend to promote discharge at planar sites, and hence favour new nucleation rather than step-wise growth.

The change in deposit growth modes with increasing overpotential from ledge-wise (epitaxial) to fine-grained nodular may now be explained in terms of an increase in the nucleation of growth centres (planar sites where 'ad-ions' have collided to form new nuclei) with rising current density. At higher current densities, the number of surface-migratory 'ad-ions' per unit area is such that the probability of collision and subsequent nucleus formation is enhanced.

At low cathode overpotentials the rate of deposition is dependent upon the rate of 'ad-ion' surface-diffusion to growth sites, and is characterized by a linear η - i relationship. At higher values of cathode polarization, this is replaced by the familiar η - log i (Tafel) association.

The mechanisms outlined above may not however pertain to chromium plating from the highly acidic solutions employed, in which the degree of complexing is likely to be much lower.

1.3.3 Concentration overpotential η_c

At high current densities, the rate of metal deposition is such that a layer of the electrolyte adjacent to the cathode surface becomes depleted in metal ions and a concentration (activity) gradient is established. At these current densities, the rate of metal deposition is therefore dependent upon mass-transfer across a cathodic diffusion layer.

Under diffusion control a maximum current density exists at which the deposition rate is controlled by the maximum diffusion rate of metal ions across the diffusion layer to the outer Helmholtz plane.

Now, , the rate of mass transport across the diffusion layer is given by

$$\frac{i}{zF} = -D.\frac{dh}{dx} \qquad (1.3.3,1)$$

which assumes a single linear activity gradient. If the diffusion layer thickness is δ, equation (1.3.3,1) may be written so that the ionic flux to the cathode is

$$\frac{i_c}{zF} = -D_M z+ . \frac{(h_M z+^{O.H.P.} - h_M z+^{bulk})}{\delta} \qquad (1.3.3,2)$$

where, $D_M z+$ = 'diffusivity' of the metal ions,

$h_M z+$ = activity of metal ions in solution.

When the deposition rate is so great that $h_M z+^{O.H.P.}$ falls to zero, the diffusional flux $\frac{i}{zF}$ attains a limiting value,

$$\frac{i_L}{zF} = -D_M z+ . \frac{(O - h_M z+^{bulk})}{\delta}$$

so that,

$$i_L = \frac{zF\ D_M z+ . h_M z+^{bulk}}{\delta} \qquad (1.3.3,3)$$

where i_L is the 'limiting current density'.

Combination of equations (1.3.3,2) and (1.3.3,3) gives

$$h_M z+^{O.H.P.} = h_M z+^{bulk} \left[1-\left(\frac{i}{i_L}\right)\right] \qquad (1.3.3,4)$$

Remembering that the Nernst equation (1.2.1,9) describes the dependence of the single potential upon the activity of the reacting

species (at the outer Helmholtz plane), it may be used with equation (1.3.3,4) to arrive at an expression for the overpotential due to mass transport across the diffusion layer,

$$\eta_C = \varepsilon - \varepsilon_M^{\circ} = \frac{RT}{zF} \ln \left[1 - \left(\frac{i}{i_L}\right)\right] \qquad (1.3.3,5)$$

Under conditions where concentration overpotential η_C controls the rate of electrodeposition, the simplest situation is described by equation (1.3.3,5) which may also be expressed in a 'Quasi-Tafel' manner,

$$\Delta i = i_L \exp (zF\, \eta_C/RT) \qquad (1.3.3,6)$$

Charge-transfer and concentration overpotential are additive, with the latter predominating at higher current densities.

1.3.4 Reaction overpotential η_R

Reaction overpotential is a phenomenon resulting from the existence of a slow (rate-determining) chemical step in the overall electrode reaction which is only manifest when other components of the total cathode overpotential (such as η_{CT} and η_C) are not rate-determining. By definition, this chemical step is a reaction with a rate independent of the electrode potential.

Rate-determining chemical reactions in electrochemical processes may be divided into two categories; those which occur in the bulk solution and those which take place at the electrode/solution interface.

1.3.4.1 Chemical reaction control in bulk solution

If the metal deposition reaction

$$Y \rightarrow M^{z+}_{(aq)} + ze^{-} \rightarrow M^{o}_{(s)}$$

is considered, wherein the $Y \rightarrow M^{z+}_{(aq)}$ step proceeds at a slower rate than the later diffusion and charge-transfer steps, it may be deduced that a limiting current density (less than i_L under conditions of concentration overpotential control) due to reaction overpotential should be observed. At this new limiting current density, the reaction rate is determined by the diffusion of species Y across a 'reaction layer' of thickness p', analogous to the Nernst diffusion layer.

It has been shown (12) that under these conditions

$$i_{lim} = zFC_{M}z+ \left(\frac{p'k}{1 + p'k.\pi^{\frac{1}{2}}t^{\frac{1}{2}}D_{Y}^{-\frac{1}{2}}} \right) \qquad (1.3.4.1,1)$$

where, k = rate constant for $Y \rightarrow M^{z+}_{(aq)}$.

When p'k is large, the rate of the chemical reaction is high and concentration overpotential predominates, with equation (1.3.4.1,1) tending towards

$$i_{lim} = \frac{zFC_{M}z+.D^{\frac{1}{2}}}{\pi^{\frac{1}{2}}t^{\frac{1}{2}}} \qquad (1.3.4.1,2)$$

This is equivalent to equation (1.3.3,3), if $\pi^{\frac{1}{2}}D^{\frac{1}{2}}t^{\frac{1}{2}}$ is the constant diffusion layer thickness (δ) under stationary conditions.

When p'k is small

$$i_{lim} = zFC_{M}z+.p'k = 'i_{r}' \quad \text{('reaction limiting current density')}. \qquad (1.3.4.1,3)$$

Under conditions where $p' << \delta$, concentration overpotential can be virtually neglected in comparison with reaction overpotential. Under these conditions, agitation should have no effect on the observed limiting current density and may be taken as an indication of possible reaction overpotential control.

1.3.4.2 Chemical reaction control at the interface

Rate-controlling chemical reactions between reactants which have been adsorbed onto the cathode surface give rise to a reaction limiting current density $i_{r'}$, the magnitude of which is dependent upon the nature of the electrode surface itself (21). Where the chemical reaction is much slower than all other steps in deposition, an equation may be derived (12),

$$i = zF\,\nu v_o\,(1 - \exp \frac{\eta_R zF\omega}{RT}) \qquad (1.3.4.2,1)$$

where, ν = the 'stoichiometric factor' of the chemical reaction

v_o = the equilibrium 'exchange reaction rate' (analogous to exchange current density in charge-transfer),

ω = the order of the chemical reaction

At high reaction overpotentials, $\eta_R \to \infty$, the reaction limiting current density is approached, and equation (1.3.4.2,1) becomes

$$i_{r'} = zF\,\nu\,v_o \qquad (1.3.4.2,2)$$

so that, by analogy with concentration overpotential,

$$\eta_R = \frac{RT}{\omega zF} \ln\left[1 - \left(\frac{i}{i_{r'}}\right)\right] \qquad (1.3.4.2,3)$$

For first order chemical reactions, $\omega = 1$ and equation (1.3.4.2,3) assumes the same form as equation (1.3.3,5).

1.3.5 Resistance overpotential η_Ω

If an electrode potential is measured (using a Luggin capillary probe) while a current is flowing, it will include a potential drop due to the resistance of the solution near to the electrode surface - the so-called 'iR drop'.

The magnitude of the iR drop component in total electrode potential is a function of measurement technique and the conductivity of the solution.

In the simplest situation, where the concentration of electrolytes at the electrode does not vary with distance from the electrode, the conductivity of the solution at the electrode may be taken to equal the bulk solution conductivity.

Under these conditions,

$$\eta_{\Omega} = \frac{i}{\Lambda_{bulk}} \qquad (1.3.5,1)$$

For electrodeposition at higher current densities, this expression is no longer valid, as the potential drop measured is across a region of bulk solution and a diffusion layer. Hence, the resistance over-potential may be separated into two components. Assuming this, and that a linear concentration gradient exists across the diffusion layer, equation (1.3.5,1) may be modified (for a large planar electrode) so that,

$$\eta\Omega = \frac{i}{\Lambda_{bulk}} + \int_{o}^{\delta} \frac{i}{\Lambda C^{x}} \cdot dx \qquad (1.3.5,2)$$

where, Λ = equivalent conductivity of electrolyte in diffusion layer,

C^{x} = electrolyte concentration at a distance x from the electrode.

The linear concentration gradient across the diffusion layer may be expressed as,

$$C^{x} = C^{O.H.P.} + \frac{x}{\delta} (C^{bulk} - C^{O.H.P.}) \qquad (1.3.5,3)$$

Assuming Λ to be constant, and that deposition (from cation M^{z+}) is from an electrolyte MB in which t_M and t_B are the transport numbers

of the M^{z+} and B^{z-} ions respectively, comparison of equations (1.3.3,4), (1.3.5,2) and (1.3.5,3) yields (22),

$$\eta_{\Omega} = \frac{i}{\Lambda bulk} + \frac{zFD}{\Lambda t_B} \ln\left[1 - \left(\frac{i}{i_L}\right)\right] \qquad (1.3.5,4)$$

where,

$$i_L = - \frac{zFD\ C_M^{bulk}}{\delta t_B} \qquad (1.3.5,5)$$

However, the diffusion coefficient D of an electrolyte is related to the equivalent conductivity by (23),

$$D = \frac{2RT}{F^2} \cdot t_M \cdot t_B \Lambda \qquad (1.3.5,6)$$

so that,

$$\eta_{\Omega} = \frac{i}{\Lambda bulk} + \frac{2zRT}{F} \cdot t_M \ln\left[1 - \left(\frac{i}{i_L}\right)\right] \qquad (1.3.5,7)$$

At low current densities, where charge-transfer or crystallization overpotential prevail, any diffusion layer is so thin that the last term in equation (1.3.5,7) tends to zero, giving a resistance overpotential component entirely due to a simple 'iR drop'.

1.3.6 Total overpotential

An overall picture now emerges when considering cathode polarization during metal electrodeposition, in which the potential drop measured between the electrode and the bulk solution may be expressed as,

$$E = \varepsilon_M + \eta_{CT} + \eta_X + \eta_C + \eta_R + \eta_{\Omega} \qquad (1.3.6,1)$$

in which every term is negative.

The predominance of any individual component of this equation during electrodeposition is largely a function of the particular process and the conditions under which it is operated (current density, temperature, concentration of metal ions, agitation). However, most electroplating is carried out at cathode current densities corresponding to conditions of mixed charge-transfer and concentration overpotential control. At these current densities, crystallization overpotential usually provides a negligible contribution. Resistance overpotential, however, must always be taken into account, although at low current densities it may tend to very low values. Reaction overpotential is, of course, only important where a chemical reaction plays a significant part in the electrodeposition process.

The diffusional and charge-transfer steps are hence usually considered the most important in electroplating.

1.3.7 Charge-transfer and diffusion under plating conditions

The variation of charge-transfer and concentration overpotential with cathode current density is described in equations (1.3.1.2,7) and (1.3.3,5). Under normal circumstances, η_{CT} is more important at lower current densities whereas η_C predominates at higher current densities.

1.3.7.1 The effect of agitation

Whilst solution agitation has little or no effect on charge-transfer overpotential, it usually reduces concentration overpotential through a thinning of the diffusion layer (which increases i_L in equation (1.3.3,5)) and can indicate whether η_C or η_{CT} is predominant.

The variation of δ with conditions of turbulence in the electrolyte is particularly relevant to those electroplating processes which involve cathodic gas evolution. Exact calculation of the effect of

turbulence upon mass transport at plating electrodes has not so far been possible (23). Nevertheless, several workers have made theoretical statements about the dependence of diffusion layer thickness on various parameters, and these have been used (24) to produce an approximate relationship,

$$\delta = 1.Re^{-0.9} . Sc^{-0.33} \qquad (1.3.7.1,1)$$

where,

l = coordinate in direction of (liquid) current flow, measured from the edge of the electrode,

Re = Reynold's number = $\frac{U.d}{\mu'}\rho$

Sc = Schmidt's number = $\frac{\mu'}{\rho.D}$

and U = fluid velocity (a function of the rate of gas evolution)

d = characteristic length of flow channel,

D = diffusion coefficient of diffusing species,

μ' = fluid viscosity, ρ = fluid density.

1.3.7.2 <u>The effect of temperature variation</u>

Differentiation of equation (1.3.3,5) with respect to temperature reveals,

$$\left(\frac{d\eta_C}{dT}\right)_{i = const} = \frac{\eta_C}{T} - \frac{RT}{F}\left(\frac{i}{i-i_L}\right)\frac{d\ln i_L}{dT} \qquad (1.3.7.2,1)$$

which becomes (if $i >> - i_L$),

$$\left(\frac{d\eta_C}{dT}\right) \simeq \frac{\eta_C}{T} - \frac{RT}{F}\frac{d\ln i_L}{dT} \qquad (1.3.7.2,2)$$

As the temperature is raised, the diffusion coefficient increases, and at the same time the diffusion layer thickness may decrease. Hence, $\frac{d\ln i_L}{dT}$ is always positive.

A survey of available data (22) indicates that $\frac{d\ln i_L}{dT}$ is approximately 0.04 per degree in many cases. This translates to (typical) values of $\left(\frac{d\eta_C}{dT}\right)_{i = const}$ in the region of -0.5 mV per degree.

Under similar conditions, the temperature coefficient of charge-transfer overpotential is considerably higher - up to -2.5 mV per degree, and is dependent upon the enthalpy of activation (see section 1.3.9.2 (24)). In simple terms,

$$\left(\frac{d\eta_{CT}}{dT}\right)_{i = const} \propto - \frac{\Delta H_A}{(1-\alpha)zFT} \qquad (1.3.7.2,3)$$

1.3.7.3 The effect of bulk solution concentration

The limiting current density (due to mass transport across the diffusion layer) of an electrode reaction is directly proportional to the bulk solution concentration of the important diffusing species (equation (1.3.3,3). An increase in bulk concentration causes an increase in i_L and therefore reduces concentration overpotential at any particular current density.

Charge-transfer overpotential is not generally strongly affected by bulk solution concentration at electroplating current densities. However, exchange current density i_o is dependent upon the bulk concentration of the discharging species (equations (1.3.1.2,1) and (1.3.1.2,3)).

The overall measured electrode potential is also, of course, affected through the dependence of the single electrode potential upon the activity (concentration) of the reacting species (equation (1.2.1,9) - the Nernst equation).

1.3.7.4 The effect of surface films

Cathodic surface films in metal electrodeposition may be

PAGE

NUMBERING

AS ORIGINAL

categorized as (25) being due to either specific organic additions (as referred to in section 1.1.4.1) or some inherent feature of the cathodic process.

From a kinetic point of view (rather than morphological), adsorbed films of organic addition agents lead to a reduction in the exchange current density for a deposition reaction, the extent of the reduction being dependent upon the nature of the addition agent and (linearly) its surface coverage (26,27).

1.3.7.4.1 Oxide and hydroxide films

Metal electrodeposition from certain plating solutions involves simultaneous hydrogen evolution which may reduce the acidity (increase pH) in the diffusion layer, with consequent precipitation of basic oxides and hydroxides. Hydrogen evolution is not only influential through its lowering of plating current efficiencies - oxide or hydroxide precipitation drastically modifies the cathode surface and the kinetics of the reactions which take place thereon.

Electrochemical kinetics in the presence of an oxide layer have been considered by a number of workers, but usually with reference to anodic dissolution processes. Such anodic dissolution through oxide films has received considerably more attention than the corresponding cathodic deposition, and is therefore better understood. Indeed, an understanding of 'quasi-passive' anodic behaviour could prove useful in the interpretation of electrodeposition through a cathodic oxide film.

Cathode films formed through localized pH changes due to concomitant hydrogen evolution in electrodeposition may be discontinuous, inhomogeneous and very thin indeed (< 10 nm). Under certain conditions however, such films are thick enough and continuous enough to provide an effective barrier to most cathode reactions other than hydrogen

evolution. So, while the presence of a film may prevent the metal deposition reaction, it will generally only hinder the hydrogen evolution reaction (modifying the kinetics of reduction).

An oxide (or hydroxide) does not conduct electricity as well as the metal, tending instead to semiconductivity although some cathodic oxide films do exhibit a tendency to 'metallic' behaviour. The degree of 'metallic' behaviour demonstrated by a cathodic oxide film may be explained in terms of a number of phenomena (28):

(a) Non-stoichiometry or unintentional doping of the oxide during the cathodic process.

(b) Flaws and micro-fissures within the oxide.

(c) Unusual surface states resulting from the chemisorption of reactants, intermediates, or products of the electrode reaction(s) (29).

(d) An oxide layer thin enough to sustain electron-tunneling.

(e) Only partial oxide-coverage, or periodic self-removal (30).

While these factors may lead to near metallic behaviour, the oxide <u>always</u> retains some residual semiconductivity, and so a fraction of the cathodic metal (oxide)/ solution potential drop (overpotential) still operates across the oxide. The potential drop across the oxide layer may be very small indeed (depending upon how 'metallic' the oxide is) but it has a considerable effect on the electrode kinetics of those cathode reactions which are able to take place (usually hydrogen evolution, if no other). Certain features are characteristic of electrode kinetics in the presence of oxide films.

(i) Anomalous Tafel slopes

The Tafel equation describing charge-transfer during the hydrogen evolution reaction gives a Tafel slope of (assuming $\alpha = 0.5$ and $z = 1$) 118 mV/decade at $25^{o}C$. Values of Tafel slope greater than this

are anomalous as they cannot be predicted by any theoretical procedure without making doubtful assumptions (30). However, Tafel slopes of greater than 118 mV/decade have been experimentally obtained for hydrogen evolution on oxide-covered electrodes. These have been explained (31) in terms of the assumption that a proportion of the metal/solution potential operates across the oxide layer and is therefore not available to assist charge-transfer at the oxide/solution interface.

Considering hydrogen evolution on an oxide-covered electrode, two energy barriers are therefore kinetically significant (31). Firstly, the charge carrying species H_3O^+ must achieve a state of activation in the double layer. Secondly, the electrons in the metal must negotiate the oxide layer before discharge of the activated species can take place.

The 'dual-barrier' model is thus defined, with two activation energy barriers to be overcome prior to reduction. For proton reduction therefore, the total overpotential driving the process may be split into a film component and a double-layer component (both 'negative' potential differences);

$$\eta = V_f + V_{dl} \qquad (1.3.7.4.1,1)$$

Considering the double-layer component first, we can write,

$$i_o = k_{dl}.a_{dl}^{H^+} \qquad (1.3.7.4.1,2)$$

where,

k_{dl} = rate constant for charge-transfer across the double-layer, and includes the term (constant) zF,

$a_{dl}^{H^+}$ = activity of hydrogen ions in the outer Helmholtz plane.

Recalling equation (1.3.1.2,6) and putting z = 1,

$$i = k_{dl}.\alpha_{dl}^{H^+} \exp\left[- (1 - \alpha_{dl}) \frac{FV_{dl}}{RT} \right] \qquad (1.3.7.4.1,3)$$

or $$V_{dl} = \left[- \frac{2.303RT}{(1-\alpha_{dl})F} \right] \left[\log i - \log (k_{dl}.\alpha_{dl}^{H^+}) \right] \qquad (1.3.7.4.1,4)$$

If electron transfer across the oxide film is now considered, a similar expression may be written,

$$V_f = \left[- \frac{2.303RT}{(1-\alpha_f)F} \right] \left[\log i - \log (k_f.\alpha_f^{e^-}) \right] \qquad (1.3.7.4.1,5)$$

and combining equations (1.3.7.4.1,1), (1.3.7.4.1,4) and (1.3.7.4.1,5),

$$\eta = \left[- 2.303\frac{RT}{F} \right] \left\{ \left[\frac{1}{(1-\alpha_{dl})} \right] + \left[\frac{1}{(1-\alpha_f)} \right] \right\} \log i + \text{constants}$$

or

$$\eta = \left[\frac{2-\alpha_f - \alpha_{dl}}{(1-\alpha_{dl})(1-\alpha_f)} \right] \left[- 2.303\frac{RT}{F} \right]. \quad \log i + \text{constants} \qquad (1.3.7.4.1,6)$$

But

$$\eta_{CT} = - \frac{2.303RT}{(1-\alpha_{dl})zF} \log\left(\frac{i}{i_o}\right) = b_c \log\left(\frac{i}{i_o}\right) \qquad (1.3.7.4.1,7)$$

where b_c is the film-free Tafel slope.

Thus, the Tafel slope in the presence of an oxide film is

$$\frac{d\eta}{d\log i} = \frac{(2 - \alpha_{dl} - \alpha_f)}{(1 - \alpha_f)} \cdot b_c \qquad (1.3.7.4.1,8)$$

Assuming α_f and α_{dl} to both be approximately equal to 0.5, the presence of an oxide film might therefore be expected to double the observed Tafel slope for hydrogen evolution. Experimentally determined

anomalously high Tafel slopes for this reaction are well documented (31,32,33,34,35,36,37).

(ii) Hysteresis in steady-state cathode polarization curves due to current rectification by the oxide.

(iii) Lowered exchange current densities due to a relative paucity of electrons at the oxide/solution interface (see Section 1.3.1).

(iv) Inflections in the cathode polarization curve, which are believed to correspond to the deposition or co-deposition of a reaction intermediate such as an oxide or hydroxide species (38,39).

1.3.7.5 Multi-electron charge-transfer

Hydrogen evolution at a cathode involves a single electron transfer for every atom of hydrogen discharged, resulting in a value of unity for z in the Tafel expression (equation (1.3.1.2,6). However, most plating metals are electrodeposited from a multi-valent state for which $z > 1$. The question therefore arises as to the feasibility of a single step multi-electron transfer.

Calculations involving a reduction of the type $Cu^{2+}_{(aq)} + 2e^{-} \rightarrow Cu_{(s)}$ have indicated (40) that the activation energy required for a simultaneous two-electron transfer would be greater than 400 kJ/mol. This is so high that the rate constant for this type of transfer would be negligible (19), and it was concluded that charge-transfer in the above reduction must take place in steps, one of which is rate-determining. This concept may be extended to include most reactions which involve multi-electron transfer.

1.3.8 Hydrogen overpotential

According to the electrochemical series of standard electrode (reduction) potentials, many metals should not be able to deposit from aqueous solutions of their ions as the hydrogen evolution

reaction is thermodynamically preferred. Fortunately however, the hydrogen evolution reaction is highly dependent upon kinetic factors, and tends to exhibit high overpotential on many surfaces.

The mechanism of hydrogen evolution varies according to conditions, and in particular, the nature of the cathode. However, the total reaction may be split into certain basic steps (41):

(a) Mass transport (diffusion) of H_3O^+ ions to the Helmholtz double-layer.

(b) Activation and discharge of H_3O^+ by an electron from the cathode;

(i) at a point on the cathode surface where no H atoms are present - $H_3O^+ + M + e^- \rightarrow MH + H_2O$, with the formation of adsorbed H atoms.

(ii) at a point on the surface where other H atoms are already present - $H_3O^+ + MH + e^- \rightarrow M + H_2 + H_2O$, with the formation of molecular H_2.

(c) Combination of two adsorbed H atoms to form molecular H_2 - $MH + MH \rightarrow 2M + H_2$.

(d) Desorption of molecular H_2 from the surface into solution.

(e) Removal of H_2 molecules by diffusion or bubble formation.

At low current densities, step (b) is usually the most important (33) and charge-transfer control predominates. However, hydrogen evolution is kinetically 'easier' on some metals than others, and on rough surfaces rather than smooth, with the result that hydrogen overpotential may determine the conditions under which other cathodic reductions may take place in aqueous solution.

1.3.9 Mechanism determination from overpotential data

As electrodeposition (in its simplest form) involves many different chemical and electrochemical steps (diffusion, charge-transfer, surface-diffusion, lattice incorporation), the individual

importance of which is dependent upon plating conditions, the determination of deposition mechanisms is problematic. Overall mechanism evaluation in chromium plating is extremely difficult and, despite the efforts of many researchers, no unequivocally accepted theory has yet been proposed.

Direct evidence with regard to deposition mechanisms in electroplating is hard to obtain, and most theories are based upon circumstantial evidence combined with a thorough knowledge of the conditions pertaining. A major means of investigation employed in electrodeposition is that of the cathode polarization curve in which the variation of (the log of) cathode current density with cathode potential (with respect to a reference potential) is used to follow the progress of the reaction.

Interpretation of overall cathode polarization curves in chromium plating (regardless of the practical difficulties inherent in their measurement) at current densities where all three cathode reactions proceed is clearly a major problem, particularly as the overall cathode overpotential may consist of a number of contituent component overpotentials (concentration, charge-transfer, reaction, crystallization, resistance) each of which varies with current density in a different manner. Attempts have recently been made to split the overall curve into three constituent 'partial' curves (157) corresponding to the individual reactions, but no systematic study has been undertaken to use these curves in mechanism determination.

If a simple metal deposition reaction is considered, the total overpotential required to drive it at a certain current density may be divided into the various overpotential types listed in section 1.3.6. The proportion of the total made up by any one constituent is mainly dependent upon the current density. However, most

electrodeposition is carried out under conditions of mixed charge-transfer (η_{CT}) and concentration (η_C) overpotential control. The predominating overpotential mode (of these two) may be determined by examining the effect of agitation on the deposition rate. A pronounced effect indicates the predominance of a concentration overpotential, whereas little effect demonstrates a tendency to charge-transfer control.

1.3.9.1 Mechanisms under charge-transfer control

Assuming 'pure' charge-transfer conditions, certain conclusions may be drawn from the corresponding straight-line Tafel region of the cathode polarization curve for the particular reduction. The slope of this line is given (under the simplest conditions) as

$$\frac{d\eta_{CT}}{d\log i} = \frac{-2.303RT}{(1-\alpha)zF} \qquad (1.3.9.1,1)$$

in which α is the so-called 'symmetry factor' (see section 1.3.1.2) and denotes the position of the activated reducible complex in the double layer. The total valence change involved in the reaction is given by z. α is usually assumed to be 0.5, and z is generally known from the observed chemistry of the process. However, the assumption of values for α and z may be unwise, as a comparison of theoretical and experimental values for Tafel slopes often indicates.

As has already been demonstrated (section 1.3.7.4.1), the presence of a film on the cathode through which deposition takes place may cause the observed Tafel slope to double, with an effective coefficient of

$$\frac{2-\alpha_{dl}-\alpha_f}{(1-\alpha_f)(1-\alpha_{dl})} \quad \text{instead of} \quad \frac{1}{(1-\alpha_{dl})}$$

assuming a value of 0.5 for α_{dl} and α_f.

When considering a cathodic deposition process which involves concomitant hydrogen evolution, the presence of a film may be checked for by measuring the Tafel slope for hydrogen reduction (using a 'partial' polarization curve) and comparing it with the fixed value (z equals unity) for an unfilmed electrode of 118 mV/decade. Steeper slopes may indicate the presence of a film.

The value of z assumed during the investigation of metal deposition from an M^{z+} species presents a further complication as the Tafel expression (in its simplest form) assumes that all charges (z) transferred in a reduction are transferred simultaneously. However, it is far more likely that the overall charge-transfer process consists of a number of individual steps which proceed at different rates under a particular set of conditions. Of these steps, the one which proceeds at the slowest rate (assuming it is an integral part of the reduction process) is the one which controls the overall rate of charge-transfer (and hence deposition, where charge-transfer is rate-controlling). This step is termed the 'rate-determining step' or R.D.S.

The nature of the R.D.S. in an overall electrodeposition is not necessarily electrochemical (i.e. involving charge-transfer), even under apparently Tafel conditions. It may be a simple chemical reaction.

1.3.9.1.1 Chemical rate-determining step

Where the R.D.S. is of a chemical nature and occurs in the bulk solution prior to any electrode reaction, it is characterized by a none agitation-dependent (usually relatively low, but varying with the reaction) limiting current density (see section 1.3.4.1). However, where the R.D.S. is chemical and occurs at the cathode/electrolyte interface, a none agitation-dependent limiting current density is encountered which is heavily dependent upon the nature of

the cathode surface (see section 1.3.4.2).

Distinguishing between chemical reaction rate control in bulk solution and at the interface is obviously difficult, and where possible is achieved through electrochemical observation combined with an idea of the overall deposition mechanism.

In chromium plating theory, the proposed mechanisms (see section 1.10) which involve a purely chemical step consider it to occur at the cathode surface. Where this is the case and the chemical reaction is rate-controlling, the relationship between over-potential and current density is given by

$$\eta_R = \frac{RT}{\omega z F} \ln \left(1 - \frac{i}{i_r'}\right) \qquad (1.3.4.2,3)$$

as defined in section 1.3.4.2, and where

$$i_{r'} = zF\, \nu v_o \text{ (assumed constant)} \qquad (1.3.4.2,2)$$

ν = stoichiometric number

v_o = equilibrium exchange rate.

A knowledge of the stoichiometry of any rate-controlling chemical step may therefore allow it to be isolated and fitted within an overall mechanism proposal (assuming a chemical R.D.S. exists in the first place).

1.3.9.1.2 Electrochemical rate-determining step

Under conditions of electrolysis where charge-transfer predominates, it is nonetheless likely that a proportion of the observed overpotential is due to concentration or possibly reaction overpotential. This proportion may be calculated from any observed limiting current densities (and equations (1.3.3,5) and (1.3.4.2,3)) and, where small, may be neglected.

Assuming that a section of a polarization curve is studied in which it is known that charge-transfer overpotential is the sole contributor to the measured polarization, the problem arises as to whether the charge-transfer is multi-step and, if so, how to isolate the R.D.S.

In chromium plating, six electrons are transferred during the overall reduction of chromic acid to metal and, as a six-electron one-step transfer is highly unlikely, the reduction must be divided into a sequence of consecutive steps. The nature and number of the steps form the basis of any theory, and are subject to controversy. However it is inevitable that charge-transfer is involved in some form, and possible that others involve chemical reduction.

If it is assumed that all the steps are electrochemical and that they proceed in a fixed sequence, the problem is to isolate the slowest one - the one which determines the overall deposition rate.

In practice, the reduction of chromic acid to chromium metal may involve more than six electrons in the overall reaction. So, z in Equation 1.3.1.2,7 may be replaced by λ (where $\lambda \geqslant z$ and is the number of electrons required for each occurrence of the overall reaction), modifying the equation (and rearranging) to the form

$$\frac{d\eta}{d\log i} = \frac{-2.303RT}{(1-\alpha)\lambda F}$$

If a value for $(1-\alpha)$ is assumed (dependent upon the presence or absence of any cathode film), λ may therefore be found from measured Tafel slopes. As λ is the number of electrons involved in the overall reaction, it can be divided into those electrons which participate in the steps preceding the R.D.S., those which participate in steps following the R.D.S., and those which participate in the R.D.S. (assuming the R.D.S. to be a charge-transfer).

This may be expressed as

$$\lambda = \vec{\gamma} + \overleftarrow{\gamma} + r\nu \qquad (1.3.9.1.2,1)$$

where, r = number of electrons participating in one occurrence of the R.D.S.

ν = stoichiometric number = number of times the R.D.S. occurs for each occurrence of the overall reaction.

$\vec{\gamma}$ = number of electrons participating in steps preceding the R.D.S.

$\overleftarrow{\gamma}$ = number of electrons participating in steps following the R.D.S.

The application of Equation (1.3.9.1.2,1) requires an initial assumption of a reaction mechanism and a R.D.S. within the mechanism, and may be used to provide evidence to support (or dispel) the mechanism chosen (170).

1.3.9.1.3 Electrochemical R.D.S. in the double layer on a film-covered cathode

Assuming a situation where reduction takes place through an oxide film, but where the R.D.S. is a charge-transfer (involving λ electrons overall) within the double layer, the 'dual-barrier' model may be adopted (see Section 1.3.7.4.1) and the Tafel slope is given by

$$\frac{d\eta}{d\log i} = \frac{-2.303RT}{\lambda F} \quad \frac{(2 - \alpha_{dl} - \alpha_f)}{(1 - \alpha_f)(1 - \alpha_{dl})} = \frac{-2.303RT}{\alpha_{term}\lambda F} \qquad (1.3.9.1.3,1)$$

where α_{term} represents the term involving α_f and α_{dl}. If values are assumed for α_f and α_{dl}, λ and ν may be calculated.

1.3.9.1.4 Cathode deactivation by film presence

Even if the R.D.S. does not take place within the film, the film has been shown to modify Tafel conditions by altering the effective value of α. In addition, the presence of a semiconducting oxide film tends to de-activate the surface and reduce the effective exchange current density of the cathode reaction (32). This reduction of i_o has no effect on the actual Tafel slope, but shifts the curve (the Tafel region) along the logi axis towards lower current densities, an effect that may be difficult to quantify.

The de-activation is due to a reduction in the density of surface sites at which charge-transfer may take place, and a reduction in the frequency with which electrons arrive at the oxide/electrolyte interface. The degree of de-activation is therefore clearly dependent upon the degree of conductivity of the film and the nature of the oxide surface (adsorbed species on the oxide surface may 'poison' the oxide in such a way as to greatly increase the density of surface states for possible charge-transfer).

1.3.9.2 Process-rate theory in electrodeposition

It was assumed by Rogers and Burr (43) that the rate at which the R.D.S. proceeds in electrodeposition is constant (if slow), and that the reaction-rate theory of Glasstone, Laidler and Eyring could apply. Based on the Arrhenius expression, this assumed a so-called free energy of activation for the process. It involved the equation (44),

$$i = \epsilon C_M z+ \cdot \frac{k'T}{h'} \cdot \exp - \frac{\Delta G_A}{RT} \cdot \exp \frac{zF(1-\alpha)\eta}{RT} \qquad (1.3.9.2,1)$$

where,

ϵ = value of ionic charge (elementary charge)

$C_M z+$ = concentration (or activity) of depositing species in concentration units per unit area

k' = Boltzmann's constant

h' = Planck's constant

G_A = free energy of activation for the process, J/mol.

η = overpotential, V.

but, $\Delta G = \Delta H - T\Delta S$

so

$$i = \epsilon C_M z+ . \frac{k'T}{h'} . \exp \frac{\Delta S_A}{R} . \exp -\frac{\Delta H_A}{RT} . \exp \frac{zF(1-\alpha)\eta}{RT} \qquad (1.3.9.2,2)$$

or

$$\log i = \log(\epsilon C_M z+ . \frac{k'T}{h'}) + \frac{\Delta S_A}{2.303R} - \frac{\Delta H_A}{2.303RT} + \frac{zF(1-\alpha)\eta}{2.303RT}$$

Plotting η versus logi gives (according to Rogers and Burr) a slope from which z and α may be found.

Measurement of the variation of logi with absolute temperature at a fixed overpotential, allows an Arrhenius-type plot of logi versus T^{-1} to be drawn, the slope of which is (from equation (1.3.9.2,2)),

$$\frac{d\log i}{d(1/T)} = -0.43T - \frac{0.43\Delta H_A}{R} + \frac{0.43zF(1-\alpha)\eta}{R} \qquad (1.3.9.2,3)$$

Assuming a representative value of T and knowing z,F,α,η and R, a value of activation enthalpy for the process (ΔH_A) may be found. With a knowledge of ΔH_A, a value of ΔS_A may be calculated provided

that values of $C_M z+$ and ε_M are available (remembering that $\eta = E - \varepsilon_M$). Rogers and Burr demonstrated that $C_M z+$ can be calculated from bulk concentration.

Once a value for ΔS_A is obtained, the free energy of activation for the process (ΔG_A) may be found. This can be a useful indicator in mechanism determination, as a significant change in ΔG_A with a variation in η (for a particular system) may indicate a change in R.D.S. Similarly, a change in ΔG_A with changes in the system (e.g., catalyst concentration, additions, in chromium plating) may explain variations in current efficiency and throwing power.

While Rogers and Burr's approach may be useful, it requires certain modifications prior to application to chromium plating:

(i) The use of 'partial' current densities instead of total cathode current density in the above equations.

(ii) The use of λ instead of z in the equations.

(iii) The value of α selected for insertion into Rogers and Burr's equations should take account of the presence of a cathodic oxide film (the expression α_{term}, as defined in Section 1.3.9.1.3, was therefore selected for use in eventual data analysis), allowing Equation 1.3.9.2,3 to be re-written;

$$\frac{d\log i}{d(1/T)} = -0.43T - \frac{0.43\ \Delta H_A}{R} + \frac{0.43\alpha_{term}\eta\lambda F}{R} \qquad (1.3.9.2.3')$$

Clearly, the choice of a value for ε_{Cr} and the measured (from Tafel slopes) value of $\lambda \times \alpha_{term}$ have an influence upon the thermodynamic quantities of activation for the plating reaction generated from equation 1.3.9.2,3'. It is therefore questionable whether the absolute values or exact meaning of these quantities can be established, but used on a comparative basis they could be a valuable aid in relating experimentally observed aspects of the plating process to the reaction mechanisms proposed.

SECTION 4

Chromium Plating

1.4.1 Types of chromium plate

Chromium plate is generally categorized, according to its use, as 'bright' or 'hard'.

Bright chromium plate consists of a very thin layer (typically 2 μm) of micro-cracked chromium deposited onto a much thicker (typically 20 μm) pre-deposited layer of nickel (and copper) in order to confer hardness and wear-resistance to what is, essentially, a decorative finish. The chromium layer is generally so thin that the observed finish is that of the (transmitted) nickel, although where a component is subject to tougher service conditions the chromium thickness may be increased accordingly. Bright chromium plate depends for corrosion resistance primarily on the thickness of the nickel layer, even though nickel is anodic to chromium in aqueous environments. Dissolution is minimised by maintaining a low anode to cathode ratio through the micro-cracks in the chromium.

Hard chromium plate is a misleading description of the deposit, as the metal deposited is usually no harder than that in bright chromium plate, both being produced under similar conditions. The difference between the two types lies in the thickness of the chromium layer and the reasons for its thickness. Whereas bright chromium has a mainly decorative purpose, the very much thicker hard chromium layer (20 - 100 μm) is directly deposited onto the component substrate and is used to confer beneficial physical properties to the surface. For this reason, hard chromium plate is often referred to as 'engineering' chromium plate, and bright chromium as 'decorative'.

1.4.2 Properties of electrodeposited chromium

1.4.2.1 Appearance

The appearance (brightness) of chromium plate depends upon the finish of the substrate (in decorative plating) and the conditions

under which plating is carried out. In general, the process may be controlled so that a fine-grained deposit is produced with a reflectivity (in the visible spectrum) of approximately 55% that of electrolytic silver and considerably greater than that of bright electrolytic nickel (45,46).

1.4.2.2 Corrosion and oxidation resistance

As outlined earlier, decorative chromium plate owes most of its corrosion resistance to the underlying nickel layer. Hard chromium deposits however, form a continuous barrier to corrosion, containing (ideally) no cracks which extend through to the substrate.

Chromium, of course, is protected by a passive oxide layer in atmospheric oxygen and (most) acid or alkaline solutions, the modification of the potential of chromium through passivation being such that it behaves as a (virtually) noble metal. It can however be attacked rapidly by hydrochloric acid and (under certain conditions) moderately by sulphuric acid and nitric acid (47).

The corrosion resistance of chromium plate generally improves with the brightness as might be expected, a smoother surface providing fewer potentially corrodible sites.

1.4.2.3 Hardness

Commercially produced chromium plate exhibits hardnesses in the range 1000 - 1100 VPN, and is hence considerably harder than any other electrolytically deposited metal (47). Various theories have been proposed to account for these high values.

1.4.2.3.1 Grain size

A simple explanation accounts for the high hardness of electrolytic chromium on the basis of the Petch analysis (48) that hardness is inversely proportional to the square root of the mean grain diameter.

The mean size of chromium grains in bright deposits has been measured as approximately 2 x 10^{-8}m (49). At these values, a slight variation in mean grain diameter may have a considerable effect on hardness (48).

It has also been observed (48) that the degree of crystal orientation is contributory to deposit hardness. Bright hard deposits tend to display a preferred orientation while less hard, matt deposits are randomly orientated.

1.4.2.3.2 Internal stresses

Chromium electrodeposits contain considerable internal stresses which are relieved to an extent by the formation of cracks in the structure, but which may also act to increase the hardness of the deposit (through work-hardening). It has been suggested that the high stresses initially within the deposited chromium are partly due to occluded hydrogen (hydrogen evolution is a concomitant cathode reaction), and partly due to the degree of faulting in the deposit (a function of overpotential) (50).

It has also been proposed that the high internal stresses observed during the early stages of deposition are as a result of lattice misfit induced by the rapid diffusion of absorbed hydrogen away from the chromium/substrate interface (51) with the consequent decomposition of an unstable chromium hydride to chromium metal (49,51).

The development of internal stresses as a result of impingement of growing metal crystallites (in thin deposits) has been shown to be indirectly dependent on substrate/deposit epitaxy (52), being lower in deposits on a smooth, strain-free substrate.

1.4.2.3.3 Oxide inclusions

The precipitation during deposition of microscopic (and submicroscopic) chromic oxide (Cr_2O_3) inclusions at grain boundaries and

within the grains of the growing deposit has been given as a reason for high deposit hardnesses (53), with inclusions being more finely dispersed in bright deposits than in matt deposits.

1.4.2.4 Wear resistance

Resistance to wear is a basic physical characteristic of hard chromium deposits but one which is difficult to measure, as wear can occur under a variety of conditions (temperature, pressure, humidity, etc). Comparative wear resistance tests (using Emery cloth as an abrasive) have shown hard chromium to be ten times as wear resistant as hard nickel plate (54), and slightly superior (using a tungsten carbide abrasive) to nitrided steel (55).

1.4.2.5 Coefficient of friction

Among metals in common use (electroplated), chromium has the lowest coefficient of friction. The coefficient of friction of hard chromium plate against steel (0.17) is approximately half that of steel against steel (47).

1.4.3 The structure of electrodeposited chromium

The structure and properties of chromium plate are closely related, both depending on the nature of the substrate and the plating conditions.

Under ideal conditions, hard chromium is deposited as an ultra-fine-grained, micro-cracked deposit with a degree of preferred orientation (during the initial stages of deposition) dependent on the pre-plating finish given to the substrate (56).

1.4.3.1 Cracking

The degree and nature of the cracking within a hard chromium deposit is of considerable importance with regard to the physical properties of the plate, and while entirely crack-free deposits have

been produced which offer a high degree of corrosion resistance (53), their relatively dull appearance and low hardness have limited their application. In general therefore, an amount of (controlled) cracking is tolerated in hard chromium deposits, providing that no cracks extend right through to the substrate (57).

The examination of crack structure in chromium deposits through electropolishing has revealed a degree of complexity which prevents comparison with true cracking in normal metals. The cracks observed are usually in the form of closed channels which contain (depending on the hypothesis) no other constituent (58,59,60), hydrides (49,61) or chromic oxide (62).

1.4.3.2 Lattice structure

The lattice structure of electrodeposited hard chromium is largely dependent upon plating variables, but conventional plate consists of body-centred cubic crystals with a cell parameter (determined in X-ray studies) of 288 pm. Variable porportions of a hexagonal close-packed structure are also sometimes observed, depending upon the electrolytic conditions under which the chromium is deposited (49).

1.4.3.3 Plate orientation

Whilst any preferred orientation of the deposit has been shown to be dependent upon the nature of the substrate, plating conditions, and the plate thickness, epitaxial effects (and internal stress due to epitaxy) are generally limited to those layers of the deposit immediately adjacent to the substrate. A strain-free polycrystalline substrate gives rise to an initial epitaxial deposition of crystallites in identical orientations on each substrate crystal, with a lessening of substrate influence as the deposit thickens.

It may therefore be concluded that structure (and hence, properties) of chromium plate is only substrate-sensitive where the

deposit is thin. Hence, the substrate initially nucleates outward or lateral epitaxial growth (63,64), but eventually loses its influence, with subsequent growth being controlled entirely by plating conditions.

Irrespective of substrate effects, the brightest chromium deposits have been shown to display a marked preferred orientation ([111] fibre texture) (65,66) at a thickness of 1 μm (67), which does not vary with deposit thickness (up to 10 μm). In less bright deposits, the variation of texture with thickness is more marked.

1.4.3.4 Deposit morphology

Morphologically, the ideal bright chromium deposit is smooth and micro-nodular with no outgrowths. However, in regions where chromium deposits at locally higher current densities than the average, deposit growth is correspondingly faster and tends toward unevenness in deposit thickness and the possibility of 'burning' (see section 1.1.8.2).

1.4.4 Chromium plating solutions

While numerous efforts have been made, since the patenting of the first commercial processes in 1925 (68,69), to develop a chromium plating solution which solves all of the problems inherent in the chromium plating process, this aim has yet to be achieved. However, some successful modifications to the original process have been made, as well as a number of interesting proposals for novel plating solutions.

1.4.4.1 The 'standard' solution

Most conventional industrial hard chromium plating is carried out from a solution based on the following:

450 g/dm^3 CrO_3 (chromic acid - in flake form),

4.5 g/dm^3 H_2SO_4 (concentrated),

as aqueous solution in de-ionised water.

A less concentrated (250 g/dm^3 CrO_3) bath is also widely used, but maintaining the CrO_3: sulphate ratio at 100:1. Chromium plating from a standard solution (and associated problems) is considered in more depth in section 1.5.

1.4.4.2 Alternative chromium plating solutions

These may be divided into those in which chromium is plated from its hexavalent state, and those in which it is plated from a lower valency state. In terms of efficiency, plating would clearly be preferred from a low valency state. However, in chromium plating, deposit properties are paramount.

1.4.4.2.1 Hexavalent (chromic acid based) solutions

(i) Self-regulating high-speed (S.R.H.S)

Control of the acid ratio (CrO_3:H_2SO_4) in a standard solution is critical and difficult, and in order to overcome this problem the S.R.H.S. bath was developed (70).

Although sulphate is commonly referred to as a 'catalyst' in standard chromium plating procedure (deposition will not take place from 'neat' chromic acid), it is in fact slowly consumed during plating. This problem is countered in the S.R.H.S. process through the use of strontium sulphate rather than sulphuric acid as the sulphate-carrying addition (1,71,72,73). The sparing solubility of strontium sulphate allows a slight excess to be maintained in the bath, keeping the acid ratio near to the optimum 100:1. The S.R.H.S. solution also contains silico-fluoride ion as a second addition, and claims considerable (e.g., 25% efficiency) advantages over conventional sulphate-catalyzed solutions (74), although the highly corrosive nature of the solution (considerably worse than standard solutions) necessitates greater care in the design and maintenance of plating hardware (47).

(ii) Mixed 'catalyst' baths

Chromic acid solutions employing sulphuric acid and silico-fluoride ion in small amounts were the fore-runners of the S.R.H.S. solution, and were shown in comparative studies (75) to exhibit slightly higher current efficiencies (under similar operating conditions) than standard solutions and slightly higher deposit hardness. They do, however, require more careful and frequent maintenance in order to prevent premature loss of control (76).

(iii) Miscellaneous chromic acid based baths

These include:

(a) fluoride catalyzed (no sulphate) chromic acid baths, which have been claimed to produce a particularly brilliant deposit under less critical plating conditions (53,77);

(b) borate catalyzed baths which apparently demonstrate higher solution conductivities while not affecting deposit properties (47);

(c) baths based on ammonium dichromate presence, which are claimed to deposit chromium with improved throwing power but which have not been widely adapted because of the high plating bath temperatures employed (70^{o}C) and the attendant problems with control (47);

(d) the Bornhauser (or Dichrome) solution which was initially developed (78,79) for the direct plating of zinc diecastings, and which contains sodium tetrachromate as a principal constituent. This solution operates at a lower bath temperature than standard solutions and exhibits a wider current density range for satisfactory deposits (80). It does, however, produce a dull deposit which is soft enough to be easily polished to a high lustre, and therefore unsuitable for most engineering (hard chromium) applications.

1.4.4.2.2 Trivalent solutions

The inherent inefficiency (according to Faraday's laws) of chromium plating from the hexavalent state has led to considerable effort being made in the development of a plating process from a lower valency state.

The trivalent state offers the best alternative to the hexavalent plating solutions, and a great many (cheaper and less toxic than chromic acid based solutions) trivalent plating solutions have been investigated, some of which have elicited considerable industrial interest, but none of which have (thus far) been adopted on a large scale.

Aqueous chromium sulphate solutions have been investigated as the basis of possible plating baths, but considerable controversy exists as to their effectiveness and the mechanisms by which they operate. While it is accepted that two modifications of aqueous chromium sulphate exist (green at elevated temperatures, violet at low temperatures) and that one (violet) has a higher ionic mobility and is more reducible than the other (81,82,83,84,85), it is not certain from which modification deposition takes place. One school of thought claims that chromium metal may only be deposited from solutions of the violet form (81,86), whereas the opposite observation has also been made (87). A noncommittal position in which it is claimed that the modification is relatively unimportant (88) may be contrasted with the proposal that a critical ratio of violet to green is necessary for efficient metal deposition to occur (89).

Some authors investigating trivalent chromium plating (90,91) have reported a straight line relationship between deposition efficiency and the concentration of divalent chromium ions in solution, with conditions favouring the $Cr^{III} \rightarrow Cr^{II}$ partial reduction step

apparently having a beneficial effect on efficiency. This has been explained (92) in terms of the divalent ions acting to catalyze the green to violet modification transformations, and hence accelerating the establishment of the critical green/violet ratio referred to earlier.

Certain variations on the trivalent chromium sulphate plating solution have claimed success with regard to improved metal deposition. These include a solution containing ammonium ions which are assumed to form hexammine complexes with trivalent chromium ions (93,94). Similarly, small quantities of organic additives such as glycine and urea (95) are reported as having a beneficial effect on deposition efficiencies in chromium sulphate baths. The action of these additives was interpreted in terms of their stabilization at the cathode surface of divalent chromium ions (previously reduced, by the action of nascent hydrogen, from the trivalent state (96) prior to discharge.

More recently, attention was shifted to the development of chromium plating baths based on trivalent chromium chloride and utilizing dimethylformamide in an aqueous/organic admixture (97,98,99). While this solution gave very high plating efficiencies and a deposit with enhanced corrosion resistance, it possessed considerable limitations (the inherently poor conductivity necessitated the use of rectifiers capable of providing up to 20V potential) and was not industrially acceptable. This work however, did suggest that solution pH was an important factor in determining the throwing power of trivalent solutions, and concluded that optimum throwing power was only attainable at pH values of greater than 2.5. The chromium chloride solution referred to was found to be unstable above pH 2 due to hydrolysis of the dimethylformamide (and subsequent precipitation of basic chromium compounds), so a more stable, inorganic

(higher conductivity), complexant was sought which would permit controlled metal deposition at a relatively high pH (2.4 to 2.9 in practice) without concomitant complexant breakdown. The solution subsequently developed (100) was based on trivalent chromium sulphate, using boric acid as a buffer to maintain the required pH range. The complexant employed was not nominated.

While this latest trivalent chromium plating both shows promise in terms of its relatively easy control and improved throwing power, the deposit is restricted to thicknesses of less than 2.5 μm for all practical applications. This fact, combined with relatively low deposit hardness, precludes its use as 'hard' chromium.

No deposit has thus far been produced from a trivalent solution which would satisfy 'hard' chromium criteria.

SECTION 5

Chromium Plating from a Standard Solution

1.5 Chromium Plating from a Standard Solution

1.5.1. The Solution

As outlined in section 1.4.4.1, the standard hard chromium plating bath is an aqueous solution of chromic acid and sulphuric acid at a concentration ratio of 100 : 1 ($450g/dm^3$: $4.5g/dm^3$).

The sulphate anion is necessary to 'catalyze' deposition. In its absence no truly metallic deposit is obtained by the electrolysis of chromic acid. The nature of the action of the sulphate anion is unclear, although 'catalyst' is a misleading term as it is consumed (albeit slowly) during deposition.

The 100 :1 concentration ratio is well documented as being that which gives maximum solution conductivity (1,47) and best deposition rates (for the production of an acceptable deposit), and is therefore, fairly closely adhered to in most industrial hard chromium plating processes.

The highly toxic and acidic nature of the standard plating solution, and the attendant problems with effluent disposal and health and safety of shop personnel (101) are undoubtedly part of the reason behind the efforts to develop a trivalent process (chromium III salts are generally non-toxic). The acidity level is also responsible for the non-use of organic brighteners such as those employed in nickel plating (see section 1.1.4.1). Such additives would break down in a standard chromium plating solution.

1.5.2. Electrodes

1.5.2.1. Anodes

Insoluble lead alloy anodes are almost always used in plating from chromic acid baths, as a film of lead dioxide forms during plating and fulfils the essential function of oxidizing trivalent chromium

(continuously formed as a cathodic side-reaction) back to the hexavalent state. A high concentration of trivalent chromium in the standard bath is detrimental to its performance.

Pure lead anodes are not used because they are soft and attacked by the solution, forming a lead-salt sludge in the bath. A lead - 4% to 8% antimony alloy has been found to offer good strength and corrosion resistance, as has a lead - 7% tin alloy (102), and these are generally employed.

An anode to cathode surface area ratio of 2 : 1 is preferred for most plating applications as this allows sufficient anodic chromic acid regeneration to prevent a build-up of trivalent chromium in the bath. Where a 2 : 1 ratio is unattainable, maximum anode surface area is often achieved through the use of corrugations. However, under these conditions care is essential to ensure that the anode corrugations are not so deep as to lead to corresponding variations in the thickness of the cathodic deposit.

The relative positioning of anodes and cathodes in a chromium plating bath is generally a function of the shape of the cathodic workpiece, with the anodes placed in such a way as to achieve the most even deposit possible. To this end, other auxiliary cathodes ('burners' or 'robbers') are often positioned in regions of locally high current density (determined by the cathode geometry and anode/cathode arrangement) in order to minimize excessive deposit build-up in these regions. Non-conducting 'shields' constructed of chromic acid resistant materials such as perspex are often used in a similar capacity.

The precise positioning (or 'jigging') of cathode, anodes, burners and shields in a plating bath is a major industrial problem (particularly under conditions of poor throwing power) as an uneven

deposit necessitates a considerable post-plating grinding operation in order to achieve agreed tolerances. In the case of hard metals such as chromium this can prove expensive.

Before plating commences, it is the usual practice to 'activate' the anode(s) and solution by passing a current (using scrap cathodes) until the protective layer of anodic lead dioxide is formed. Failure to do this leads to an early build up of trivalent chromium in solution with the attendant drawbacks.

1.5.2.2. Cathodes

As well as the care required to ensure optimum positioning of the cathode with respect to the other components in the bath, it is often necessary to carry out a pre-plating cathodic treatment. This may consist of a simple mechanical finish or a complex chemical (or electrochemical) polishing process. In general, the finer the finish on the pre-plated cathode, the more even (on a microscopic level) the deposit will be. Any roughness on the pre-plated cathode is amplified during plating as a result of the very poor throwing power of the chromium plating solution.

A simple grinding and polishing process is sufficient to give the finish required for much hard chromium plating. However, where the density and severity of micro-cracking in the deposit has to be minimized, it has been shown that a pre-plating electrolytic polish may be effective (56). Cathodes of complex shape are clearly more easily polished electrolytically than mechanically.

Following a pre-plating mechanical finishing process, it is essential that the cathode is thoroughly cleaned and degassed as any surface residue may insulate and hinder deposition or react unfavourably with the plating solution. Any areas of the cathode which need

to remain unplated are generally protected or 'stopped off' by special waxes or lacquers which resist chromic acid attack (103).

Hard chromium may be deposited with ease onto carbon steels, engineering steels, fine-grained cast irons, nickel, and copper and its alloys. Good deposits are more difficult to obtain, and special pre-treatment is generally required, on metals which exhibit strong passive oxide layers in air, and certain alloyed or surface-treated steels.

The concomitant cathodic reduction of hydrogen ions during chromium electrodeposition inevitably results in a degree of diffusion of atomic hydrogen into the substrate metal (although most reduced hydrogen is liberated as gas) with consequent embrittlement. Indeed, embrittlement of steels during chromium plating has been shown (104) to be much more severe than that produced by cathodic acid pickling (100% hydrogen evolution) under the same conditions of temperature and current density, and a post-plating anneal is required to restore substrate toughness (105).

15.3. Temperature control

The accurate control of bath temperature is critical in hard chromium plating from standard solutions.

The highly corrosive nature of the plating solution means that direct immersion heating is usually impractical. The most generally adopted industrial alternative is to employ a water-jacketted plating tank, with water temperature controlled thermostatically.

1.5.4. Agitation

The vigorous evolution of hydrogen and oxygen during plating provides considerable agitation of the solution adjacent to the

electrodes without recourse to any external source. However, in industrial plant, solution circulation is achieved (on a larger scale) by various means, such as pumps and stirrers.

1.5.5. Electricity supply

In chromium plating it is essential that the current employed should be a steady, low voltage direct supply with minimum ripple. In industry this is generally provided by a low-voltage generator or by a rectifier unit with three-phase rectification.

The sensitivity of deposit structure, properties and appearance to current density means that it is usually preferable to install some form of automatic regulator to ensure that once the plating conditions have been set, they are closely maintained irrespective of mains voltage (and other) variations.

On a laboratory scale a steady direct current supply is easily obtained through the use of a potentiostat as a power source.

1.5.6. Fume control

Gas evolution during chromium plating throws up a fine spray of chromic acid which is harmful to the skin and respiratory system (101) and demands some means of control. Spray may be reduced by approximately 90% through the use of plastic floats on the surface of the solution (106). However, the remaining 10% still exceeds the legal safe working limit and necessitates the use, in industry, of fume exhaust systems. These are usually constructed in such a way as to recover airborne chromic acid while removing hydrogen gas, and are often made of stainless steel to avoid contamination of the recovered acid.

SECTION 6

Control Problems in Chromium Plating

1.6. Control Problems

The appearance, structure and properties of hard chromium are highly sensitive to plating conditions in a standard plating bath, and considerable work has been carried out in establishing ranges (in terms of plating variables) in which satisfactory deposits may be obtained. The ranges in which bright hard chromium deposits (corresponding to optimum physical properties, in general) are produced from standard solutions are rather narrow, but well documented.

In terms of the two major control variables, solution temperature and cathode current density, a number of workers have presented graphical data (1, 47, 67, 50, 107, 108) to illustrate the so-called 'bright range'. An example (50) is given in Figure 1.

The narrowness of this range places considerable constraints on hard chromium platers, particularly with respect to current density (constant temperature is relatively easy to maintain).

The poor throwing power of chromic acid plating solutions combined with the (geometrical) likelihood of locally high (and low) current density regions on the cathode, means that the plater must aim at an overall cathode current density somewhere in the middle part of the 'bright range'. Failure to control current density accurately, especially where jigging is inadequate, may lead to uneven and unsatisfactory deposits.

1.6.1. Throwing power in standard solutions

Standard chromic acid based plating solutions exhibit negative throwing power (see section 1.1.7) as they give an increase in plating efficiency with cathode current density. The rate of increase however,

is not uniform as efficiency rises less steeply at higher current densities. In other words, although chromic acid based solutions always demonstrate negative throwing power, it tends to be slightly less negative at high current densities. This is not particularly helpful to the plater who must avoid burnt deposits and therefore usually operates in the middle of the 'bright range'.

Other factors determining the throwing power of standard solutions are the variation of cathode polarization with current density, and the conductivity of the solution. The latter is usually reasonably high but is faily insignificant when compared to the effects of polarization and current efficiency variation. Throwing power may be slightly bettered by increasing the chromic acid/sulphate ratio to 200 :1, but only at the expense of plate properties (109).

To date, the only solution to the negative throwing power problem in these solutions is accurate 'jigging' (see section 1.5.2).

1.6.2 Current efficiency in standard solutions

Three competitive cathodic reactions take place during metal deposition from a chromic acid plating solution; the deposition reaction itself, the hydrogen evolution reaction, and the partial reduction of hexavalent chromium ions to the trivalent state.

Each reaction proceeds at an efficiency (see section 1.1.1) determined by the particular set of plating conditions, but usually varying with current density. In chromium plating practice, the metal deposition reaction generally exhibits an efficiency of 10 - 15%, with the greatest proportion of the cathode current being used in hydrogen evolution (the partial reduction reaction accounts for the difference). As plating efficiency is clearly related to the deposition rate, it might be assumed that a high values is aimed for in the

development of chromium plating solutions. Indeed, under cetain conditions of current density, temperature, and solution concentration, plating current efficiencies may be boosted to over 20% in a standard solution. However, such conditions exist only outside the 'bright' range, and the plate produced has poor appearance and properties. An increase in plating efficiency is, therefore desirable but not at the expense of plate properties.

1.6.3. Bath composition

The extent of the 'bright' range and the throwing power of the solution are dependent upon (in addition to temperature and current density) the ratio of chromic acid to sulphate concentration, and the concentration of trivalent chromium salts in solution.

During heavy industrial plating, the chromic acid in the bath becomes diluted, with (it is estimated) 25 g of chromic deposited per 500 amp-hours of operation. Losses due to drag-out and spray are also appreciable. The chromic acid content in industrial baths is, therefore usually estimated daily through density measurements, and once a month, by chemical analysis (titration).

The importance of maintaining the 100 : 1 chromic acid to sulphate ratio has been observed, as has the fact that sulphate is not a true catalyst, being consumed slowly during plating. The measurement of sulphate concentrations in plating solutions is generally carried out by the accurate precipitation of barium sulphate (using barium chloride with a sample of solution) using a chrome reducing mixture, and then weighing the deposit (102).

A certain controlled concentration of trivalent chromium in a standard plating solution improves throwing power and indicates that the partial reduction of Cr VI to Cr III at the cathode is taking place. As it is widely thought that cathodic Cr III production is essential in the deposition mechanism, its presence in the bath is to be expected. However, too high a concentration of trivalent chromium leads to a considerable drop in plating current efficiency and conductivity, and causes a reduction in the extent of the 'bright' range.

A simple pointer to the presence of excess trivalent salts in a chromic acid solution is given by colour. If on dilution of a sample of the plating solution, a green tinge is present in the orange of the chromic acid, further (chemical) analysis is usually carried out. Any excess of trivalent chromium in the bath may be removed by working the solution at a high temperature (80°C), high cathode current densit and low anode current density until satisfactory levels are attained (110).

1.6.4. Summary

There is, thus far, no simple answer to the problems inherent in the control of hard chromium plating baths.

The negative throwing power of the solutions used may be countered to an extent by careful jigging, but the necessity for a post-plating grinding treatment usually still remains.

The inherently poor efficiencies at which chromium deposits from chromic acid plating solutions are tolerated provided satisfactory plate is produced. Indeed, the lengthy plating times required, the constant attention needed during plating, and the hazardous nature of the process say much for chromium's importance as a plating metal.

Alternative plating solutions such as those referred to in section 1.4.4.2.2 have not found widespread acceptance principally befause where they may solve one problem they generally create another. For this reason, chromic acid based baths appear to have a relatively secure future, with much current research concentrating on improving process control through a more scientific approach to jigging (111, 112).

SECTION 7

Standard Solution Chemistry

1.7 Standard solution chemistry

Despite the long history of chromium plating from standard chromic acid based solutions, no definite conclusions have yet been drawn with regard to their precise chemical and ionic nature. This situation is largely due to the aggressive character of the highly concentrated solutions employed, and the attendant difficulties in research techniques.

1.7.1. Species and equilibria

The composition of a standard solution in terms of the major components and their relative concentrations is well established (see section 1.5.1), however, the nature of the ionic species present is still subject to controversy.

A study of polarization data obtained at identical current densities in a standard solution revealed that as the chromic acid concentration was increased, the cathode potential became more negative (113), behaviour which led to the conclusion that more than one chromium-bearing species exist in a standard solution, the relative concentrations of which depend upon the initial chromic acid concentration.

It has been suggested (113) that a standard plating solution should be considered as a mixture of two acids, H_2CrO_4 and $H_2Cr_2O_7$, in unstable equilibrium with each other -

$$2H_2CrO_4 \rightleftharpoons H_2Cr_2O_7 + H_2O$$

and that the electrolyte contains three anions, $HCrO_4^-$, CrO_4^{2-}, and $Cr_2O_7^{2-}$, in ratios which depend upon the initial CrO_3 concentration

and (importantly) pH, a dependence illustrated in Figure 2.

Under certain conditions, equilibria are established between these ions (114) -

$$HCrO_4^- \rightleftharpoons CrO_4^{2-} + H^+$$

$$2HCrO_4^- \rightleftharpoons Cr_2O_7^{2-} + H_2O$$

These equilibria are shifted towards the formation of dichromate ion by an increase in the CrO_3 concentration, and vice versa. However, it has also been shown that an increase in solution pH, such as occurs adjacent to the cathode as a result of hydrogen evolution during plating, tends to shift the equilibria towards formation of the chromate ion (115). Indeed, species identification in the region of the solution immediately adjacent to the cathode surface is extremely difficult because of the complicated local variations in concentration and pH. The nature of the chromium-bearing species in the bulk electrolyte is, however, unaffected by these localized cathodic changes and is generally assumed to be dichromate (116, 117), although one school (118) suggested the predominance of the trichromate ($HCr_3O_{10}^-$) ion, and possibly the tetrachromate ($HCr_4O_{13}^-$) ion (by linking the degree of polymerization to the solution colour (119)) in highly concentrated solutions.

A similar lack of agreement exists with regard to the form adopted by the sulphate 'catalyst' in the bulk solution and in the region of the cathode, with some authors tending to the view that the sulphate group is bound up in a complicated polynuclear species and others assuming its existence as a simple aqueous ion such as SO^{2-} or HSO_4^-.

SECTION 8

Electrode reactions

1.8 Background

The uncertainty which exists with regard to the ionic nature of chromium plating solutions extends to many other aspects of the process. Indeed, although chromic acid based plating solutions have been used in industry for over fifty years, agreement is still to be reached on the nature of the chromium plating mechanism. Various (often conflicting) theories have been proposed, but none has yet been universally accepted as correct. Meanwhile, the industrial hard chromium plater continues to employ the same techniques (often 'trial and error') as always, with no satisfactory 'back-up' theory available to explain, prevent or solve the problems encountered in practice.

The various theories mooted are considered in section 1.9. However, certain generally agreed-upon observations may be made.

1.8.1 Basic observations

In the absence of the sulphate (or alternative) catalyst, no pure metallic deposit is obtained at the cathode through the electrolysis of a concentrated pure chromic acid solution, the sole observable product being hydrogen gas. Using dilute solutions under similar conditions, a dark cathodic 'oxide' layer is seen to form through which hydrogen reduction takes place. Addition of sulphate to such solutions causes the dark layer to stream away from the surface, with subsequent metal deposition (120). The electrolysis of pure chromic acid is, therefore seen to lead to the formation of a cathodic (probably hydrated) chromium III oxide film which is maintained at a relatively high pH through localized hydrogen ion exhaustion, and through which ionic and atomic hydrogen may migrate.

(assuming hydrogen ion reduction takes place at the cathode/film interface). Its passivity with respect to metal deposition is only overcome through its apparent breakdown in the presence of the sulphate ion.

When sulphate is present at the prescribed concentration and ratio, the observed electrode reactions during plating may be represented, in their simplest form, as -

$$Cr\ III_{(aq)} \longrightarrow Cr\ VI_{(aq)} + 3e^-$$

$$2H_2O \longrightarrow O_2 + 4H^+ + 4e^-$$

Cathode

$$Cr\ VI_{(aq)} + 6e^- \longrightarrow Cr^o$$

$$Cr\ VI_{(aq)} + 3e^- \longrightarrow Cr\ III_{(aq)}$$

$$2H^+ + 2e^- \longrightarrow H_2$$

1.8.1.2. Anode reactions

Following the establishment of a semiconducting lead dioxide film upon the anode surface by means of a pre-plating period of electrolysis (activation), subsequent application of an increasingly positive electrical potential causes the following changes at the anode :-

At low positive potentials, no anodic reaction takes place and no anodic current flows. However, at a potential determined by the system (+1.25V vs S.H.E. in a 250g/dm^3 CrO_3, 2.5g/dm^3 H_2SO_4 solution

at 45°C (121)) an anodic current starts to flow as oxygen evolution commences. Contemporary with oxygen evolution, the oxidation of trivalent chromium back to chromic acid takes place at the anode. The form taken by the trivalent chromium is subject to controversy, although it is generally assumed (1, 118, 122) to exist as the stable hexaquo complex, $Cr(H_2O)_6^{3+}$. The oxidation may, therefore be represented as -

$$Cr(H_2O)_6^{3+} \longrightarrow CrO_3 + 3H_2O + 6H^+ + 3e^-,\ 3CrO_3 + H_2O \longrightarrow HCr_3O_{10}^- + H^+$$

Hydrogen ions are regenerated in both anode reactions, thereby maintaining bath acidity.

The oxygen evolution reaction and the Cr III $\longrightarrow$ Cr VI oxidation reaction are competitive, with their current efficiencies varying with current density. At the lowest anode current densities, the oxygen evolution efficiency is relatively low and the regeneration reaction is correspondingly favoured. However, at high current densities, oxygen may evolve at an efficiency of greater than 90%, thereby reducing the ability of the anode to control the Cr III concentration in the bath. Indeed, at very high current densities ($> 100\ kA/m^2$) oxygen evolves at nearly 100% efficiency. The need to maintain a high anode to cathode surface area ratio is hence critical in order to avoid high anode current densities.

1.8.1.3. Cathode reactions

The mechanisms by which the three cathode reaction take place are, despite a considerable research effort, still in dispute.

Numerous theories have been expounded as to the precise nature of what occurs at the cathode surface during plating from

a standard solution. However, certain fundamentals are agreed upon :-

The presence of a 'catalyst' is (as already stated) essential for deposition, its absence resulting in a 'passive' Cr III based cathode layer through which only hydrogen ion reduction may take place.

Chromium is held in bulk solution predominantly as an anionic species.

On application of a negative potential to the cathode in a standard plating solution, the first reduction to commence is that of Cr VI to Cr III, followed at a more negative potential by the hydrogen evolution reaction.

During plating all three cathode reactions occur and demonstrate a high degree of interdependence.

The overall stoichiometry of the cathode reactions may be represented thus (assuming the predominant chromium bearing species to be trichromate) ;

$$HCr_3O_{10}^- + 6H^+ + 6e^- \longrightarrow Cr^o + 3H_2O + HCr_2O_7^-$$

$$HCr_3O_{10}^- + 6H^+ + 3e^- \longrightarrow Cr^{3+} + 3H_2O + HCr_2O_7^-$$

$$2H^+ + 2e^- \longrightarrow H_2$$

SECTION 9

Chromium plating research techniques

1.9. History

Since the advent of the first commercial chromium plating process, numerous efforts have been made to determine the mechanism by which chromium deposits from a standard solution. The various theories proposed over the past fifty years tend to reflect the research techniques available at the time, with the earliest being based upon solution chemistry combined with circumstantial evidence and a degree of intuition. More recently, advances in technology have led to greater accuracy in electrochemical techniques of investigation with consequently more substantial evidence as to the nature of the electrode reactions. However, despite the improvements in research techniques, controversy still dominates the field, and to date no generally accepted theory of chromium deposition has been proposed.

Any investigation of the chromium plating process is obviously severely hampered by the physical and chemical conditions which prevail in the plating bath. The plating solution is extremely acidic, which means that great care has to be taken in the design of any research device to be immersed therein. The (working) solution is also opaque and, therefore prevents the direct observation of electrodes during plating.

1.9.1. Means of investigation

The available means of gathering information about the chromium plating process may be classified thus :

1.9.1.1 Deposit examination

The nature (morphology, microstructure, physical properties, cathodic distribution) of the metal deposit often provides

strong circumstantial evidence as to the deposition mechanisms, especially when related to variations in operating conditions.

1.9.1.2. Direct optical process observation

Although the opacity of the plating solution makes observation of the electrodes virtually impossible, the accompanying hydrogen evolution may be followed quite closely with regard to its vigour, average bubble size, etcetera.

The direct observation of cathodic oxide films is widely reported in the literature, and is considered in section 1.10.3.

1.9.1.3. Electrochemical techniques

The development of more sophisticated apparatus with which to monitor the progress of electrochemical reactions has led to a corresponding widening of understanding, particularly with regard to cathode polarization during chromium plating. Indeed, most recent treatments of the problem employ cathodic polarization data (usually obtained by means of a potentiostat) to analyse the situation at the cathode during deposition.

Attempts have been made to study the cathodic reduction processes using polarography. However, it was found (123) that concentrated standard plating solutions gave highly irreproducible results. When diluted plating solutions were used (123), it was observed that the cathode film was permeable to certain foreign (deliberately introduced) metal cations, whereas, under normal plating conditions, the film is entirely impermeable to the aforesaid ions (124). This illustrates that conclusions drawn through extrapolation of data from dilute solutions up to concentrated working solutions are not always accurate.

SECTION 10

Deposition mechanisms

1.10. Deposition mechanisms

Early investigations into chromium plating resulted in divided opinions as to the deposition mechanism and the action of the 'catalyst'.

1.10.1 Step-wise reduction

Sargent (125) maintained that the direct deposition of chromium metal from the hexavalent state was impossible, and that deposition could only proceed from a trivalent species produced through the action of (sulphate) 'catalyst' on the basic reduction product layer adjacent to the cathode ('passive' in the absence of a catalyst'). Under these conditons, he proposed that trivalent chromium in the layer next to the cathode surface is partially reduced to the divalent state from which chromium actually deposits. In his view therefore, the sulphate acts to stabilize trivalent chromium in the cathode layer prior to further reduction to the divalent and, ultimately, metallic state.

Liebreich (126) agreed that the last step in deposition was from the divalent state, and took Sargent's ideas further in postulating the existence of a complex Cr III/Cr II based cathode film (distinct from the film present in the absence of a 'catalyst') produced through the action of sulphate ion on chromic hydroxide. On the basis of cathode polarization data (and apparent breaks in the curves) and a knowledge of reduction potentials, he proposed that three major steps occurred in the reduction of chromic acid to metal :-

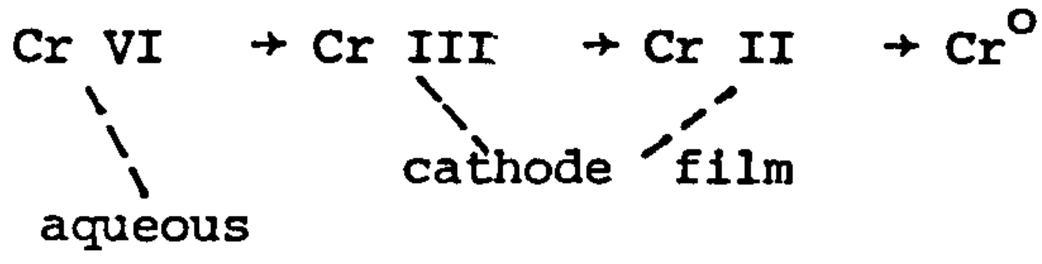

The cathode film was considered to consist mainly of colloidal hydrated chromic and chromous oxide (chromic at the solution boundary; chromous at the cathode boundary), with the ultimate deposition step from the divalent state being facilitated by the dissolving action of sulphuric acid on such basic chromium compounds (a chemical thinning of the film). Liebreich's polarization data must be subject to some doubt with regard to its accuracy in view of the research techniques available at the time, and particularly in the lack of agreement with data obtained by contemporary researchers. A comparison of Liebreich's polarization curve with that according to Muller (127) under identical conditions illustrates the difficulties (Figures 3 & 4).

Birynkov (128) developed Liebreich's thesis by nominating three cathodic reaction zones as opposed to a cathode film as such; an outer zone of chromic acid (or hexavalent species thereof), a middle zone consisting mainly of hydrated chromic oxide ($Cr_2O_3.nH_2O$), and an inner zone (adjacent to the cathode surface) of divalent chromous oxide (CrO). His approach thus far was clearly similar to Liebreich's. However, he differed in that he introduced the idea that the Cr III → Cr II reduction was due to atomic hydrogen produced at the cathode. Expressed simply, this may be written as

$$Cr^{3+}_{film} + H_{film} \rightarrow Cr^{2+}_{film} + H^{+}_{aq}$$

In the middle zone he proposed that sulphuric acid reacts with trivalent cathodic reduction products to form a highly soluble species of the form $Cr_2(CrO_4)SO_4$, and result in a 'liquid protective layer'. Within this layer, chromic acid is reduced to trivalent chromium by chromous oxide from the inner zone :-

$$CrO_3 + 3CrO \rightarrow 2Cr_2O_3$$

A so-called 'chromic-chromous couple'.

The notion that atomic hydrogen in the cathode film plays a critical part in the deposition process was also adopted by Rogers (129). However, he maintained that the final reduction step of divalent chromium to the metal was accomplished in this way (having drawn no conclusions on the preceding reduction of Cr VI to Cr II). Simply put :-

$$Cr^{2+}_{(film)} + 2H_{(film)} \rightarrow Cr_{(metal)} + 2H^+$$

He also explained the production of poor deposits at high current densities in terms of the atomic hydrogen in the film reaching such high activities that it formed compounds with the chromium. In other words, he introduced the concept of a critical film pH, so that below a certain pH a metallic deposit (through reduction of Cr II by atomic hydrogen) will not form, and above a particular higher pH any deposit will be a chromium compound.

The divalent state prior to deposition was, according to Rogers, that of colloidal particles of chromous hydroxide which were positively charged and hence attracted to the cathode (where reduction by hydrogen occurred). If the pH of the cathode film became too great, the chromous hydroxide particles reached the cathode in larger quantities than could be reduced and the alkalinity increased until further deposition was prevented. Once this barrier to reduction was established, pH fell once more and deposition recommenced (this idea of a 'dynamic

equilibrium' was later taken up by other workers). The effect of the sulphate was to increase the bath pH and solution viscosity, thereby facilitating the maintenance of film pH within the nominated range.

Rogers' concept of ultimate deposition through atomic hydrogen reduction was supported by Kato and Murakami (130), who observed that plating current efficiency variation with cathode current density was virtually identical to that of theoretically determined atomic hydrogen concentration with current density.

A discussion of Rogers' work by Kasper and Blum (131) considerably discredited this hypothesis, even though Kasper had earlier (88) suggested that film pH might be important.

Snaveley (49) used Rogers' conclusions, together with his own observations and those of others (132, 133) on the atomic structure of plate, to arrive at an overall coherent theory of deposition. Like Rogers, he considered that hydrogen played an important part in the cathode surface reactions, and that film pH was considerably higher than bulk solution pH. He also agreed with the proposal of Kasper (in his earlier work) that, in the absence of sulphate, the cathode film (which only permits hydrogen ion reduction) contains a complex basic electropositive dispersoid, $Cr(OH)_3 . Cr(OH)CrO_4$, which has been prepared synthetically and shown to have (88) an isoelectric point of about 6. Below a pH of about 6 therefore, the dispersoid particles (in the film) are positively charged and attracted to the cathode. The film produced in the absence of a 'catalyst' is, therefore viscous and 'locked' to the cathode surface.

Snavely's concept of the cathode film invokes a 'dynamic equilibrium' similar to that according to Rogers, but more specific. According to Snavely, any localized increase in film pH (due to increased rates of hydrogen evolution) above 6 would cause the dispersoid to be repelled by the cathode. Under these conditions, hydrogen ions (normally impeded by the dispersoid within the film) gain free access to the cathode, film pH drops and the dispersoid moves back. This 'dynamic equilibrium' is, therefore governed by the isoelectric point of the dispersoid, all else being equal. He treated the effect of the sulphate 'catalyst' in terms of Kasper's observation (88) that the presence of sulphate reduced the electrophoretic velocity of the dispersoid referred to above, and that a reduction of electrophoretic velocity (of a dispersoid) corresponds to a lowering of the isoelectric point (134). The dispersoid particles strongly adsorb the sulphate ion and, it is proposed, have their isoelectric point lowered to about 3.

Snavely therefore concluded that a film pH range exists within which chromium deposits, and that the nature (atomic structure) of the deposit depends critically upon the precise pH within the range (Figure 5).

He considered the reduction of chromic acid based plating solutions to be entirely step-wise, although only the final steps determined the eventual plate structure. The first reduction step was assumed to be via a chromic-chromous couple (after Birynkov), $Cr^{6+} + 3Cr^{2+} \rightarrow 4Cr^{3+}$ (towards the 'outer' edge of the film), following by reduction (within the film) of trivalent chromium to divalent chromium by atomic hydrogen. Any divalent chromium which was not then subsequently reduced further, would be free to participate in the chromic-chromous couple.

The mechanism of the final reductions of divalent to metallic chromium was believed to be through an intermediate hydride stage, with the nature of the deposit being determined by the activity of atomic hydrogen within the film. At high current densities, the rate of reduction of hydrogen ions is such that the activity reaches a level at which chromium begins to be deposited as a (Cr_2H - CrH) hexagonal hydride as well as the body-centred cubic metal. At higher current densities, the deposit takes the form of a face-centred cubic hydride (CrH - CrH_2). Eventually, at very high current densities, film pH is increased to the point where no metallic or hydride deposit is obtained, and the sole products are basic hydrolysis products.

Snavely found that the hexagonal hydride had a bright appearance when deposited in thin layers, although continued electrolysis resulted in considerable deposit darkening. The colour of the face-centred cubic hydride was uniformly black. Using these observations and the fact that decreasing bath temperature increases the film pH by lowering diffusion rates within the film, he produced a basis for an explanation of the so-called 'bright range' in terms of cathode film pH. He also assumed that film pH was sensitive to overall bath viscosity, and hence explained the dependence of deposit structure upon the concentrations of chromic acid and trivalent chromium.

Apart from the relatively unstable hexagonal and stable face-centred cubic hydrides referred to, Snavely considered the body-centred cubic metallic chromium, deposited under conditions of relatively low film pH, to pass initially through an intermediate, highly unstable, 'hydride' state of the form Cr_2H. Despite deposition

as a hydride, the rate of subsequent decomposition of the deposit to a metallic form was assumed by Snavely to have no effect on the deposition overpotential, as the spontaneous nature of the decomposition (Cr_2H to Cr) implies a net negative free energy change (i.e. no extra energy input is required to effect the decomposition).

The highly unstable intermediate 'hydride' state of the deposit was considered essential in the production of a bright hard deposit as it was proposed that the rapid decomposition of small grains of chromium 'hydride' from the outside inwards halts the subsequent grain growth and favours the further nucleation of new 'hydride' crystals. By such a mechanism, formation of an aggregate of fine grains may be envisaged. A further refinement of grain size may also take place by virtue to the shrinkage which inevitably accompanies 'hydride' decomposition: if it is assumed that each 'hydride' grain decomposes from the outside, the subsequent 'shell' of metal produced occupies a smaller volume and, as a result, ruptures. This allows further decomposition from the centre of the grain with further rupturing until decomposition is complete and each original hydride grain has split into many microscopic crystallites.

Snavely's extensive treatment of the chromium plating process also included an experiment in which he demonstrated (in agreement with Rogers, but contrary to Kasper) that the reduction of chromic acid to the trivalent state could be effected chemically by atomic hydrogen, an observation which certain later workers did not apparently consider in their experimentation (particularly with regard to physical 'examination' of the cathode film).

Reinkowski and Knorr (135), while not accepting the major role of atomic hydrogen in the reduction of chromic acid, were of the opinion that reduction was step-wise via the formation of 'intermediate reducible combinations' within the cathode film, with the precise nature of the film (in terms of the type and proportions of intermediates present) being assumed to change at potentials corresponding to steps in observed cathode polarization curves (after Liebreich). The intermediate combination which characterizes film composition under plating conditions is assumed to contain divalent chromium as a complex species, and it is from this state that metallic discharge ultimately takes place (in agreement with Liebreich, Birynkov, Snavely, et al).

The cathode film according to Reinkowski and Knorr was composed of an insoluble and non-reducible basic chromium chromate sol which, in the absence of a 'catalyst', allowed the sole passage of hydrogen ions and atoms. The idea of a chromium chromate film was originally proposed by Muller (127), and will be considered later. Indeed Reinkowski and Knorr's ideas are remarkably akin to Muller's with respect to film composition, and to Liebreich's with respect to mechanism. Even their 'intermediate reducible compound' during plating, which contained sulphate, hexa, tri and divalent chromium, seems similar to Snavely's earlier 'complex basic electropositive dispersoid'. One positive conclusion which may be drawn from Reinkowski and Knorr's work is that experimental polarization data in chromium plating is very hard to reproduce accurately. If their cathode polarization curve (Figure 6) is compared to those obtained under identical conditions by Liebreich and Muller (Figure 3 & 4),

the differences are marked. As reproducibility of data should be a prerequisite to theorizing on the basis of that data, conclusions drawn by early workers on the strength of polarization data must be subject to question.

Following Snavely's theories and Reinkowsi and Knorr's 'summary', the most recent account of chromium deposition via a step-wise mechanism was proposed by Hoare (118). As with Liebreich, Muller, and Reinkowski and Knorr, Hoare used low potential cathode polarization data (using a platinum cathode) to draw conclusions about plating mechanisms. However, he based his proposals on the premise that any theory should account for the existence of Cr III (at the cathode) in a reducible state, and explain why the highly stable trivalent aquo-complex, $Cr(H_2O)_6^{3+}$, is not formed. His theory combines Muller's concept of a chromium chromate film with the idea of step-wise reduction, but with certain important developments and modifications. He started from the assumption that the main chromium-bearing species in concentrated ($250g/dm^3$) chromic acid is the trichromate ion, $HCr_3O_{10}^-$ (based upon solution colour) and that, in the absence of a 'catalyst', this ion approaches the cathode surface but is held (through its negative charge) at a point just outside the outer plane of the Helmholtz double layer. This is because most of the potential drop between the cathode and the bulk solution (highly concentrated) occurs across the double layer (21, 136). As the double layer thickness was assumed to be of the order of 0.5 nm (137), he considered that electron transference to the ion could be achieved through quantum mechanical tunneling.

In the first step of reduction, an electron is transferred through the Helmholtz double layer to one end of the waiting trichromate ion, thereby reducing a Cr VI ion to the pentavalent state :-

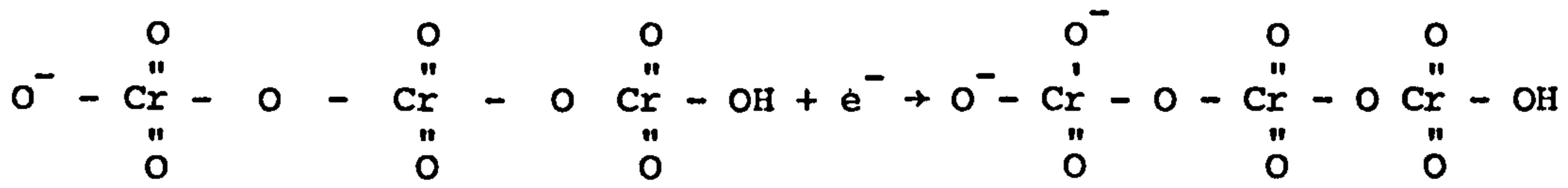

Upon a further electron transfer, the Cr IV state is obtained :-

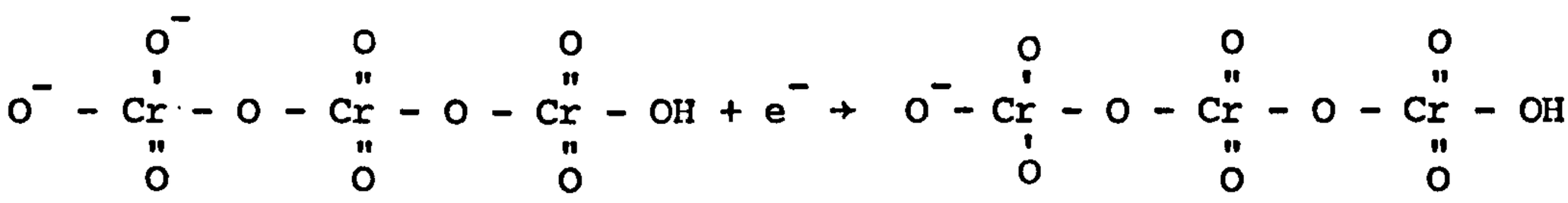

Finally, with a third electron transfer, a Cr III species is produced, with the loss of oxygen which combines with hydrogen ions to form water :-

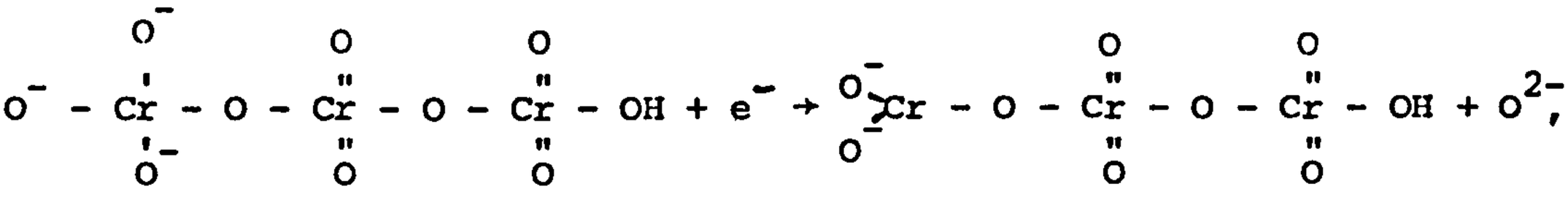

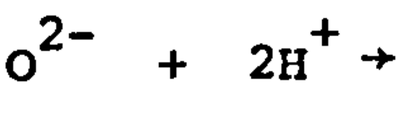

The species

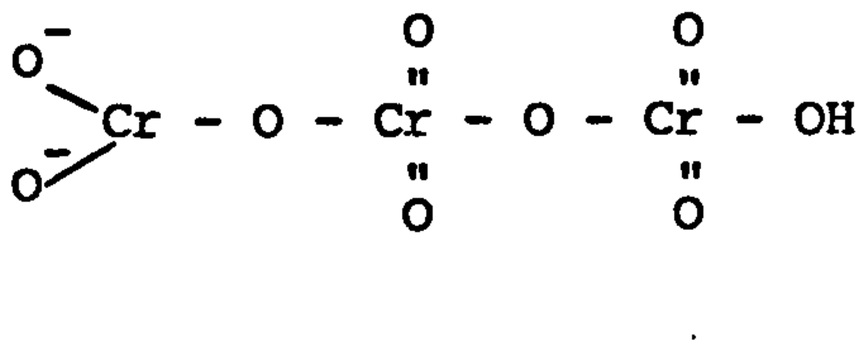

is chromium dichromate and may be identified with the blocking film of Muller and other workers, which exists in the absence of a'catalyst'.

In strongly acidic conditions, a further electron transfer may result in the divalent chromium-containing chromous dichromate :-

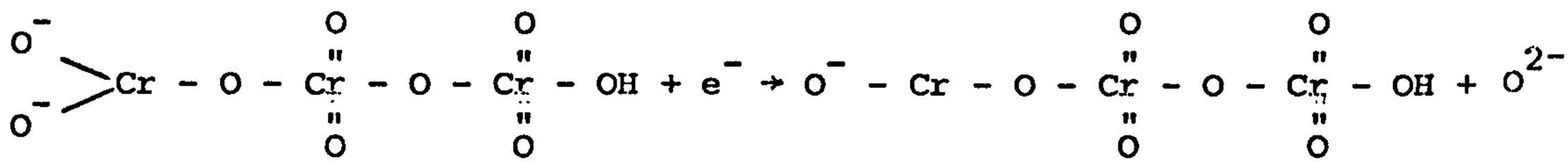

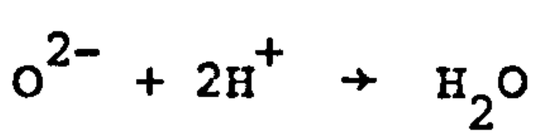

Decomposition of chromous dichromate may then take place :-

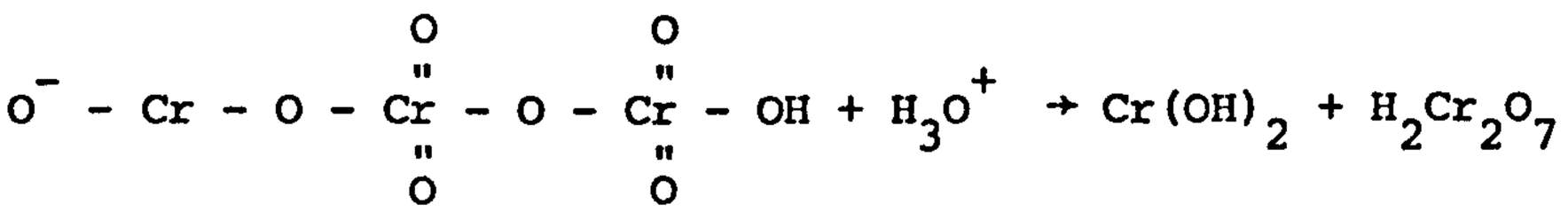

forming basic chromous hydroxide and a dichromate which may undergo condensation back to trichromate in solution.

In the absence of the 'catalyst', the chromous hydroxide dischargesas 'black chromium', provided the current density is high enough.

The cathode surface is, therefore covered by a chromium dichromate/chromous dichromate/chromous hydroxide film from which, under favourable conditions, black chromium may deposit, and through which hydrogen evolution takes place.

Hoare then proposed that the sulphate 'catalyst' in strong acid adopted the form of a bisulphate ion HSO_4^-, and that it was through the action of this that plating took place. In support of this he provided equilibrium data and a highly plausible mechanism by which the bisulphate ion affects (and effects) cathodic processes. His theory provides not only an explanation of bisulphate catalysis, but also a reason for the existence of an optimum chromic acid/'catalyst' concentration ratio.

His explanation of bisulphate as 'catalyst' involves its influence at the final stages of deposition (i.e. once the chromous hydroxide has formed).

If the chromous hydroxide is considered to be hydrated chromous oxide :-

$$Cr(OH)_2 \rightleftharpoons Cr = O + H_2O,$$

the bisulphate ion may attach itself to the chromous oxide via hydrogen bonding :-

$$Cr = O + HSO_4^- \rightleftharpoons Cr = O\cdots H - O - \overset{\overset{O}{\|}}{\underset{\underset{O}{\|}}{S}} - O^- \rightleftharpoons Cr^+ - O - H\cdots O = \overset{\overset{O}{\|}}{\underset{\underset{O}{\|}}{S}} - O^-$$

The positive charge on the end of this complex causes it to swing around in the outer Helmholtz plane so that the chromium end is specifically adsorbed onto the cathode surface with the sulphate tetraheda extending into the solution. Two electrons may then be transferred to the specifically adsorbed Cr II ion, forming first Cr I ion, and then metallic chromium with the HSO_4^- ion regenerated :-

$$Cr^+ - O\langle\cdot\rangle H\langle\cdot\rangle O - \overset{\overset{O}{\|}}{\underset{\underset{O}{\|}}{S}} - O^- + e^- \rightarrow Cr - O\langle\cdot\rangle H\langle\cdot\rangle O - \overset{\overset{O}{\|}}{\underset{\underset{O}{\|}}{S}} - O^- + e^- + 2H^+$$

$$\rightarrow Cr^o + H_2O + HSO_4^-$$

This model provides a reason for the non-formation of a stable trivalent chromium aquo-complex, as Cr III is held in the chromium dichromate species and suggests the existence of a thin cathodic 'film' based upon Cr = O during plating.

It also explains the action of the bisulphate as being that of a true catalyst as it forms an intermediate which facilitates electron transfer before being subsequently regenerated. At high current densities where hydrogen evolution is sufficiently rapid to raise the film pH and thus lower the local HSO_4^- concentration, the effectiveness of the catalyst is impaired and a deposit containing non-metallics results. Finally, Hoare accounts for the high observed deposition overpotential in terms of the fact that two thirds of the electron transfer involved is via tunnelling across the double layer. This barrier to electron transfer, along with the comparative ease of hydrogen evolution, also accounts for the relative current efficiencies of the two reactions.

The second part of Hoare's theory accounts for the narrow range of concentrations in which HSO_4^- is effective in catalysis of chromium deposition.

His thesis for the deposition mechanism assums that one end only of the trichromate ion is reduced step-wise with HSO_4^- participation. However, should both ends of the ion be reduced (in the absence of HSO_4^-) to the trivalent chromium state (step-wise, with a six-electron transfer in total), a dichromic chromate complex would be formed;

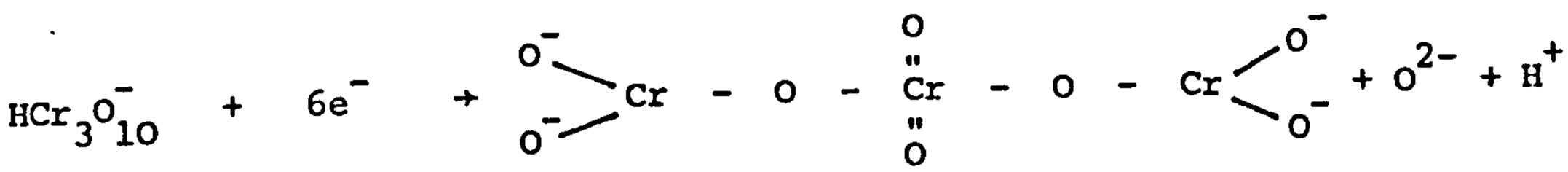

In acidic solutions this could decompose, yielding chromate ions and trivalent chromium;

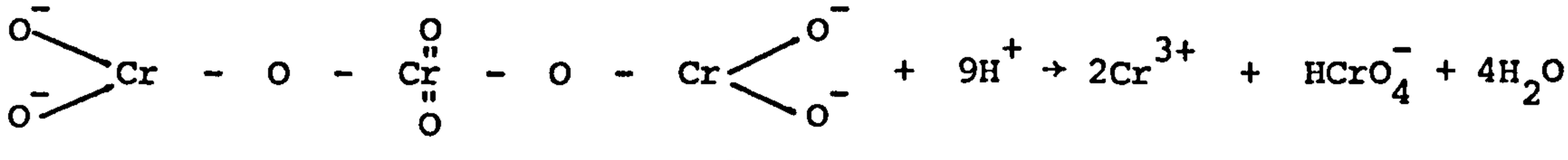

Under these circumstances, the Cr^{3+} ions would immediately form the highly stable hexaquo complex $Cr(H_2O)_6^{3+}$, through which further reduction of Cr III is impossible. In the absence of HSO_4^- then, either 'black chromium' or the stable trivalent complex is formed, depending on the local solution (film) pH (and hence, on current density).

In order to prevent the formation of the dichromic chromate species, one end of the trichromate must be protected. Hoare considered this to be accomplished by hydrogen bonding with HSO_4^- ions when these are present. He assumed that such bonding may occur with any or all of the four terminal double-bonded oxygen atoms of the trichromate ion;

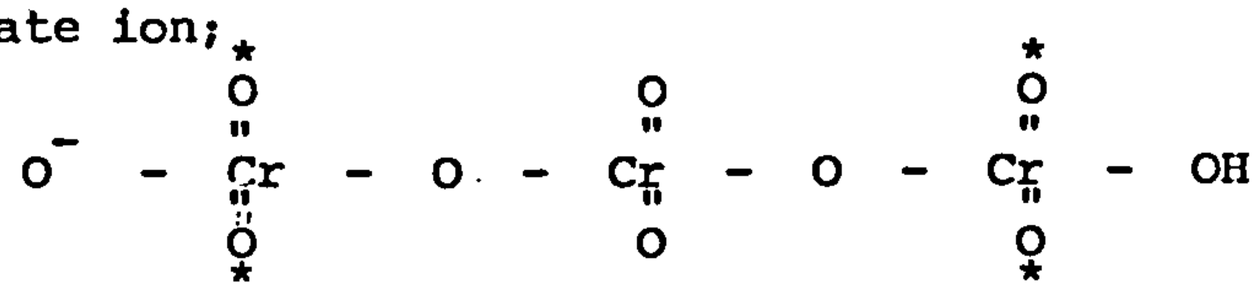

On this basis, optimum 'protection' would be afforded the trichromate species when two HSO_4^- ions bond in the following way;

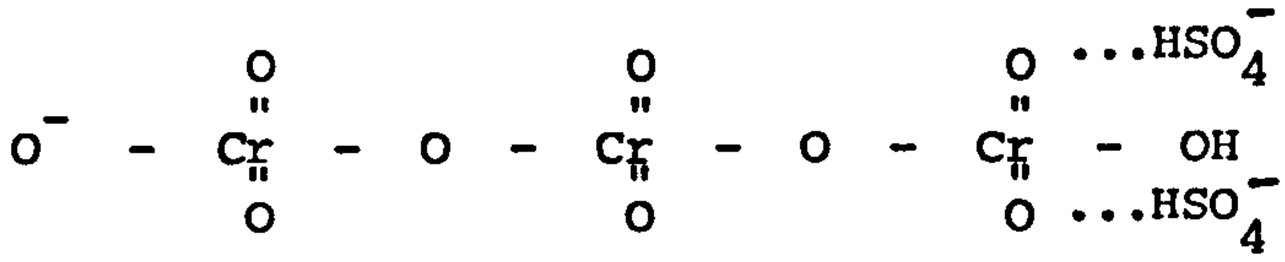

In this condition, reduction could only take place at the 'innermost' chromium ion, thus avoiding the possibility of dichromic chromate formation.

Should HSO_4^- ions form bonds with all four of the corner oxygen atoms in the trichromate ion, both ends would be blocked, with most current consequently diverted to the hydrogen evolution reaction and little or no metallic deposit produced.

If the hydrogen bonding of HSO_4^- ions to trichromate ions is written thus;

$$HCr_3O_{10}^- + nHSO_4^- \rightleftharpoons \left[HCr_3O_{10}^-.nHSO_4\right]^{(n+1)-}$$

where n may take values of 0 to 4, it is clear that the optimum situation for metal deposition corresponds to n = 2. This condition is apparently satisfied when the chromic acid/sulphate concentration ratio is 100 : 1. At higher ratios $n < 2$, and the tendency is towards Cr III production, and at lower ratios $n > 2$ and the tendency is towards hydrogen evolution only.

Hoare's ideas are well-explained and generally plausible, although they do not account for the drop in sulphate concentration with time which undoubtedly does occur (i.e. the sulphate is <u>not</u> a true catalyst). It is felt, nonetheless, that Hoare's mechanism proposals provide the best explanation to date of the chromium plating process.

1.10.2 <u>Direct reduction from the hexavalent to the metallic state</u>

While the idea of a basic chromium chromate ($Cr(OH)CrO_4$) film was initially mooted by Muller (127), he did not consider reduction to be completely step-wise. In the absence of sulphate, he proposed that the relatively high pH (as a result of hydrogen evolution) at the cathode causedthe formation of a chromium chromate layer, through which the

relatively large CrO_4^{2-} ions (which he considered to be the active species) could not pass, but through which hydrogen ion reduction could take place;

$$2H_2CrO_4 + 3e^- \rightarrow Cr(OH)CrO_4 + 3OH^-,\ 3OH^- + 3H^+ \rightarrow 3H_2O$$

With the addition of sulphuric acid to the solution, Muller proposed a partial electrostatic dissolution of the film;

$$2Cr(OH)CrO_4 + H_2SO_4 \rightarrow 2Cr^{3+} + SO_4^{2-} + 2CrO_4^{2-} + 2H_2O$$

He considered that this film dissolution would not commence until the cathode potential reached a certain 'penetration potential'. At this potential, the reduction of Cr VI to Cr III could occur. At the same time, film breakdown allowed easier access of CrO_4^{2-} ions to the cathode surface, with subsequent discharge to metallic chromium. He, therefore assumed deposition to be from the hexavalent state, with the sulphate acting to electrostatically dissolve the cathode film down to a thickness and structure which allowed hexavalent ion transmission.

Muller later (138) abandoned this theory for one in which he assumed that sulphate in the form of the HSO_4^- ion passed through interstices in a colliodal basic dispersoid ($Cr(OH)_3.Cr(OH)CrO_4$), thus allowing higher hydrogen ion concentrations in the cathode film. This drop in pH did not favour the dispersoid's existence and hence allowed easier access of hexavalent ions for subsequent reduction to metal.

Muller's work was by no means definitive and provided no explanation for a number of phenomena peculiar to chromium deposition

(e.g. the optimum 'catalyst' ratio). However, the idea of chromium chromate formation was adopted by later researchers (e.g. Hoare) as a basis for step-wise reduction theory.

Muller's proposal that reduction took place from the hexavalent state prompted later workers' attempts at confirmation.

Kasper (88) was originally of the opinion that reduction was step-wise and that sulphate allowed metal deposition through lowering (through adsorption) the electrophoretic velocity of a basic chromium chromate ($Cr(OH)_3.Cr(OH)CrO_4$, after Muller) sol. Subsequent reduction was then achieved via the establishment of a chromic/chromous couple. His introduction of the importance of film pH combined with multi-step reduction within the film was used later by Snavely in his theory (although with important modifications). However, Kasper later (139) proposed that chromium was deposited directly from the hexavalent state, and that deposition from the trivalent state (as an intermediate) was impossible. As evidence of this, he demonstrated that other metal (e.g., Cu, Cd, Ni) cations with reduction potentials more positive than trivalent chromium could not be co-deposited. This assumption that metal deposition was impossible from the trivalent state in a chromic acid bath was seemingly confirmed by Muller (138), who added trivalent chromium to a plating bath and observed no change in deposition efficiency. This is contrary to the observations of other workers, as an excess of trivalent chromium is generally accepted to decrease the plating current efficiency. It could however be explained in terms of a failure on Muller's part to take into account the relative surface areas of his anode and cathode, as this affects the efficiency with which trivalent chromium is removed from the solution.

Levin and Falicheva (113) also considered metal deposition to be from the hexavalent chromium state, and used ionic equilibrium data together with assumed cathode pH values to predict that ultimate discharge takes place chiefly from the CrO_4^{2-} ion. They supported this assertion by using paper chromatography analysis of the catholyte during deposition, and observing lines characteristic of $HCrO_4^-$, $Cr_2O_7^{2-}$, and CrO_4^{2-}. of which the latter was the strongest. However, their use of relatively dilute (180g/dm^3 CrO_3) test solutions must place some doubt on the applicability of their findings to industrial-strength solutions.

The question of the oxidation state from which chromium deposits in a standard solution became subject to renewed interest with the development of radioactive tracer techniques.

Ogburn and Brenner (140) used the Cr^{51} isotope in an effort to determine whether deposition was step-wise (via the Cr III and Cr II states) or directly from the hexavalent state. Their conclusion was in accordance with that of Vagramyan and Usachev (141) (who used a similar technique), and stated that reduction takes place exclusively from the hexavalent state in standard chromium plating solutions. These conclusions were based on the observation that when the radio-active tracer was added to the solution as trivalent chromium prior to plating, no radioactivity (or very little) was traceable in the subsequent deposit. Radioactive labelling of the hexavalent ions, however gave highly radioactive deposits.

Objections (142) to Ogburn and Brenner's conclusions, based on the cathode film acting as a barrier to incoming Cr^{3+} ions, were proved

unfounded through investigations which used interrupted current to ensure film breakdown (141). Similar objections based upon the different modifications of trivalent chromium (green or violet) which may exist in solution were also shown to be unsound (143).

Hoare (and others) however showed that the trivalent chromium which participates in the actual deposition mechanism is held in a completely different form to that which exists in bulk solution. Deposition, while not possible from stable trivalent species ($Cr(H_2O)_6^{3+}$) in solution,can, therefore occur via reducible trivalent-based intermediate species present in the cathode film. In a review of proposed deposition mechanisms, Ryan (144) cited this as a reason for non-acceptance of the 'hexavalent' theories of Ogburn and Brenner (and others), and instead favoured the notion that reduction takes place step-wise through products formed in the sulphate-modified cathode film (after Snavely and others).

The film composition in the absence of sulphate is, according to Ryan, similar to that of Muller and others, i.e., a basic chromium chromate. However, he proposes that the addition of sulphuric acid leads to an anion exchange between hydroxyl groups in the film and sulphate ions in solution;

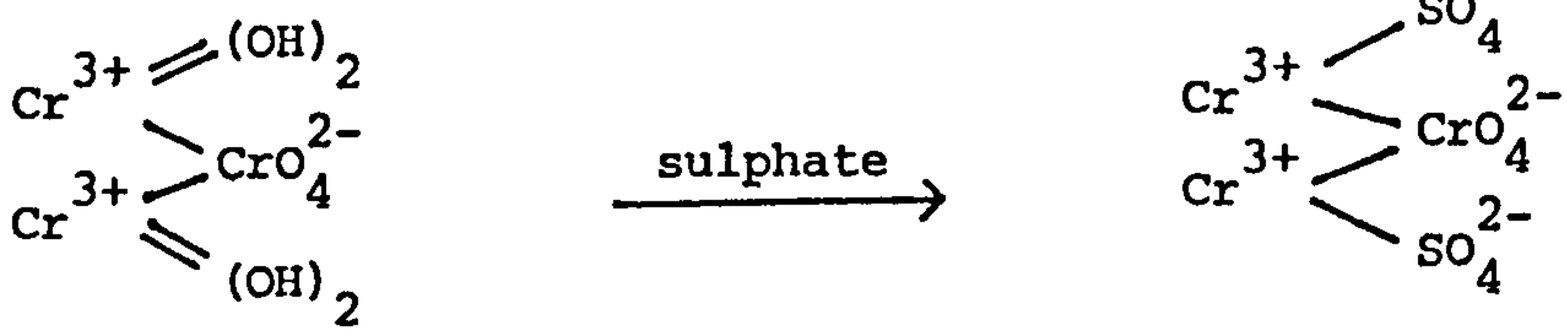

Sulphate ions therefore facilitate electron transfer within the film by allowing bridging through anionic components of the cationic complex.

This fits with the observation that metals other than chromium can only co-deposit with chromium if present as anions which can exchange with CrO_4^{2-} (e.g., MnO_4^{2-}, SeO_4^{2-}, ReO_4^{2-}) (145).

Hoare (118) did not invoke the concept of a cathode 'film' as such, but one (based upon Cr II oxide) may be inferred from his mechanism, and, although he proposed that a chromium dichromate species (similar to Muller's chromium chromate) is formed as an intermediate, it is short-lived and is not involved in 'film' formation.

1.10.3 Cathode film composition

In addition to the main theories regarding the deposition mechanisms involved in chromium plating, a number of workers have attempted to analyse the structure and composition of the cathode film through which plating takes place, and their findings may be compared with those predicted by the various theories. Indeed, in many cases research has been concentrated simply on the nature of the cathode film (chemical and physical), with no attempt to venture into the complexities of deposition mechanism.

Two schools of thought exist as to the nature of the film and how it differs from the film formed in pure chromic acid (i.e., in the absence of sulphate).

It is generally accepted that electrolysis of pure chromic acid leads to the formation of an amorphous oxide film of considerable thickness (dependent on plating conditions, but of the order of μm) through which hydrogen ion reduction is the sole reaction able to take place. The precise chemical and structural nature of the film varies with current density (as pH conditions change) but it is generally assumed to be a non-porous chrome oxide of the form $Cr = O.nH_2O$ or $Cr_2O_3.nH_2O$. Such films are plainly visible during the electrolysis

of dilute (less opaque) pure chromic acid solutions. However, on the addition of sulphuric acid to pure chromic acid (at the prescribed ratio) a change in the film takes place, the exact nature of which is controversial.

One school has it that the sulphate modifies the amorphous film in some way, while another maintains that chromium deposition is brought about through the formation of an entirely different type of film.

Theories of film modification by sulphate have been proposed by Muller (127) (via partial film disruption through electrostatic dissolution), Weiner (146) (via partial chemical dissolution), Reinkowski and Knorr (135) (through the formation of intermediate reducible compounds) and Kappel and Gerischer (147) (through the inhibition of film growth). However, none of these workers employed direct film observation as a research tool, preferring instead to draw inferences from (possibly suspect) electrochemical data.

An alternative view was presented by Vagramyan and Usachev (148), Vagramyan and Solov'eva (143), and Shluger and Kazakov (149). They maintained, through visual observation, that an entirely different (colloidal as opposed to amorphous oxide) type of film is formed in the presence of sulphate. This film may *apparently* be observed (150) on cathodes extracted from plating solutions with the current still flowing. It is soluble in dilute chromic acid, sulphuric acid and (even) distilled water, and while its thickness may vary with conditions of electrolysis, it is always macroscopic.

Saiddington and Hoey (120), in an attempt to end the controversy, carried out detailed research into the nature of the two films, corr-

elating microscopic observations of cathode film formation with polarization data. They observed that the addition of sulphate to pure (250g/dm^3) chromic acid caused an increase in cathode polarization (at a constant current density of 175 mA/cm^2) and a corresponding break up of the amorphous oxide film. Before completion of break-up, the presence of a 'transparent' viscous film was noted in the vicinity of the cathode surface. Using a fixed concentration ratio however, it was found that at low potentials an amorphous oxide film of the first type existed (in the presence of sulphate). The sequence of events during cathode polarization in a chromium plating bath suggested by Saiddington and Hoey may be summarized :-

(i) At very low cathode potentials, in the initial stages of polarization, trivalent chromium is produced and accumulates at the interface prior to the onset of the hydrogen evolution reaction (151).

(ii) The commencement of hydrogen evolution at a more negative potential lowers the hydrogen ion concentration at the interface and creates conditions favouring the formation of an amorphous oxide type film which is visible under a microscope. The process of film formation is observed to be faster at lower chromic acid/sulphate ratios (Saiddington and Hoey drew no conclusions as to the precise mechanism of formation of this film).

This 'pre-plating' amorphous film was also observed by Weiner and Schiele (152), who demonstrated that it consisted of two layers: a very thin (0.02 μm) pore free initial layer and a thicker (0.1 μm), more porous upper layer. Saiddington and Hoey assumed their films to be the upper of these layers.

(iii) At a still more negative cathode potential a point is reached at which the amorphous oxide film is observed to disintegrate into fragments (Weiner and Schiele's lower layer was assumed to be destroyed simultaneously). At the same time, a transparent viscous film is formed on the cathode surface and a complete cessation of visible gas evolution is perceived (153). As this potential also marks the commencement of metal deposition, the temporary gas disappearance has been explained in terms of the deposition of an initial metal layer rich in hydrogen (154).

At potentials corresponding to metal deposition, Saiddington and Hoey therefore favoured the formation of a completely different type of film which was transparent and viscous in contrast with the opaque and solid nature of the amorphous oxide film. However, all their conclusions were restricted to the physical nature of the film(s), making no suggestions with regard to deposition mechanisms.

Saiddington and Hoey's work, and that of Weiner and Schiele and the Soviet workers from whom they drew heavily, is subject to certain criticisms.

Saiddington and Hoey proposed the presence of a transparent viscous cathode film during electrodeposition on the basis of their observation of hydrogen bubble behaviour. This implies that the viscous film is macroscopic. However, Snavely (49) showed that the viscosity of a chromic acid solution increases considerably with the percentage of trivalent chromium ions present, suggesting that Saiddington and Hoey's viscous cathode film may, in fact, be due simply to the high trivalent concentrations (reduction products) which inevitably prevail in the vicinity of the cathode, and that any true (plating) cathode film is so thin as to be undetectable.

A similar explanation may be given to Shluger and Kazakov's observations that a viscous film is apparent around the cathode after the polarizing current is switched off (during electrolysis it is assumed to be masked by hydrogen evolution). Alternatively, it is possible that Shluger and Kasakov's layer is one of trivalent chromium reduction products, produced through the reduction of chromic acid at the cathode surface by desorbing hydrogen (after Snavely).

Weiner and Co-workers drew conclusions on the basis of the examination of 'films' stripped from cathodes in the presence and absence of 'catalysts'. They found, using electron diffraction techniques (155), that films obtained through the electrolysis of pure chromic acid were essentially Cr_2O_3 based, and that those obtained during plating contained oxides of the cathode substrate metal as well as Cr_2O_3. From this they deduced that the substrate played some immediate part in the chromium deposition mechanism.

Any 'film' stripped from a cathode during plating must be subject to doubt. It is considered more likely that the films examined by Weiner and Schiele were simply trivalent chromium rich solution dried onto the cathode surface on removal of the cathode from the bath. Parallel work in Japan (156) used electron diffraction of 'films' to arrive at similar conclusions, which must be similarly subject to question.

1.10.4 Polarization data as a basis for deposition theory

Cathode polarization data obtained during chromium plating are notoriously irreproducible, as the polarization curves of Muller, Liebreich, and Reinkowsi and Knorr testify (Figures 3, 4 and 6).

Each was produced under 'identical' conditions of electrolysis, yet the differences are obvious (taking into account differences in scale, etc). However, many researchers have employed polarization data as a basis for theories of chromium plating, a practice which, in the absence of other supporting evidence, is precarious.

The problems involved in the measurement of cathode polarization during the electrolysis of chromic acid based plating solutions are formidable and are considered in greater depth under 'Experimental'. However, it is worth stressing that :-

(i) The electrolyte is extremely acidic and hence, corrosive.

(ii) The conditions at the cathode surface (due to metal deposition and gas evolution) are constantly changing.

(iii) The cathode surface area changes with time during plating.

(iv) The probe employed to measure cathode surface potential (with respect to a reference electrode) must be positioned at a point on the cathode surface where the current density reflects the overall average.

These problems serve to indicate the technical difficulties inherent in the accurate collection of polarization data from chromium plating solutions, and go some way to explain the irreproducibility of results of early workers.

Expressed simply, polarization measurements may be made in two ways :- potentiostatically or galvanostatically. In the latter, the current through the system (current density at an electrode) is held at a constant value while the potential of the electrode investigated is monitored via a cappilary electrode probe (versus a standard

reference electrode and via a salt bridge). In the former, the potential of the test electrode is held constant (with respect to a reference electrode), and the corresponding current density measured. Potentiostatic methods of polarization measurement are often favoured because they tend to yield more information. However, the maintenance of a strictly constant electrode potential during polarization measurement is essential for accuracy.

Earlier researchers used simple electrical circuits in order to maintain 'constant' electrode potentials. Such circuits were assumed sufficiently accurate if high polarization currents were not required. The irreproducibility of data obtained by such methods however places doubt on this assumption.

More recently, the development of the 'potentiostat' has greatly improved accuracy in polarization measurement. First used in the 1940's, these instruments work electronically by comparing two signals. The principle is that an increase (for whatever reason) in the potential between the test electrode and a reference (usually a calomel) electrode causes an increase in the negative potential of the grid of the electronic valve (later instruments employ transistors) and a reduction of the current in the amplifier circuit. This in turn reduces the polarizing current and leads to a decrease in the potential of the test electrode back to the original value.

The introduction of the potentiostat was a great aid to research into electrode kinetics as it permitted greater accuracy of measurement and the use of high polarizing currents (where required). However, even using a potentiostat, the accumulation of polarization data

is subject to considerable error, which may be divided into that connected with experimental technique and that related to the complexity of the process under investigation. The possible level of error involved is important and is a major factor in dictating the unwisdom of comparing polarization curves obtained by different workers under so-called 'identical' conditions.

No authors of polarization data in chromium plating have provided sufficient information on accuracy of technique to be considered 'definitive'.

Cathode polarization curves obtained in chromic acid plating baths may be divided into three (not always distinct) regions :-

(i) A low-potential - low current density section in which the curve describes an inconsistent path, and which corresponds to changes at the cathode surface prior to the commencement of metal deposition.

(ii) A range of higher potentials and current densities in which all three cathode reactions (as defined earlier) take place, and which describes a reasonably constant variation of current density with potential.

(iii) A region of high cathode potential in which there is a tendency towards a limiting current density, and which corresponds to a general deterioration in deposit properties and appearance.

It is reasonably fair to state that most attention has thus far been focussed on the low potential end of the curves, with attempts to

relate its shape to the reduction potentials of certain cathode reactions and observed changes at the cathode surface. No realistic analysis of the higher potential regions of the curves has been carried out due to the complicating factor that in these regions polarization is due to three competing reactions, the efficiencies of which vary individually with total current density. One group of Soviet workers have, however attempted to split the overall curve into its three component parts (157) by combining current efficiency data with overall polarization data to yield 'partial polarization curves'. Subsequent analysis of 'partial' curves may yield new information helpful in the development of a definitive chromium-plating theory.

While partial polarization curves have been plotted and investigated with regard to the effect of certain solution variables on the polarization behaviour of each reaction during chromium plating, a systematic analysis of such data (with regard to cathode reaction kinetics) has not been undertaken. The Soviet researchers did, however use partial polarization ('decomposition') curves to explain the optimum chromic acid/sulphate ratio in terms of the interaction of the individual cathode reactions at varying sulphate concentrations. They found that as the concentration of sulphuric acid was increased, the deposition reaction and partial reduction (Cr VI to Cr III) reactions were favoured at the expense of hydrogen evolution. At higher sulphate concentrations a further repression of the hydrogen evolution reaction corresponds to an increase in the rates of the other two reactions, with the partial reduction predominating at the expense of metal deposition. This conflicts directly with Hoare's observation that at low chromic acid/sulphate ratios the

tendency is towards hydrogen evolution only, a lack of agreement which may perhaps be explained in terms of the different experimental conditions and techniques employed.

An example of a cathode polarization curve divided into its component partial curves (after Vagramyan, Usachev and Cherchova (157)) is given in Figure 7.

In addition to their analysis of the higher potential regions of the curves, the Soviet workers also considered the low density, quasipassive region which is usually assumed to correspond to film formation on the cathode (Saiddington and Hoey's pre-plating, amorphous oxide film). They deduced from fixed potential current versus time curves, that a film does indeed exist at these potentials and that once established, electrochemical reactions taking place through the film proceed at a rate governed by the presence and concentration of sulphate catalyst.

The use of copper as cathode material by the Soviet workers prevents comparison of their polarization curves with those of previous researchers (Muller, Liebreich, Reinkowski and Knorr, Hoare) who employed platinum cathodes, particularly as Weiner (146) has shown polarization behaviour to be sensitive to cathode material (in a manner related to the standard reduction potential of the cathode metal). Polarization data obtained during chromium deposition on ferrous metal is difficult to find, surprisingly so as most chromium plating is of steels. Okada and Yamamoto (156) have published polarization curves obtained on mild steel cathodes, but they employed very dilute plating solutions (which do not accurately reflect normal plating conditions) and concentrated their attention on the low potential, pre-plating region of the curves.

The use of reproducible partial cathode polarization curves in the analysis of chromium plating mechanisms clearly holds considerable promise as a research technique. However, the development of research techniques does not (in the short term) assist the industrial hard chromium plater, and while a definitive theory of chromium plating may suggest practical improvements to the process, no such theory exists and most proposed improvements have been as a result of 'trial and error'. Published results of such speculative experiments may, nonetheless, be of interest to the research scientist. Of particular interest is work in which small chemical additions (as alternatives to, or in addition to, proven catalysts) are reported as producing considerable changes in plate appearance, properties, current efficiencies and throwing power.

1.10.5 Additions to standard plating solutions

Although no unequivocally accepted deposition mechanism exists, it is accepted that the presence in solution of sulphate (or silicofluoride) anion is necessary for plating to take place. The controversy surrounding the precise action of the sulphate has led some researchers to investigate other acid anions as possible alternative catalysts in chromium plating.

Levin and Falicheva (113) explained the ineffectiveness of NO_3^-, Cl^-, Br^-, and I^- as alternative catalysts in terms of their inability to be absorbed by the hydroxides and basic salts of trivalent chromium present at the cathode surface during the electrolysis of chromic acid. Their interpretation of the action of the sulphate anion as a catalyst was similar to that of Muller (127) in that they assumed the sulphate to be absorbed by the 'passive'cathode film with the formation of easily soluble complex species which promote film

dissolution and allow easier access of chromate ions, from which direct reduction takes place.

Griffin (158) carried out a far more extensive programme of tests on possible alternative catalysts and, while drawing no conclusions as to their catalytic mechanisms, listed six which gave metallic deposits when added to chromic acid (at various ratios). These were trichloroacetate anion (Cl_3CCOO^-), bromate anion (BrO_3^-), fluoborate anion (BF_4^-), chloride anion (Cl^-), fluoride anion (F^-) and silicofluoride anion (SiF_6^-). That the latter two additions could function as catalysts in chromium plating was already well accepted prior to Griffin's work. He did, however establish optimum operating conditions for their use.

Griffin's approach was to vary temperature, current density and chromic acid/additon ratio, and measure the corresponding current efficiency for each cathode reaction. In addition (sic), he commented on the appearance of the resultant deposit, realizing that plate appearance is a major criterion when considering the effectiveness of proposed new catalysts. He made no attempt to investigate the effect of the new catalysts on throwing power or cathode polarization. However, it may be concluded that, in terms of the variation of plating efficiency with current density (at least),none of his alternative catalysts would improve on the throwing power of a sulphate-catalyzed solution. This is supported by his own conclusion that the deposits produced from solutions containing the new catalysts 'did not appear to be useful'. Indeed, he was able to draw no real conclusions from his work, other than that the role of sulphuric acid as a catalyst is more specific than just that of a strong acid.

Although no literature is apparently available regarding the effectiveness of inorganic chemicals as <u>additions</u> to standard plating solutions (as opposed to substitutes for the conventional 'catalysts'), it is apparent that of the substitutes for the sulphate ion investigated, halogen-based chemicals have proved the most promising.

This observation is borne out by work carried out (159) at a local chromium plating company where the addition of an organic chlorine-containing chemical to standard plating solutions has resulted in an apparent improvement in 'throwing-power' combined with better properties and a wider 'bright range'. The chemical, DCMA or di-chloro-malonic acid, is thought to break down in the acidic environment of the plating solution to yield the perchlorate ion, ClO_4^-.

The apparent benefits afforded by the use of DCMA (or perchlorate ion) have prompted investigations into the bromate ion, BrO_3^- (for its similarity) and the borate ion $B_2O_4^{2-}$ (boron-based chemicals have shown promise as alternative'catalysts' in chromium plating (158)).

EXPERIMENTAL

SECTION 1

Apparatus

2.1 Introduction

Polarization data obtained at a working cathode were used with current efficiency measurements to construct partial polarization curves for each of the three cathode reactions which take place during chromium plating. These were used to provide an insight into the mechanisms by which the reactions proceed, and a pointer towards possible rate-determining steps.

In addition, the effect of solution temperature variation upon partial polarization characteristics was analysed and used (for the plating reaction only) to provide approximate values of activation enthalpy, entropy and free energy of activation for the deposition reaction.

Following an investigation into the effects of three novel solution additions (to a Standard Solution) upon the solution throwing power, current efficiencies, physical properties and appearance of deposit, an attempt was made to explain these effects by means of an extensive programme of investigation employing the polarization analysis technique outlined above (and initially evaluated using a Standard Solution alone).

The measurement of electrode polarization as a means of investigating the chromium plating process is not valid unless strict reproducibility can be guaranteed. So although potentiostatic and potentiodynamic means of obtaining polarization data are well-tried (160) it was initially necessary to develop a particular procedure which satisfied this proviso.

Supplementary experiments, complementing the main thrust of experimentation, were carried out in an attempt to clarify certain points and present a more complete consideration of the chromium plating process.

2.2.1 General

2.2.1.1 The plating cell

The cell was constructed in the form of an 'H' (Figure 8) from tubular silica glass. It was fabricated so that it contained a porous pot barrier at the centre of the cross-arm to prevent gas from passing between anolyte and catholyte, as this would introduce errors in current efficiency measurements. The cell held approximately one litre of plating solution and was suspended in a water bath by means of a clamp attached to its middle.

2.2.1.2 Plating solutions

All solutions used were based upon a 450g/l solution of (99% pure) flake chromic acid (CrO_3) in deionised water. To this were variously added concentrated sulphuric acid (H_2SO_4), potassium perchlorate ($KClO_4$), potassium bromate ($KBrO_3$) and potassium borate ($K_2B_2O_4$). The additions (to the standard 100:1 chromic acid/sulphuric acid plating solution) of perchlorate, bromate and borate were made at concentrations of 5g/l, 10g/l, and 15g/l. Each addition was made as a pre-dissolved solution of the salt in deionised water and added to highly concentrated fresh Standard Solution prior to making up to a 1.5l quantity with further deionised water.

A fresh solution was prepared for each series of experiments in an effort to reduce possible errors due to concentration changes during experimentation.

2.2.1.3 Electrodes

2.2.1.3.1 Anodes

All anodes were constructed from a polished strip of a lead-4% antimony alloy.

Prior to immersion and electrolysis, each anode was stopped-off using adhesive tape and lacquer in such a way as to present a working

2 cm^2 area which faced the entry to the cross-arm in the 'H' cell when immersed. The anode was suspended in the anolyte compartment of the cell by simply bending the top of the strip and hanging it on the cell wall. At this (top) end of the anode an area was left unmasked and abraded ready for the attachment of an electrical contact.

The approximate dimensions of the anodes used were 150 mm x 25 mm x 2 mm, although the actual working area was 200 mm^2.

2.2.1.3.2 Cathodes

The cathode material employed in this work was a type 304 stainless steel, bright annealed strip. This was cut into sections measuring 200-250 mm x 25 mm x 1 mm prior to polishing, stopping-off and insertion into a perspex cathode-holder.

Each cathode was carefully polished using 'Wet or dry' paper to a finish of 600 grit. Following a thorough wash in deionised water and then methanol, the cathode was stopped-off for most of its length with adhesive tape (after weighing where this was required). At the top end of the cathode a small section was left unmasked for the attachment of an electrical contact.

The working end of the cathode was secured in a perspex cathode-holder designed in such a way as to give an optimum current density distribution across a 100 mm^2 working cathode area (see Section 2.2.1.4).

Prior to immersion and subsequent electrolysis the cathode strip was bent in such a way as to facilitate its suspension from the cell wall with the working cathode area facing the entrance to the cross-arm in the 'H' cell.

2.2.1.4 The cathode-holder

This was constructed, in a number of sections, from perspex, and held together with six stainless steel screws (Figure 9). Its design was such that it presented a cathode area of 100 mm^2 ($\pm$ 2.5 mm^2), thus enabling current density measurements to be made directly.

The nature of the securing plate and the position of the deflector plate were designed (161) for optimum evenness of primary current distribution in an attempt to reduce errors in polarization measurement due to probe position (in the plane of the cathode surface).

The tapered shape of the cathode holder towards its upper end was necessary to accommodate the positioning of an inverted solution-filled glass funnel (attached to an inverted solution-filled burette). This was used to collect cathodically produced hydrogen as part of the experiments to determine the cathode reaction current efficiencies.

2.2.1.5 Heating

The plating solution was heated by immersion of the 'H' cell (to above the surface level of the solution within) in a thermostatically controlled, immersion heated water bath which contained a motorised stirring mechanism to ensure against 'hot-spots'.

The temperature of the water bath and that of the plating solution were monitored regularly and compared by means of a conventional mercury thermometer. However, following a settling-down period of thirty minutes after reaching temperature, no unintentional temperature variation was ever observed during experimentation.

2.2.2 Polarization measurement apparatus

In the course of experimentation the apparatus and technique used in the collection of polarization data required modification in

order to ensure reproducibility. As a result, two sets of apparatus were employed.

2.2.2.1 Potentiodynamic

The initial approach was to record the variation of cathode current density with cathode potential potentiodynamically by means of a potential ramp generator and an X-Y plotter together with a 10 Amp range potentiostat.

The ramp generator produced a gradual (negative) increase in cathode potential with time (and with respect to a S.C.E.), while the X-Y plotter recorded the change in cathode current with potential. The rate of increase of potential with time was adjustable and could be varied from 1 mV/s to 300 mV/s (in either direction).

Rather than providing a true continuous increase of potential with time, the ramp generator operated in a forward or reverse direction by means of short steps, each of which consisted of a forward and a reverse component. When the forward component was greater than the reverse component an overall positive change (in a negative direction when considering a cathode) in potential with time was applied. The ratios of forward to reverse potential change components available were 4:1, 3:2, 2:3, 1:4.

Hence, polarization curves obtained using this method were essentially potentiodynamic but in terms of a sequence of consecutive finite steps.

As will be shown, the shape of the polarization curve recorded was found to depend upon the rate of increase of cathode potential with time to an extent where it was decided that a potentiostatic step-wise approach might provide greater accuracy (although at the expense of expediency). The polarization curves obtained potentio-

dynamically are included in the results presented in order to demonstrate this sweep-rate effect.

2.2.2.2 Step-wise, potentiostatic

Although limiting cathode current densities were observed during the potentiodynamic experiments, it was realized that these were probably influenced by potentiostat saturation and were hence largely ignored. Indeed, very little practical chromium plating is undertaken at current densities greater than 10 kA/m^2.

Bearing these points in mind, it was decided that an analysis of polarization data at current densities corresponding to Tafel behaviour (and below) might yield the most accurate and useful information, particularly as errors in measured current density due to surface area change (during deposition) are minimized at lower current densities. The potentiodynamic experiments were therefore repeated (in the low current density range) using a 1 Amp range potentiostat and a step-wise method in which a potentiometer (with a sensitivity of $\pm$ 100 μV) was employed to measure the potential difference between the cathode and the reference, and (via a known resistance) the current flowing through the cell.

The potentiodynamic and step-wise potentiostatic arrangements are given diagrammatically in Figures 10 and 11. The same electrical leads and contacts were used throughout all polarization measurements.

In both techniques the arrangement of the Luggin probe and reference half-cell was the same.

2.2.2.3 The Luggin probe

The potential of the working cathode surface with respect to a reference electrode was measured by means of a Luggin capillary probe and a salt-bridge. The probe was constructed from fine silica tube

(4 mm i/d, 6 mm o/d) which was drawn down (in a flame) to a very fine point and bent in such a way that it could be clamped to the cathode-holder with the probe tip in close proximity to the metal cathode surface but pointing slightly upwards to prevent gas entrapment during deposition. In every test an effort was made to position the probe tip exactly 2 mm higher (in a vertical plane) than the centre of the cathode, thereby ensuring minimum error due to possible uneven current distribution across the cathode. The width of the probe tip was difficult to measure accurately but was estimated as being approximately 250 μm radius (using a travelling microscope).

The other end of the Luggin probe was attached to a length of plastic tubing (i/d 6 mm) which, when filled with an electrolyte, acted as a salt-bridge from the cathode to the reference half-cell.

The electrolyte employed in the salt-bridge was a 43 g/l aqueous (in deionised water) solution of K_2SO_4 in an Agar gel. This was prepared at a temperature of 85°C and drawn into the salt-bridge/Luggin probe arrangement (by vacuum) just prior to solidification, thereby minimizing shrinkage (and the consequent possibility of breaks) within the tube. Care was taken not to stir too vigorously during gel preparation in an attempt to avoid bubbles within the gel.

With the electrolyte gel solidified inside the Luggin probe (filled to the tip) and plastic tubing, the probe was then securely attached to the cathode-holder by means of strong adhesive tape and strategically placed rubber bands, with the probe tip adjacent to the electrode surface (1 mm away). The other end of the salt-bridge (gel-filled tubing) was led away from the cell to the reference half-cell.

2.2.2.4 The reference half-cell

The same reference half-cell was used in all polarization measurements, namely a standard calomel electrode in a saturated KCl solution ($\mathcal{E}_M$ = + 0.2415V vs S.H.E. (46). See section 1.2.2.2).

The salt-bridge tubing length limited the distance from the plating cell at which the reference could be placed so, to avoid contamination by chromic acid spray, the reference cell was covered during experimentation.

A sufficient depth of saturated KCl was maintained in the reference cell to ensure that the end of the salt-bridge could not escape.

2.2.3 Current efficiency apparatus

Measurement of the weight of metal deposited and volume of hydrogen evolved in a fixed time under a particular set of conditions allowed (via Equations 1.1.1,1 and 1.1.1,2) the current efficiencies of each of these cathode reactions to be calculated. The efficiency of the third, partial reduction, reaction (CrVI to CrIII) was found by subtraction from 100%. A similar procedure adopted at the anode (measuring oxygen evolution and assuming two anode reactions only) revealed the efficiencies of the oxygen evolution reaction and the re-oxidation (CrIII to CrVI) reaction.

2.2.3.1 Cathode efficiencies

Following careful polishing and cleaning the length of stainless steel strip was accurately weighed (to $\pm$ 100$\wedge$ g) before being stopped-off with adhesive tape and lacquer and secured in the cathode-holder. Careful bending of the strip prior to immersion in the solution-filled cell allowed the positioning of an inverted burette with a funnel attachment above the cathode as a means of gas collection (see

Figure 13). With the cathode and gas-collector thus arranged, and using a conventional pre-oxidized (2 cm^2) anode, the plating current was passed for a fixed period of time (measured with a stop-clock). The consequent changes in weight of cathode and solution level in the burette during the chosen time period were then used to find the reaction efficiencies.

In order to ensure accuracy with regard to the cathode current density employed in current efficiency determination, a potentiostat was modified (by placing a 4 Ω resistor in parallel) for use as a source of stable direct current (see Figure 12).

2.2.3.2 Anode efficiencies

A similar procedure, using an inverted solution-filled burette, was employed at the anode. However, as no weight change is involved in either of the two anode reactions, gas evolution was used as the sole means of determining the current efficiencies.

A working anode area of 2 cm^2 (stopped-off with tape and lacquer) was used for all anode current efficiency measurements, with a corresponding (scrap stainless steel) cathode area of 1 cm^2.

2.2.4 Throwing power apparatus

The relative throwing power of the various solutions tested was investigated by means of the rudimentary Haring-Blum cell shown in Figure 14.

Instead of the 'H' cell a large (2 litre) glass beaker was employed to hold the plating solution. Following solution and anode activation using scrap cathodes, the two working cathodes (A and B in Figure 14) were ground and polished (to 600 grit finish), and then weighed before being carefully wired together and stopped off to each present an area of 1 cm^2 to the anode. After careful positioning of

the cathode with respect to the anode (4 cm^2) within the solution (using a shaped block of wood - see Figure 14), a current was passed for a fixed length of time and the resulting weight difference were used to arrive at a number representing the throwing power.

The wood block employed was shaped in such a way as to present cathode B at a distance from the anode of five times that of cathode A. Cathodes A and B were electrically linked by an insulated (stopped off at all points save the contacts) lead running beneath the wood block through a machined groove. Anode and cathode arrangements were secured by means of clamps and retort stands.

2.2.5 The appearance, morphology and physical properties of the plate

In every solution tested, measurement of polarization and current efficiency was followed by the production of sample plates at various current densities. Each sample was plated for long enough (calculated from previously calculated current efficiency data) to give a 20 μm thick deposit across a 1 cm^2 area (using the cathode-holder). Following production, samples were cleaned in deionised water and ethanol prior to examination and testing.

2.2.5.1 Appearance

The appearance of each sample was subjectively assessed through comparison with a set of colour standards produced earlier from a Standard Solution and classed as White, Mid-grey, Dark-grey or Black. Sample smoothness was judged in terms of the relative adherence of a water droplet to the dry surface at increasing tilt angles, and was classed as Mirror, Smooth, Matt or Rough.

2.2.5.2 Physical properties

A complete examination of the physical properties of the various plates produced is beyond the scope of this thesis. However, it was considered that representative trends could be obtained via average

microhardness measurements (using a Leitz Micro-hardness tester and a 300 g load) in scans across the sample plates produced (impression positions are given in Figure 15). No diamond impression exceeded one third of the sample thickness.

2.2.5.3 Morphology

Following hardness-testing, a sample of plate from each solution was investigated by means of a Philips (400) Scanning Electron Microscope. A representative morphology of the deposit was recorded photographically, as were any unusual features.

2.2.6 Ancillary experiments

In addition to the main thrust of experimentation to monitor cathode polarization characteristics (and the effect of new additions thereon) and relate these to specific theoretical and practical aspects of the chromium plating process, a number of ancillary experiments were carried out. Certain of these involved the use of additional apparatus to that already listed.

2.2.6.1 Agitation

As is already clear, the co-deposition of hydrogen gas during chromium plating provides considerable catholyte stirring and hence probably reduces any concentration overpotential component in the total cathode overpotential. In an effort to determine the cathode potential (overpotential) at which η_c becomes significant, total polarization curves (in a Standard Solution at $55^{o}C$) were recorded in (a) the presence and (b) the absence of supplementary agitation.

The extra stirring was provided by means of a motorized perspex stirrer introduced alongside the cathode holder during polarization measurement.

2.2.6.2 Gas evolution

In addition to the measurement of the volume of hydrogen evolved as a way of calculating current efficiencies, notes were also made of

(i) The nature of the gas evolved in terms of estimated average bubble size.

(ii) The presence within the cathode gas of any other constituents beside hydrogen when halogen-based new additions were present in the solution. This was investigated by bubbling the cathode gas through barium sulphate solution for lengthy periods (3 hours). The gas was led away via a plastic tube from the top of the inverted burette (Figure 13).

2.2.6.3 Polarography

An effort was made to use mercury-drop polarography as a means of investigating cathode polarization in chromium plating solutions. However, reproducibility of results was found impossible to obtain (even in highly diluted solutions) and this method of investigation was abandoned.

SECTION 2

Procedure

Prior to all plating, the anode (and the solution) was activated by solution electrolysis for 30 minutes at 5 kA/m^2 (anodic current density) using a scrap cathode.

2.3.1 Polarization data measurement

2.3.1.1 Potentiodynamic (Figure 10)

Following immersion of the cathode (and attachments), the system was activated immediately (to reduce the reaction of the steel with the plating solution). The X-Y plotter recorded a trace of cathode potential (versus S.C.E.) along the Y axis versus cathode current (cathode current density in A/cm^2) along the X axis. In each test, the potential was increased until a limiting cathode current (density) became apparent. At this point the current was noted (from the potentiostat ammeter) and the potential sweep was reversed so that the curve was re-plotted back to zero current density. Knowing the value of the (apparent) limiting current, the X axis on the plot was calibrated and the entire trace was transposed onto log-linear graph paper with current density on the log scale (after the Tafel equation). The values of potential plotted were first converted to S.H.E. scale values by the addition to each of 0.2415V.

In this way, potentiodynamic cathode polarization curves were recorded in a number of plating solutions containing various concentrations of the three additions. Each curve was recorded at a potential sweep rate of 30 mV/s in the forward direction (increasing recorded current density).

The results are illustrated in Figure 16, with each curve representing average current density values from three scans.

Although limiting current density phenomena were apparently observed higher current densities had been obtained during plating

using a dc rectifier as a power source (and in the absence of the cathode holder), leading to the conclusion that at higher current densities the technique might be suspect. In addition, high plating current densities inevitably involve considerable errors in measured current (morphological outgrowths increase the real surface area) density and surface potential (the distance between probe tip and surface decreases with time).

These factors, together with an observed variation of curve shape with sweep rate (using a Standard Solution at 55°C and sweep rates of 1 mV/s, 10 mV/s and 30 mV/s. See Figure 18) led to the conclusion that more useful and reproducible data could be obtained by employing a slow, step-wise potentiostatic investigation and concentrating on the low current density (Tafel) region of the curves.

A further aspect of high sweep-rate potentiodynamically recorded polarization data in chromium deposition is illustrated in Figure 17. This apparent difference between curves recorded in forward and reverse directions (hysteresis) is considered in Section 4.3.1.1.

2.3.1.2 Potentiostatic (step-wise)

2.3.1.2.1 Stabilization time

During the potentiodynamic measurement of polarization data it became clear that at the potential sweep-rates employed the current densities recorded were dependent upon the sweep-rate (Figure 18). That is, a certain stabilization time was required at each cathode potential for the current density to attain a steady-state value. Experiments were therefore carried out to determine the minimum time reqiured (between step-wise potential increases) to produce reproducible polarization curves. To this end a number of low current density (<10 kA/m^2) cathode polarization curves were obtained (in a Standard

Solution) using step-wise potential increases but varying the time between each step. The resulting curves are shown in Figure 19. All were obtained unidirectionally (increasing potential negatively) and repeated twice. The curves in Figure 19 are averaged.

During current density stabilization, deposition is of course taking place with a consequent effect on the surface area (and the recorded current density). A stabilization time was therefore selected which ensured steady-state attainment but minimized errors due to surface area change. Five minutes was adopted as stabilization time and used in the measurement of all subsequent step-wise potentiostatic polarization data.

2.3.1.2.2 Luggin probe position

When the tip of the Luggin capillary probe does not touch the cathode surface during electrodeposition, the potential it records inevitably includes an 'iR drop' (see Section 1.3.5) the magnitude of which might be expected to increase with the distance of the probe from the surface. With this in mind, it was decided to investigate the effect of probe position (in a horizontal plane) upon the recorded polarization curve in a Standard Solution at 55°C.

The gap between the probe tip and the cathode surface was measured by feeler gauge prior to polarization measurement. The resulting curves (averaged over 5 scans) are given in Figures 20 and 21. Subsequent polarization curves were recorded using a probe distance of 1 mm and corrected accordingly (see 'Results', Figure 21 and Appendix I).

2.3.1.2.3 Curve measurement

Having established the importance of stabilization time and probe position, the following procedure was adopted in the measurement of cathode polarization curves by a step-wise potentiostatic method.

With the circuit connected as shown in Figure 11, the cathode-holder/Luggin attachment was lowered into the solution and the system was switched on. Using the potentiometer, the cathode current density and cathode potential (with respect to an S.C.E.) were recorded after a settling down period of one minute. The cathode potential was then increased by 10 mV and allowed to settle for five minutes before a reading of cathode current density (again using the potentiometer) was made. This operation was repeated until a cathode current density of 10 kA/m^2 was approached. As this involved a potential range of approximately 1 Volt, each curve took approximately eight hours to record.

Before and after each run, the position and condition of the Luggin probe and salt-bridge were checked. Whenever a bubble in or discolouration (by chromic acid) of the Agar gel medium was discovered, the corresponding data was shelved.

In general, the technique was found to give highly reproducible results. However, in an effort to ensure accuracy, each step-wise total cathode polarization curve given in the results represents the mean of three potential scans unless stated otherwise (a maximum deviation in current density of $\pm$ 2% was observed).

2.3.1.2.4 Agitation

It was assumed that at cathode current densities of less than 10 kA/m^2 the predominant overpotential component in the measured overpotential was due to charge-transfer, as any diffusion layer present at such current densities would be relatively thin and reduced still further by the local stirring action of the hydrogen evolution reaction.

However, in order to investigate the contribution of concentration overpotential to the overall polarization, a total cathode polarization curve was measured (in a Standard Solution) in the presence and absence of additional catholyte stirring via the introduction (close to the face of the working cathode) of a rotating propellor. At the current densities investigated (<10 kA/m^2), no effect on curve shape was observed.

With a reproducible technique defined, a series of cathode polarization curves were recorded in a Standard Solution at 55°C. The mean of these is given in Figure 22.

2.3.2 Current efficiency measurement

Following careful polishing (to 600 grit finish) and cleaning, the length of stainless steel strip used as a cathode was carefully weighed using a laboratory balance and the weight noted. The strip was then stopped-off using adhesive tape and inserted into the cathode holder in such a way as to present a working area of 1 cm^2 to the anode. The top end of the strip was bent in a manner which allowed accommodation of an inverted funnel (see Figure 13) before being suspended from the wall of the 'H' cell. The inverted funnel/burette arrangement shown in Figure 13 was then lowered carefully over the cathode-holder to a position well below the level of the plating solution. With the valve at the top (bottom) of the burette open, a gentle vacuum was applied and solution drawn up into the inverted burette. With the solution level in the burette at a point on the volume scale, the valve was closed and the said point was noted. Leads were then attached to the (pre-oxidized) anode and cathode and, using a potentiostat as a power source (Figure 12), a pre-determined cathode current (measured by means of a potentiometer across the 0.1 Ω resistor shown in Figure 12) was passed until most of the

solution in the inverted burette had been displaced by hydrogen evolved at the cathode. At this point, the current passage was halted and, after a thirty second settling down period, a note was made of the new solution level in the burette. Having calculated the volume of hydrogen evolved over the duration (measured by means of a stop-clock) of electrolysis the valve was opened (in the absence of a vacuum), the remaining solution allowed to re-enter the 'H' cell, and the entire gas-collection unit lifted away from the cathode.

After removal of the cathode-holder, and hence cathode, from the solution, the weight of chromium deposited was calculated (after very careful removal of adhesive tape, and subsequent cleaning in deionised water and methanol) by subtracting the initial cathode weight from the final cathode weight.

Knowing the weight of chromium and hydrogen (volume) deposited in a particular time at a known cathode current density, Equation 1.1.1,1 was used to determine the number of Coulombs/second (Amperes) involved in each reaction during plating. This partial current, when expressed as a percentage of the overall cathode current, gave a direct value for the current efficiency of the reaction at the overall cathode current density being investigated (Equation 1.1.1,2). Clearly, the current efficiency of the third cathode reaction which takes place during plating (the partial reduction of CrVI to CrIII) cannot be measured directly. It is determined by subtracting calcu lated values for the plating and hydrogen evolution efficiencies from 100%.

An equivalent procedure was employed to monitor corresponding anode current efficiencies. However, reliance on stopping off of the anode to give a fixed working area (as opposed to the use of the accurately dimensioned perspex holder when determining cathode current

efficiences) resulted in a greater degree of inaccuracy in anode current efficiency results.

Each current efficiency value related in this work refers to an average of three values unless otherwise stated. The deviation from the mean in cathode current efficiency results was a maximum at the lowest overall cathode current densities employed (as might be expected) and at maximum solution addition concentrations.

Two series of cathode reaction current efficiency measurements were made in each solution tested at 55°C (values for a Standard Solution are given in Figures 23 to 28). The first were obtained at total cathode current densities of between 10 kA/m^2 and 50 kA/m^2, in an attempt to correlate throwing power with the variation of plating efficiency with (high) current density. The second series were obtained at total cathode current densities of less than 10 kA/m^2 and were intended for combination with total cathode polarization curves to produce partial polarization curves.

2.3.2.1 Partial polarization data evaluation

Following the determination of the overall cathode polarization curve for a Standard Solution at 55°C (Figure 22), closer examination revealed a range of current densities and corresponding cathode potentials in which Tafel conditions might be assumed to prevail. This region is shown magnified in Figure 29.

In order to plot partial polarization data, current efficiency values corresponding to certain total cathode current densities in this range were determined (Figures 23, 25 and 27) for a Standard Solution. The plotting of partial current densities at potentials corresponding to total cathode current densities (on a log-linear scale) gave the partial cathode polarization curves (for a Standard Solution) shown in Figures 30, 31 and 32.

2.3.3 Throwing power measurement

The apparatus shown in Figure 14 was used to determine the throwing power of a solution at a particular and current density by simply passing a current through the circuit and measuring the weight of metal deposited on each of cathodes A and B. Knowing the deposit weight difference between A and B, and the ratio of anode to cathode distances (P = 5), the Field formula (1),

$$T = \frac{P - M}{P + M - 2} \times 100 \qquad (2.3.3,1)$$

was employed to determine the solution throwing power, T. The results of tests carried out in a number of solutions at 55°C and a current density of 3 kA/m^2 are given in Table 1.

2.3.4 Deposit appearance, properties and morphology

Samples of chromium plate were produced from fresh solutions by electrolysis for two hours at a cathode current density of 3 kA/m^2. The deposits produced (using the cathode holder to give 1 cm^2 samples) were used in comparative tests in an attempt to correlate throwing power, current efficiency variation with current density, polarization gradient, deposit appearance and properties.

Physical properties of the plate produced were represented by deposit micro-hardness. Each sample was subjected to 22 diamond impressions (Figure 15) at specific points on the surface, and the resulting values of imprint diameter (in μm), mean imprint diameter, standard deviation in imprint diameter and resultant mean VPN are given in Table 2.

Prior to micro-hardness testing, the macro-appearance of each sample was compared to a series of pre-prepared 'standard' samples

of varying colour. The resulting observations are given in Table 3. Following visual observation of plate colour, the relative finish of each sample was estimated (approximately) in terms of the angle of inclination at which the plate sample could just hold a drop of water (from a pipette) during progressive tilt. Whilst clearly not accurate, this procedure provided a reasonable test of relative surface finish. The estimated finish is included in Table 3.

A more accurate impression of relative surface finish is given in the photomicrographs of plate morphology included as Plates 1 to 16.

2.3.5 Arrhenius plot determination

From the shape of a plating partial polarization curve, a value for the expression $\lambda \times \alpha_{term}$ was obtained. This was then used with the modified Rogers and Burr (43) equation (1.3.9.2,3) to provide a means of calculating the thermodynamic constants for activation in the deposition process. This first necessitated the practical determination of the variation of log of the partial (plating) current density with the inverse of the absolute plating temperature (i.e., an Arrhenius-type plot).

Initially using a Standard Solution at temperatures of 45^{o}, 50^{o}, 55^{o}, 60^{o}, and $65^{o}C$, the arrangement shown in Figure 11 was adopted and used in the following way.

The plating partial polarization curve at $55^{o}C$ was examined and a number of cathode potentials corresponding to the apparent Tafel region were selected. Maintaining a fixed cathode potential, and using the arrangement shown in Figure 11, the solution temperature was varied in 5^{o} increments (with a 15 minute settling down period at each temperature prior to measurement) and the corresponding total cathode current density (i_t) was noted. Then at each temperature

and corresponding total cathode current density, the arrangement shown in Figures 12 and 13 was employed to determine a plating current efficiency and a plating partial current density (i_{Cr}). A plot of log i_{Cr} versus 1/T (with T in Kelvin) resulted in an Arrhenius-type slope from which the activation enthalpy could be approximately determined.

Calculation of ΔH_A required (see Equation 1.3.9.2,2) the pre-determination of a value for the overpotential η at the particular cathode potential chosen. As overpotential represents the difference between the measured cathode potential E and the single potential ε_M, this in turn required a value for the single potential for chromium deposition from a 450 g/l solution of chromic acid. Rogers and Burr (43) took ε_{Cr} to be - 0.8V versus S.C.E. as a rough average of values in the literature for reversible chromium metal to ion couples (using a 2.5M solution of CrO_3 and a sulphate ratio of 100:1).

The precise value of ε_{Cr} for metal deposition from a chromic-acid based plating solution is difficult to define, particularly in view of the controversy over the ions present. It was therefore decided to employ the Nernst equation (Equation 1.2.1,9) to estimate ε_{Cr} for the 4.5M solution employed in this work.

In order to calculate ε_{Cr} using the Nernst equation, it was first necessary to assign values to ε_{Cr}^{o} (standard single potential) and CrVI ion activity.

Values for ε_{Cr}^{o} from the hexavalent state are not directly available in the literature, but it was possible to calculate the concentration-dependent contribution to ε_{Cr};

$$\varepsilon_M = \varepsilon_M^o + \frac{RT}{zF} \ln(h_M z+)$$

where h = n f (m/m^{o}), and

n = number of moles of chromium-bearing ionic species produced through salt ionization

f = mean molal activity coefficient

m/m^{o} = molality.

According to Hoare (118), the predominant species in concentrated aqueous chromic acid is the trichromate ion $HCr_3O_{10}^-$:

$$3CrO_3 + H_2O \rightarrow HCr_3O_{10}^- + H^+$$

For this ionization, n = 1/3.

Molality = 4.5 moles of CrO_3/kg of solvent water.

A value for the mean molal activity coefficient is not available. However, on the basis of data for other salts (162), it was estimated that a reasonable value for f might be 0.25.

On the basis of these assumptions the concentration-dependent contribution was calculated to be approximately 0.005 Volts. As this is very low, particularly when the uncertainty of ε_{Cr}^{o} is considered, the concentration-dependent contribution was ignored and ε_{Cr} is assumed equal to ε_{Cr}^{o} in subsequent calculations.

Initially, Rogers and Burr's value for ε_{Cr} of -0.8V (S.C.E.) or -0.56V (S.H.E.) was considered for use in equations 1.3.9.2,2 and 1.3.9.2,3. However, ε_{Cr} = -0.565V (incorporating the concentration term) yields considerably negative values for ΔG_A (the so-called free energy of activation) in many of the solutions at the potentials selected (Table 7c). As this seemed unlikely, scrutiny of the relevant overall polarization curves (Figures 22,34,35,36) and a knowledge of the approximate potential in each solution at which chromium deposition commences, was used to select another value for

ε_{Cr}. Using ε_{Cr} = -0.7V (S.H.E.), the values for ΔH_A, ΔS_A and ΔG_A given in Table 7a were generated. This time, ΔG_A values are positive with the exception of those from a solution containing 10 g/l ClO_4^-. However, it is considered that this anomaly is due to the apparently abnormally high value for $\lambda \times \alpha_{term}$ of 4 in this solution. Substitution of $\lambda \times \alpha_{term}$ = 3 (as is the case in a solution containing 5 g/l ClO_4^-) gives more reasonable values and serves to indicate the sensitivity of ΔG_A to errors in $\lambda \times \alpha_{term}$.

With this in mind, the calculations were repeated, but using ε_{Cr} = -0.65V (S.H.E.), in order to determine the sensitivity of ΔG_A, ΔH_A and ΔS_A to the value of η employed in equations 1.3.9.2,2 and 1.3.9.2,3. As Table 7b shows, the values of ΔH_A and ΔG_A are changed (ΔS_A is unaffected), but the trends remain the same.

In all of these calculations it was first necessary to determine a value for the constant $C_M z+$ in equation 1.3.9.2,2 (ϵ, k' and h' are known constants and T was taken to be 328K throughout), the number of depositing species per square metre of the cathode surface.

A molar concentration of 4.5M/l is equivalent to 2.813×10^{21} M/cm^3, which is in turn equivalent to a distribution of 1.928×10^{14} M/cm^2. Assuming a mole fraction of 0.0749 (4.5/(55.6 + 4.5)), this equates to a distribution of chromium-bearing molecules on the cathode surface of approximately 5.2×10^{12} molecules/cm^3. When combined with the other constants this (5.2×10^6 molecules/m^2) yielded a value for the first term in equation 1.3.9.2,2 of

$\epsilon C_M z+.\frac{k'T}{h'} \approx 5.687 \times 10^{10}$, and $\log (\epsilon C_M z+.\frac{k'T}{h'}) = 10.755$.

The $\log_{10} i_{Cr}$ values used in equation 1.3.9.2,2 are given in Tables 6.

2.3.6 New solution additions

2.3.6.1 Introduction

An initial series of experiments were undertaken in an attempt to determine the effect of the three new solution additions (to a Standard Solution) in various concentrations upon industrially important properties of chromium plate and the chromium plating process, such as current efficiency, throwing power, appearance (macro and morphological) and hardness.

The techniques applied in the investigation of plating mechanism outlined earlier were then employed with each solution tested in an attempt to correlate the effect of solution additions on properties with their effect upon such quantities as Tafel slope, α_{term}, ΔG_A, ΔH_A, ΔS_A.

Each new solution was therefore subjected to tests which yielded results for (a) current efficiency variation with total cathode current density, (b) throwing power, (c) appearance of deposit (macro and morphological), (d) hardness of deposit, (e) overall cathode polarization data (including pre-plating data), (f) partial cathode polarization data, (g) Tafel slopes, (h) α_{term}, (j) ΔG_A, ΔH_A, ΔS_A.

2.3.6.2 Throwing power

The effect of the new solution additions upon the throwing power of a Standard Solution is given in Table 1. All solutions were tested at $55^{o}C$ and a cathode current density of 3 kA/m^2.

2.3.6.3 Current efficiency

Current efficiency measurements were made for each cathode reaction at total cathode current densities of 10, 20, 30, 40, and 50 kA/m^2 in every solution tested. The results are given in

Figures 24, 26, 28, 40, 42, 44, 46, 48 and 50. The procedure adopted was the same as that outlined earlier for the measurement of Tafel region current efficiencies. A temperature of 55°C was maintained throughout.

Corresponding anode data is given in Figures 60 to 65.

2.3.6.4 Deposit appearance

As already explained, samples of plate from each solution were prepared using a standard procedure of electrolysis for 2 hours at 3 kA/m^2 and 55°C.

Following observations of macro-appearance (relative to a series of 'standard' samples), each deposit sample was mounted for electron-microscopic examination by means of a Philips S.E.M. 400. From a total of 200 photomicrographs subsequently taken, 18 have been selected to represent the morphology of plate produced from each solution tested (Plates 1 to 18).

2.3.6.5 Hardness of deposit

Subsequent to macro and micro observations of plate appearance, each sample was subjected to a series of micro-hardness tests, using a Leitz micro-hardness tester and a 300 g load. The impression positions are shown in Figure 15 and the results are given in Table 2.

It should be noted that the intense hardness of certain deposits led to values beyond the scope of the conversion tables provided and necessitated the use of the equation

$$VPN = \frac{1854 \times P^*}{d^2}$$

where P^* = load in grams, and d = mean impression diameter in μm.

From this equation it is apparent that errors in mean impression diameter correspond to greater errors in VPN at higher hardness values.

For this reason it is suggested that VPN values of greater than 1250 (in Table 2) be read as trends rather than definitive.

2.3.6.6 Overall cathode polarization curves

The same procedure was employed with the solutions containing new additions as was defined with regard to a Standard Solution in section 2.3.1.2. The results for each solution tested are given in Figures 22, 34, 35 and 36, and include the low potential-low current density regions prior to the onset of deposition. More detailed curves showing the apparent Tafel regions are given in Figures 29, 37 and 38.

2.3.6.7 Partial cathode polarization data

Again, the technique outlined in section 2.3.2.1 for a Standard Solution was employed in each solution tested. Low current density values of reaction current efficiencies (illustrated in Figures 23, 25, 27, 39, 41, 43, 45, 47 and 49) were used with overall polarizatio curves (Tafel regions) to produce the individual reaction partial polarization curves shown in Figures 30, 31, 32, 51 to 56.

The Tafel slopes of these partial curves were then analysed (for the plating and hydrogen evolution reactions) to give the values for $\lambda \times \alpha_{term}$ and (assuming certain values of λ, and $\alpha_{dl} = 0.5$) α_{film} recorded in Tables 4 and 5.

2.3.6.8 Thermodynamic activation data (deposition reaction)

The technique defined in section 2.3.5 was used for each of the new solutions (selecting constant cathode potentials corresponding to the particular Tafel region observed for the plating reaction in each solution) over the same temperature range. The data obtained was tabulated in Tables 6, used to plot the Arrhenius curves shown in Figures 33, 57, 58 and 59, and given as values of ΔH_A, ΔS_A and ΔG_A in Tables 7a, 7b and 7c.

2.3.6.9 New addition exhaustion

In an effort to discover whether the new additions investigated were consumed during deposition, an experiment was carried out to determine the variation (if any) of plating efficiency with time (using long periods of electrolysis) in each new solution tested.

A fresh solution of each solution was made up and worked at 3 kA/m^2 and 55°C for a period of 16 hours. At 4 hour intervals the electrolysis was temporarily halted and a measurement of plating current efficiency made. The results are given in Table 8.

2.3.6.10 New addition combinations

An extensive investigation into the effect of various addition combinations upon the appearance of the plate produced (the major criterion of the industrial plater) revealed that the presence of $KBrO_3$ at low concentrations (5 g/l) in any plating solution always had a deleterious effect (even in the presence of $KClO_4$ at high concentrations). Similarly, the presence of $K_2B_2O_4$ in any solution had the effect of greatly increasing the incidence of cracking and flaking in the resulting deposit.

For these reasons, and in an effort to avoid any further difficulties in interpretation, the techniques employed in mechanism determination were only applied to Standard Solutions containing one additional component, and not to 'cocktails'.

RESULTS

3.1 Technique establishment for the reproducible measurement of polarization data

3.1.1 Potentiodynamic polarization curves

Polarization curves were measured potentiodynamically by means of the apparatus and technique referred to in sections 2.2.2.1 and 2.3.1.1. Five curves were recorded in each solution (at 55°C, 30 mV/s and using a touching Luggin probe), representative means of which are shown in Figure 16. The shapes of the curves are similar, consisting of a low current density region of shallow slope followed by an abrupt change to a higher current density region in which the slope steepens considerably. A limiting current density is apparent in all curves.

The degree of spread apparent during the recording of the five scans used to provide the mean curves given in Figure 16, combined with the inherent scale inaccuracies (when examining the region of the curves corresponding to current densities of less than 10 kA/m^2), prompted an investigation into the effect of sweep rate upon curve shape and reproducibility. For this, and subsequent technique establishment tests, a Standard Solution was employed at 55°C.

3.1.1.1 The influence of sweep rate

Figure 18 shows the effect of sweep rate upon the shape and reproducibility of the potentiodynamic cathode polarization curve in a Standard Solution at 55°C (each curve represents the mean of five scans). A change in curve shape and an improvement in reproducibility was observed as sweep rate was reduced, although no variation in 'limiting current density' was apparent.

Acknowledging the apparent sensitivity of polarization curve shape and reproducibility to sweep rate, it was decided to employ the 1 Amp range (10 kA/m^2 on a 1 cm^2 cathode) potentiostat in a step-wise potentiostatic mode (thereby permitting effective sweep rates of considerably less than 1 mV/s) to record polarization data (see Sections 2.2.2.2 and 2.3.1.2).

One phenomenon of the potentiodyanically recorded curves which disappeared with decreasing sweep rate was curve hysteresis. Figure 17 shows a typical potentiodynamic overall polarization curve (Standard Solution) recorded at a high sweep rate (100 mV/s) in which hysteresis is evident at current densities greater than 10 kA/m^2. At moderate sweep rates (10 mV/s) no hysteresis was evident.

3.1.2 Potentiostatic (step-wise) polarization curves

3.1.2.1 The influence of stabilization time

The results are given in Figure 19 (each curve is an average of five scans), from which it is apparent than an increase in stabilization time from 1 minute (= 0.167 mV/s) to 3 minutes (= 0.056 mV/s) caused an increase in the slope of the overall cathode polarization curve (at current densities greater than 1 kA/m^2), and that a further increase from 3 minutes to 5 minutes (= 0.033 mV/s) had no further effect upon the slope. As a result of this (and the observed decrease in error with increasing stabilization time) it was decided to record all subsequent polarization curves using a step-wise potentiostatic method with the 1 Amp potentiostat and employing a 10 mV potential increment at time intervals of 5 minutes - an effective 'sweep rate' of 0.033 mV/s.

A further argument for the adoption of a step-wise potentiostatic technique was the lack of curve resolution (and hence accuracy) at low current densities (< 1 kA/m^2) inherent in the potentiodynamic technique. Data subsequently obtained potentiostatically revealed facets of the curves which had not hitherto been apparent (compare Figure 16 and 22).

3.1.2.2 The influence of Luggin probe position

The polarization curves measured potentiostatically to illustrate the effect of stabilization time upon curve shape were all obtained using a Luggin capillary probe (the same one throughout) positioned

1 mm away from the cathode surface, a position selected after a series of experiments had been carried out to determine the appropriate (iR drop) correction factor.

Quantification of the iR drop correction was undertaken through the recording of a series of potentiostatic polarization curves (in a Standard Solution at 55°C) in which everything was maintained constant except the distance of the (same) Luggin probe tip from the cathode surface. The results are given in Figures 20 and 21, and show that the probe tip to cathode distance has a bearing on the curve shape at current densities greater than 2 kA/m^2, and that the effect increases with current density in an apparently non-linear manner. At a current density of 3 kA/m^2 the additional potential drop corresponding to a probe distance of 1 mm (and 2 mm) was found to be 1 mV, increasing to a value of 5 mV at a current density of 9 kA/m^2. (Figure 20). The non-linearity of the potential drop variation with current density hinted at a two-component aspect to the potential drop between the probe and the surface, a predominant current density-sensitive component combined with a probe gap-sensitive component of less importance. An effort has been made to derive an approximate expression linking potential drop with probe gap and cathode current density, and this is outlined in Appendix I.

Figure 21 shows the effect of probe position upon the polarization curve in the apparent Tafel region (subsequently analysed in mechanism determination), magnified to illustrate the apparent constancy of the potential drop in this region (<2 mV - see Appendix I).

All subsequently measured overall cathode polarization curves were corrected accordingly prior to inclusion in the Results section of this work, having been recorded using a 1 mm gap instead of a touching probe.

Barnartt (163) used a potential mapping device to monitor primary current distribution around capillary tips at electrodes, and concluded (with other researchers (164,165,166,167,168) that a touching probe shields the working electrode, thereby decreasing the recorded polarization. His analysis revealed that for a probe of tip radius r, greater accuracy in measurement is afforded at a probe tip to cathode distance of 4r, although employment of such a system necessitated a correction to all values of cathode potential recorded.

Figures 20 and 21 show that at a cathode current density of 9 kA/m^2, the additional potential drop due to a probe tip to cathode distance of 1 mm is 5 mV. A proportionate correction (see Appendix I) was applied at lower current densities in all polarization data subsequently presented.

One inaccuracy in technique which could not be overcome was the difference in real and recorded cathode current density which existed at higher current densities as a result of the effect of the growing deposit upon the real cathodic surface area. This inaccuracy was counteracted to an extent by the masking effect of the hydrogen evolution reaction which decreased the effective area of the cathode available for deposition. A further consideration of the errors introduced into recorded data as a result of changing surface area is given in Section 3.6.

3.2 Chromium plating mechanism evaluation using partial polarization measurements in a Standard Solution

Using the apparatus described in sections 2.2.2.2 and 2.2.3.1 and the technique referred to in sections 2.3.1.2 and 2.3.2.1, current efficiencies (Figures 23, 25 and 27) were used with the overall cathode polarization curve (Figure 29) to give the partial

polarization curves shown in Figures 30, 31 and 32 for a Standard Solution.

The partial polarization curves corresponding to the plating reaction and the hydrogen evolution reaction demonstrated two distinct regions - a low current density region in which the gradient was relatively constant, followed by a higher current density section in which an increasing gradient was observed. It was assumed that the low current density, shallow gradient sections of the curves corresponded to conditions in which charge-transfer was the major contributor to the total recorded overpotential, and that the subsequent change in gradient at higher current densities corresponded to an increase in influence of diffusion-controlled processes. Attention was concentrated upon the sections of the curves where charge-transfer was assumed to predominate, and the Tafel equation could apply.

The Tafel slopes of the plating and H.E.R. partial polarization were measured (to accuracies of $\pm$ 7 and $\pm$ 30 mV/decade) for a Standard Solution at 55^{o}C and are included in Table 4. Data subsequently derived from the measured Tafel slopes were then used in the consideration of plating and hydrogen evolution mechanisms (see Discussion).

3.3 Rate process theory in the chromium deposition reaction

Using the modified Arrhenius approach outlined in sections 1.3.9.2 and 2.3.5, the variations in plating partial current density with absolute temperature were obtained at three cathode potentials within the Tafel region for a Standard Solution. The results are given in Tables 6a to 6c, and are plotted as Arrhenius curves in Figure 33.

Subsequent analysis of the Arrhenius slopes obtained for deposition from a Standard Solution yielded (using the methods outlined in section 2.3.5) values of ΔH_A, ΔS_A, and ΔG_A given in Table 7.

The values of the thermodynamic constants generated for the plating reaction in a Standard Solution are considered in the Discussion.

3.4 The effect of the new additions upon the plating process and the plate produced

The influence of additions of $KClO_4$, $KBrO_3$ and $K_2B_2O_4$ (at concentrations of 5, 10 and 15 g/l in freshly prepared Standard Solutions) upon certain practical aspects of the plating process and the plate produced is illustrated in Tables 1, 2 and 3, Figures 24, 26, 28, 40, 42, 44, 46, 48 and 50, and Plates 1 to 16.

3.4.1 The influence on throwing power

The effect of the additions upon a Standard Solution throwing power as measured by the Field formula (equation 2.3.3,1) was apparently considerable, and is shown in Table 1.

The presence of $KClO_4$ has an apparently profound effect upon the throwing power in that it causes a change from negative (in Standard Solution) to slightly positive values at all concentrations. This contrasts markedly with the effects of $KBrO_3$ and $K_2B_2O_4$ which both worsen the throwing power of the solution, making it more negative. The $KBrO_3$ demonstrates the most negative effect at even the lowest concentrations.

3.4.2 The influence on current efficiencies

The variation of cathode reaction current efficiencies with current density (>10 kA/m^2) in each of the solutions investigated is given in Figures 24, 26, 28, 40, 42, 44, 46, 48 and 50. The corres-

ponding variations in anode reaction current efficiencies are given in Figures 60 to 65.

3.4.2.1 Cathode current efficiencies

In all solutions tested, a general increase in plating efficiency with current density was observed with the exception of those containing $KClO_4$, in which plating efficiency peaked and subsequently fell at current densities greater than 30 kA/m^2.

The efficiency of the hydrogen evolution reaction shows a gentle decrease with increasing current density in all solutions.

Maximum plating efficiencies (~30%) were obtained in solutions containing $KBrO_3$. The other solutions demonstrated peaks of 25% ($K_2B_2O_4$) and 22% ($KClO_4$).

Hydrogen evolution was evidently encouraged in the presence of ClO_4^- at higher current densities but repressed by BrO_3^-, $B_2O_4^{2-}$ (Figures 26, 42, 48).

3.4.2.2 Anode current efficiencies

With each new addition present, the variation of the efficiency of the re-oxidation reaction (CrIII to CrVI) did not appear to differ by much from that observed for a Standard Solution. In all solutions tested, the re-oxidation efficiency was seen to drop considerably at anode current densities of greater than 20 kA/m^2. The one exception was the solution which contained a concentration of 15 g/l $KBrO_3$ (Figure 63). In this solution, the re-oxidation efficiency levels off at approximately 20% for all current densities greater than 20 kA/m^2.

3.4.3 The influence on macro-appearance

The influence of the specific solution additions upon the macro-appearance of 'standard' samples of plate produced at current densities of 3, 10 and 30 kA/m^2 (at 55^oC) is given in Table 3, after comparison with a series of standard colour samples.

The effect of the presence of each addition was apparently clear. $KClO_4$ had the effect of extending the so-called bright range at all concentrations tested, whereas $KBrO_3$ had an opposite deleterious effect, producing unsatisfactory deposits at the lowest current densities. While $K_2B_2O_4$ caused a general darkening of the deposit (compared to that produced in a Standard Solution), its worst effect was on deposit smoothness.

3.4.4 The influence on morphology

Plates 1 to 16 show the effect of the additions upon the morphology of plate produced at 3 kA/m^2 and 10 kA/m^2 (and 30 kA/m^2 in a Standard Solution) and at 55^oC. The plates shown are representative of a greater number.

Plates 1 and 2 give the morphology of chromium deposited from a Standard Solution within the so-called bright range. The morphology is fine, nodular and contains a crack network. At higher current densities the deposit becomes more dendritic (Plates 3 and 4).

In the presence of 10 g/l $KClO_4$, the morphology is nodular once again but with a very much lower crack density and demonstrating no tendency to dendrites at the higher current density (Plates 5, 6, 7 and 8). Under higher magnification (Plate 8) it is apparent that each nodule has a 'raspberry' appearance, consisting of an agglomeration of smaller nodules.

Plates 9 and 10 show the effect of 10 g/l of $KBrO_3$ in a Standard Solution upon the deposit produced at a current density of 3 kA/m^2. In contrast to plate produced from the previous solutions, this deposit exhibits a highly cracked morphology with flaky outgrowths. At higher current densities, the deposit shows an extremely dendritic morphology (Plates 11 and 12).

The presence of 10 g/l of $K_2B_2O_4$ in a Standard Solution caused a change in morphology to that shown in Plates 13, 14, 15 and 16. At low current densities, the deposit exhibits a nodular appearance in whic fine cracks are evident, and in which some nodules are apparently growing at a faster rate than others. At higher current densities, it is apparent that the outgrowths evident at the lower current density have formed dendrites which have grown out of control, while the severity of cracking has increased.

Plates 17 and 18 show severe cracking and flaking in a deposit produced from a solution containing 10 g/l $K_2B_2O_4$ at 3 kA/m^2. The flaking was produced through the inadvertant bending of a sample of plate, but allowed certain observations to be made which are given in Appendix II.

3.4.5 The influence upon micro-hardness

The effect of solution additions upon the micro-hardness of the deposits produced is given in Table 2 along with the variations in diamond impression diameter with position on the sample. Standard deviations in impression diameter are included as it is thought that these might relate to deposit morphology.

The presence of all three solution additions (separately) caused a change in deposit hardness when compared to that produced from a Standard Solution. The greatest increase in hardness was

observed in plate produced in the presence of $KClO_4$ with increasing concentration corresponding to increasing hardness. Plate produced from solutions containing $K_2B_2O_4$ demonstrated increased hardness (compared to Standard Solution plate) but only a slight increase, whereas the hardness of chromium deposited from solutions containing $KBrO_3$ was somewhat lower than that produced in a Standard Solution alone.

3.5 The influence of the new solution additions upon those aspects of the deposition process investigated using the (Tafel and Arrhenius) techniques referred to earlier

3.5.1 Polarization curve analyses

In each solution investigated, overall cathode polarization curves recorded step-wise using 10 mV potential increments, a five minute stabilization time and a probe tip to cathode gap of 1 mm, were corrected for probe position and plotted on log-linear scales (Figures 22, 34, 35 and 36). The apparent Tafel region of each curve (all measured at 55°C) was magnified and is presented in greater detail in Figures 29, 37 and 38.

Cathode current efficiency measurements for each reaction in each solution and corresponding to the current density range in Figures 29, 37 and 38, were carried out and are presented in Figures 23, 25, 27, 39, 41, 43, 45, 47 and 49. When combined with the data given in Figures 29, 37 and 38, these yielded partial polarization curves for each cathode reaction in each solution tested, and these are illustrated in Figures 30, 31, 32, 51, 52, 53, 54, 55, and 56.

Using the resulting partial polarization data for the plating and hydrogen evolution reactions (the curves plotted for the CrVI

to CrIII reaction were considered inconclusive in terms of Tafel slopes), apparent Tafel slopes were measured and are presented in Table 4. From the measured Tafel slopes, values for the expression $\lambda \times \alpha_{term}$ were obtained for the two reactions in each solution tested, and these are given in Table 4 as well.

Further interpretation of this and subsequently derived data is undertaken in the Discussion.

3.5.2 Arrhenius data

With the employment of the technique developed using a Standard Solution to determine the thermodynamic constants of activation for the plating reaction, a series of two Arrhenius-type plots (at values of cathode potential corresponding to the apparent Tafel regions in Figures 30, 51, and 54) were drawn for each solution, and are given in Figures 35, 57, 58 and 59 (in tabular form in Tables 6a to 6y).

From the slopes of these plots, and using the pre-determined values of η and $\lambda \times \alpha_{term}$, values of ΔH_A, ΔS_A and ΔG_A were obtained for the plating reaction in each solution. These are given in Table 7.

The apparent effects of the solution additions upon the thermodynamic constants of activation for the plating reaction are considered in the Discussion.

3.6 Errors

Despite the stress placed upon accuracy and reproducibility of technique, a degree of spread was apparent in all results recorded and is given with the results (Tables 2, 4 and 5) where appropriate.

Experiments showed that the shape of the potentiodynamically recorded overall cathode polarization curve in a Standard Solution was sensitive to the sweep-rate and probe position employed. The error due to sweep-rate was reduced from a maximum of $\pm$ 8% (of

current density) at 30 mV/s to a maximum of ± 6% at 1mV/s. Subsequent potentiostatically recorded cathode polarization curves demonstrated a further reduction in the maximum spread in current density to ± 2% at an effective sweep-rate of 0.033 mV/s (having corrected for potential drop due to probe position - see Appendix I). However, the application of measured current efficiencies (with the inherent errors - ± 8% in efficiency at current densities <5 kA/m^2, ± 5% in efficiency at current densities >5 kA/m^2) to overall cathode polarization data introduced errors into the partial polarization data subsequently generated, and thus into the measured Tafel slopes given in Table 4. The errors introduced into the data at this point are carried through subsequently derived values for $\lambda \times \alpha_{term}$, α_{term}, α_f, and ΔH_A, ΔG_A and ΔS_A.

In the case of the thermodynamic quantities of activation for the plating reaction, a further error is introduced through the experimental determination of the Arrhenius slopes (in which each i_{Cr} value is the mean of three), estimated as being approximately ± 10% (maximum) of the gradient. The errors in $\lambda \times \alpha_{term}$ and Arrhenius slope translate to a maximum calculated error in ΔH_A of ± 18% in a Standard Solution, ± 29% in Standard + 10 g/l $KClO_4$, ± 12% in Standard + 15 g/l $KBrO_3$, and ± 19% in Standard + 15 g/l $K_2B_2O_4$. For this reason, all values for thermodynamic quantities presented are intended only to indicate trends.

Although a straight-line relationship is apparent in a number of the Arrhenius plots, this is in itself erroneous, as Equation (1.3.9.2,3) predicts that the slope should in fact be slightly temperature-dependent (remember that an average value for T in the term -0.43T had to be selected in order to allow the technique to

be applied). Obviously, an apparent straight-line relationship cannot be ignored, but the anomaly should be noted.

Measured throwing power data were recorded using a fairly rudimentary technique and, although each measurement was repeated and averaged for inclusion in Table 1, it is not intended that the results should be taken as anything other than trend-indicators (particularly in view of some of the low deposit weights recorded).

3.6.1 Cathode surface area variation during plating

One further, important, source of error in recorded polarization data which must be accounted for is the error in current density measurement which exists due to cathode surface area change once cathodic metal deposition has commenced.

The current density recorded during the measurement of polarization data is a function of the cathode surface area, which is assumed to remain unchanged (1 cm^2 in this work) as long as no metal deposition has occurred. However, this assumption becomes invalid at cathode potentials more negative than that at which plating commences because the metal deposit (unless absolutely flat and parallel to the original surface) causes an effective increase in cathode surface area. The extent of this increase depends upon the morphology of the deposit. Plates 1 to 16 indicate that chromium deposits with a nodular morphology in the solutions tested (at industrial plating current densities). This being the case, it is reasonable to assume that every πr^2 (area of a circle) of initial uncovered cathode surface becomes $2\pi r^2$ (surface area of a hemisphere) once metal deposition is underway. This infers that the current density recorded is double the actual current density (at potentials more negative than the deposition potential). However, a corresponding correction has not been applied. For two reasons;

(i) Assuming a nodular deposit the applied correction would be the same at all current densities and would therefore simply shift the overall polarization curves (in the plating potential range) to lower current densities without affecting the slopes.

(ii) Exactly the same correction would have to be applied to current densities used for current efficiency measurements. The partial polarization curves generated by combining current efficiency measurements with overall polarization curves would therefore remain unchanged.

Circumstantial support for the validity of these assumptions regarding the non-application of a surface-area error correction lies in the partial polarization curves generated for the plating and hydrogen evolution reactions, which (as will be shown) demonstrate fairly well-defined straight-line (Tafel) regions.

However, it is accepted that at high current densities in some solutions where a dendritic deposit morphology results, a complex correction to current density is required. For this reason, no attempts have been made to analyse the high current density regions of the partial polarization curves.

3.6.2 The application of the dual barrier model

The cathode film is obviously important in influencing the kinetics of chromium deposition but it has been assumed that the dual barrier model (and therefore equation 1.3.9.1.3,1) applies to all charged transfers including those which occur within the film. This assumption implies that the importance of the film lies more in its ability to allow electrons through prior to charge transfer in the double layer (where it is assumed the R.D.S. occurs) rather than in its effect upon intra-film charge transfer. Obviously the application of the dual barrier model to include charge transfer within the film

is doubtful (as a dual barrier does not exist for these charge transfers), it is considered that this assumption provides the only way to analyse data. It is, moreover, likely that the contribution to the total overpotential from the final charge transfers within the film is relatively very small.

DISCUSSION

4.1. Introduction

This work undertaken may be divided into four categories :-

(a) The establishment of an accurate, reproducible method of determining cathode polarization data during the electrolysis of concentrated, chromic acid-based chromium plating solutions.

(b) The use of the said technique to record overall, and then partial (by means of selective low current density current efficiency measurements) cathode polarization curves for each of the cathode reactions in a Standard Solution. The subsequent use of the Tafel regions of the curves (in conjunction with previously proposed mechanisms) to give an indication of the nature of the rate-determining step (R.D.S) in the plating reaction. The determination of the enthalpy, entropy and free energy of activation for the plating reaction by means of a modified Arrhenius-type expression employing data obtained from the reaction partial polarization curves mentioned earlier (and varying the solution temperature).

(c) An evaluation of the beneficial (or otherwise) effects of three new inorganic additions to a Standard Solution in terms of their influence upon solution throwing power, current efficiencies, physical properties and appearance of the deposit produced (under working conditions).

(d) An investigation of the new solutions using the techniques outlined in (a) and (b). An attempt to interpret the 'property' effects of the new solution additions in terms of the mechanism elucidation approaches employed.

4.2. Accuracy and reproducibility in data measurement

Although overall cathode polarization curves obtained during

electroplating have been used in the past to provide the basis for chromium plating mechanism theories (126, 127, 135, 118) in most cases insufficient information has been provided with regard to the accuracy of the technique employed in their measurement. It has been demonstrated in this work that curve shape is apparently sensitive to the rate of potential change (in potentiostatic and potentiodynamic data measurement) employed, and the distance between the Luggin probe tip and the cathode surface.

Although Hoare (118) indicated that his curves were recorded by taking steady-state measurements, he neglected to expand upon this or comment upon the relative positioning of the probe he employed. A schematic diagram of the apparatus he used reveals that in place of a Luggin capillary probe he simply positioned the cathode end of the salt bridge (plugged with glass wool) in the vicinity of the cathode. The (albeit small, in all probability) additional potential drop measured as a result is not apparently accounted for in his results. Comparison with polarization data recorded in this work is further complicated by his use of a platinum bead cathode and a 1M $H_2Cr_3O_{10}$ solution at $23^{o}C$.

The cathode polarization curves recorded by Okada and Yamamoto (156) were obtained potentiostatically under implied steady-state conditions but no details were given as to the means employed to monitor changes at the cathode surface (i.e. the nature of the probe and its position relative to the cathode). Like Hoare, they investigated relatively dilute (50g/l CrO_3) 100 : 1 ratio solutions with platinum cathodes, but also recorded some data using mild steel cathodes (which allows some limited comparison with polarization curves obtained in this work).

Earlier workers' data must be subject to doubt as curves which were recorded ostensibly under similar conditions demonstrate differences (witness Figures 3, 4, 6, 7). Even more recently recorded potentiostatic polarization curves obtained by Hoare and Okada and Yamamoto in catalyzed chromic acid solutions show some disagreement (Figures 66 and 67). However, in the absence of more thorough descriptions of the techniques employed (and any errors inherent therein), this is not particularly surprising. Particularly as it has been demonstrated (146) that low-potential polarization data recorded in plating solutions is sensitive to substrate composition (actually the film of cathode metal oxide which exists prior to the application of a potential). As stainless steel has been used as the cathode material throughout this work, it is considered that the cathode film which exists naturally (prior to immersion in the solution and application of potential) is probably chemically similar to that which is formed on the initial application of a pre-plating potential.

Where polarization data have been used as a basis for deposition mechanism theory in chromium plating, emphasis has been placed upon an analysis of the curve reversals which take place at less negative cathode potentials than that at which plating commences. Whilst accepting that this region of the cathode polarization curve may provide insights into the formation of the initial pre-plating film which could be useful in theorizing about the (apparently different type of) film that exists during plating, it is curious that no workers have attempted to analyze systematically the higher potential regions of the curves which correspond to industrial plating current densities. Furthermore, it is apparent that many of the contradictory conclusions regarding deposition mechanism have been made on the basis of fundamentally similar data (pre-plating

cathode polarization data). For example, Muller (127) (Figure 4) proposed that the action of the sulphate ion was to break up the 'blocking' film and allow access of hexavalent ions to the cathode surface where they undergo reduction to metal. However, Liebreich (126) and Reinkowski and Knorr (135) stated, on the basis of similar polarization data (Figures 3, 6) that the cathode film during plating consists of intermediates in the reduction of hexavalent ions to the metal, an altogether different mechanism.

In the current work, stress has been placed upon the accuracy and reproducibility of the recorded polarization data. Hence, the first part of the experimental programme was concerned with the establishment of a technique by which accurate, reproducibile curves could be recorded. Initially, the set-up illustrated in Figure 10 was used (with a touching probe and a sweep-rate of 30mV/s) to record the potentiodynamic curves shown in Figure 16. Each curve in Figure 16 represents the mean of three potential scans, the reproducibility of which was found to be low, giving an estimated maximum error in current density of $\pm$ 8% (less at lower current densities). Realizing that the attainment of a 'steady-state' current density prior to the recording of a point on the curve was important (for reproducibility), potentiodynamic curves at lower sweep-rates were recorded in a Standard Solution and are given in Figure 18. As expected, a slight change in the shape of the curve is observed as sweep-rate is lowered, with a tendency toward lower current densities recorded. A corresponding increase in curve reproducibility was noted (again using the mean of three curves) with the estimated maximum error in recorded cathode current density falling to approximately $\pm$6%.

Corrections to the potentiodynamically recorded curves in order to account for errors due to non-attainment of steady state were considered

likely to be complex and approximate. As a result, it was decided to implement a step-wise potentiostatic technique in which a closer approximation to 'steady state' conditions could be ensured.

At this stage a decision was taken to concentrate upon the low current density region ($< 10\ kA/m^2$) of the cathode polarization curve and neglect those current densities where concentration over-potential might be presumed to predominate, a decision taken for the reasons given in Section 2.3.1.

4.2.1. Potentiostatic polarization data

The apparatus shown in Figure 11 and the technique outlined in Section 2.3.1.2 were used to record a series of step-wise potentiostatic cathode polarization curves in a Standard Solution at $55^{o}C$. The results were obtained using a 10mV incremental potential step every five minutes. The Luggin capillary probe was positioned at the onset of measurement at a distance of 1mm from the cathode surface, and inclined at an angle which prevented the possibility of hydrogen gas entrapment. Using this technique and applying the correction referred to in Section 3.1.2.2 and quantified in Appendix I, good reproducibility was ensured with an estimated maximum deviation in recorded current density of $\pm 2\%$ (compared with $\pm 8\%$ for the potentiodynamic technique employed originally).

The values of current efficiency (for each cathode reaction) used with overall polarization data to produce partial polarization curves were each the mean of three values. The maximum estimated error in these efficiency values was found to be $\pm 8\%$ (of the percentage efficiency), a high number but to be expected in view of the low current densities employed. At higher current densities (greater than $5kA/m^2$) the observed error in current efficiency fell to approximately $\pm 5\%$. The higher degree

of uncertainty in the low current density efficiency values is obviously reflected in the slopes of the partial polarization curves constructed. For this reason all data derived subsequently are approximate, their estimated accuracy reflected in the number of decimal places given (Tables 4ff).

The partial polarization curves from a Standard Solution at 55°C shown in Figures 30, 51 and 54 were all assumed to illustrate cathode behaviour under charge-transfer control as none were influenced by the presence of additional localized forced agitation. The shapes of the curves were assumed to discount the possibility of any significant contribution to the total overpotential by crystallization overpotential (this does provide a contribution but is considered negligible at the current densities being employed (1.3.6.)) or reaction overpotential (limiting current densities were not encountered other than in the original, suspect, potentiodynamic curves).

4.3. Chromium plating in a Standard Solution

4.3.1. The plating reaction

Using the techniques outlined in Sections 2.3.1.2 and 2.3.2.1, the plating partial polarization curve in a Standard Solution at 55°C was constructed and analyzed and a Tafel slope of 21.5mV/decade was measured (Table 4). This information may be interpreted in a number pf ways depending upon the particular assumptions made with regard to deposition mechanism (although all mechanisms have been assumed to be multi-step). In most instances chromium deposition is assumed to occur via some sort of cathodic 'oxide film' and the current work has yielded indirect evidence to support this.

4.3.1.1. The Cathode film

(i) Hysteresis.

Hysteresis in polarization curves was only apparent at high current densities when a potentiodynamic,high sweep-rate, technique was employed (Figure 17). The lower current densities corresponding to the reverse cycle (decreasing potential) indicate the presence of an additonal resistance to the passage of current during that part of the cycle. This suggests a build-up of reaction products during the forward (increasing potential) cycle which subsequently act as a barrier during the reverse cycle.

At lower sweep-rates, hysteresis was not as evident, suggesting that, under these circumstances, there is sufficient time available for the dispersal of the layer (film) of intermediate reaction products during the reverse cycle (decreasing potential).

On a smaller scale, hysteresis was also observed with each individual (biased) reversal of potential during the recording of potentiodynamic polarization data (Section 2.3.1.1.) on the X-Y plotter. Again, this was more evident at higher sweep-rates (and with additives present).

(ii) Pre-plating behaviour

Examination of Figure 22 reveals that electrode reactions occur at less negative potentials than those associated with the onset of plating. As the potential is increased (negatively) the reduction of chromium VI to chromium III takes place exclusively at an increasing rate (current density) until a potential is reached at which the rate of removal of chromium III (aqueous) from the cathode surface is unable to keep up with the rate of production. At this point, a chromium III

rich layer is formed which effectively passivates the cathode and which is based upon the chromic dichromate species, $HCr_3O_9^{2-}$, identified with the blocking film of Muller (127). A further increase in potential allows an increase in current density as hydrogen evolution commences. The stirring which accompanies gas evolution tends to break up the CrIII layer so that (once the deposition potential is attained) the plating reaction is able to commence. Whether the 'low-potential' CrIII-rich layer should be termed a 'film' is a moot point, but it is apparently insoluble, suggesting that perhaps a layer of Cr_2O_3 is formed from the chromic dichromate species ($HCr_3O_9^{2-}$) in the vicinity of the cathode surface.

4.3.1.2 Film Composition

In the absence of the sulphate 'catalyst' plating will not take place, although a high enough applied cathode potential causes the reduction of chromic dichromate to chromous dichromate ($HCr_3O_8^{-}$). This species subsequently decomposes to give chromous hydroxide which may discharge to form black chromium. Should both ends of the trichromate be reduced to the trivalent state, the resulting dichromic chromate ($Cr_3O_8^{4-}$) species may decompose, yielding trivalent chromium ions and chromate -

$$Cr_3O_8^{4-} + 9H^+ \rightarrow 2Cr^{3+} + HCrO_4^- + 4H_2O$$

The Cr^{3+} ions would immediately form the highly stable hexaquo complex ($Cr(H_2O)_6^{3+}$), preventing further reduction.

In the presence of the sulphate 'catalyst' the mechanism is (according to Hoare (118)) similar to that in the absence of the 'catalyst' at potentials less negative than that at which deposition commences. The difference being that in the former case the

chromic dichromate species which produce the CrIII blocking film are hydrogen-bonded to HSO_4^- ions. The hydrogen-bonding to one end of the reducible species provides an explanation for the existence of a trivalent chromium species which does not form the stable hexaquo complex. The trivalent chromium intermediate is, as it were, 'protected' by the catalyst.

In the catalyzed solution, HSO_4^- may also bond to Cr=O (from chromous hydroxide), producing a polarized species which is adsorbed onto the cathode surface (chromium end on) to form an effective divalent 'film', and reducing the likelihood of the establishment of a so-called chromic-chromous couple.

In other words, the film which exists during plating differs from the one that exists upon the cathode at less negative 'pre-plating' potentials. The plating film is very much thinner (it cannot be seen by the naked eye during deposition from dilute plating solutions) and is not based upon an accumulation of reaction products (such as chromic dichromate in uncatalyzed solutions), but rather upon a layer of reaction intermediates based upon the Cr=O composition and in a continuous state of flux (as CrII $\rightarrow$CrI $\rightarrow Cr^{o}$, and new CrII arrives to reconstruct the film). This change in the fundamental nature of the film in the present of sulphate was supported by Vagramyan et al (157) who demonstrated (using oscilloscopic recording of the variation of current with time immediately following the abrupt application of a constant potential to a test cathode) that the presence of sulphate greatly increases the effective conductivity of the cathode film. A similar technique yielded

similar results for Okada et al (156).

The mechanism of plating film formation given above is due to Hoare (118) whose overall plating mechanism is considered to be the most feasible of those thus far proposed, particularly his elegant explanation of the action of sulphate (actually HSO_4^-) in catalyzing the reaction and his reasons for the limited range of effective sulphate concentration ratios. Any subsequent references to a cathode film in this work are, therefore alluding to an organized congregation of the cathode surface of those divalent and monovalent chromium species involved in the final steps of Hoare's mechanism for chromium depositon (unless specified otherwise). A schematic representation of the mechanism is given in Appendix III.

Hoare does not actually invoke the concept of a cathode film in the way that earlier workers do. He simply imples that certain reaction intermediates congregate at the cathode surface prior to further reduction. However, the interpretation of his mechanism in terms of a definite cathode film is necessary, as all polarization (and other) data suggest that such a film does indeed exist during chromium plating.

4.3.1.3. Rate control in the plating reaction

If it is assumed that the rate-determining step (R.D.S.) in the plating reaction at industrial plating current densities is a charge-transfer of some description within Hoare's mechanism, it would be helpful to know which one.

Hoare recorded polarization curves (potentiostatic and galvanostatic) under exactly similar conditions in a catalyzed (with SO_4^{2-}) and uncatalyzed solution. He noted that the overall shape of the curves in the 'pre-plating' region was not affected by the presence

of SO_4^{2-} and concluded that the catalytic action of the ion did not influence the early reduction steps of Cr VI to Cr III. He subsequently reasoned that the SO_4^{2-} acted to facilitate the later reduction steps of Cr III to Cr metal. In other words, that the catalyst operated upon the 'film' rather than in the solution. Hoare's theory in this respect is similar to those of Muller (127), Kasper (139), Liebreich (126) and Reinkowsi and Knorr (135), who all proposed that sulphate ions acted (in different ways) to modify a chromic dichromate type film. Where Hoare differs is in his consideration and explanation of the specific action of the catalyst, which he reasons to be the HSO_4^- ion.

Although Hoare's mechanism is the best-argued and most complete available, it does not offer any thoughts as to which step in the process (if any) controls the overall deposition rate.

Hoare's mechanism can be divided into three phases :-

(i) The approach of the bulk ionic species $HCR_3O_{10}^-$ to the vicinity of the Outer Helmholtz Plane. Subsequent reduction to $HCr_3O_{10}^{2-}$ by quantum-mechanical electron tunneling. Reduction of $HCr_3O_{10}^{2-}$ to $HCr_3O_{10}^{3-}$ by electron tunneling. Reduction of $HCr_3O_{10}^{3-}$ to $HCr_3O_9^{2-}$ (and O^{2-}) by electron tunneling, followed by the immediate reaction of O^{2-} with $2H^+$ to give water. The species $HCr_3O_9^{2-}$ (containing a trivalent chromium ion) may then undergo further reduction.

(ii) The transfer of an electron from the cathode across the 'film' to reduce $HCr_3O_9^{2-}$ (chromic dichromate) to $HCr_3O_8^-$ (chromous dichromate) + O^{2-}, followed by the immediate reaction of O^{2-} with $2H^+$ to form water. The chemical reaction of $HCr_3O_8^-$ with H_3O^+ to give $Cr(OH)_2$ (chromous hydroxide which is equivalent in form to hydrated chromous oxide; $CrO.H_2O$) and a dichromate which may undergo condensation with other

chromates to regenerate the trichromate. This chemical reaction is clearly pH-dependent.

(iii) The formation of a highly polarized complex through hydrogen bonding between CrO and HSO_4^-. The positive charge associated with the chromium in this complex causes the complex to swing around until the positive end of the complex is specifically adsorbed on the cathode surface, with the sulphate tetrahedron extending out into the solution. In this end-on configuration rapid transfer of electrons from the cathode to the divalent chromium ion in the complex is possible, reducing it to monovalent chromium and finally chromium metal (with the regeneration of HSO_4^-).

Of these three phases in reduction, one must contain the rate-determining step (if one exists).

It is considered that phase (iii) is an unlikely candidate as the final two charge-transfers are to a specifically adsorbed (i.e. 'close') target. Of the steps involveed in phase (iii) it is likely that the 'slowest' would be the film-incorporation step as the polarized, hydrogen-bonded, complex would need to find a suitable site for adsorption.

Phase (ii) involves one charge-transfer within the double layer as chromic dichromate is reduced to chromous dichromate, and two chemical reactions both of which are dependent on local pH. Assuming that pH is generally low enough so as not to present a problem, the charge-transfer might be expected to be the slowest step in this phase. In regions where pH is relatively high (where hydrogen evolution is favoured) the decomposition of chromic dichromate to chromous dichromate would be hindered, stabilizing the trivalent species and tending to slow down deposition.

Phase (i) involves one (rapid) chemical reaction in the Outer Helmholtz Plane and three charge transfers involving electron-tunneling. The electrons transferred thus have to first negotiate the cathode 'film' then tunnel across the double-layer to the reducible ion in the particular species which probably sits just outside the O.H.P. The ion is located here as this is the closest approach of the ion to the cathode surface because most of the potential drop between the cathode and the bulk solution operates across the Helmholtz double-layer in such a highly concentrated solution. Hoare estimated the double-layer thickness as being approximately 3 to 6 x 10^{-10} m.

Although the 'film' constitutes a barrier to the passage of electrons from the metal out to the ionic species at the O.H.P. (and must be taken into account) and should be considered semiconductive, it may exhibit nearly-metallic behaviour. Vijh (28) listed many factors which may tend to mask the semi-conducting nature of such a film, among which are a number that could certainly apply to the 'film' in chromium plating:

(a) Nonstoichiometry or unintentional doping of the oxide may be produced during the electrode reaction.

(b) Surface states may result from the chemisorption of reactants, intermediates or reaction products.

(c) The electrode surface could only be partially covered by islands of surface oxide, or the oxide could undergo periodic self-removal.

It is, therefore assumed that in the transfer of an electron from the cathode to (say) the $HCr_3O_{10}^-$ species at the O.H.P., the charge-transfer from the film/solution interface to the ion is the most difficult aspect. However, there are four consecutive electron

transfers which must involve electron tunneling (CrVI to CrV, CrV to CrIV, CrIV to CrIII, to CrII. The question arises as to which of these transfers (if any) is the most difficult.

The principles of quantum mechanics which govern the probability of an electron tunneling through an energy barrier lay down certain conditions. The tunneling probability of an electron P_T is given by (170) -

$$P_T = |\psi|^2 = \exp(-2\rho'_2 x/h') \qquad (4.3.2,1)$$

ψ = probability amplitude

ρ'_2 = real part of electron momentum

x = distance from interface

h' = Planck's constant

It is evident from equation (4.3.2,1) that the likelihood of encountering an electron decreases with increasing distance from the electrode. One might, therefore expect that the particular chromium-bearing species which allows closest approach of the reducible chromium ion to the cathode would be the most easily reduced by a tunneling electron. However, it is also necessary to consider the 'ability' of each species to receive the electron. This involves consideration of the position of the chromium ion within the species in terms of its geometry and charge distribution.

In each of the three species under consideration the reducible chromium ion (hexavalent, pentavalent or tetravalent) is surrounded by four oxygen atoms (or ions) in an approximately tetrahedral arrangement. In the case of the hexavalent species,

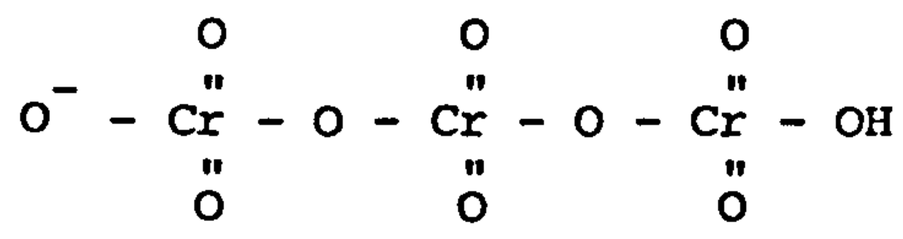

only one of the 'protective'oxygens has an extra negative charge in the form of a free electron. This negative charge would tend to repel any incoming electron, and would also tend to hinder any electron access by contracting the bond through electrostatic reaction with the chromium. In the case of the tetravalent species :-

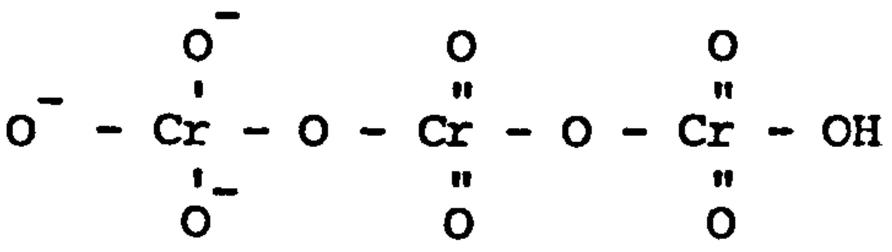

the reducible (in this case, tetravalent) chromium ion is 'protected' by a greater concentration of negative charge because three of the four oxygens to which it is bonded have a free electron. This charge concentration is assumed to have a greater influence on an incoming electron than any geometric changes due to bond-stretching and mutual repulsion between adjacent oxygen ions. If this is so, then the chances of reduction by a tunneling electron are greater for the hexavalent chromium ion in the $HCr_3O_{10}^-$ species than for the tetravalent chromium ion in the $HCr_3O_{10}^{3-}$ species. The probability of reduction of the CrV ion in the $HCr_3O_{10}^{2-}$ species would logically fall between the two extremes.

It, therefore seems likely that the R.D.S at plating current densities is either the CrIV →CrIII charge transfer (from phase (i)) or the CrIII → CrII charge transfer from (phase (ii)).

Having expanded Hoare's mechanism to the point where a R.D.S. may be proposed, measured polarization data may be employed to characterize it.

Figure 30 yields a value of 21.5mV/decade for the Tafel slope of the plating reaction at $55^{o}C$ in a Standard solution. Remembering that this represents all charge-transfer steps in the reduction of $HCr_3O_{10}^-$ to chromium metal (i.e. z = 6), substitution into equation (1.3.9.1.3,1) -

$$\frac{d\eta}{d\log i} = \frac{-2.303RT}{\alpha_{term}\lambda F}$$

yields a value for λ of 12.11. Twelve electrons are, therefore required from the cathode in order to complete one overall deposition reaction.

Substitution of $\lambda = 12$ into Equation (1.3.9.1.2,1) implies that the R.D.S. in the reaction mechanism is repeated 7 times (i.e., $\nu = 7$), assuming all the reaction steps to be single electron transfers and that all steps other than the R.D.S. are in virtual equilibrium. Explaining this in terms of Hoare's mechanism :-

(i) $HCr_3O_{10}^- + e^- \rightleftharpoons HCr_3O_{10}^{2-}$

(ii) $HCr_3O_{10}^{2-} + e^- \rightleftharpoons HCr_3O_{10}^{3-}$

(iii) $HCr_3O_{10}^{3-} + e^- \rightleftharpoons HCr_3O_9^{2-} + O^{2-}$

(iv) $HCr_3O_9^{2-} + e^- \rightleftharpoons HCr_3O_8^- + O^{2-}$

(v) $HCr_3O_8^- + H_3O^+ \rightleftharpoons Cr{=}O + H_2O + H_2Cr_2O_7$

(vi) $Cr{=}O + e^- \rightleftharpoons Cr{-}O$

(vii) $Cr{-}O + e^- \rightleftharpoons Cr^o$

is difficult. It is considered that the step which is most likely to require more than one molecule of the reactant species in order to ensure reaction step completion is step (v) above, in which a reaction product is necessary for cathode film construction. This being the case, Equation (1.3.9.1.2,1) could only be satisfied for λ = 12 if the preceding charge-transfer (step iv) above) is the R.D.S. and has a stoichiometric number of 7. However, 7 seems an unlikely stoichiometric number and it is difficult to understand why the (ongoing) reconstruction of the cathodic oxide film network should require 7 Cr=O species in unison. A different value for ν may be generated if a different (lower) value for λ is assumed. From the Tafel slopes recorded (and the value for $\lambda \times \alpha_{term}$ of 3 generated in a Standard Solution), it is clear that any value of between 6 and 12 for λ (dependent upon the α_{term} value assumed) may be extracted. However, as λ = 6 is only possible if no cathode film exists (i.e. α_{term} = 0.5) and knowing that a film <u>does</u> exist, λ probably takes a value intermediate between 7 and 11.

As will be shown, the presence of $B_2O_4^{2-}$ causes an evident increase in film conductivity and yields a value for λ of 8, assuming α_{term} = 0.31 (the only reasonable value of α_{term} which satisfies the conditions that λ is an integer and that $0.5 > \alpha_{term} > 0.25$). Clearly, α_{term} for plating in a Standard Solution must be less than 0.31 because film conductivity is lower in a Standard Solution (assuming that α_{dl} is constant and equal to 0.5). However, $\lambda \times \alpha_{term}$ for plating in a Standard Solution is equal to 3 (Table 4), so $\lambda_{(plating, Standard Solution)}$ must be greater than 3/0.31 = 9.7. λ for plating in a Standard Solution can therefore only be equal to

10, 11 or 12, which in turn give stoichiometric numbers of 5, 6 or 7. Of these, 6 seems the more likely, meaning that Hoare's mechanism becomes -

(i) $HCr_3O_{10}^- + e^- \rightleftharpoons HCr_3O_{10}^{2-}$

(ii) $HCr_3O_{10}^{2-} + e^- \rightleftharpoons HCr_3O_{10}^{3-}$

(iii) $HCr_3O_{10}^{3-} + e^- \rightleftharpoons HCr_3O_9^{2-} + O^{2-}$

(iv) $6(HCr_3O_9^{2-} + e^- \longrightarrow HCr_3O_8^- + O^{2-})$ R.D.S. ($\gamma = 6$)

(v) $6HCr_3O_8^- + 6H_3O^+ \rightleftharpoons 6Cr{=}O + 6H_2Cr_2O_7$

(vi) $Cr{=}O + e^- \rightleftharpoons Cr{-}O$

(vii) $Cr{-}O + e^- \rightleftharpoons Cr^O$

This mechanism, if accepted, makes $\lambda = 11$ and $\alpha_{term} = 0.27$, and suggests that the film which exists during plating from a Standard Solution is flawed in some way, as described by Vijh (28).

4.3.1.4. Arrhenius data for the plating reaction in a Standard Solution

Data obtained from the apparent Tafel region of the plating partial polarization curve in a Standard Solution was used in Equation 1.3.9.2,3 to generate values for the thermodynamic quantities (of activation) at three different potentials. Accepting that errors in Tafel data would transmit to the thermodynamic data generated, it was nonetheless hoped that this approach might yield information to clarify the nature of the R.D.S.

While the thermodynamic (activation) data probably do not pertain directly to the R.D.S., it may be assumed that they constitute 'upper limit' values, representing as they do the overall plating

reaction (i.e. all steps). So, whereas a recorded value of ΔG_A does not necessarily refer to the R.D.S. in the plating reaction ($\Delta G_{A(RDS)}$ cannot be greater than ΔG_A), it may act as a useful pointer to the nature of the R.D.S. Unfortunately, the situation is complicated by the presence of an oxide 'film' on the cathode during plating. This tends to 'de-activate' the cathode and could be expected to increase the activation enthalpy for charge-transfer as compared to a 'bare' metal (assuming the R.D.S. is a charge-transfer). In fact, ΔH_A for plating in a Standard Solution is recorded as being of the order of 100kJ/mol (Tables 7) whereas charge-transfer on 'bare' metals typically involves a ΔH_A of $\leqslant$70kJ/mol (15). This cathode 'de-activation (along with the approximateness of the data) makes it impossible to conclude unequivocally that the R.D.S. during plating at 3kA/m^2 in a Standard Solution is a charge-transfer. However, there is circumstantial evidence to support this proposal, as will be shown (e.g. the presence of 15g/l BrO_3^- in a Standard Solution increases the 'film' conductivity and reduces ΔH_A to approximately 70kJ/mol - see Section 4.5.3 and Tables 7).

It is noteworthy that a considerable increase in activation enthalpy of the plating reaction occurs with an increase in cathode potential to -0.85V (vs S.H.E). Reference to Figure 30 reveals that at this potential a deviation from straight-line Tafel behaviour is apparent, which could indicate a change to a different R.D.S. within the deposition mechanism. Snaveley's observation (49) that at higher current densities the tendency to deposit a chromium hydride becomes more pronounced, together with the increase in the

ΔH_A value generated leads to the tentative suggestion that at these current densities (beyond the Tafel straight-line region) deposition rate-control may shift away from charge-transfer to hydrogen diffusion.

Thus, evidence is presented to support the hypothesis that the R.D.S. in the chromium deposition reaction (at industrial plating current densities) is a charge-transfer (CrIII → CrII) with a stoichiometric number of 6.

4.3.2. The hydrogen evolution reaction

The different mechanisms by which hydrogen evolves in the presence and absence of a thin oxide film were examined by Makrides (171) who noted that the overall stoichiometry of the reaction could be affected substantially. He proposed that in the absence of a film the mechanism -

$$H^+ + e^- \longrightarrow H_{ads(metal)} \qquad \text{(slow step)}$$

$$H_{ads(metal)} + H_{ads(metal)} \rightleftharpoons H_2$$

predominated, whereas when a film was present,

$$H^+ + e^- \rightleftharpoons H_{ads(film)}$$

$$H_{ads(film)} + H^+ + e^- \longrightarrow H_2 \qquad \text{(slow step)}$$

became the mechanism. The effect of the oxide was considered to be via the restriction of the motion of adsorbed hydrogen atoms.

If the presence of a cathode 'film' is assumed, hydrated protons are reduced by electrons which must negotiate both the

'film' and the Helmholtz double-layer. Equation (1.3.9.1.3,1) therefore applies.

Reference to Figure 31 and Table 4 reveals that the measured Tafel slope for the hydrogen evolution reaction in a Standard Solution at 55°C is 124mV/decade. Substitution of this value into Equation (1.3.9.1.3,1) assuming $\alpha_{term} = 0.25$ (i.e., $\alpha_f = \alpha_{dl} = 0.5$), yields a value for λ of 2.10.

Remembering Equation (1.3.9.1.2,1), this gives

$$2 = \vec{\gamma} + \overleftarrow{\gamma} + r\nu$$

Accepting that there are two possible mechanisms for hydrogen evolution in an acid solution (Section 1.3.8) and that each is two-step, there are four possible rate determining steps (170),

(a) $M(e^-) + H_3O^+ \longrightarrow MH + H_2O$ R.D.S. ($\nu = 1$)

$M(e^-) + MH + H_3O^+ \rightleftharpoons 2M + H_2O + H_2$

(b) $M(e^-) + H_3O^+ \rightleftharpoons MH + H_2O$

$M(e^-) + MH + H_3O^+ \longrightarrow 2M + H_2O + H_2$ R.D.S. ($\nu = 1$)

(c) $M(e^-) + H_3O^+ \rightleftharpoons MH + H_2O$

$MH + MH \longrightarrow 2M + H_2$ R.D.S. ($\nu = 1$)

(d) $M(e^-) + H_3O^+ \longrightarrow MH + H_2O$ R.D.S. ($\nu = 2$)

$MH + MH \rightleftharpoons 2M + H_2$

As in this case, $2 = \vec{\gamma} + \overleftarrow{\gamma} + r\nu$ (and r must = 1 or 0), it is clear that any mechanism other than (c) will satisfy this condition. However, it will be shown that the addition of BrO_3^-

to a Standard Solution causes λ_{HER} to become equal to 1, making $1 = \vec{\gamma} + \overleftarrow{\gamma} + \nu r$, a condition that may only be satisfied by mechanism (c). This is taken as evidence to suggest that the mechanism which applies in a Standard Solution is probably mechanism (d) and supports the idea that the nature of the film influences hydrogan evolution (as proposed by Makrides (171)). Furthermore, it is known (170) that mechanisms (a) and (b) require a high cathode coverage of adsorbed hydrogen, a condition that is less likely to obtain where the hydrogen evolution reaction takes place on a filmed electrode.

The conductivity of the cathode film (demonstrated to be dependent upon the presence of certain of the new additions) might be expected to affect the ease with which hydrogen atoms (discharged protons) are able to diffuse towards one another prior to combination and eventual escape as hydrogen gas. This is supported by Snavely's proposal (49) that chromium deposits as hydride which subsequently decomposes, yielding an intensely hard deposit. A higher film conductivity might be expected to allow fewer hydrogen atoms to linger long enough in the region of the film/cathode interface to form hydrides. Consequently, solutions which apparently cause an increase in film conductivity (such as those containing BrO_3^-) should produce softer deposits (at Tafel current densities), which they do (Table 2).

The hydrogen evolution reaction in chromium plating is clearly complicated by the presence of a cathode film (under continuous destruction and regeneration). For this reason, all conclusions

drawn from Tafel data for this reaction are not intended as definitive, although data obtained in different solutions has been used comparatively (as will be shown) to yield insights into deposition mechanisms.

4.4. The effect of the new additions upon plate and plating parameters

This section of the work was carried out in an attempt to determine the potential industrial applications of the observed effects of the new additions (to a Standard Solution at 55°C) upon aspects of the plating process of most interest to practitioners.

4.4.1. Potassium perchlorate

Reference to Table 1 reveals that the presence of $KClO_4$ in a Standard Solution causes a change in the measured solution throwing power from a negative value to a slightly positive one. The greater the concentration of $KClO_4$, the more positive the throwing power.

Although these results are no meant to be taken as definitive, the observed trend must be encouraging because the negative throwing power of conventional chromic acid based plating solutions is the cause of many of the practical problems associated with the hard chromium plating process. For this reason alone $KClO_4$ is considered to be of potential use to the industrial chromium plater, and to merit further investigation.

The variation of plating current efficiency with cathode current density in solutions containing $KClO_4$ (Figure 24) at concentrations of 5, 10 and 15g/l shows a gradual increase up to a current density of $\sim 30 kA/m^2$ whereafter the efficiency falls. In a Standard

Solution alone no downturn in efficiency is apparent. This may be related to the measured solution throwing powers, in that it demonstrates a tendency to lower deposition rates in areas of locally higher (than the mean) cathode current density (i.e. better 'levelling') with a consequently beneficial effect on deposit distribution.

The macro-appearance (Table 3) and morphology of chromium deposits produced in solutions containing $KClO_4$ further reflect the observed effect on throwing power. The presence of $KClO_4$ appears to extend the current density range in which satisfactory deposits are obtainable (Table 3), and reduces the tendency to a dendritic morphology at higher current densities (Plates 5 to 8) observed in plate produced in a Standard Solution (Plates 1 to 4).

The nodular deposit produced in the presence of $KClO_4$ at $3kA/m^2$ was similar in appearance to that produced in a Standard Solution at the same current density, but was observed to contain significantly fewer cracks, a property of the deposit which was later found to influence considerably the high temperature oxidation behaviour of plated mild steel. (Jha (173) reported that chromium plate produced from a solution containing $KClO_4$ conferred better high temperature oxidation resistance than conventionally deposited chromium).

The micro-hardness values measured from the deposit produced in solutions containing $KClO_4$ were found to be very high, even by hard chromium plate standards (Table 2). Allowing for errors in measurement, an average micro-hardness of greater than 1500VPN

(compared with 1175VPN for plate from a Standard Solution) should have commercial implications. The combination of increased hardness and fewer cracks is undoubtedly a desirable one, but it presents a problem in terms of Snavely's theory for deposit hardness. According to Snavely (49) the decomposition of (initially deposited) chromium hydrides to chromium metal which increases deposit hardness through grain-size refinement should also lead to (via a lattice contraction of ~15%) increased cracking, a theory reinforced by reference to Plates 1 to 4 in which an increase in current density (in a Standard Solution) is seen to lead to a decrease in crack frequency. The apparent contradiction observed in plate produced in the presence of $KClO_4$ may perhaps be explained in terms of the stability of the chromium hydride initially deposited. A slower release of atomic hydrogen from the deposit would tend to lessen the incidence of cracking (through a more even stress distribution within the deposit), but this would result in a softer deposit unless the original hydride grains deposited from a solution containing $KClO_4$ are smaller than those deposited from a Standard Solution (i.e. if $KClO_4$ somehow favours grain nucleation at the expense of growth). Another problem with the idea of deposition of a more stable hydride is that the slow decomposition of such a hydride (and reduction of the associated chromium) might be expected to be the R.D.S. in deposition. Comparison of the Tafel slopes for plating in solutions with $KClO_4$ and Standard Solution (Table 4) indicates no difference in R.D.S. So, although one solution produces cracked deposits and the other doesn't, the electrochemical evidence suggests that the R.D.S. is the same in both instances (that proposed in Section 4.3.2.).

The effect of $KClO_4$ presence in solution upon deposit hardness and crack density is considered further in Appendix IV.

4.4.2. Potassium bromate

Whereas the presence of perchlorate in solution appeared to have a uniformly beneficial effect upon the plating process and the deposit produced, the bromate addition had the opposite tendency (with one exception).

Table 1 shows that BrO_3^- at all concentrations had a negative effect upon the recorded solution throwing power, and this (as with the ClO_4^- addition) is reflected in its effect upon other parameters. No downturn in the variation of plating current efficiency with current density was observed. Indeed, Figure 39 shows that a very steep increase occurred. In practice, this would lead to an extremely non-uniform deposit distribution as areas of locally high current density would plate at progressively faster rates and eventually lead to the formation of outgrowths. On a microscopic scale the presence of bromate caused a change at low current densities from a finely nodular deposit (Standard Solution) to a highly-cracked, flakey morphology with outgrowths (Plates 9 and 10). At higher current densities the deposit became highly dendritic and porous (Plates 11 and 12).

The addition of $KBrO_3$ to the solution therefore led to a contraction of the bright range (Table 3) for chromium deposition, rendering it apparently useless as a potential industrial additive. The slight reduction in deposit hardness may be attributed to the increased porosity of the plate (Table 2, Plates 9 to 12). (See Appendix IV).

The one beneficial effect of $KBrO_3$ presence in solution (although outweighed by negative effects) upon the plating process is its influence upon the anode efficiency of CrVI regeneration (Figure 63), which at a $KBrO_3$ concentration of 15g/l, remains consistently high (∿20%) at all current densities studied. This suggests the possible use of BrO_3^- as a plating addition in situations where plate appearance is non-critical, but in which anode area is less than cathode area (the inside of gun-barrels, for example).

4.4.3. Potassium borate

The addition of $K_2B_2O_4$ to a Standard Solution appeared, in general, to have an effect on the measured plate and plating parameters similar to that of $KBrO_3$ but to a lesser extent.

The throwing power of a solution containing $K_2B_2O_4$ was recorded (Table 1) as being worse (more negative) than that of a Standard Solution but not as poor as a solution containing $KBrO_3$. Again, this could be related to the measured variation in plating current efficiency (Figure 46) in which no downturn is evident, and which varies in a manner intermediate between that recorded in a Standard Solution and a solution containing $KBrO_3$.

The macro-appearance and morphology of the deposits (Table 3 and Plates 13 to 16) reflect the intermediate throwing power of the solutions containing $K_2B_2O_4$ in that their appearance seems to fall between that of plate produced in a Standard Solution and a solution containing $KBrO_3$, and their morphology whilst (unevenly) nodular and (very finely) cracked at lower current densities (i.e. similar to Standard Solution plate) demonstrates a dendritic appearance when produced a higher current densities (Plates 15 and 16).

The micro-hardness measurements made on plate produced in solutions containing $K_2B_2O_4$ yielded results which fell somewhere between those from a Standard Solution and a solution containing $KClO_4$ (closer to the Standard Solution plate). Despite the marginally harder deposit produced, the more negative throwing power and consequently poor appearance of the plate deposited in the presence of $K_2B_2O_4$ would seem to consign it the same fate as $KBrO_3$ when considered as a potential industrial chromium plating additive.

Like $KBrO_3$, the presence of $K_2B_2O_4$ allows a high rate of anodic CrVI regeneration (efficiency of up to ~30%), but one which falls rapidly (Figure 65) with increasing anode current density (in contrast to $KBrO_3$). As any benefits from this type of behaviour would be confined to plating conditions in which the anode is unavoidably small (as a result of the geometry of the component to be plated) and anodic current density is correspondingly high, it is important that the rapid rate of CrVI regeneration should be maintained over a wide range of current densities. Whilst the solution containing 15g/l $KBrO_3$ best fulfils this requirement (Figure 63), none of the solutions containing $K_2B_2O_4$ appear to (Figure 65). For this reason, $K_2B_2O_4$ must be classified as demonstrating even less potential than $KBrO_3$ as a chromium plating solution additive.

4.4.4. Mixed additions

In view of the uniformly beneficial effects of the addition of $KClO_4$ to a Standard Solution and the specific benefit of $KBrO_3$ in aiding the regeneration of CrVI, it was hoped that a solution containing both additives might demonstrate the beneficial properties associated with each. Alas, the presence of $KBrO_3$ (or $K_2B_2O_4$) at

the lowest concentrations investigated (5g/l) in a Standard Solution containing $KClO_4$ tended to 'swamp' the beneficial effects of the $KClO_4$, causing the solution to behave as if $KBrO_3$ was the only additive present (i.e. producing a relatively soft, dark deposit at all current densities).

4.4.5. Summary

The present of $KClO_4$ in a Standard Solution has a uniformly beneficial effect upon all plating and plate parameters investigated when compared to a Standard Solution alone, and is considered to demonstrate potential with regard to possible industrial applications. In general, an increase in concentration of $KClO_4$ causes a corresponding improvement in those aspects of plating considered (the maximum concentration of 15g/l was selected in view of safety considerations). It was noted that at concentrations of 5g/l and 10g/l, lengthy electrolysis of a solution containing $KClO_4$ caused no apparent exhaustion of the additive, whereas at a concentration of 15g/l the $KClO_4$ was apparently used up (Table 8), but only down to a concentration of ∿10g/l (according to the plating efficiencies recorded). This observation is considered in a later section.

Apart from plating conditions in which a high rate of anodic CrVI regneration is necessary, neither $KBrO_3$ or $K_2B_2O_4$ are considered to exhibit industrial potential, because of their negative effects upon solution throwing power and related properties.

4.5. The influence of the new additions upon electrochemical aspects of hard chromium plating

4.5.1. Introduction

The partial polarization curve Tafel region analysis and modified Arrhenius technique employed during the investigation of the deposition

mechanism in a Standard Solution were also applied to each solution tested containing the new additions.

In every case, it was assumed that the mechanism of deposition was essentially the same as that outlined for a Standard Solution. On this basis, partial polarization curves (Figures 30, 51, 54) and Arrhenius data (Tables 6a to 6y and Figures 33, 57, 58, 59) were used to generate values for α_{term}, ΔG_A, ΔH_A and ΔS_A for the deposition reaction in each solution (Tables 5 and 7).

Breakdown of α_{term} values into α_f and α_{dl} components was carried out on the assumption that either α_f or α_{dl} was equal to 0.5. Table 5 gives values for α_f assuming $\alpha_{dl} = 0.5$. However, the values generated are equally applicable if α_f is assumed to equal 0.5, and those given are for α_{dl}. So, while it is apparent that the new additions do affect α_{term} for the plating reaction (assuming $\lambda = 12$), it is not possible from the data to state unequivocally whether their effect is in the 'film' or double-layer. The splitting of α_{term} into its constituent parts was, therefore undertaken mainly in an attempt to clarify the situation.

4.5.2. Potassium perchlorate

The overall cathode polarization curves for a Standard Solution containing $KClO_4$ at various concentrations (Figure 34) show a slight shift in the low current density pre-plating regions of the curves to more positive potentials when compared to that for a Standard Solution. However, they are so similar as to suggest that $KClO_4$ has no really pronounced effect upon the nature of the cathode reaction products in this region, other than to maybe somehow affect the conductivity of any 'film' (the maximum current density of the CrVI → CrIII 'loop' is changed from approximately $0.4 kA/m^2$ to $0.5 kA/m^2$).

At more negative potentials the overall polarization curves are very similar in shape to that produced in a Standard Solution alone.

Analysis of the Tafel regions of the plating reaction partial polarization curves for solutions containing $KClO_4$ revealed (assuming $\lambda = 12$) similar values for α_{term} to that (0.25) recorded in a Standard Solution (Table 5), with the exception of the solution containing 10g/l $KClO_4$ in which an anomalously high value (0.33) was recorded.

The almost identical values for α_{term} for the plating reaction in the presence and absence of $KClO_4$ present a problem in the interpretation of the specific action of this addition. However, it is clear that the addition has a consistently positive influence upon the ease with which hydrogen evolves during plating. α_{term} for the hydrogen evolution reaction is increased consistently in the presence of $KClO_4$ when compared with a Standard Solution, a phenomenon which may help to explain the high hardness of $KClO_4$ catalyzed deposits if Snavely's theories are accepted. Obviously, the action of $KClO_4$ in facilitating the hydrogen evolution reaction would have a converse (indirect) effect upon metal deposition, an effect reflected in the relevant current efficiency versus current density plots (Figures 23, 24, 25, 26).

If it is accepted that its action upon the plating reaction is indirect, the question then arises as to how ClO_4^- is able to facilitate the hydrogen evolution reaction (particularly at higher current densities). Reference to the electrochemical series (46) reveals that it is possible that any ClO_4^- in the proximity of the cathode will be reduced to some other species as the standard reduction potentials for the reductions involving ClO_4^- are highly

positive (versus S.H.E.). The particular reductions which take place are probably a function of the availability of protons at the cathode (46). Remembering that ClO_4^- appears to act at higher current densities where pH is higher, it is assumed that the first reduction in the sequence could be

$$ClO_4^- + 2H^+ + 2e^- \rightarrow ClO_3^- + H_2O \qquad 1.19V$$

followed by

$$ClO_3^- + 2H^+ + e^- \rightarrow ClO_2 + H_2O \qquad 1.15V$$

and

$$ClO_2 + H^+ + e^- \rightarrow HClO_2 \qquad 1.27V$$

and finally (perhaps) by

$$HClO_2 + 2H^+ + 2e^- \rightarrow HClO + H_2O \qquad 1.64V$$

At highly negative cathode potentials (and high current densities) $HClO_2$ and HClO will probably exist in the vicinity of the cathode. These species are polarized and could possibly hydrogen bond to trichromate ions in solution in the same manner as HSO_4^- (according to Hoare (118)). If this were true the action of the perchlorate addition may be explained.

Hoare proposed that HSO_4^- could hydrogen bond to any of the four 'corner' oxygen atoms in the bulk trichromate species $HCr_3O_{10}^-$ (see Page 92). He noted that if bonding took place with all four oxygen atoms the species would be impotent with regard to participation in deposition, whereas if none of the oxygen atoms were affected, both ends of the complex could be reduced to produce a stable trivalent aqueous species (of no further use in deposition). He concluded that the optimum condition for plating would involve the hydrogen bonding of two HSO_4^- to the two oxygen atoms at one end only of the trichromate as this would permit subsequent step-wise reduction at the end (as detailed earlier), and that this situation corresponded to a bulk solution concentration ratio of 100 : 1 for CrO_3 : H_2SO_4.

It is considered possible that if $HClO_2$ and HClO are produced cathodically at high current densities in a solution containing $KClO_4$, these species could act to 'seal up' the trichromate species via hydrogen bonding -

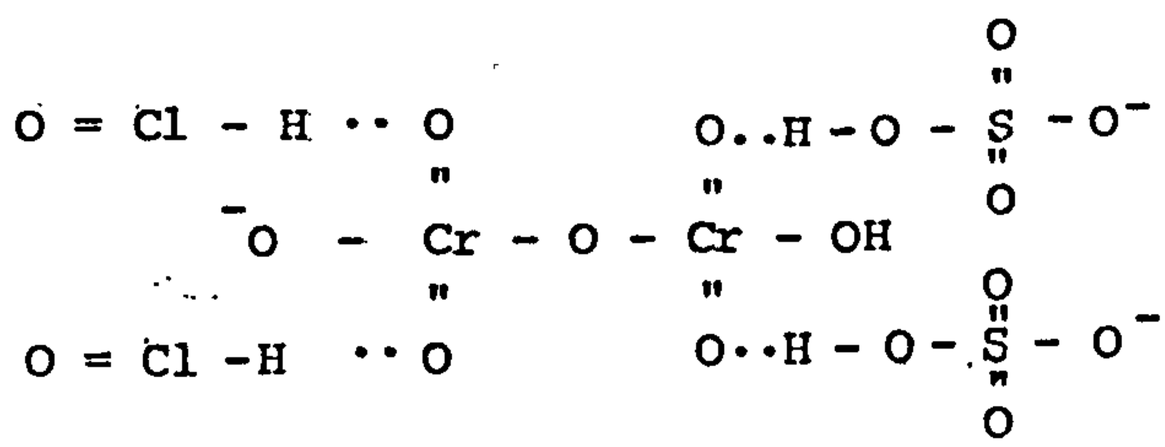

thus preventing the particular ion from being reduced and diverting current to the competing reactions at higher current densities (as is observed).

It could be argued that if HClO or $HClO_2$ can act in the same way as HSO_4^- in bonding to oxygen atoms in the trichromate

species they should be able to do the same thing during the actual plating mechanism step in which HSO_4^- hydrogen bonds to Cr = O. This is -

$$CrO + HClO \rightarrow Cr = O \cdot\cdot H - Cl = O$$

instead of

$$CrO + HSO_4^- \rightarrow Cr = O \cdot\cdot H - O - \overset{\overset{O}{\|}}{\underset{\underset{O}{\|}}{S}} - O^-$$

and that ClO_4^- should therefore be able to act as a catalyst in its own right in the absence of HSO_4^-. In practice, ClO_4^- will in itself catalyze the chromium plating reaction in aqueous chromic acid (158) but only at high concentrations (a molar ratio of 10 : 1 for CrO_3 : $HClO_4$) where it yields a metallic but dark deposit at $2kA/m^2$. This suggests that the electrolytic production of HClO and $HClO_2$ is slow despite the positive values of ε^o, and would require a higher concentration of ClO_4^- or a more negative cathode potential in order to produce the quantities of HClO or $HClO_2$ required for the production of a more acceptable deposit. The instability of a chromic acid solution containing still higher concentrations of $HClO_4$ would appear to rule out this option. However, the application of a higher cathode potential might produce sufficient HClO or $HClO_2$ from a 10 : 1 molar ratio solution of $HClO_4$ in chromic acid to catalyze successfully the plating reaction. Unfortunately, it is apparent from Griffith's work (158) that this would probably involve higher current densities and so introduce further problems.

At the low concentrations of $KClO_4$ employed in conjunction with H_2SO_4 in this work (maximum molar ratio of 42 : 1 for CrO_3 : $KClO_4$) the production of HClO and $HClO_2$ might be expected to be insignificant at low current densities (and potentials) where HSO_4^- is the principal active 'catalyst'. However, as the cathode potential is increased the production and subsequent action of HClO and $HClO_2$ might become progressively more influential (assisting the action and bolstering the 'effective' concentration of HSO_4^-).

The negligible effect of ClO_4^- upon α_{term} for the plating reaction and the similarity between the overall polarization curves and that for Standard Solution alone suggest that ClO_4^- has little or no effect upon the cathode 'film' and support the mechanism already proposed.

At cathode current densities between 2 and 5 kA/m^2 plating efficiency is greater in the presence of ClO_4^- than in a Standard Solution alone (Figure 23). These current densities correspond to cathode potentials of between -0.86V and -0.89V (S.H.E), at which thermodynamic quantities for activation are given in Table 7a. As may be seen from Table 7a, ΔG_A is reduced in the presence of ClO_4^- at these potentials (in agreement with the effect upon plating efficiencies). So, plating is promoted by ClO_4^- at 'low' potentials but depressed at higher (more negative) potentials. This may be explained in terms of the mechanism already outlined in which HClO and $HClO_2$ are assumed to be the active species.

$HClO$ and $HClO_2$ require high cathode potentials to be produced in quantity and are, therefore in relatively short supply at low potentials (e.g. -0.89V) where they are able to supplement the action of the HSO_4^- in 'catalysing' the deposition reaction. At higher potentials $HClO$ and/or $HClO_2$ are produced at faster rates and, therefore tend to swamp the solution in the region of the cathode and 'block' reducible chromium species.

The increase in ΔS_A accompanying the addition to a Standard Solution is presumably due to the different structure and charge distribution of the species. For example -

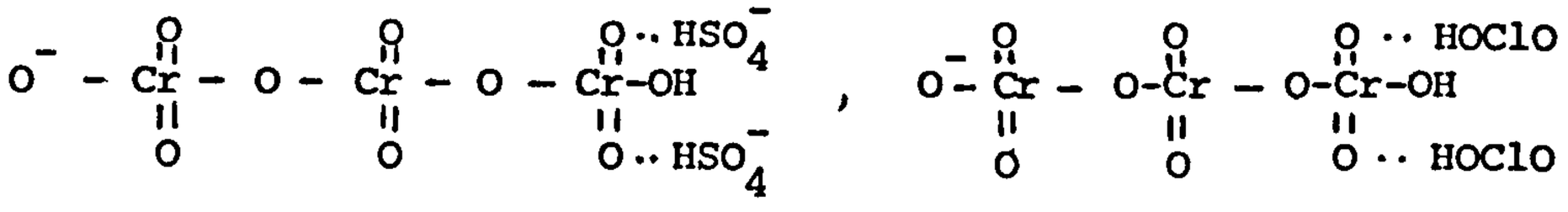

In other words, a greater increase in the degree of disorder accompanying activation takes place when $HClO_2$ (or $HClO$) is the catalysing agent, implying that the reducible species is less disordered in this case.

4.5.3. Potassium bromate

The presence of the bromate ion in a Standard Solution has a number of effects upon the properties monitored.

The overall cathode polarization curves are similar to that produced in a Standard Solution alone but with some differences. In the presence of BrO_3^- an increase in the maximum current density of the CrVI→CrIII 'loop' is apparent (from 0.4kA/m^2 to 0.9kA/m^2). In addition, a further 'loop' is evident at more negative potentials (prior to the onset of chromium deposition which commences at less negative potentials than in a Standard Solution alone) which

corresponds to the commencement of hydrogen evolution (Figure 35) and indicates a reduction in hydrogen overpotential through a modification of the layer of reaction products which exists on the cathode surface. The change in the nature of the first 'loop' and in the existence of a second 'loop' therefore indicate that the influence of BrO_3^- in altering polarization characteristics is through an increase in 'film' conductivity and/or reduction in 'film' thickness.

The commencement of hydrogen evolution (and then metal deposition) at less negative potentials than in a Standard Solution alone may be explained in terms of the formation of more soluble reaction products at the cathode surface. In a Standard Solution alone, as the potential is increased, an insoluble layer of trivalent (and probably divalent) chromium reaction products is formed. A further increase in potential allows hydrogen evolution to commence at the surface with a subsequent increase in pH and modification of the surface layer in such a way as to permit chromium deposition. The bromate ion apparently acts to break down the initial reaction product layer, thus making hydrogen evolution (and, therefore deposition) easier. It is possible that this occurs via -

$$BrO_3^- + 6H^+ \rightarrow Br^- + 3H_2O \qquad 1.44V(vs\ S.H.E)$$

followed by

$$Cr_2O_3 + 6Br^- \rightarrow 2CrBr_3 + 3O^{2-}$$

or

$$CrO + 2BR^{-} \rightarrow CrBr_2 + O^{2-}$$

and

$$nO^{2-} + 2nH^{+} \rightarrow nH_2O$$

Chromium bromides are considerably more soluble than the corresponding oxides (46). A thinning of the cathode layer thus occurs, allowing hydrogen evolution to commence at less negative potentials.

Analysis of the Tafel regions of the partial polarization curves for plating in solutions containing BrO_3^- revealed an increase in slope when compared with a Standard Solution alone. Such a change in Tafel slope indicates an increase in polarization and a reduction in the value of the expression $\lambda \times \alpha_{term}$ (Equation 1.3.9.1.3,1). Variation in this expression could be due to a change in λ, α_{dl}, α_f, or all three. This makes interpretation difficult.

However, other experimental evidence (the effect of BrO_3^- upon the low-potential regions of the overall cathode polarization curves, and its apparent reduction of hysteresis in potentiodynamically recorded polarization data) suggests that the addition of BrO_3^- to a Standard Solution affects the cathode film in a way which causes an increase in its conductivity. But, an increase in film conductivity would be expected to reduce polarization in the plating reaction (and hydrogen evolution reaction), a phenomenon which is not observed.

From Table 7, it may be seen that the presence of BrO_3^- in a Standard Solution causes an increase in ΔG_A (free energy of activation) indicating that a reduction in the exchange current density (i_o) has taken place, an observation that does not support an increase in cathode film conductivity. Reference to the recorded pertinent values of ΔH_A and ΔS_A given in Tables 7 may provide an explanation for this. It is apparent that both quantities are considerably reduced by the presence of BrO_3^-, but that ΔS_A is affected to the greater extent, so that from -

$$\Delta G_A = \Delta H_A - T \Delta S_A$$

a nett increase in ΔG_A is the result.

A reduction in the values of ΔH_A and ΔS_A may be explained in terms of an increase in the conductivity of the cathode film.

It has already been observed that the enthalpy of activation for plating in a Standard Solution is considerably greater than might be expected for a reaction with a charge-transfer as the R.D.S., the explanation provided being that the presence of a cathodic oxide film 'de-activates' the electrode. The reduction of ΔH_A recorded in the presence of BrO_3^- therefore, suggests that this addition somehow 're-activates' the cathode, this being the case, a mechanism is required to explain the action of BrO_3^- in this 're-activation' which increases film conductivity.

A possible explanation is -

(i) $BrO_3^- + 6H^+ + 6e^- \rightarrow Br^- + 3H_2O$ +1.44V (vs.S.H.E)

(ii) $CrO + 2Br^- \rightarrow CrBr_2 + O^{2-}$, $O^{2-} + 2H^+ \rightarrow H_2O$

The film is thus disrupted -

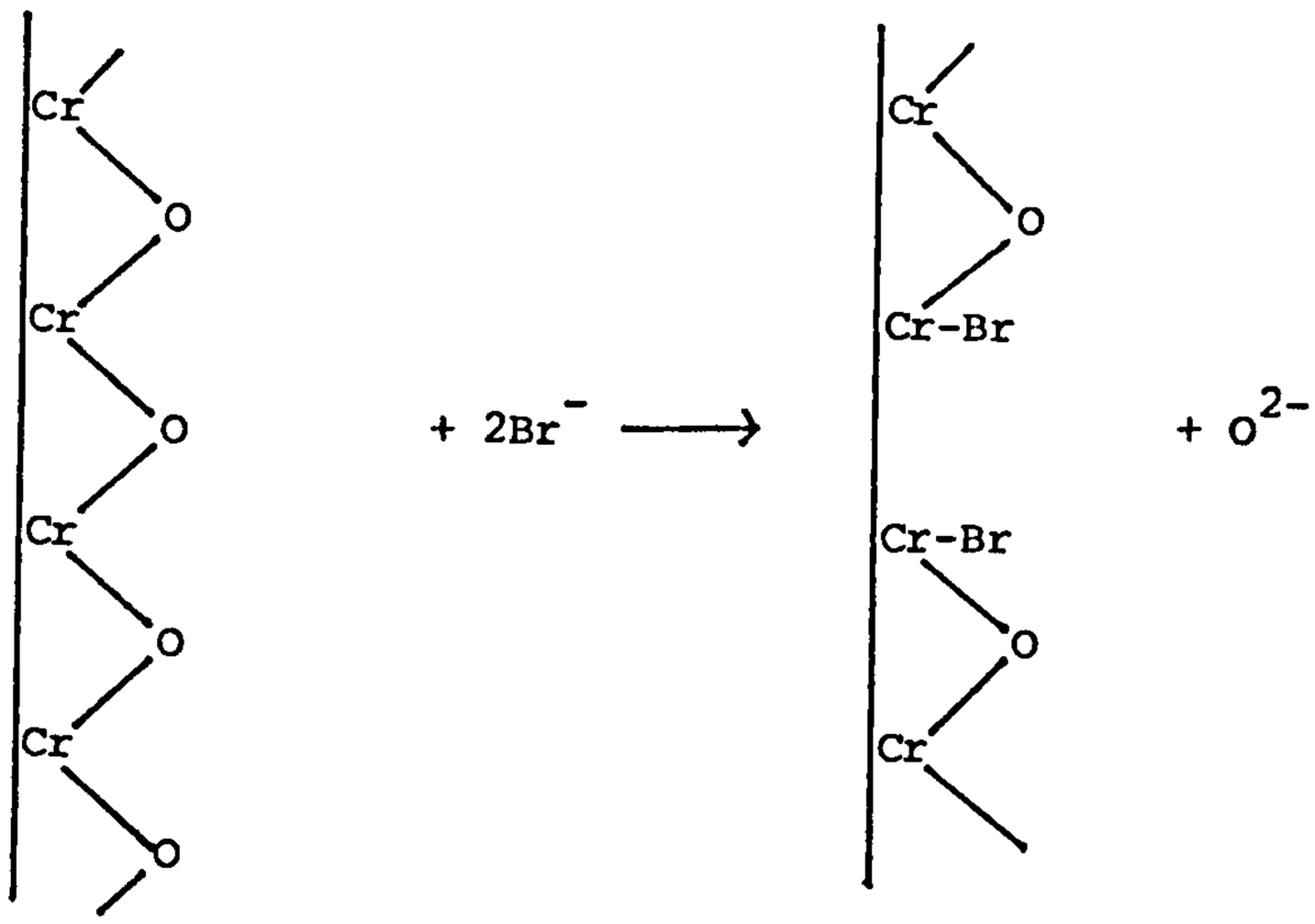

A breakdown of the CrO network in this way could also help to explain the observed drop in ΔS_A for the plating reaction, as the film is clearly in a much less ordered state in the presence of BrO_3^- (Br^-).

A problem arises in the reconciliation of increased Tafel slopes for plating with reduced throwing power in solutions containing BrO_3^-, a contradictory effect. However, an explanation may be found in the Tafel slopes for the competing hydrogen evolution reaction which are increased to a greater degree (Table 4). In other words, although BrO_3^- presence causes an increase in deposition overpotential it causes a greater increase in hydrogen evolution overpotential. As the two reactions are in competition for electrons the deposition reaction is the more successful and so its efficiency rises with current density (total) whereas the hydrogen evolution efficiency gradually falls (Figures 39, 40, 41, 42). A steep increase in plating efficiency with current density is a prime cause of poor throwing power.

The increase in Tafel slope for plating associated with the presence of BrO_3^- presents a further problem in that it argues against other observations which suggest that BrO_3^- causes an increase in film conductivity. Because other evidence points to BrO_3^- (or product thereof) operating within the cathode film, it is reasonable to assume that the observed increase in polarization accompanying the presence of BrO_3^- might also be attributed to a film effect. If it is assumed that the R.D.S. is the same in a solution containing BrO_3^- as in a Standard Solution alone, and that λ remains equal to 12, α_{term} is reduced from 0.25 to $\sim$0.19 (Table 5) with a corresponding increase in α_f (assuming α_{dl} remains equal to 0.5) from 0.5 to $\sim$0.7. Unfortunately, this contradicts all the evidence which suggests that BrO_3^- increases film conductivity.

The anomaly may be explained if a different value for λ is adopted. If a mean value for $\lambda \times \alpha_{term}$ of 2.2. is taken from Table 4 for solutions containing BrO_3^- (ignoring the value for Standard + 15g/l $KBrO_3$ as being anomalous), substitution of $\lambda = 8$ yields a value for α_{term} of 0.275 which (assuming $\alpha_{dl} = 0.5$) reduces α_f to 0.39, satisfying the condition that film conductivity is increased. The assumption that λ changes from 12 to 8 when BrO_3^- is added to a Standard Solution therefore allows the increased Tafel slope for plating to be reconciled with an increase in film conductivity as suggested by the mechanism outlined earlier.

If λ is assumed to be equal to 8 for plating in a Standard Solution containing BrO_3^-, and if the R.D.S. is taken to be the same as in a Standard Solution alone, the reaction mechanism in the presence of BrO_3^- may be written -

(i) $HCr_3O_{10}^- + e^- \rightleftharpoons HCr_3O_{10}^{2-}$

(ii) $HCr_3O_{10}^{2-} + e^- \rightleftharpoons HCr_3O_{10}^{3-}$

(iii) $HCr_3O_{10}^{3-} + e^- \rightleftharpoons HCr_3O_9^{2-} + O^{2-}$

(iv) $3(HCr_3O_9^{2-} + e^- \longrightarrow HCr_3O_8^- + O^{2-})$ R.D.S. ($\nu = 3$)

(v) $3HCr_3O_8^- + 3H_3O^+ \rightleftharpoons 3Cr{=}O + 3H_2O + 3H_2Cr_2O_7$

(vi) $Cr{=}O + e^- \rightleftharpoons Cr{-}O$

(vii) $Cr{-}O + e^- \rightleftharpoons Cr^O$

The effect of BrO_3^- is, therefore to reduce the stoichiometric number of the R.D.S. from 6 to 3. In other words, the number of Cr=O species required for film incorporation/reconstruction is reduced from 6 to 3 when BrO_3^- is added to a Standard Solution. The question then arises as to why this should be so. The answer may lie in a more detailed consideration of the (critical) step -

$$HCr_3O_8^- + H_3O^+ \rightleftharpoons Cr{=}O_{film} + H_2O + H_2Cr_2O_7$$

which actually (according to Hoare) consists of a number of further steps -

$$HCr_3O_8^- + H_3O^+ \rightleftharpoons Cr{=}O_{dl} + H_2O + H_2Cr_2O_7$$

$$Cr{=}O_{dl} + HSO_4^- \rightleftharpoons Cr{=}O\cdots\cdots HSO_4^-\ dl$$

$$Cr{=}O\cdots\cdots HSO_4^-\ dl \rightleftharpoons Cr{=}O\cdots\cdots HSO_4^-\ ads.film$$

$$Cr{=}O\cdots\cdots HSO_4^- \text{ ads.film} \rightleftharpoons Cr{=}O_{film} + HSO_4^-$$

in which the hydrogen-bonding of HSO_4^- to a Cr=O species in the double-layer provides sufficient polarization in the resulting species to allow it to adsorb onto the cathode surface (i.e. 'shoulder in' on the existing cathode film) and be incorporated into the film. The ease with which this polarized, hydrogen-bonded species is able to become accepted into the film network is probably a function of the structural integrity of the film. It would, therefore encounter more difficulty being incorporated into an unflawed film network than into a structurally disrupted film network of the type which (it is proposed) exists in the presence of BrO_3^-. This being the case, it might be expected that the production in association of fewer of these polarized species would be necessary prior to incorporation into the cathode film during plating from a solution which contains BrO_3^-, an observation which could explain the reduction in ν from 6 to 3.

The explanation of increased Tafel slopes for plating in solutions containing BrO_3^- in terms of a reduction in ν combined with an increase in α_{term} presents a further problem because the increased film conductivity might also be expected to increase α_{term} for the hydrogen evolution reaction. However, this is not the case if λ is assumed to remain equal to 2 (as in a Standard Solution alone - see Table 5). In fact, the presence of BrO_3^- leads to a reduction in α_{term} for hydrogen evolution to $\sim$0.16 (from 0.27 in a Standard Solution alone). The measured value for α_{term} of 0.33 (averaged) for solutions containing BrO_3^- must, therefore be due to a decrease in λ_{HER} if the condition that film conductivity is increased (i.e. α_f is decreased) is to be met. λ_{HER} can only be reduced to 1, which gives a more

agreeable value for $\alpha_{term(HER)}$ of 0.33, and would mean that r in Equation (1.3.9.1.2,1) becomes equal to 0 (i.e. the R.D.S. is not a charge-transfer). This indicates a change in mechanism of hydrogen evolution when BrO_3^- is added to a Standard Solution from -

$$M(e^-) + H_3O^+ \longrightarrow MH + H_2O \qquad \underline{R.D.S.}\ (\nu = 2)$$

$$MH + MH \rightleftharpoons 2M + H_2$$

to

$$M(e^-) + H_3O^+ \rightleftharpoons MH + H_2O$$

$$MH + MH \longrightarrow 2M + H_2 \qquad R.D.S.\ (\nu = 1)$$

as already indicated in Section 4.3.2.

The active species Br^- appears to influence deposition in solutions containing $KBrO_3$ from relatively low (negative) cathode potentials, whereas the active species (HClO and/or $HClO_2$) during deposition from solutions containing $KClO_4$ apparently only operate at high cathode potentials (and current densities). This could explain why the influence of BrO_3^- is predominant in solutions which contain both BrO_3^- and ClO_4^-, producing unacceptable deposits (dark and porous) at industrial plating current densities despite the presence of the (beneficial, when the sole additive) ClO_4^-.

Figures 61 and 63 demonstrate that the present of $KBrO_3$ in higher concentrations (15g/l) in a Standard Solution has an interesting and potentially useful effect upon the anodic regeneration of hexavalent chromium ions during plating. The re-oxidation of trivalent chromium ions produced at the cathode -

$$3Cr^{3+} + 10H_2O \rightarrow H_2Cr_3O_{10} + 18H^+ + 9e^-$$

is important as it prevents a build-up of trivalent chromium in solution which could lead to a drop in solution conductivity and an eventual exhaustion of hexavalent chromium. For this reason, it is essential in normal plating practice that an anode to cathode surface area ratio of at least 2 : 1 is maintained. Unfortunately, this area ratio obviously places geometrical constraints upon where chromium plating may be employed as a practical finishing technique. The high efficiency (and therefore rate per unit area) of anodic hexavalent chromium regeneration observed in solutions containing high concentrations of $KBrO_3$ may, therefore prove useful in situations where a high anode to cathode area ratio is impossible.

As no electrochemical investigations (other than current efficiency measurements) were carried out into anode reactions during plating in this work, the mechanism by which BrO_3^- influences these reactions is moot.

Table 8 reveals that the exhaustion of BrO_3^- with time during electrolysis is apparently somewhat more rapid than ClO_4^-. This could be through the production of bromine at the anode alongside oxygen evolution and hexavalent chromium regeneration, following the migration of Br^- ions from the cathode (where they are produced) to the anode. This would lend creedence to the theory that BrO_3^- (as Br^-) has a direct effect upon deposition at all plating current densities via a modification of the cathode film, as an exhaustion of BrO_3^- in solution with time would reduce the presence of Br in the film (and hence film conductivity) and lead to the observed drop in

plating efficiency with time, an observation which tends to support the earlier conclusion that this addition only influences the plating process at higher current densities.

4.5.4. Potassium borate

As a generalization, it is true to say that the presence of the borate ion in a Standard Solution appears to have an influence upon those properties monitored similar to that of the bromate ion but to a lesser degree.

As with BrO_3^-, $B_2O_4^{2-}$ affects both the low current density (pre-plating) region and the higher current density (Tafel) region of the overall polarization curves. In each instance, the effect is similar but not as marked (compared Figures 22, 35 and 36).

A second slight pre-plating 'loop' (in addition to the CrVI→ CrIII 'loop') in the overall cathode polarization curves measured in solutions containing $K_2B_2O_4$ (at 5g/l, 10g/l, 15g/l) is evident, suggesting that this addition may act to modify the reaction product layer which exists on the cathode surface at these postentials in the same way as the BrO_3^- addition which allows hydrogen evolution to commence at less negative potentials than in a Standard Solution alone. Once again, the maximum current density of the CrVI→ CrIII 'loop' is increased when compared with a Standard Solution (from 0.4kA/m^2 to 0.6kA/m^2 - compare Figures 22 and 36), providing evidence that $B_2O_4^{2-}$ acts to alter the nature of the surface film. The $B_2O_4^{2-}$ therefore appears to act in a similar way to BrO_3^- (actually Br^-) to break down the initial reaction product layer on the cathode surface, making the hydrogen evolution reaction (and ultimately deposition) easier. Unfortunately, there is

little information on electrode reactions involving $B_2O_4^{2-}$ in the literature, and as a result all conclusions made about the mechanism by which $B_2O_4^{2-}$ acts must be tentative. Nonetheless, the evidence from the pre-plating region of the overall cathode polarization curves recorded in solutions containing $B_2O_4^{2-}$ (together with a reduction in hysteresis observed in the potentiodynamically recorded polarization data from these solutions) suggests that this addition affects the cathode film.

As in the case of BrO_3^-, analysis of the Tafel regions of the partial polarization curves for plating and hydrogen evolution in solutions containing $B_2O_4^{2-}$ (Figures 54 and 55) yield increased Tafel slopes which contradict the concept of this addition acting to increase film conductivity. So, once again, the assumption that $\lambda = 12$ for plating gives an anomalously decreased value for α_{term} (compared to a Standard Solution alone) and requires the selection of a different, lower value for λ in order to satisfy the condition that $B_2O_4^{2-}$ causes an increase in α_{term} (α_{term} in Standard Solution alone is 0.25) and film conductivity. Again, $\lambda = 8$ seems to provide the most likely answer, giving a value for α_{term} of 0.31 (assuming an average $\lambda \times \alpha_{term}$ for these solutions of 2.5 - see Table 4) and a stoichiometric number for the R.D.S. of 3 (assuming the same R.D.S. as in solutions containing BrO_3^-).

If it is assumed (and the evidence points to the fact) that $B_2O_4^{2-}$ acts to increase the conductivity of the cathode film, a mechanism for this may be proposed -

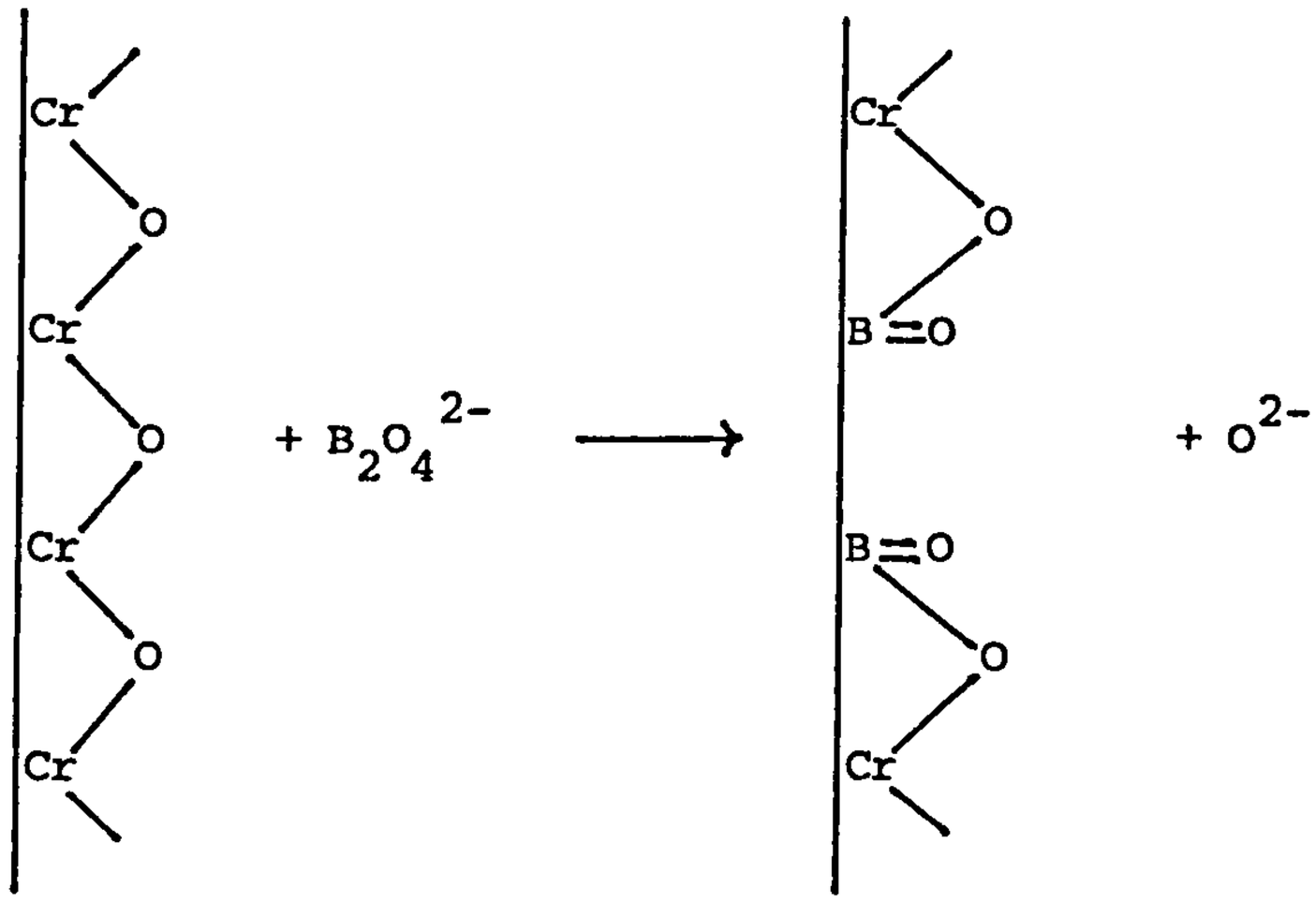

Here again, the addition is assumed to cause a disruption in the cathode film which would explain an increase in film conductivity.

It is interesting to note that the proposed siting of the foreign atoms in the Cr=O network is different, with B essentially occupying a Cr position whereas Br occuies an O position. This helps to reinforce the idea (see below) that B may be incorporated to a degree into the growing deposit (leading to an increase in hardness) whereas Br^- is regenerated as the film undergoes final reduction to metal.

Assuming $\lambda = 8$ and that $B_2O_4^{2-}$ increases film conductivity, it might be expected that α_{term} for the hydrogen evolution reaction would be similarly increased to a value greater than that for a Standard Solution alone (0.27). As $\lambda x\ \alpha_{term}$ for hydrogen evolution in solutions containing $B_2O_4^{2-}$ averages ~0.38, this would once more (as with BrO_3^-) require λ to equal 1 and suggest a similar mechanism for hydrogen evolution to that in solutions containing BrO_3^-.

The thermodynamic quantities for activation given in Tables 7 indicate that the presence of $B_2O_4^{2-}$ in a Standard Solution causes a slight increase in ΔG_A which in turn indicates a slight

increase in film conductivity. Once more (as in the case of BrO_3^-) this increase in ΔG_A is due to a slight reduction in ΔH_A combined with a relatively larger reduction in ΔS_A, both of which could be attributed to a 're-activation' and disruption of the film by $B_2O_4^{2-}$ (as predicted by the mechanism proposed earlier).

Although polarization for both plating and hydrogen evolution is increased by the presence of $B_2O_4^{2-}$ (compared to a Standard Solution alone), the hydrogen evolution reaction is affected to a greater extent (Table 4). As a result, plating takes place at slightly higher efficiencies than in a Standard Solution alone (Figures 23, 24, 45, 46). Figure 46 demonstrates no drop in plating efficiency similar to that observed in the presence of ClO_4^- (Figure 24) and, as a result, helps to explain the poor throwing power of solutions containing $B_2O_4^{2-}$ (Table 1) which is intermediate between that of a Standard Solution alone and solutions containing BrO_3^-. In addition, it is considered that the apparent argument between reduced throwing power and steeper Tafel slopes in solutions containing $B_2O_4^{2-}$ may also be due in part to the mechanics of gas evolution as invoked in the earlier explanation of the same phenomenon in solutions containing BrO_3^-.

The slight increase in deposit hardness caused by the $B_2O_4^{2-}$ in solution is somewhat unexpected, bearing in mind the similarity of this addition to BrO_3^- in terms of its influence upon the other properties monitored. The effect is also rather too consistent to be explained by statistical means (sic). It is unlikely that the increase in hardness is via Snavely's mechanism of hydride decomposition (49) as, unlike solutions containing ClO_4^-, $B_2O_4^{2-}$ does not favour the hydrogen evolution reaction. It is, therefore considered possible that the

hardening mechanism is the co-deposition of some boron in regions of locally high potential, with a subsequent formation of a solid solution in chromium or chromium boride particles.

Reference to Figure 65 demonstrates that although $B_2O_4^{2-}$ presence leads to a considerably increased rate of anodic CrVI regeneration atlow anode current densities (< 20kA/m^2), this rapidly decreases at higher current densities where such a phenomenon could be of possible use (as is the case in a solution containing 15g/l BrO_3^-) and is, therefore considered to be of little significance.

CONCLUSIONS

5. Conclusions

(i) Analysis of Tafel data for both the plating reaction and the hydrogen evolution reaction (during chromium plating at industrial current densities) appears to confirm that deposition takes place via a cathodic (CrII oxide) film. This is supported by observed polarization hysteresis at high sweep-rates and subsequently determined high values for the enthalpy of activation for the plating reaction (suggesting a de-activated cathode surface).

(ii) The rate-determining step in the plating reaction in the chromium deposition process at these current densities appears to be a charge-transfer (following a Tafel regime) involving the reduction of (probably) a trivalent chromium bearing species to a divalent chromium bearing species in the double layer.

(iii) The rate-determining step in the plating reaction takes place 6 times for every occurrence of the overall reaction.

(iv) The presence of $KClO_4$ in a Standard chromium plating solution leads to an improvement in the throwing power of the solution together with an extended 'bright range' and increased deposit hardness.

Analysis of polarization data, current efficiency data and calculated thermodynamic quantities of activation for the plating reaction led to the conclusion that $KClO_4$ modifies the deposition mechanism in regions of locally higher cathode current density through the electrolytic production of HClO and/or $HClO_2$ which are able to replace/assist the sulphate catalyst (actually HSO_4^-) in its action upon chromium bearing species in the outer Helmholtz plane (i.e., not in the cathode film) and divert current to the hydrogen evolution reaction.

(v) The addition of $KBrO_3$ to a Standard Solution appears to have a generally adverse effect upon the plating process and the deposit produced, causing a worsening of throwing power, a reduction in the 'bright range', and softer plate.

These effects may be explained in terms of the observed changes (due to $KBrO_3$ presence) to polarization curves, current efficiencies and thermodynamic quantities of activation for the plating reaction, which pointed to the action of $KBrO_3$ as being confined (as a reduction product - Br^-) to a disruption of the cathode film favouring both the hydrogen evolution reaction and the plating reaction, but the latter to a greater extent.

A positive aspect of $KBrO_3$ presence in a Standard Solution is its tendency (at higher concentrations - 15 g/l) to increase consistently the rate of anodic CrVI regeneration.

(vi) $K_2B_2O_4$ in a Standard Solution has a generally similar effect to, but less pronounced than, $KBrO_3$, in that both the throwing power and 'bright range' are reduced. A slightly harder deposit is produced (possibly as a result of boron or boride incorporation) but this is of little use in a solution which exhibits a poor throwing power and 'bright range'.

Again, the interpretation of experimental data suggested that the effect of $K_2B_2O_4$ on the process and the deposit produced was via a modification of the cathode film.

(vii) Attempts to combine the beneficial effects of one addition with those of another in a Standard Solution proved fruitless, as $KBrO_3$ 'swamped' any other addition in its effects.

SUGGESTIONS FOR FURTHER WORK

6. Suggestions for further work

(i) The investigation of the variation of current density with time during the first few seconds (using a sensitive recording technique) following the abrupt application of a fixed negative potential (corresponding to a current density within the plating range) to a cathode in a catalyzed and uncatalyzed solution has been used (157) to demonstrate that the presence of the sulphate ion affects the conductivity of the cathodic film formed. This technique could be applied to the solutions tested in this work in an attempt to confirm the conclusions drawn regarding the effect of the new additives upon film conductivity during plating.

(ii) The application of rate-process theory to the hydrogen evolution reaction during chromium plating in a Standard Solution, in an attempt to further categorize the rate-determining step.

(iii) A repetition of (ii) in solutions containing $KClO_4$ and $KBrO_3$ in order to investigate their effects upon ΔH_A, ΔS_A and ΔG_A for the hydrogen evolution reaction and yield a more complete picture of the influence of these additives upon the overall plating process.

(iv) A determination of the concentration of ClO_4^- and cathode potential required to produce an acceptable deposit (assuming one is obtainable) in a sulphate-free Standard Solution.

(v) Industrial-scale tests on $KClO_4$ as a potentially commercial addition to a Standard chromium plating solution.

(vi) Industrial-scale tests on $KBrO_3$ as a plating additive where component geometry determines a low anode to cathode surface area ratio, and plate appearance is of secondary importance.

REFERENCES

REFERENCES

1. F.A.Lowenheim. Electroplating, Mc-Graw-Hill, 1978.

2. A.R.Despic and K.I.Popov. Modern Aspects of Electrochemistry No. 7, pp 199, Butterworth's 1972.

3. H.J.Reed and A.K.Graham. Trans.Am.Electrochem.Soc., 778, 78, (1940).

4. W.N.Nernst and E.S.Merriam. Z.Phys.Chem., 237, 53, (1905).

5. J.A.V.Brunner. Z.Phys.Chem., 56, 47, (1904).

6. D.A.Vermilyea. J.Chem.Phys., 1254, 25, (1956).

7. M.Volmer. Z.Phys.Chem., 267, 102(A), (1922).

8. G.Wranglen. Trans.Roy.Inst.Tech. (Stockholm), (1950).

9. H.J.Pick and J.Wilcock. Trans. Inst.Met.Fin., 298, 35, (1958).

10. A.Stranski in "Crystal Growth", Ed. H.E.Buckley, John Wiley 1951.

11. S.A.Watson and J.Edwards. Trans.Inst.Met.Fin., 167, 34, (1957).

12. G.Kortum. Treatise on Electrochemistry, 2nd edition, Elsevier (1965).

13. N.E.Khomutov in "Electrodeposition of Metals and Alloys", I.P.S.T. Press, Jerusalem 1969.

14. J.M.West. Basic Electrochemistry, Van Nostrand Reinhold 1973.

15. J.M.West. Basic Corrosion and Oxidation, Ellis Horwood Ltd 1981.

16. J.Tafel. Z.Phys.Chem., 641, 50, (1905).

17. W.Lorenz. Z.Phys.Chem., 275, 202, (1953).

18. W.Lorenz. Nature., 716, 99, (1954).

19. J.O'M.Bockris and G.A.Razumney. Fundamentals of Electrocrystallization, Plenum Press, New York 1967.

20. J.O'M.Bockris and B.E.Conway. Proc.Roy.Soc., 394, A248, (1958).

21. K.J.Vetter. Z.Phys.Chem., 284, 194, (1950). Z.Elektrochem., 121, 55, (1951). ibid, 931, 56, (1952).

22. J.N.Agar and F.P.Bowden. Proc.Roy.Soc., 206, A169, (1939).

23. K.J.Vetter. Electrochemical Kinetics: Theoretical Aspects, Academic Press London 1967.

24. J.N.Agar. Trans.Faraday Soc., 81, 44, (1948).

25. G.E.Gardam. Trans.Faraday Soc., 182, 43, (1947).

26. A.Armata and P.Delahay. J.Phys.Chem., 880, 68, (1964).

27. T.Biegler and H.A.Laitinen. J.Electrochem.Soc., 852, 113, (1966).

28. A.K.Vijh. Electrochemistry of Metals and Semiconductors, Marcel Dekker New York 1973.

29. H.Gerischer. Physical Chemistry: An Advanced Treatise Vol.IX(A), Academic Press New York 1970.

30. B.E.Conway. Progress in Reaction Kinetics Vol.4, Pergamon Press Oxford 1967.

31. R.E.Meyer. J.Electrochem.Soc., 847, 107, (1960).

32. A.K.Vijh. J.Phys.Chem., 506, 73, (1969).

33. A.N.Frumkin. Disc.Faraday Soc., 57, 1, (1947).

34. J.Weiss. Disc.Faraday Soc., 68, 1, (1947).

35. A.C.Makrides. J.Electrochem.Soc., 1158, 113, (1966).

36. J.W.Diggle, T.C.Downie and C.W.Goulding. Corrosion Sci., 907, 8, (1968).

37. J.Kunze. Corrosion Sci., 273, 7, (1967).

38. B.E.Conway and D.Gilroy. J.Phys.Chem., 1259, 69, (1965).

39. V.S.Bagotskii and Y.B.Vasilev. Electrochimica Acta., 869, 9, (1964).

40. J.O'M.Bockris and B.E.Conway. Electrochimica Acta., 340, 3, (1961).

41. J.O'M.Bockris and E.C.Potter. J.Electrochem.Soc., 169, 99, (1952).

42. J.M.West. Electrodeposition and Corrosion Processes, Van Nostrand Reinhold 1970 (2nd Edition).

43. D.G.Rogers and A.A.Burr. J.Electrochem.Soc., 92, 97, (1950).

44. S.Glasstone, J.K.Laidler and H.Eyring. The Theory of Rate Processes, McGraw-Hill New York 1941.

45. British Standards Institution: Electroplated Coatings of Nickel and Chromium on Steel and Brass. BS 1224 (1953).

46. C.R.C. Handbook of Chemistry and Physics (60th Edition), C.R.C. Press Boca Raton, Florida 1980.

47. P.Morriset, J.W.Oswald, C.R.Draper and R.Pinner. Chromium Plating, R.Draper 1954.

48. W.A.Wood. Phil.Mag., 1073, 10, (1930).

49. C.A.Snavely. Trans.Electrochem.Soc., 537, 92, (1947).

50. D.R.Gabe. Ph.D. Thesis, University of Sheffield, November 1962.

51. W.H.Cleghorn and J.M.West. Trans.Inst.Met.Fin., 105, 44, (1966).

52. W.H.Cleghorn and J.M.West. Trans.Inst.Met.Fin., 43, 45, (1967).

53. A.Brenner, P.Burkhead and G.Jennings. J.Nat.Bur.Standards., 31, 40, (1948).

54. D.J.MacNaughton and A.W.Hothersall. J.Electrodep.Tech.Soc., 63, 5, (1930).

55. A.Swain. Machinist., 496, 77, (1933).

56. P.A.Jacquet and A.R.Weill. Chrome Dur., p4 (1949).

57. A.S.T.M. Specification. Chromium Plating on Steel for Engineering Use, No. B177.

58. P.Bastien and A.Popoff. Chrome Dur., p13 (1948).

59. K.Gebauer. Oberflachentechnik., February (1941).

60. L.E.Grant and L.F.Grant. Trans.Am.Electrochem.Soc., 509, 53, (1928).

61. M.Cymboliste. Trans.Electrochem.Soc., 353, 73, (1938).

62. J.B.Cohen. Trans.Electrochem.Soc., 441, 86, (1944).

63. G.I.Finch and D.N.Layton. Trans.Inst.Met.Fin., 215, 27, (1951).

64. D.N.Layton. Trans.Inst.Met.Fin., 239, 28, (1952).

65. W.Arkharow. Tech.Phys.U.S.S.R., 1072, 3(12), (1936).

66. R.Glocker and E.Kaupp. Z.Phys., 121, 24, (1924).

67. W.Hume-Rothery and M.R.J.Wyllie. Proc.Roy.Soc., 331, A181, (1943).

68. C.G.Fink. U.S.Patent 1,581,188 (1926).

69. E.Liebreich. German Patent 488,526 (1924). Z.Electrochem., 94, 27, (1921). ibid, 208, 29, (1923). ibid, 186, 30, (1924).

70. J.E.Stareck, F.Passal and H.Mohlstedt. Proc.Am.Electroplaters' Soc., 31, 37, (1950).

71. H.Silman. Trans.Inst.Met.Fin., 43, 32, (1955).

72. J.Solanze. Galvano., 13, 22, (1953).

73. British Patent 697,786 (1953).

74. V.M.Semin in "Theory and Practice of Chromium Electroplating", Ed. Vagramyan and Kudrayetsev (1959).

75. H.Wahl and K.Gebauer. Metalloberflache., No. 2 (1948).

76. K.Gebauer and K.Sommer. Oberflachentechnik., May (1942).

77. A.J.Steiger. Metal Finishing., 56, 56, (1958).

78. French Patent 754,299 (1951).

79. A.Kozelnigg. Metalloberflache., 156, 5, (1953).

80. F.Taylor. Electroplating., 109, 5, (1952).

81. O.Deny-Henault. Z.Electrochem., 319, 12, (1906).

82. A.Recoura. Bulg.Soc.Chem., 1155, 3, (1902).

83. S.I.Orlova and N.I.Petin. Z.Obs.Khim., 345, 1, (1931).

84. P.F.Kalyuzhnaya and K.N.Pimenova., Z.Prikl.Khim., 1057, 35, (1962).

85. S.Morioka and H.Yamaoka., Tohoku daig.sen.sitr.kon.ikho., 45, 14, (1958).

86. W.Machu and M.F.M.El-Gandour. Werkstoffe und Korrosion, 556, 10, (1959). ibid, 617, 10, (1959). ibid, 274, 11, (1960).

87. G.Fuseya and K.Sasaki. Trans.Electrochem.Soc., 445, 59, (1931).

88. C.Kasper. J.Nat.Bur.Standards., 519, 11, (1923). ibid., 353, 9, (1922).

89. A.I.Falicheva, A.I.Matantsev, N.V.Savinova and V.A.Kostyreva in "Theory and Practice of Bright Electroplating", Pub. Vil'nyus 1963.

90. S.Morioka and H.Yamaoka. Tech.Rep.Tohoku.Univ., 121, 22, (1959).

91. R.W.Parry, S.Swann and J.C.Bàiler. Trans.Electrochem.Soc., 507, 92, (1947).

92. L.P.Zosimovich, A.I.Zayets and L.K.Rudaya. Ukrain.Khim.Zh., 150, 28, (1962).

93. R.R.Lloyd, W.T.Rowles and R.G.Fleney. Trans.Electrochem.Soc., 443, 89, (1946).

94. W.H.Wade and L.F.Ynterna. Trans.Electrochem.Soc., 461, 74, (1938).

95. T.Joshida and R.Joshida. J.Chem.Soc.Japan., 89, 58, (1955).

96. T.Joshida. J.Chem.Soc.Japan., 8, 58, (1955).

97. N.R.Barucha and J.J.B.Ward. Prod.Finishing, 4, 64, 33, (1969).

98. British Patent 1,144,913 (1969).

99. J.J.B.Ward, I.R.A.Christie and V.E.Carter. Trans.Inst.Met.Fin., 97, 49, (1971).

100. C.Barnes, J.J.B.Ward and J.R.House. Trans.Inst.Met.Fin., 74, 55, (1977).

101. D.L.C.Burges. Trans.Inst.Met.Fin., 138, 54, (1976).

102. G.Dubpernell. Trans.Electrochem.Soc., 589, 80, (1941).

103. R.Schneidewind. Mich.Eng.Bulletin., 60pp (1930).

104. C.A.Zapffe and M.E.Haslem. Trans.A.S.M., 241, 39, (1947).

105. C.Levy and G.A.Consolazio. J.Electrochem.Soc., 624, 103, (1956).

106. A.C.Stern. J.Electrochem.Soc., 67N, 93, (1948).

107. H.E.Haring. Chem. and Met.Eng., 692, 32, (1925).

108. J.Gabriel. Metal Finishing., 55, 64, (1966).

109. H.L.Farbera and W.Blum. J.Res.Nat.Bur.Standards, 661, 4, (1931).

110. R.Seegmiller and V.A.Lamb. Proc.Am.Electroplaters' Soc., 125, 35, (1948).

111. S.Y.S.Parn, Private communications.

112. D.Howe, M.McCormick, C.Yonnet and G.Glossop. Finishing Industries, 34, January, (1979).

113. A.I.Levin and A.I.Falicheva. Z.Fiz.Khim., 1652, 28 (1954).

114. E.Muller and A.Kossow. Z.Elektrochem., 833, 38, (1932).

115. N.Hackerman and R.Powers. Z.Elektrochem., 139, 57, (1953).

116. A.I.Levin and A.I.Falicheva in "Theory and Practice of Chromium Electroplating", Ed. Vagramyan and Kudrayetsev (1959).

117. J.Levitan. J.Electrochem.Soc., 286, 111, (1964).

118. J.P.Hoare. J.Electrochem.Soc., 190, 126, (1979).

119. T.Moeller. Inorganic Chemistry, J.Wiley and Sons, New York 1952.

120. J.C.Saiddington and G.R.Hoey. J.Electrochem.Soc., 1011, 117, (1970).

121. H.E.Haring and W.P.Barrows. Tech.Pub.Nat.Bur.Standards, 413, 21, (1926).

122. J.P.Hunt and H.Taube. J.Chem.Phys., 757, 18, (1950).

123. I.M.Kolthoff and A.M.Shams El Din. J.Phys.Chem., 1564, 60, (1956).

124. D.G.Rogers and A.A.Burr. Trans.Electrochem.Soc., 97, 97, (1950).

125. G.J.Sargent. Trans.Am.Electrochem.Soc., 479, 37, (1920).

126. E.Liebreich. Z.Elektrochem., 628, 39, (1933). ibid., 73, 40, (1940).

127. E.Muller. Z.Elektrochem., 399, 32, (1926).

128. N.D.Birynkov and A.Nelikhov. Korrosion u.Metall., 294, August, (1947).

129. R.R.Rogers. Trans.Electrochem.Soc., 391, 68, (1935).

130. Y.Kato and T.Murakami. J.Soc.Chem.Ind.Japan., 124, 31, (1928).

131. C.Kasper and W.Blum. Trans.Electrochem.Soc. (discussion)., 412, 68, (1935).

132. E.A.Ollard and A.Bradley. Nature., 122, 117, (1926).

133. J.Hume-Rothery. The Structure of Metals and Alloys, Institute of Metals, London, (1962).

134. A.Svedberg. Colloid Chemistry pp243, Chemical Catalog Co. Inc. (1928).

135. D.Reinkowski and C.A.Knorr. Z.Elektrochem., 709, 58, (1954).

136. D.G.Grahame. Chem.Rev., 441, 41, (1947).

137. P.Delahay. Double-layer and Electrode Kinetics pp44, Interscience New York 1965.

138. E.Muller. Arch.Metallkunde., 110, 2, (1948).

139. C.Kasper. J.Nat.Bur.Standards., 693, 14, (1935).

140. F.Ogburn and A.Brenner. Trans.Electrochem.Soc., 347, 96, (1949).

141. A.T.Vagramyan and D.N.Usachev in "Theory and Practice of Chromium Electroplating", Ed. Vagramyan and Kudrayetsev (1959).

142. Discussion. Trans.Electrochem.Soc., 385, 96, (1949).

143. A.T.Vagramyan and Z.A.Solov'eva in "Electrodeposition of Metals and Alloys", I.P.S.T.Press Jerusalem 1969.

144. N.E.Ryan. Metal Finishing., 73, 63, (1965).

145. A.T.Vagramyan, D.N.Usachev and N.L.Klimarenko. Proc.Acad.Sci. U.S.S.R., 828, 127, (1959).

146. R.Weiner. Trans.Inst.Met.Fin., 46, 43, (1966).

147. M.Kappel and H.Gerischer. Z.Elektrochem., 235, 64, (1960).

148. A.T.Vagramyan and D.N.Usachev. Zh.Priklad.Khim., 1900, 32, (1958).

149. M.A.Shluger and V.A.Kazakov. Zh.Fiz.Khim., 752, 36, (1959).

150. Z.A.Solov'eva, Y.S.Petrova, N.L.Klimasenko and A.T.Vagramyan. Zh.Priklad.Khim., 1806, 35, (1962).

151. H.Feigl, L.Kandler and J.Rheinhold. Metalloberflache., 229, 17, (1963).

152. R.Weiner and C.Schiele. Metalloberflache., 357, 14, (1960).

153. J.C.Saiddington and G.R.Hoey. J.Electrochem.Soc., 1475, 120, (1973).

154. G.Levy and G.A.Consolazio. J.Electrochem.Soc., 624, 103, (1956).

155. R.Weiner and C.Schiele. Z.Phys.Chem., 248, 26, (1960).

156. H.Okada and K.Yamamoto. Electrochem.Technol., 389, 6, (1968).

157. A.T.Vagramyan, D.N.Usachev and G.I.Cherchova. in "Electrodeposition of Metals and Alloys" Issue 1. Ed. D.Slutzkin. Pub. IPST Press (1969).

158. J.L.Griffin. Plating., 196, 53, (1966).

159. J.A.Naismith. Private communications.

160. J.A.Fraunhofer and C.H.Banks. Potentiostat and its applications, Butterworths 1972.

161. S.Y.S.Parn, D.Howe and M.McCormick. Private communications.

162. R.Parsons. Handbook of Electrochemical Constants, Butterworth's (1969).

163. S.Barnartt. J.Electrochem.Soc., 549, 99, (1952).

164. A.L.Ferguson and G.M.Chen. J.Phys.Chem., 1166, 36, (1932).

165. A.L.Ferguson. Trans.Electrochem.Soc., 113, 76, (1939).

166. A.L.Ferguson and S.Kleinheksel. J.Phys.Chem., 171, 42, (1938).

167. F.Haber. Z.Phys.Chem., 208, 32, (1900).

168. A.M.Azzam and J.O'M.Bockris. Nature., 403, 165, (1950).

169. Y.Y.Matulis and D.Rimdzhyute in "Contributions to the Theory of Chromium Plating", I.P.S.T.Press, Jerusalem 1965.

170. J.O'M.Bockris and A.K.N.Reddy. Modern Electrochemistry Vols 1 and 2, Plenum Press 1970.

171. A.C.Makrides. J.Electrochem.Soc., 1158, 113, (1966).

172. A.V.Shreider in "Theory and Practice of Chromium Electroplating", Ed. Vagramyan and Kudrayetsev (1959).

173. R.Jha Private Communication.

174. D.R.Gabe and J.M.West. Trans. I.M.F., 197, 40, (1963).

175. A.Hall. Final year undergraduate project, Sheffield University, 1982.

APPENDICES

APPENDIX I

A simplified model to account for the variation in potential drop with Luggin probe gap.

During polarization measurement, assume the Luggin probe tip to be positioned a distance of x metres from the cathode surface and the cathode current to be I_t Amps.

Under these circumstances, the potential drop must consist of two components (additive);

(i) A bubble layer component (the evolution of hydrogen at the cathode introduces an extra resistance to current passage).

(ii) A component corresponding to the solution gap between the probe tip and the outer edge of the bubble layer.

(i) Bubble layer component

If the bubble layer thickness is δ_{BL} metres, the potential drop across the bubble layer is given by

$$\Delta V_1 = \frac{\rho \delta_{BL} I_t}{A'} \qquad 1$$

where ρ = resistivity of solution = 6.4×10^{-4} m

A' = effective cathode area for deposition in metres (area unmasked by hydrogen bubbles).

If it is assumed that bubbles of evolved hydrogen adopt a quasi-F.C.C. arrangement at the cathode surface with the plane of the surface coinciding with the (100) plane of the unit cube, the situation may be represented thus;

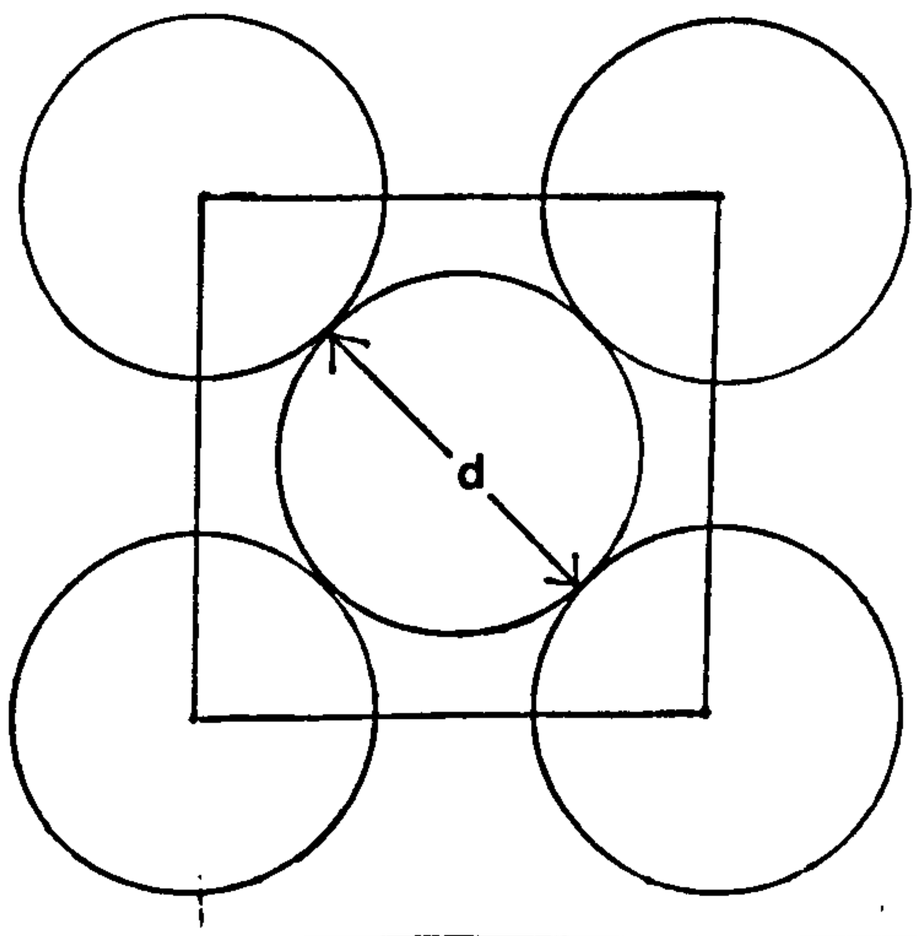

If the bubble diameter is d, the fraction of the unit area masked by bubbles is $\frac{1}{2}\pi d^2/2d^2 = \pi/4$. This leaves the fraction of the surface unmasked equal to $1 - \pi/4$, so

$$A' = (1 - \pi/4)A \qquad 2$$

Combining equations 1 and 2 gives

$$\Delta V_1 = \frac{\rho \delta_{BL} I_t}{(1 - \pi/4)A} \qquad 3$$

If the bubble layer is B bubbles thick, then

$$\delta_{BL} = B\ d \qquad 4$$

and the necessity to determine d arises.

The volume of hydrogen (in bubbles) adjacent to the cathode surface at time t is

$$V_H = 2A\pi \frac{d^3}{6} . A . \frac{1}{2d^2} \qquad 5$$

However, according to Faraday, the volume of hydrogen may also be given by

$$V_H = \frac{I_H . t}{2F} \times 2.47 \times 10^{-2} \text{ (molar volume of } H_2 \text{ at } 55^{\circ}C) \qquad 6$$

but $d = D_H^{\frac{1}{2}} . t^{\frac{1}{2}}$, where D_H is the diffusivity of H^+, so

$$V_H = \frac{I_H . d^2}{2F . D_H} \times 2.47 \times 10^{-2} \qquad 7$$

Assuming D_H to = $2 \times 10^{-5} m^2/s$ and equating equations 5 and 7

$$d = \frac{\pi A^2}{I_H} \times 156.25 \qquad 8$$

Recalling equation 4,

$$\delta_{BL} = \frac{B\pi A^2}{I_H} \times 156.25 \qquad 9$$

Substitution of equation 9 in equation 1 yields

$$\Delta V_1 = \frac{\rho}{(1 - \pi/4)} \times \frac{B\pi A}{CE_H} \times 156.25 \qquad 10$$

where CE_H = current efficiency of hydrogen evolution = I_H/I_t

(ii) Solution gap component

The thickness of the gap according to this model is $\varkappa - \delta_{BL}$, and the corresponding potential drop is given by

$$\Delta V_2 = \frac{I_t \times \rho \times (\varkappa - \delta_{BL})}{A} \qquad 11$$

Substituting equation 9 into this expression gives

$$\Delta V_2 = \frac{I_t \rho \varkappa}{A} - \frac{B\pi A\rho \times 156.25}{CE_H} \qquad 12$$

Combination of equations 10 and 12 gives an expression for the total potential drop

$$\Delta V_3 = \frac{\rho}{(1 - \pi/4)} \times \frac{B\pi A}{CE_H} \times 156.25 + \frac{I_t \rho \varkappa}{A} - \frac{B\pi A\rho \times 156.25}{CE_H}$$

Substitution of typical values of $B = 1$, $\varkappa = 10^{-3}$m, $A = 10^{-4}$m^2, $\rho = 6.4 \times 10^{-4}$, $I_t = 0.3$ Amps, $CE_H = 0.6$, yields

$$\Delta V_3 = 0.244\text{mV} + 1.920\text{mV} - 0.052\text{mV} = \underline{2.112\text{mV}}$$

This is of the order of measured values corresponding to the conditions defined.

APPENDIX II

During the course of testing and examination, a sample of plate produced from a Standard Solution containing 10 g/l $K_2B_2O_4$ was inadvertently bent, causing the deposit to crack and flake away from the substrate.

When viewed by means of a Philips SEM 400, it was apparent that the nature of the flaking allowed a lateral examination of the chromium deposit. Plates 17 and 18 illustrate this at two magnifications.

The photomicrograph taken at the higher magnification (Plate 18) apparently demonstrates that each nodule of plate produced consists of an agglomeration of very fine micro-nodules, an observation supported by close examination of Plate 8 (plate produced from a solution containing 10 g/l $KClO_4$).

APPENDIX III

A schematic representation of Hoare's mechanism (118) for chromium electrodeposition modified slightly to involve the concept of a cathode 'film' based upon Cr=O.

To ease congestion in the diagram, the following species which take part in the reaction are represented by letters;

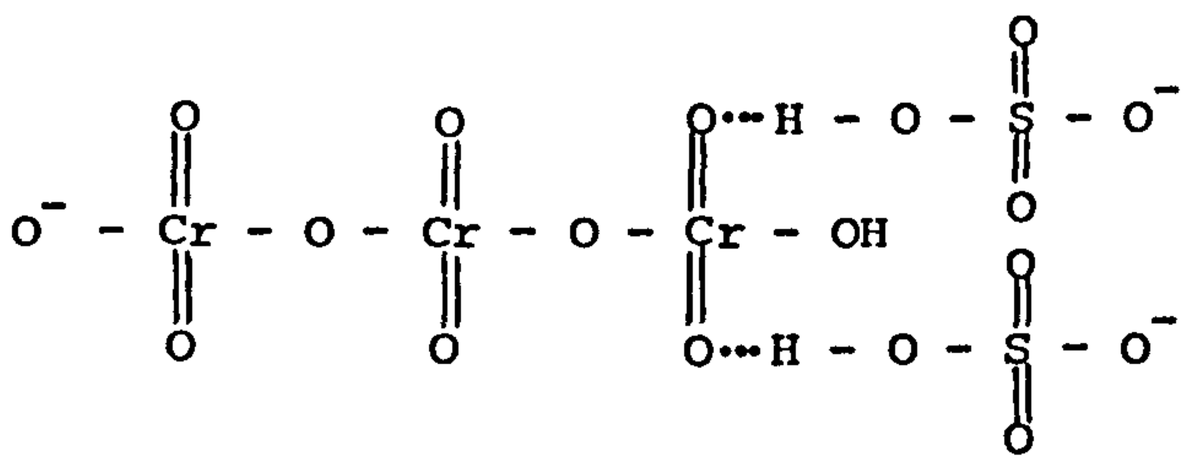

or $HCr_3O_{10}^-$ = Species A

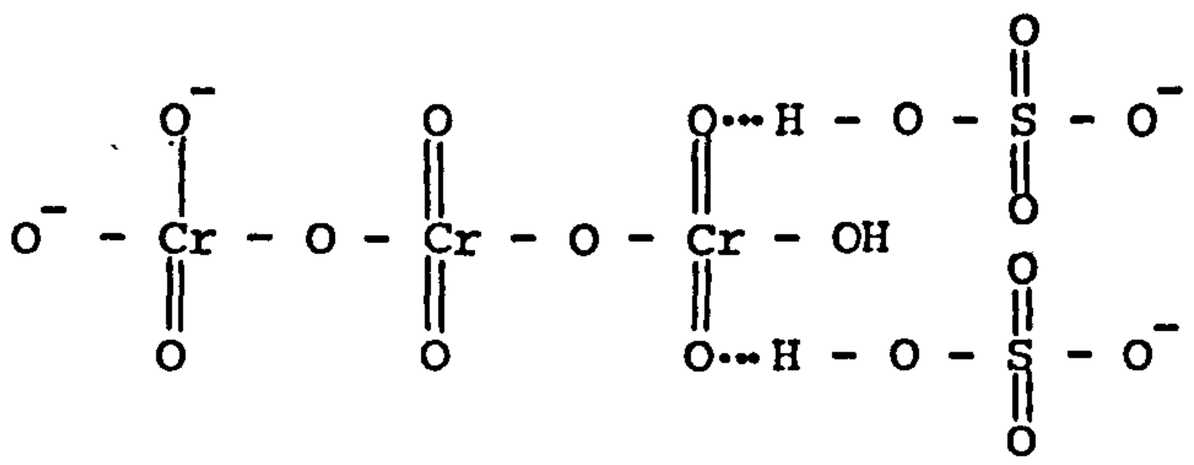

or $HCr_3O_{10}^{2-}$ = Species B

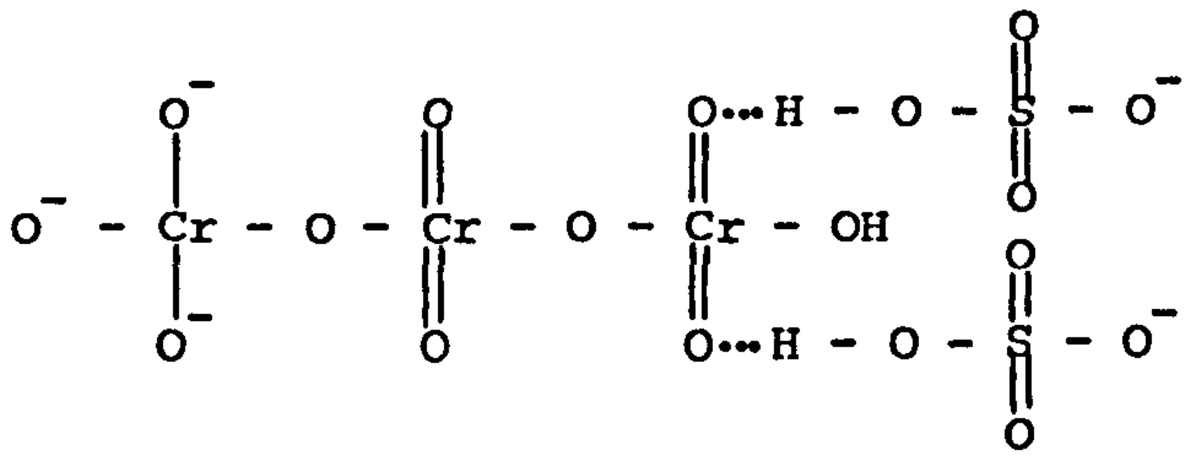

or $HCr_3O_{10}^{3-}$ = Species C

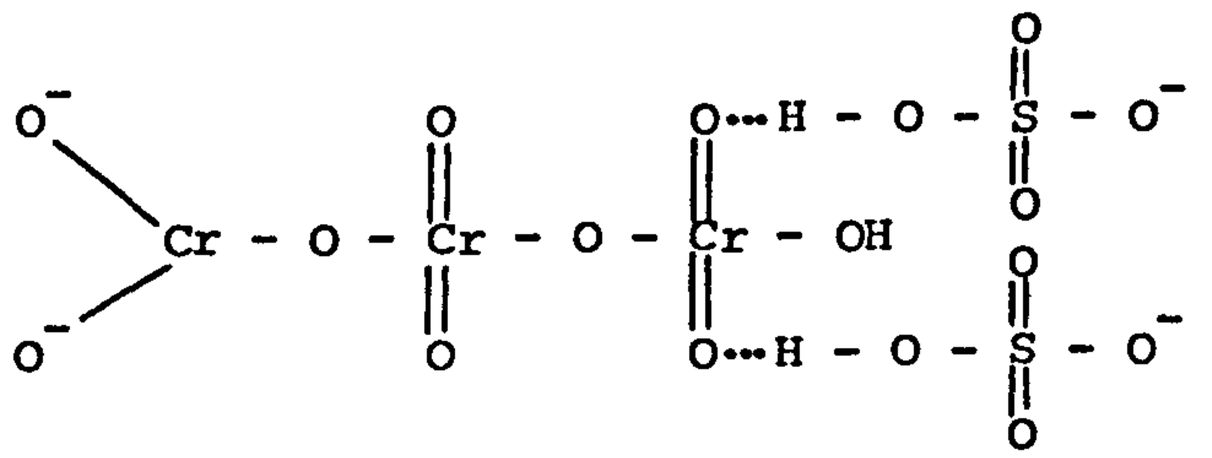

or $HCr_3O_9^{2-}$ = Species D

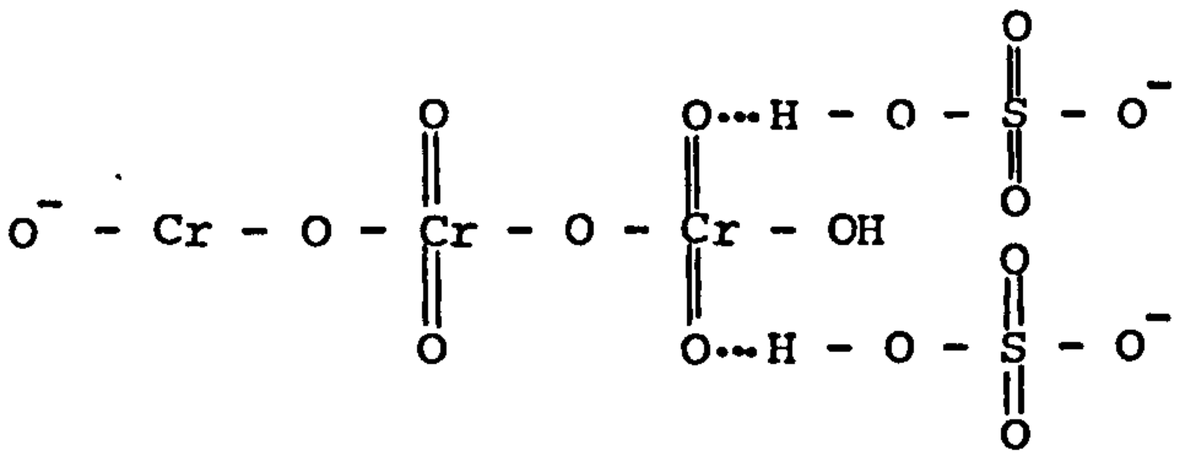

or $HCr_3O_8^-$ = Species E

$Cr(OH)_2 \longrightarrow H_2O + Cr{=}O$ $Cr{=}O$ = Species F

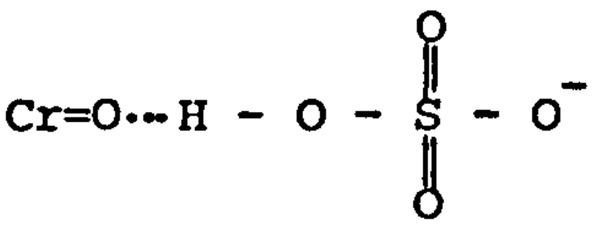

= Species G

Hydrogen atoms are represented as H, and hydrogen ions are shown as H^+. Water molecules are assumed to occupy the spaces between the various ionic species.

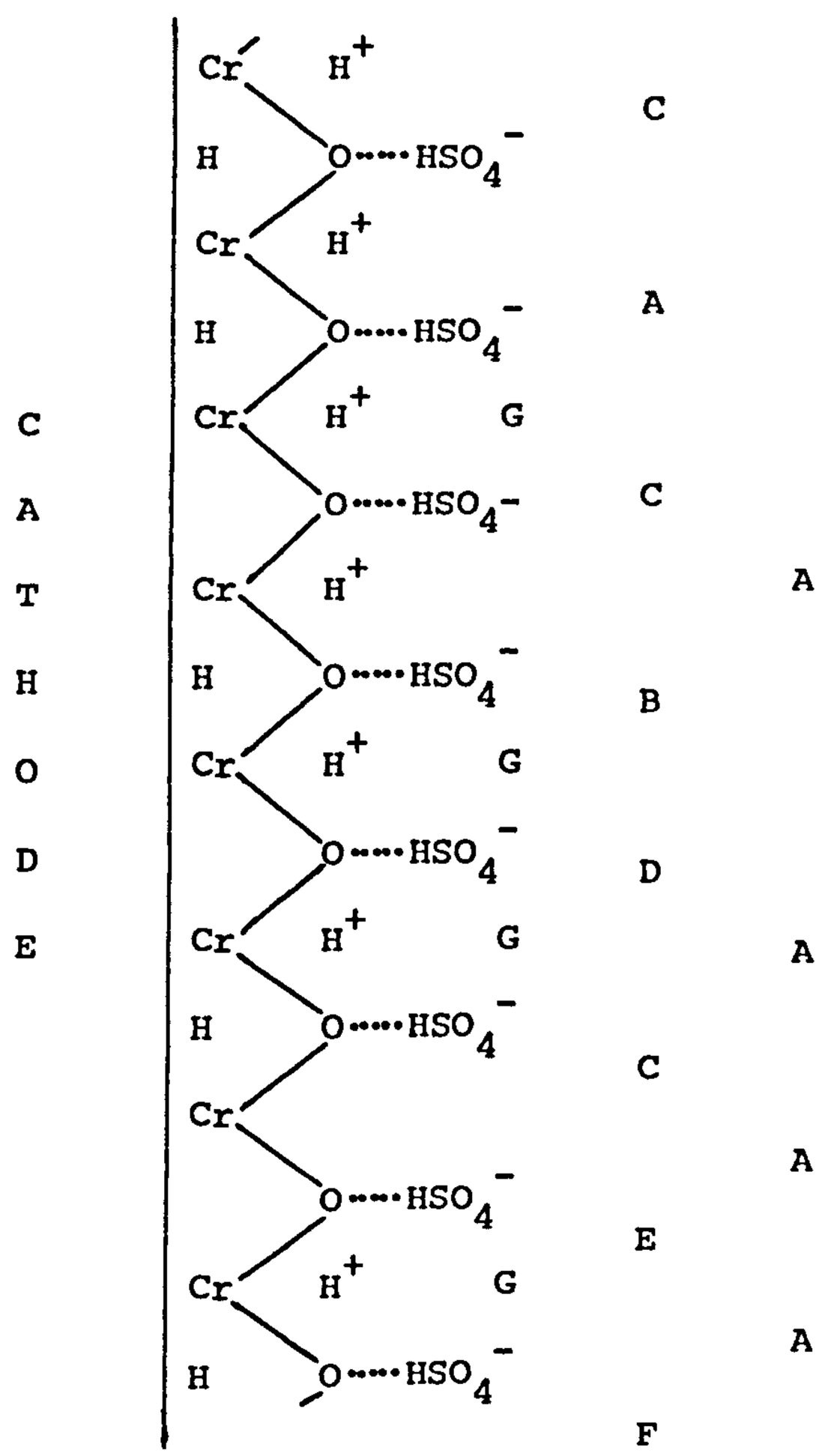

It is assumed here that once the $Cr{=}O\cdots HSO_4^-$ species (G) is formed it is polarized and wheels around in the double layer so that the Cr is adjacent to the cathode surface. At this stage, a Cr=O network is formed as illustrated, constituting a very thin cathode 'film' to which HSO_4^- are hydrogen-bonded. Upon subsequent reduction of the divalent chromium, HSO_4^- are regenerated freeing them to bond with newly produced Cr=O in the double layer. The final steps of deposition (reduction of the 'film') may be represented thus;

(i) 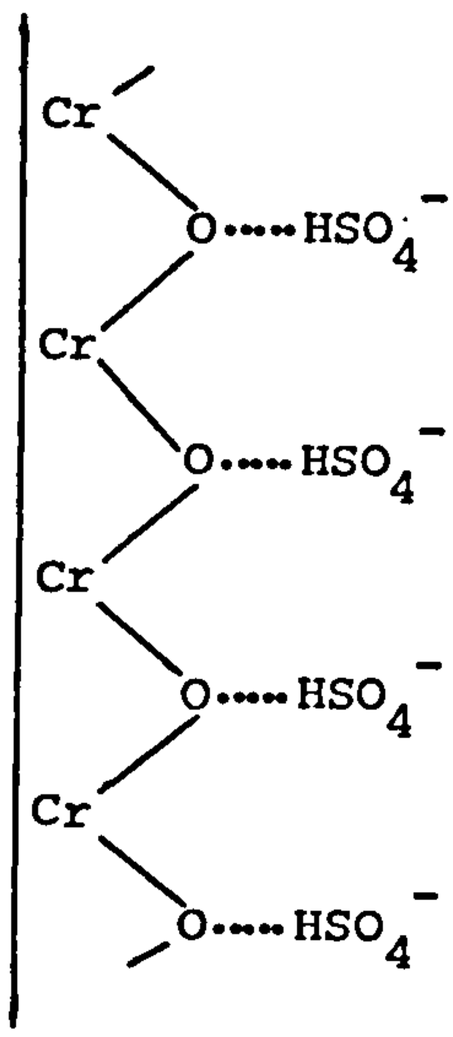

$+ e^- \longrightarrow$

(ii) 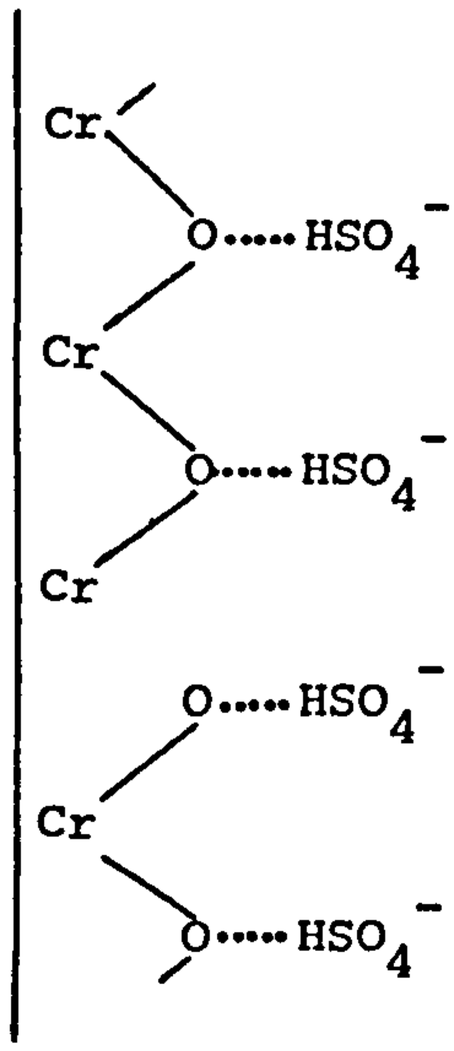

(iii) $+ e^- + 2H^+ \longrightarrow$ 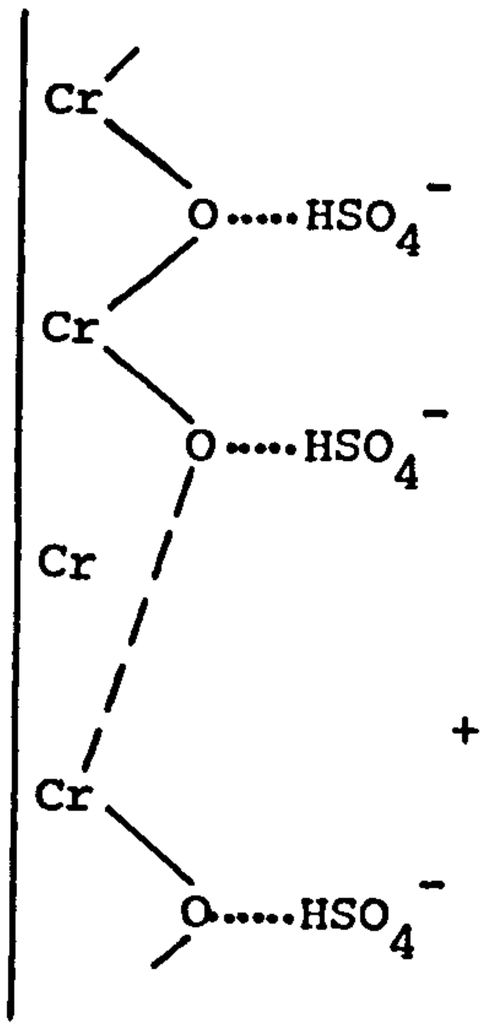

$+ HSO_4^- + H_2O$

The cathode 'film' is thus reformed over the newly deposited metal.

APPENDIX IV

It is well known that electrodeposited chromium is generally highly stressed and intensely hard, with a crack network that forms in order to relieve some of the stress.

Snavely (49) proposed that the hardness of chromium deposits could be attributed to an extremely fine grain size resulting from the decomposition of (initially deposited) chromium hydride grains to chromium metal and the subsequent breakdown into smaller crystals. Hydride deposition would require a high partial pressure of hydrogen in the depositing chromium layer, conditions which are more likely to exist at high overpotentials (and current densities) where the rate of hydrogen evolution is high, or (interestingly) under conditions where the plating reaction is repressed. The presence of ClO_4^- in a Standard Solution has been demonstrated to reduce the efficiency of plating at higher current densities (diverting current to hydrogen evolution), and has also been shown to increase considerably the hardness of the deposit produced. Snavely's theory would explain these observations. However, chromium deposited in the presence of ClO_4^- is not as cracked as that produced in a Standard Solution alone. If Snavely's mechanism was the sole mechanism of hardening, the converse might be expected. As a result, it is considered that as the grains of hydride break up (during decomposition) the atomic hydrogen liberated diffuses through the deposit to the surface, into the substrate metal, or possibly into the pores which undoubtedly exist between growth nodules in the deposit (see Plate 18). These pores (which probably contain entrapped 'film' material) could act as sites for the liberation of hydrogen gas, leading to very high local hydrogen pressures sufficient to nucleate a brittle crack (174).

The fact that solutions containing ClO_4^- produce less cracking in the deposits suggests that the deposit contains fewer sites for such gas liberation, a suggestion that is supported by the increased throwing power of such solutions.

In contrast, the presence of BrO_3^- in a Standard Solution leads to an increase in cracking together with a decrease in hardness (Table 2, Plates 9 and 10). This may be attributed to a reduced tendency for hydride deposition in these solutions, along with an increase in porosity of the deposits which provides more sites for hydrogen gas liberation and subsequent crack nucleation. $B_2O_4^{2-}$ appears to have little effect upon the crack density (effecting a slight increase) but does produce a marginally harder deposit. In this case it is considered unlikely that the increased hardness is due to enhanced hydride formation because the hydrogen evolution reaction is not favoured in the way that it is in solutions containing ClO_4^-. Rather, it is possible that this unexpected (albeit slight) increase in hardness is through the incorporation of boron into the growing deposit.

Supporting evidence for the enhanced deposition of hydrides in solutions containing ClO_4^- has recently been provided (175) via X-ray diffraction investigations of deposits produced in these solutions.

TABLES, FIGURES, PLATES

Throughout this section of the thesis, the following abbreviations and symbols have been employed;

Standard Solution	S	●
Standard + 5g/l $KClO_4$	S + 5A	○
Standard + 10g/l $KClO_4$	S + 10A	X
Standard + 15g/l $KClO_4$	S + 15A	■
Standard + 5g/l $KBrO_3$	S + 5B	+
Standard + 10g/l $KBrO_3$	S + 10B	□
Standard + 15g/l $KBrO_3$	S + 15B	△
Standard + 5g/l $K_2B_2O_4$	S + 5C	⊥
Standard + 10g/l $K_2B_2O_4$	S + 10C	⊤
Standard + 15g/l $K_2B_2O_4$	S + 15C	▲

In the current efficiency versus current density graphs relating to current densities below 5kA/m^2 the maximum observed error in efficiency was $\pm$8%, each point representing the average of three measurements.
At current densities greater than 5kA/m^2 the maximum observed error was $\pm$5%. Again, three measurements were averaged for each point.

TABLES

TABLE 1.

The relative throwing power of the solutions investigated, illustrating the effect of the three new additions to a Standard Solution.

Solution	Deposit weight g		M (= A/B)	$T=\left[\frac{P-M}{P+M-2}\right]$ x100
	A	B		
S	0.0149	0.0025	5.96	- 10.71
S + 5A	0.0143	0.0029	4.93	0.88
S + 10A	0.0094	0.0019	4.95	0.63
S + 15A	0.0194	0.0040	4.85	1.91
S + 5B	0.0126	0.0018	7.00	- 20.00
S + 10B	0.0210	0.0027	7.78	- 25.80
S + 15B	0.0175	0.0023	7.61	- 24.60
S + 5C	0.0177	0.0028	6.32	- 14.16
S + 10C	0.0174	0.0027	6.41	- 14.98
S + 15C	0.0183	0.0027	6.69	- 17.44

TABLE 2.

Measured diamond impression diameters at positions on the sample surface as defined in FIGURE 15.

Mean values, standard deviations and average VPN hardness values for plate produced at 3 kA/m^2 in each of the solutions investigated.

All impression diameters are given in μm.

S + 15C	S + 10C	S + 5C	S + 15B	S + 10B	S + 5B	S + 15A	S + 10A	S + 5A	S	
21.0	21.3	21.5	23.9	24.0	23.5	18.3	18.9	19.1	21.9	1
21.2	21.2	21.4	23.5	24.3	23.3	18.3	18.9	19.1	21.7	2
21.2	21.3	21.5	23.5	24.4	23.3	18.2	18.6	19.2	21.5	3
21.1	21.4	21.5	23.6	24.3	23.2	18.3	18.4	19.1	21.8	4
21.3	21.2	21.5	23.4	24.6	23.2	18.0	18.4	18.8	21.7	5
21.4	21.0	21.4	23.6	24.4	23.0	18.2	18.9	18.7	21.7	6
21.0	21.0	21.3	23.6	24.4	23.0	18.2	18.8	19.0	21.9	7
21.0	21.2	21.4	23.8	24.4	23.1	18.0	18.6	19.0	21.7	8
21.1	21.1	21.5	23.5	24.6	23.4	18.2	18.5	18.8	21.5	9
21.1	21.1	21.4	23.6	24.5	23.1	18.3	18.5	19.0	21.5	10
21.2	21.1	21.4	23.6	24.3	23.2	18.1	18.5	18.9	21.6	11
21.2	21.2	21.3	23.7	24.1	23.1	18.1	18.8	19.2	21.6	12
21.4	21.2	21.3	23.7	24.0	23.1	18.0	18.8	19.1	21.7	13
21.3	21.0	21.5	23.8	24.1	23.3	18.2	18.7	19.0	21.7	14
21.1	21.0	21.5	23.4	24.4	23.3	18.0	18.7	19.1	21.9	15
21.2	21.0	21.3	23.4	24.3	23.4	18.1	18.7	19.1	21.8	16
21.2	21.1	21.4	23.4	24.3	23.2	18.2	18.8	19.1	21.7	17
21.0	21.3	21.6	23.6	24.4	23.4	17.9	18.7	18.8	22.0	18
21.1	21.3	21.3	23.7	24.3	23.0	18.1	18.9	19.0	21.8	19
21.1	21.0	21.4	23.5	24.2	23.1	18.3	18.7	18.9	21.8	20
21.1	21.1	21.4	23.5	24.3	23.2	18.2	18.6	19.2	21.9	21
21.3	21.0	21.3	23.4	24.1	23.5	18.1	18.6	19.0	22.0	22
21.2	21.1	21.4	23.6	24.3	23.2	18.2	18.7	19.0	21.8	Mean
0.1	0.1	00.1	0.1	0.2	0.2	0.1	0.2	0.1	0.2	σ
1238	1249	1215	999	942	1033	1679	1591	1541	1170	VPN

TABLE 3.

The macro-appearance of samples of plate produced at three cathode current densities in each of the solutions investigated.

Solution	3kA/m^2	10kA/m^2	30kA/m^2
S	Mirror	Matt White	Matt mid-grey
S + 5A	Mirror	Smooth white	Matt white
S + 10A	Mirror	Smooth white	Matt white
S + 15A	Mirror	Smooth white	Matt white
S + 5B	Matt mid-grey	Matt dark-grey	Matt dark-grey
S + 10B	Matt dark-grey	Matt dark-grey	Matt black
S + 15B	Matt dark-grey	Matt black	Matt black
S + 5C	Smooth mid-grey	Matt mid-grey	Matt mid-grey
S + 10C	Matt mid-grey	Matt mid-grey	Rough mid-grey
S + 15C	Matt mid-grey	Rough mid-grey	Rough mid-grey

TABLE 4.

The influence of the three new solution additions upon the measured Tafel slope of the partial polarization curves for the plating and hydrogen evolution reactions. The corresponding values of $\lambda x \alpha$ term.

Estimated errors.

Solution	PLATING				H.E.R			
	Tafel slope (mV/dec)	±	$\lambda \times \alpha_{term}$	±	Tafel slope (mV/dec)	±	$\lambda \times \alpha_{term}$	±
S	21.5	3	3.0	.3	124	15	0.53	.06
S + 5A	21.5	3	3.0	.3	112	16	0.58	.07
S + 10A	16.5	4.5	4.0	1.0	106	20	0.61	.12
S + 15A	21	3	3.1	.5	105	15	0.62	.08
S + 5B	32	3.5	2.0	.2	224	22	0.29	.03
S + 10B	27.5	3	2.4	.2	198	20	0.33	.03
S + 15B	39	7	1.7	.3	214	30	0.30	.05
S + 5C	24	3	2.7	.3	180	21	0.36	.04
S + 10C	26	3	2.5	.3	162	23	0.40	.07
S + 15C	28.5	3	2.3	.3	185	20	0.35	.05

TABLE 5.

The influence of the three new solution additions upon the cathode reaction overall α_{term} (assuming λ = 12 for the plating reaction and 2 for the hydrogen evolution reaction). The corresponding values of α_f (assuming α_{dl} = 0.5).

Estimated errors.

α_{term} and α_f values for the plating reaction in Standard Solutions containing $KBrO_3$ and $K_2B_2O_4$, assuming λ = 8.

Solution	PLATING		H.E.R	
	α_{term} if $\lambda = 12$	α_f if $\alpha_{dl}=1/2$	α_{term} if $\lambda = 2$	α_f if $\alpha_{dl}=1/2$
Standard	0.25 ±0.03	0.50 ±0.12	0.27 ±0.04	0.45 ±0.18
S + 5A	0.25 ±0.03	0.50 ±0.12	0.29 ±0.04	0.31 ±0.23
S + 10A	0.33 ±0.08	0.04 ±0.45	0.31 ±0.06	0.18 ±0.32
S + 15A	0.26 ±0.04	0.47 ±0.18	0.31 ±0.04	0.18 ±0.27
S + 5B	0.17 ±0.02	0.74 ±0.05	0.15 ±0.02	0.79 ±0.05
S + 10B	0.20 ±0.02	0.66 ±0.05	0.17 ±0.02	0.74 ±0.05
S + 15B	0.14 +0.03	0.81 +0.05	0.15 +0.03	0.79 +0.05
S + 5C	0.23 ±0.03	0.59 ±0.10	0.18 ±0.02	0.72 ±0.05
S + 10C	0.21 ±0.03	0.64 ±0.09	0.20 ±0.03	0.66 ±0.08
S + 15C	0.19 ±0.03	0.69 ±0.08	0.18 ±0.03	0.72 ±0.08

PLATING	
α_{term} if $\lambda = 8$	α_f if $\alpha_{dl}=1/2$
0.26	0.46
0.30	0.25
0.21	0.64
0.35	< 0.0
0.32	0.11
0.29	0.31

TABLES 6a to 6y.

Arrhenius data obtained at selected potentials corresponding to the Tafel range in plating partial polarization curves for each of the solutions investigated.

Standard Solution

E = -0.83 V

Table 6a

T (K)	$T^{-1} \times 10^3$	i_t (kA/m^2)	C.E %	i_{Cr} (kA/m^2)	$\log_{10} i_{Cr}$
318	3.145	0.09	3.33	0.003	-2.523
323	3.096	0.38	2.11	0.008	-2.097
328	3.049	1.50	1.40	0.021	-1.678
333	3.003	3.76	1.25	0.047	-1.328
338	2.959	8.92	1.20	0.107	-0.971

E = -0.84V

Table 6b

T (K)	$T^{-1} \times 10^3$	i_t	C.E %	i_{Cr}	$\log_{10} i_{Cr}$
318	3.145	0.23	4.78	0.011	-1.959
323	3.096	0.60	4.33	0.026	-1.585
328	3.049	1.95	3.39	0.066	-1.181
333	3.003	5.40	3.00	0.162	-0.791
338	2.959	> 10			

E = -0.85V

Table 6c

T (K)	$T^{-1} \times 10^3$	i_t	C.E %	i_{Cr}	$\log_{10} i_{Cr}$
318	3.145	0.19	8.95	0.017	-1.770
323	3.096	0.83	7.23	0.060	-1.222
328	3.049	2.65	6.76	0.179	-0.747
333	3.003	8.55	5.73	0.490	-0.310
338	2.959	> 10			

E = -0.86V

Table 6d

T (K)	$T^{-1} \times 10^3$	i_t (kA/m^2)	C.E %	i_{Cr} (kA/m^2)	$\log_{10} i_{Cr}$
318	3.145	0.16	5.04	0.008	-2.118
323	3.096	0.58	3.62	0.021	-1.672
328	3.049	2.60	2.27	0.059	-1.229
333	3.003	8.21	1.96	0.161	-0.793
338	2.959	> 10			

E = -0.87V

Table 6e

T (K)	$T^{-1} \times 10^3$	i_t	C.E %	i_{Cr}	$\log_{10} i_{Cr}$
318	3.145	0.25	8.91	0.022	-1.651
323	3.096	0.86	7.44	0.064	-1.196
328	3.049	2.90	6.14	0.178	-0.750
333	3.003	9.76	5.01	0.489	-0.311
338	2.959	> 10			

S + 10A

E = -0.88V

Table 6f

T (K)	$T^{-1} \times 10^3$	i_t (kA/m^2)	C.E %	i_{Cr} (kA/m^2)	$\log_{10} i_{Cr}$
318	3.145	0.11	6.36	0.007	-2.155
323	3.096	0.45	5.11	0.023	-1.638
328	3.049	2.83	3.00	0.085	-1.071
333	3.003	> 10			
338	2.959	> 10			

E = -0.885V

Table 6g

T (K)	$T^{-1} \times 10^3$	i_t	C.E %	i_{Cr}	$\log_{10} i_{Cr}$
318	3.145	0.16	8.54	0.014	-1.854
323	3.096	0.80	6.47	0.052	-1.284
328	3.049	3.12	5.98	0.187	-0.729
333	3.003	> 10			
338	2.959	> 10			

S + 15A

E = -0.88V

Table 6h

T (K)	$T^{-1} \times 10^3$	i_t (kA/m^2)	C.E %	i_{Cr} (kA/m^2)	$\log_{10} i_{Cr}$
318	3.145	0.15	7.88	0.012	-1.941
323	3.096	0.59	6.07	0.036	-1.446
328	3.049	2.33	4.42	0.103	-0.987
333	3.003	9.79	3.32	0.325	-0.488
338	2.959	> 10			

E = -0.89V

Table 6j

T (K)	$T^{-1} \times 10^3$	i_t	C.E %	i_{Cr}	$\log_{10} i_{Cr}$
318	3.145	0.18	11.12	0.020	-1.699
323	3.096	0.76	9.29	0.071	-1.149
328	3.049	2.72	8.46	0.230	-0.638
333	3.003	9.96	7.39	0.736	-0.133
338	2.959	> 10			

S + 5B

E = -0.78V

Table 6m

T (K)	$T^{-1} \times 10^3$	i_t (kA/m^2)	C.E %	i_{Cr} (kA/m^2)	$\log_{10} i_{Cr}$
318	3.145	0.55	6.03	0.033	-1.482
323	3.096	1.19	4.95	0.059	-1.229
328	3.049	2.53	4.11	0.104	-0.983
333	3.003	5.17	3.52	0.182	-0.740
338	2.959	> 10			

E = -0.79V

Table 6n

T (K)	$T^{-1} \times 10^3$	i_t	C.E %	i_{Cr}	$\log_{10} i_{Cr}$
318	3.145	0.69	9.47	0.065	-1.187
323	3.096	1.47	8.11	0.119	-0.925
328	3.049	3.11	6.82	0.212	-0.674
333	3.003	6.63	5.71	0.379	-0.421
338	2.959	> 10			

E = -0.77V

Table 6p

T (K)	$T^{-1} \times 10^3$	i_t (kA/m^2)	C.E %	i_{Cr} (kA/m^2)	$\log_{10} i_{Cr}$
318	3.145	0.30	14.53	0.044	-1.361
323	3.096	0.82	10.05	0.082	-1.084
328	3.049	1.81	8.55	0.155	-0.810
333	3.003	4.47	6.37	0.285	-0.546
338	2.959	9.63	5.33	0.513	-0.290

E = -0.78V

Table 6q

T (K)	$T^{-1} \times 10^3$	i_t	C.E %	i_{Cr}	$\log_{10} i_{Cr}$
318	3.145	0.55	12.47	0.069	-1.159
323	3.096	1.23	11.02	0.136	-0.867
328	3.049	2.75	9.56	0.263	-0.580
333	3.003	6.02	8.13	0.489	-0.311
338	2.959	> 10			

E = -0.76V

Table 6r

T (K)	$T^{-1} \times 10^3$	i_t (kA/m^2)	C.E %	i_{Cr} (kA/m^2)	$\log_{10} i_{Cr}$
318	3.145	0.41	7.89	0.032	-1.495
323	3.096	0.88	6.02	0.053	-1.276
328	3.049	2.18	3.95	0.086	-1.066
333	3.003	4.69	2.88	0.135	-0.870
338	2.959	9.91	2.17	0.215	-0.668

E = -0.77V

Table 6s

T (K)	$T^{-1} \times 10^3$	i_t	C.E %	i_{Cr}	$\log_{10} i_{Cr}$
318	3.145	0.73	11.42	0.083	-1.081
323	3.096	1.37	9.91	0.136	-0.867
328	3.049	2.75	8.15	0.224	-0.650
333	3.003	5.39	6.88	0.371	-0.431
338	2.959	> 10			

E = -0.84V

Table 6t

T (K)	$T^{-1} \times 10^3$	i_t (kA/m^2)	C.E %	i_{Cr} (kA/m^2)	$\log_{10} i_{Cr}$
318	3.145	0.22	6.40	0.014	-1.853
323	3.096	1.04	4.05	0.042	-1.377
328	3.049	2.19	3.52	0.077	-1.114
333	3.003	5.94	2.88	0.171	-0.767
338	2.959	> 10			

E = -0.85V

Table 6u

T (K)	$T^{-1} \times 10^3$	i_t	C.E %	i_{Cr}	$\log_{10} i_{Cr}$
318	3.145	0.25	11.84	0.029	-1.518
323	3.096	0.74	9.66	0.071	-1.149
328	3.049	2.45	6.82	0.167	-0.777
333	3.003	7.50	5.20	0.390	-0.409
338	2.959	> 10			

S + 10C

E = -0.83V

Table 6v

T (K)	$T^{-1} \times 10^3$	i_t (kA/m^2)	C.E %	i_{Cr} (kA/m^2)	$\log_{10} i_{Cr}$
318	3.145	0.29	5.19	0.015	-1.822
323	3.096	0.74	3.66	0.027	-1.568
328	3.049	2.17	2.72	0.059	-1.229
333	3.003	6.19	1.97	0.122	-0.913
338	2.959	> 10			

E = -0.84V

Table 6w

T (K)	$T^{-1} \times 10^3$	i_t	C.E %	i_{Cr}	$\log_{10} i_{Cr}$
318	3.145	0.35	7.23	0.025	-1.597
323	3.096	0.96	5.96	0.057	-1.243
328	3.049	2.51	4.82	0.121	-0.917
333	3.003	7.85	3.44	0.270	-0.569
338	2.959	> 10			

S + 15C

E = -0.83V

Table 6x

T (K)	$T^{-1} \times 10^3$	i_t (kA/m^2)	C.E %	i_{Cr} (kA/m^2)	$\log_{10} i_{Cr}$
318	3.145	0.29	7.16	0.021	-1.678
323	3.096	0.81	5.33	0.043	-1.367
328	3.049	2.10	3.86	0.081	-1.092
333	3.003	6.72	2.41	0.162	-0.790
338	2.959	> 10			

E = -0.84V

Table 6y

T (K)	$T^{-1} \times 10^3$	i_t	C.E %	i_{Cr}	$\log_{10} i_{Cr}$
318	3.145	0.39	12.79	0.050	-1.301
323	3.096	1.03	10.12	0.104	-0.903
328	3.049	2.49	8.35	0.208	-0.627
333	3.003	6.10	7.11	0.434	-0.363
338	2.959	> 10			

TABLE 7.

Arrhenius slopes and thermodynamic quantities of activation for the plating reaction (at 328K) corresponding to the potentials referred to in Tables 6a to 6y:

7a) ε_{Cr} taken to be -0.7V (S.H.E.)

7b) ε_{Cr} taken to be -0.65V (S.H.E.)

7c) ε_{Cr} taken to be -0.565V (S.H.E.)

N.B. In Table 7a values for Standard + 10g/l $KClO_4$ have been recalculated using $\lambda x \alpha_{term} = 3$ (instead of the measured, but apparently anomalous, value of 4) and are given at the foot of the table.

In Tables 7b and 7c values for Standard + 15g/l $KBrO_3$ have been recalculated using $\lambda x \alpha_{term} = 2.2$ (instead of the measured, but apparently anomalous, value of 1.7) and are given at the foot of the tables.

7a

Solution	E −V vs S.H.E	Arrhenius slope K	ΔH_A kJ/mol	ΔS_A J/mol.K	ΔG_A kJ/mol
Standard	0.83	-8200	118	235	41
	0.84	-8000	111	232	35
	0.85	-10500	157	388	30
S + 5A	0.86	-9000	125	291	30
	0.87	-9200	126	312	24
S + 10A	0.88	-10000	121	353	5
	0.885	-11000	139	418	1
S + 15A	0.88	-10500	147	401	15
	0.89	-10800	149	408	15
S + 5B	0.78	-5300	84	94	53
	0.79	-5500	86	95	55
S + 10B	0.77	-5700	91	104	57
	0.78	-5800	91	114	53
S + 15B	0.76	-4400	73	23	65
	0.77	-4600	75	42	61
S + 5C	0.84	-8000	116	234	39
	0.85	-7700	107	223	34
S + 10C	0.83	-6500	92	143	45
	0.84	-7300	105	196	40
S + 15C	0.83	-6200	88	129	46
	0.84	-5800	78	113	41

S + 10A $\lambda \times \alpha_{term}$ = 3	0.88	-10000	139	353	23
	0.885	-11000	156	418	19

7b

Solution	E −V vs S.H.E	Arrhenius slope K	ΔH_A kJ/mol	ΔS_A J/mol.K	ΔG_A kJ/mol
Standard	0.83	-8200	104	235	27
	0.84	-8000	97	233	21
	0.85	-10500	142	388	15
S + 5A	0.86	-9000	111	291	15
	0.87	-9200	112	312	9
S + 10A	0.88	-10000	102	352	-13
	0.885	-11000	119	418	-18
S + 15A	0.88	-10500	132	384	6
	0.89	-10800	134	408	1
S + 5B	0.78	-5300	75	77	49
	0.79	-5500	77	95	46
S + 10B	0.77	-5700	80	104	46
	0.78	-5800	79	114	42
S + 15B	0.76	-4400	64	23	57
	0.77	-4600	67	42	53
S + 5C	0.84	-8000	103	234	26
	0.85	-7700	94	223	21
S + 10C	0.83	-6500	80	143	33
	0.84	-7300	93	196	28
S + 15C	0.83	-6200	77	128	35
	0.84	-5800	67	113	30

S + 15B $\lambda x \alpha_{term}$ = 2.2	0.76	-4400	59	23	52
	0.77	-4600	61	42	47

7c

Solution	E –V vs S.H.E	Arrhenius slope K	ΔH_A kJ/mol	ΔS_A J/mol.K	ΔG_A kJ/mol
Standard	0.83	-8200	79	235	2
	0.84	-8000	72	233	4
	0.85	-10500	118	388	-10
S + 5A	0.86	-9000	86	291	-9
	0.87	-9200	87	312	-15
S + 10A	0.88	-10000	69	353	-47
	0.885	-11000	87	418	-51
S + 15A	0.88	-10500	106	401	-26
	0.89	-10800	109	408	-25
S + 5B	0.78	-5300	58	94	27
	0.79	-5500	60	95	29
S + 10B	0.77	-5700	60	104	26
	0.78	-5800	60	114	22
S + 15B	0.76	-4400	50	23	43
	0.77	-4600	53	42	39
S + 5C	0.84	-8000	80	234	4
	0.85	-7700	72	223	-1
S + 10C	0.83	-6500	59	143	12
	0.84	-7300	72	196	8
S + 15C	0.83	-6200	58	129	16
	0.84	-5800	48	113	11

S + 15B $\lambda \times \alpha_{term}$ = 2.2	0.76	-4400	41	23	34
	0.77	-4600	43	42	29

TABLE 8.

The effect of lengthy electrolysis at 3kA/m^2 upon the plating current efficiency in each solution investigated.

An indication of the relative rates at which new addition exhaustion takes place.

Solution	Plating Current Efficiency (%) at 3kA / m^2				
	'0' hrs	4	8	12	16
Standard	7.0	6.5	6.5	6.0	6.0
S + 5A	4.0	4.5	4.5	6.0	6.0
S + 10A	5.0	5.0	5.0	6.0	6.0
S + 15A	9.5	8.0	7.5	6.5	6.5
S + 5B	5.5	6.0	5.0	4.5	5.0
S + 10B	10.5	8.5	6.5	6.5	6.0
S + 15B	9.5	7.5	7.0	6.0	6.0
S + 5C	9.5	9.5	9.0	9.0	8.5
S + 10C	9.5	9.0	9.0	9.0	8.5
S + 15C	9.5	9.0	9.0	9.0	8.0

FIGURES

FIGURE 1.

The so-called 'Bright Range' in Chromium Plating.

(2.5M CrO_3, 100:1 ratio)

a) After D. R. Gabe (50).

b) After W. Hume-Rothery and M. R. J. Wyllie (67).

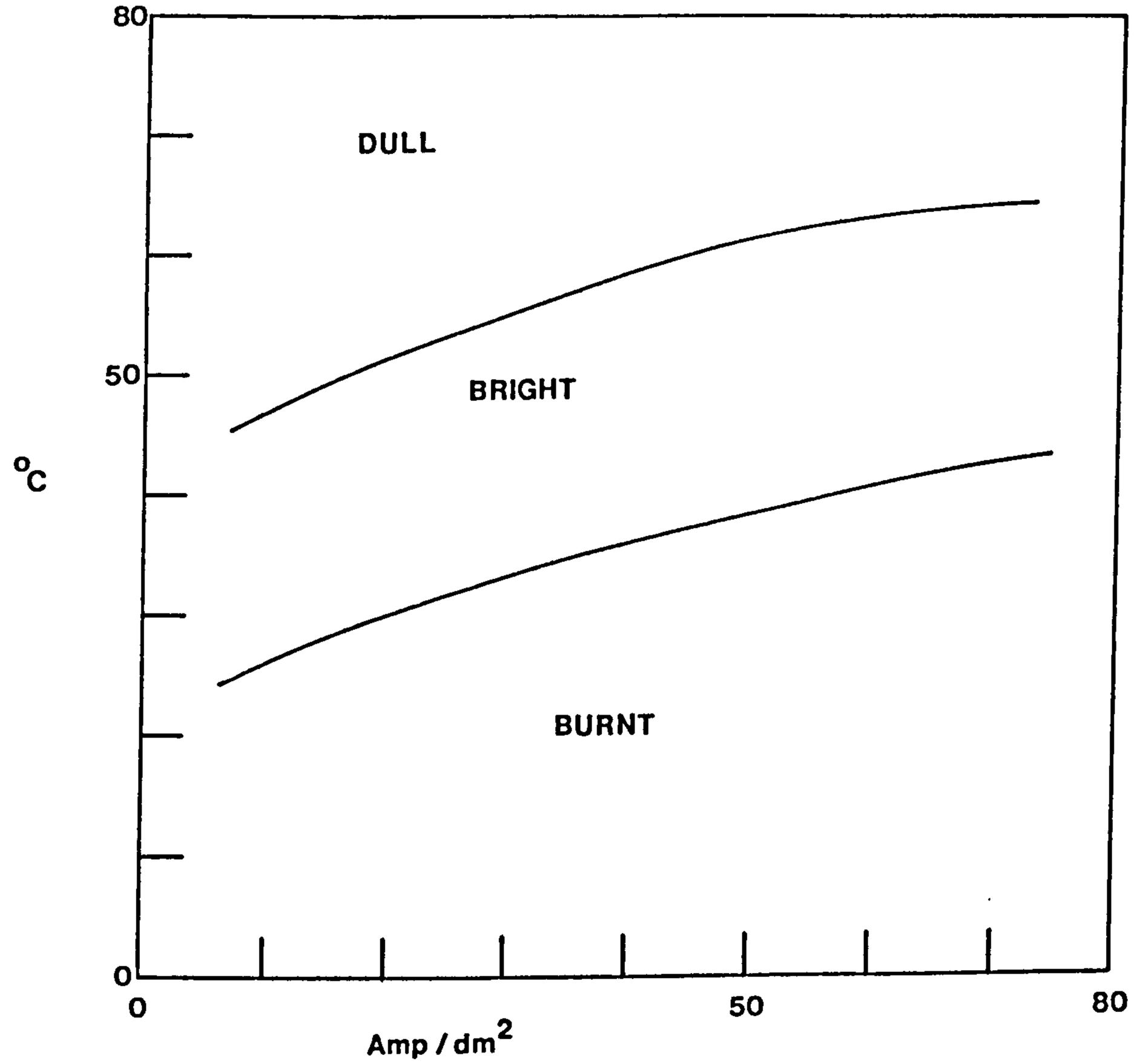
80
50
0
°C
DULL
BRIGHT
BURNT
0
50
80
Amp / dm2

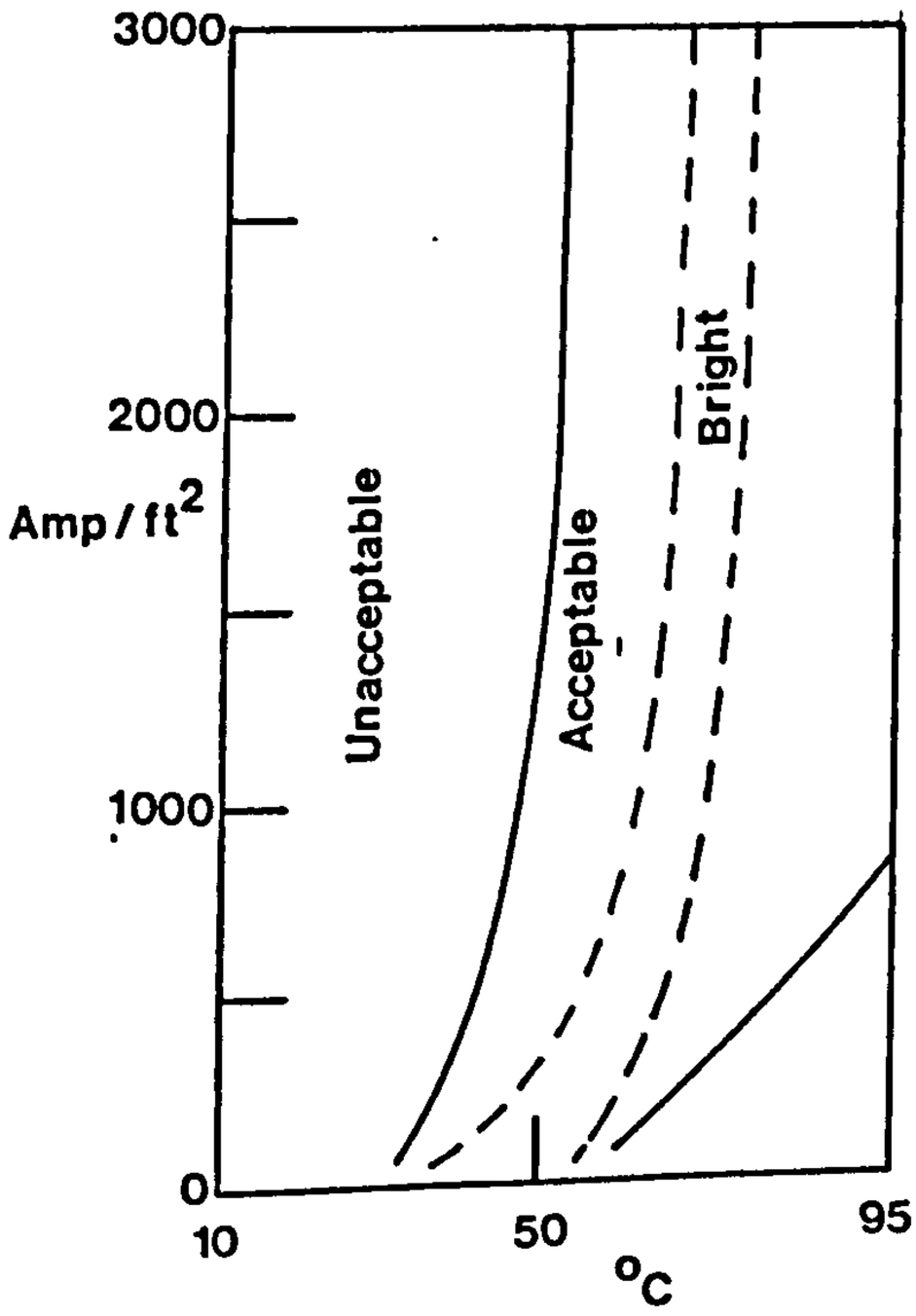
3000
2000
1000
0
Amp / ft2
Unacceptable
Acceptable
Bright
10
50
95
°C

FIGURE 2.

The pH-dependence of the concentration of certain chromium-bearing anionic species in dilute chromic acid.

After R. A. Powers and N. Hackerman (115)

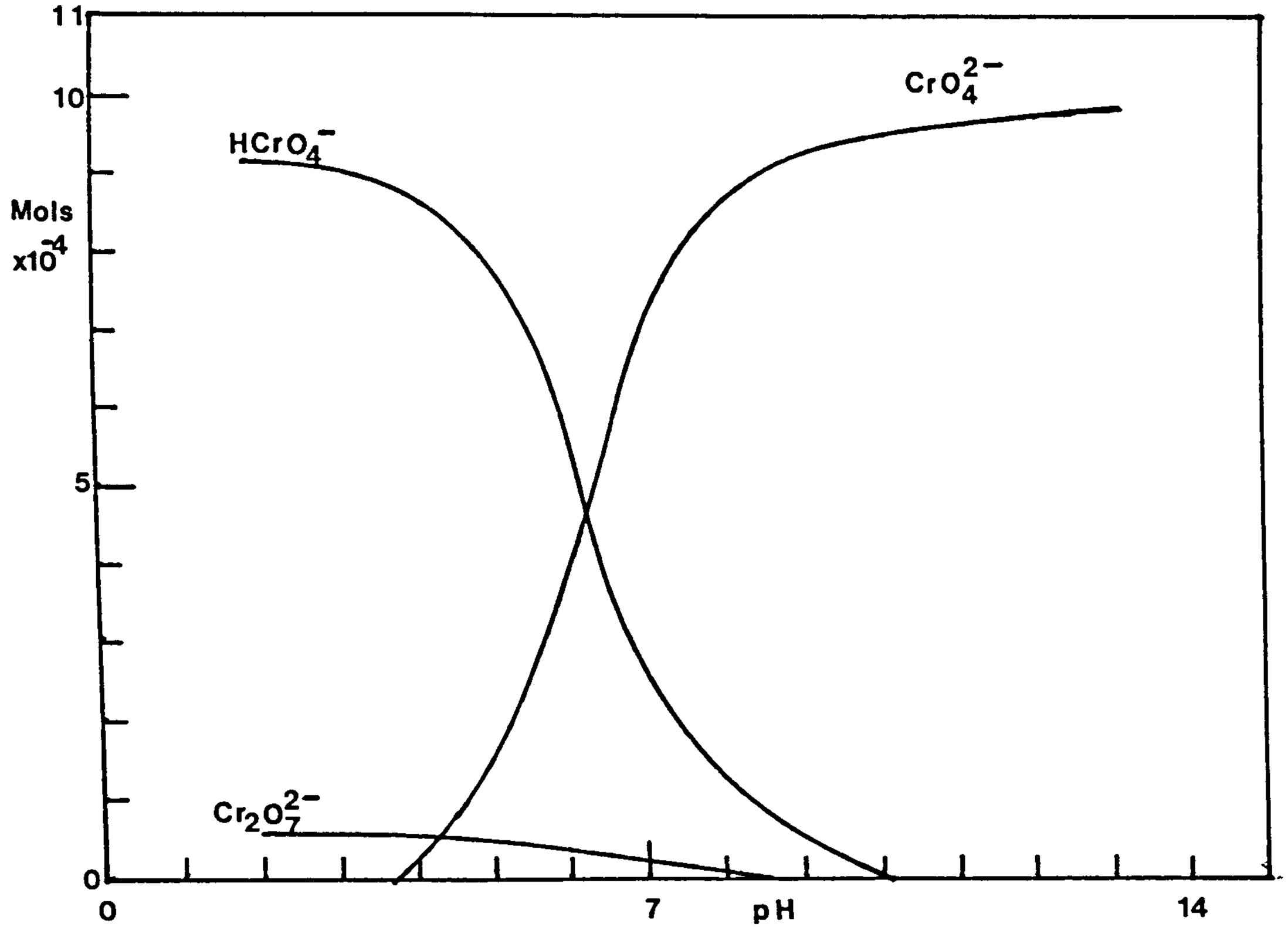
11
10
5
0
Mols
x10⁻⁴
HCrO4⁻
CrO4²⁻
Cr2O7²⁻
0
7
pH
14

FIGURE 3.

Cathode polarization curve for the electrolysis of a 2.5M, 100:1 ratio, chromic acid plating solution. Platinum cathode.
After E. Liebreich (126).

FIGURE 4.

Cathode polarization curve obtained under same conditions as FIGURE 3.
After E. Muller (127).

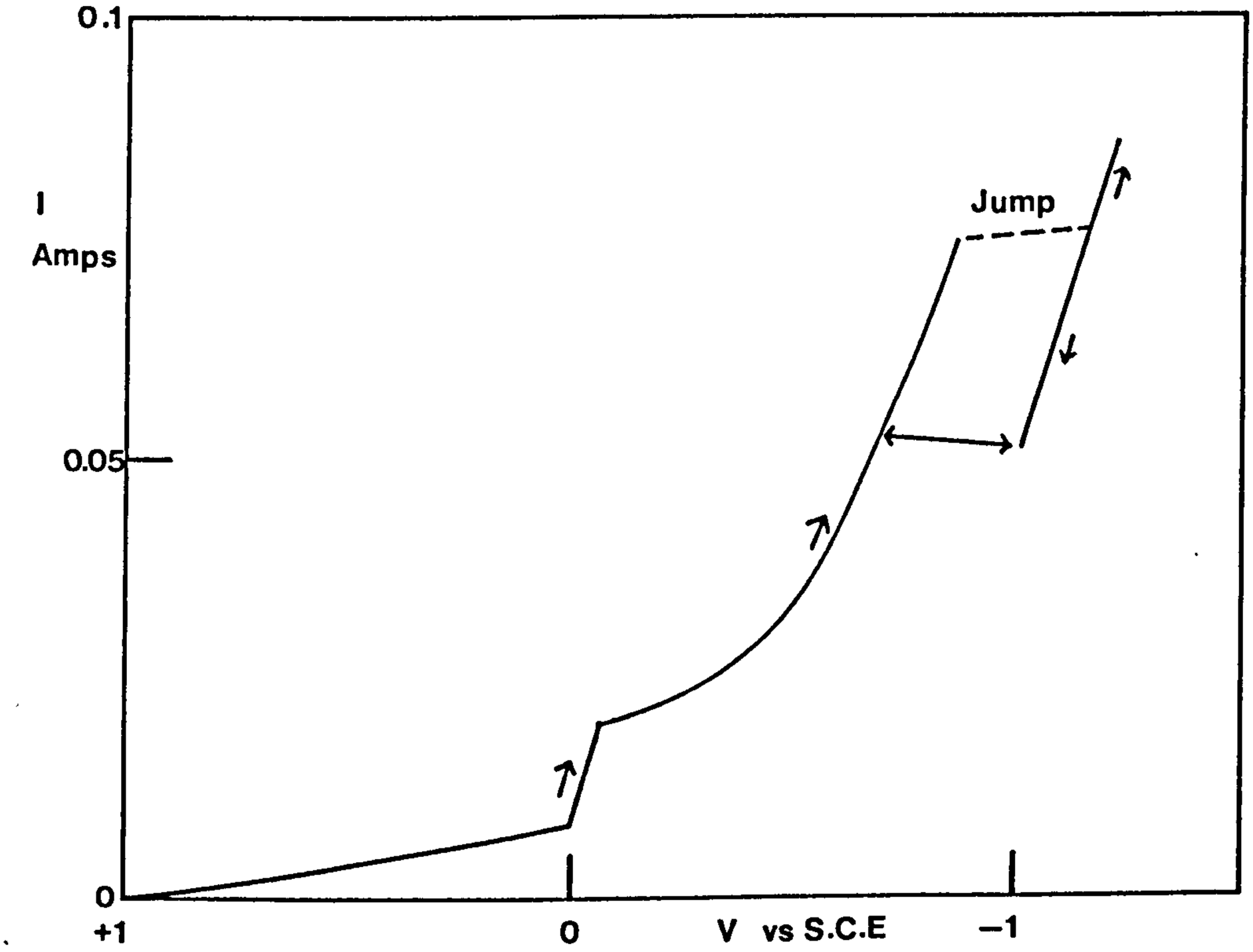
0.1
I
Amps
0.05
Jump
0
+1
0
V vs S.C.E
−1

40
30
I
mA
20
10
Jump
0
0
V vs S.C.E
−1

FIGURE 5.

The approximate dependence of deposit structure upon cathode film pH during deposition.

After C. A. Snavely (49)

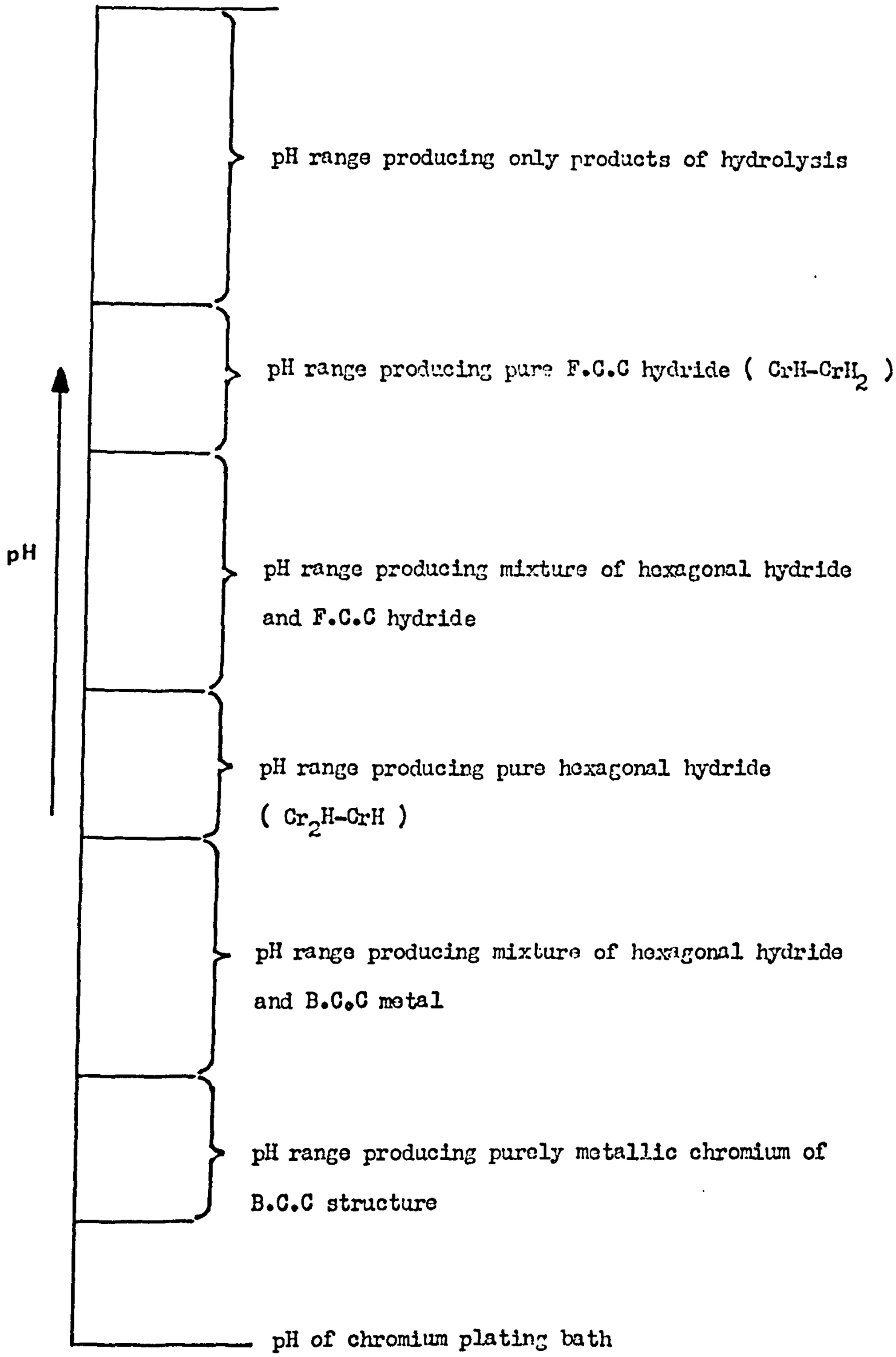
pH range producing only products of hydrolysis
pH range producing pure F.C.C hydride (CrH-CrH2)
pH
pH range producing mixture of hexagonal hydride and F.C.C hydride
pH range producing pure hexagonal hydride (Cr2H-CrH)
pH range producing mixture of hexagonal hydride and B.C.C metal
pH range producing purely metallic chromium of B.C.C structure
pH of chromium plating bath

FIGURE 6.

Cathode polarization curve for the electrolysis of a 3.0M, 100:1 ratio, chromic acid plating solution. Platinum cathode. ○

After D. Reinkowski and C. A. Knorr (135).

The same, but for a 10:1 ratio solution. ●

FIGURE 7.

Overall cathode polarization curve divided into its component partial curves.

After A. T. Vagramyan, D. N. Usachev and G. I. Cherchova (157).

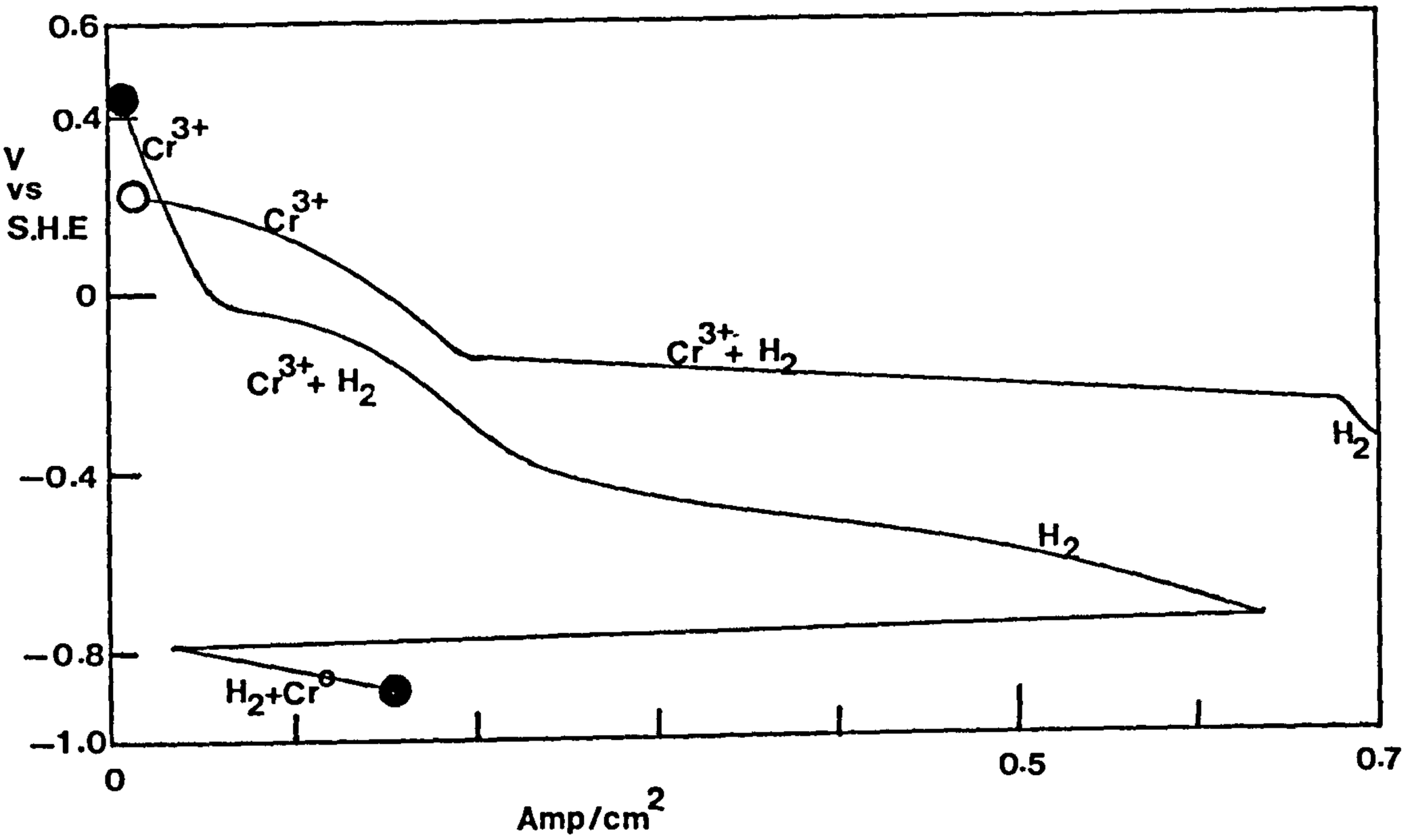
0.6
0.4
V
vs
S.H.E
0
−0.4
−0.8
−1.0
0
0.5
0.7
Amp/cm2
Cr3+
Cr3+
Cr3+ + H2
Cr3+ + H2
H2
H2
H2+Cr°

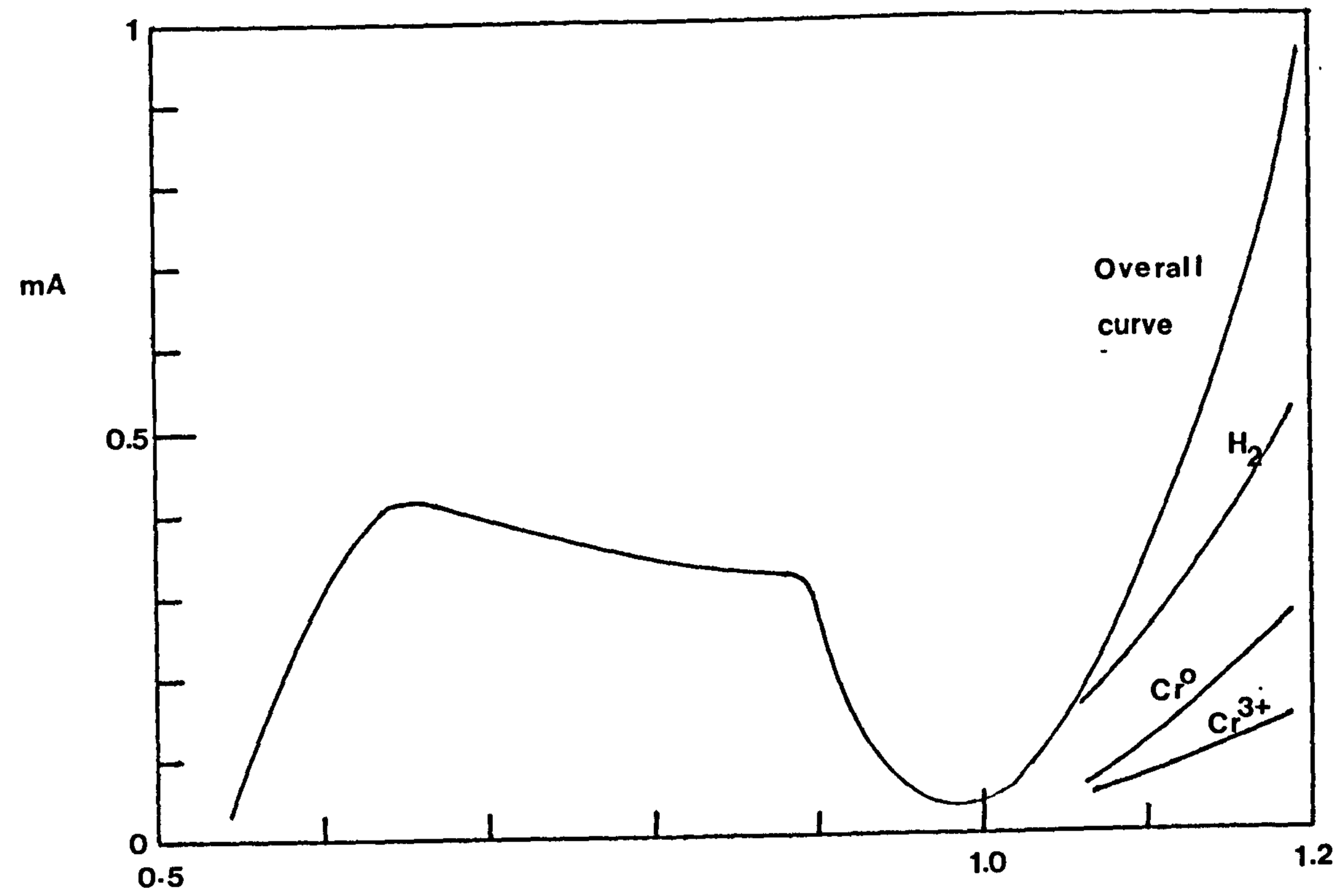
1
mA
0.5
0
0.5
1.0
1.2
−V vs S.C.E
Overall
curve
H2
Cr°
Cr3+

FIGURE 8.

Schematic diagram of the 'H-Cell' used for most experimental work.

FIGURE 9.

Schematic diagram of the perspex cathode-holder. (The shaded area represents the position of the steel strip within the holder).

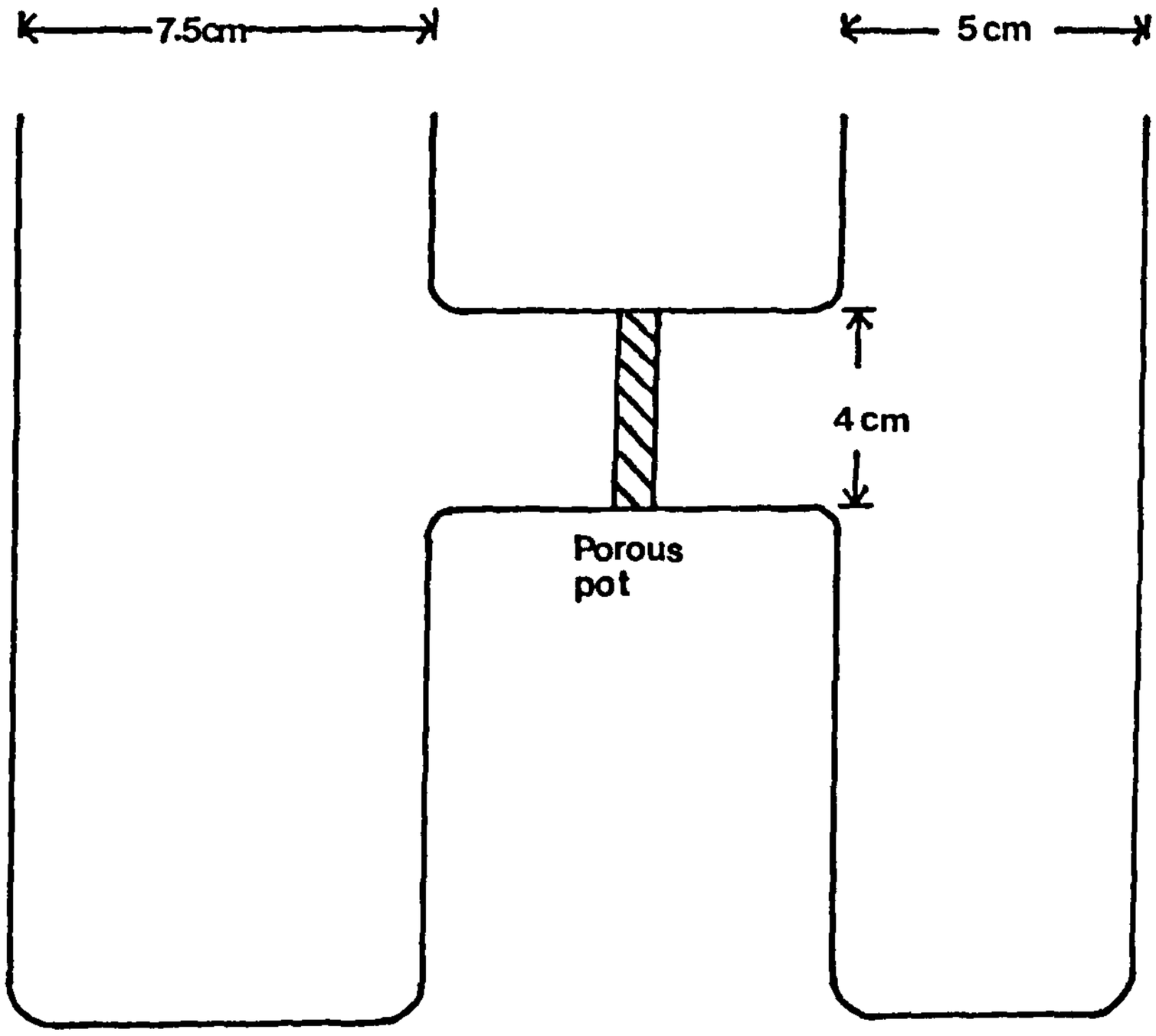
7.5cm
5 cm
4 cm
Porous
pot

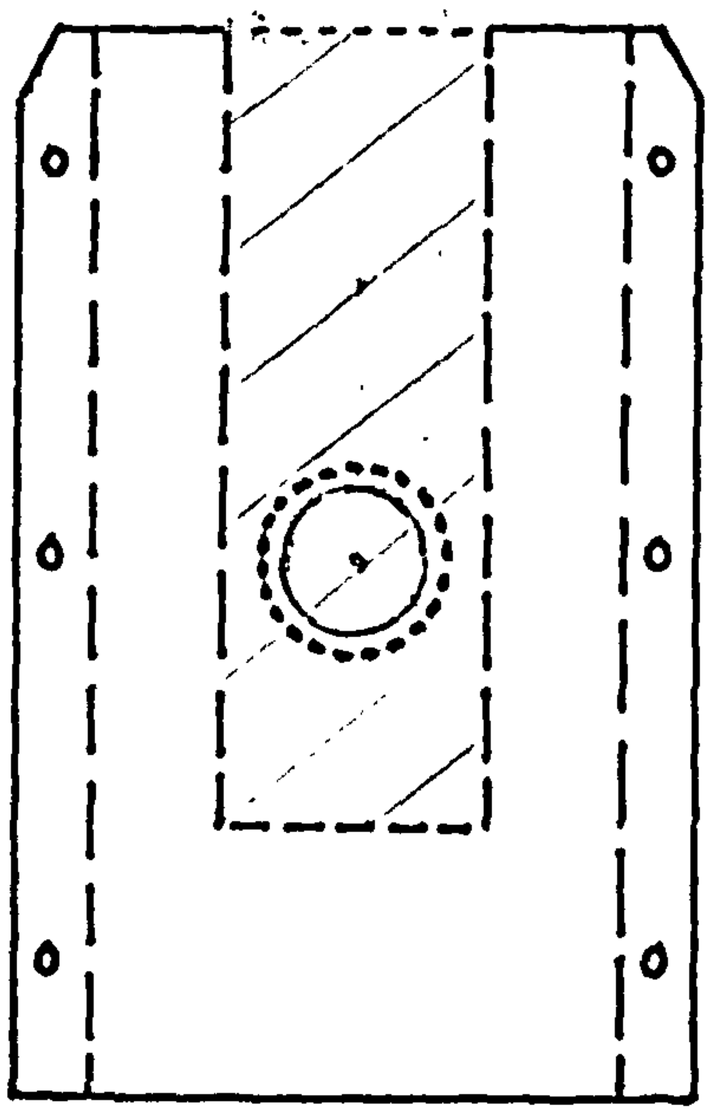

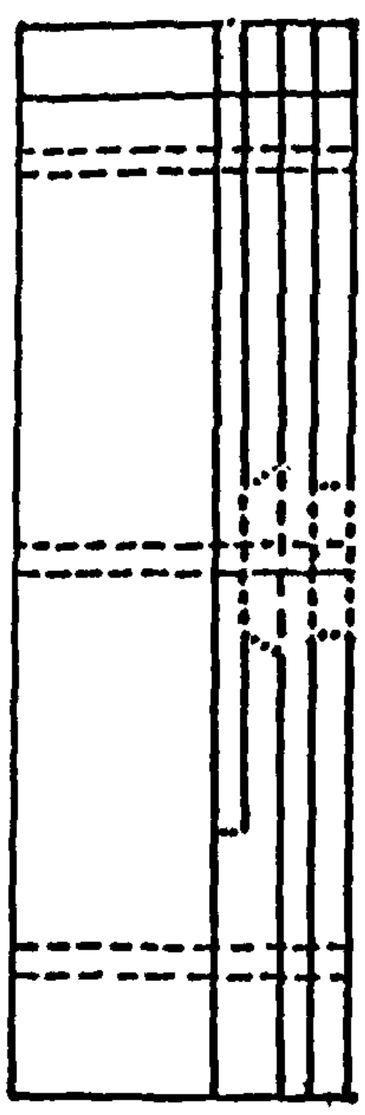
1.128 cm

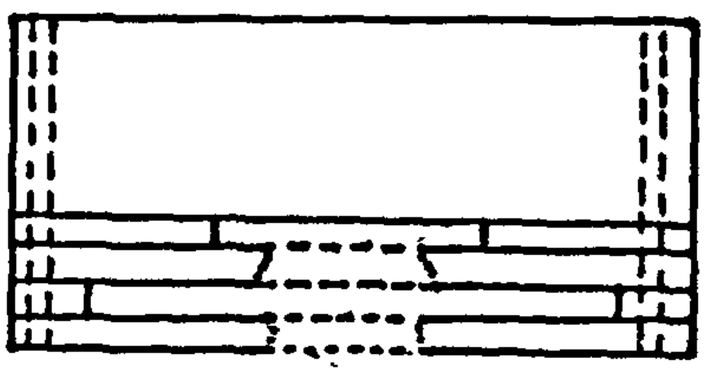

FIGURE 10.

Schematic representation of the circuit arrangement employed in the measurement of potentiodynamic polarization curves.

FIGURE 11.

Schematic representation of the circuit arrangement employed in the measurement of potentiostatic polarization curves.

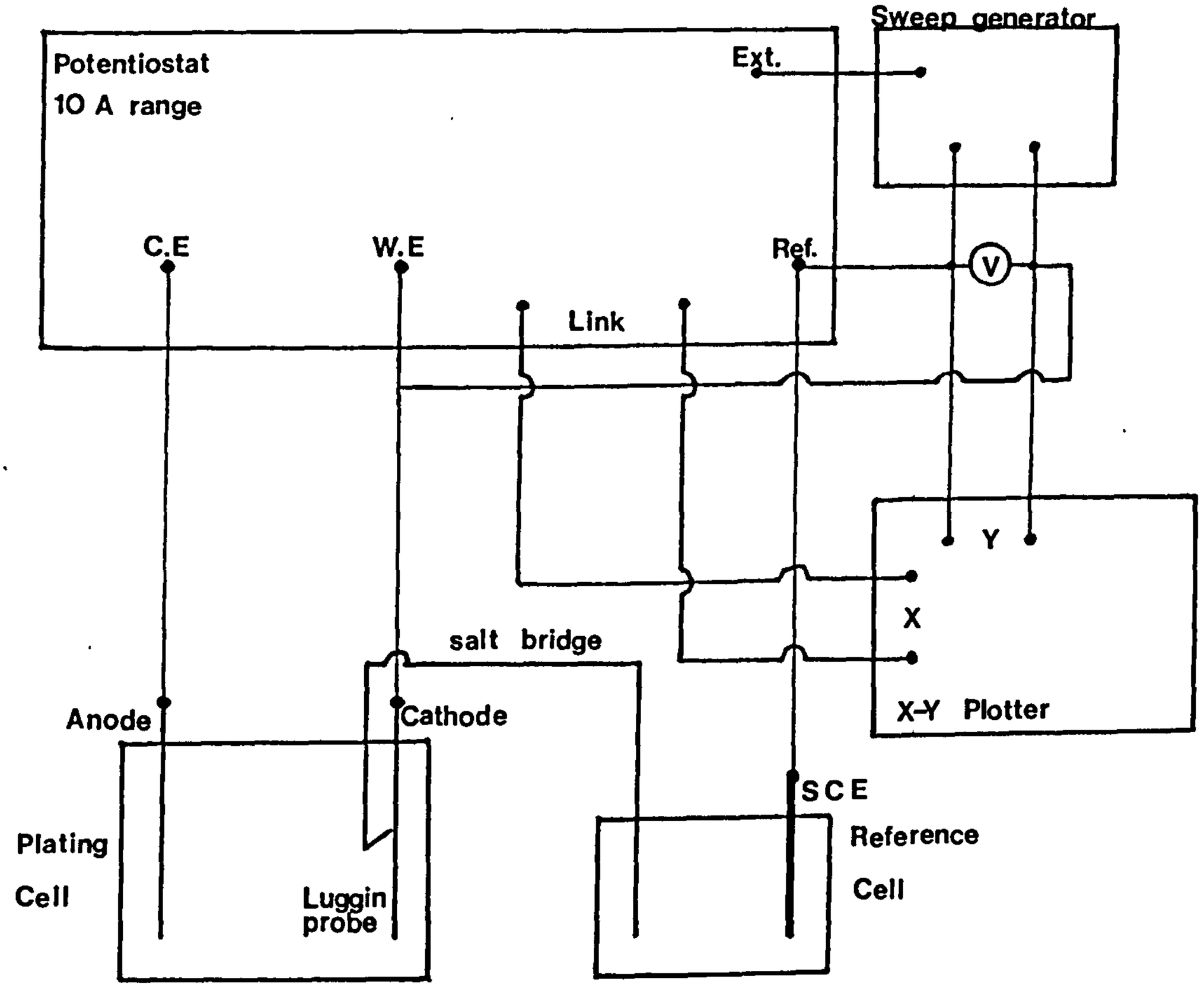
Potentiostat
10 A range
Sweep generator
Ext.
C.E
W.E
Ref.
V
Link
Y
X
salt bridge
X-Y Plotter
Anode
Cathode
SCE
Reference
Cell
Plating
Cell
Luggin
probe

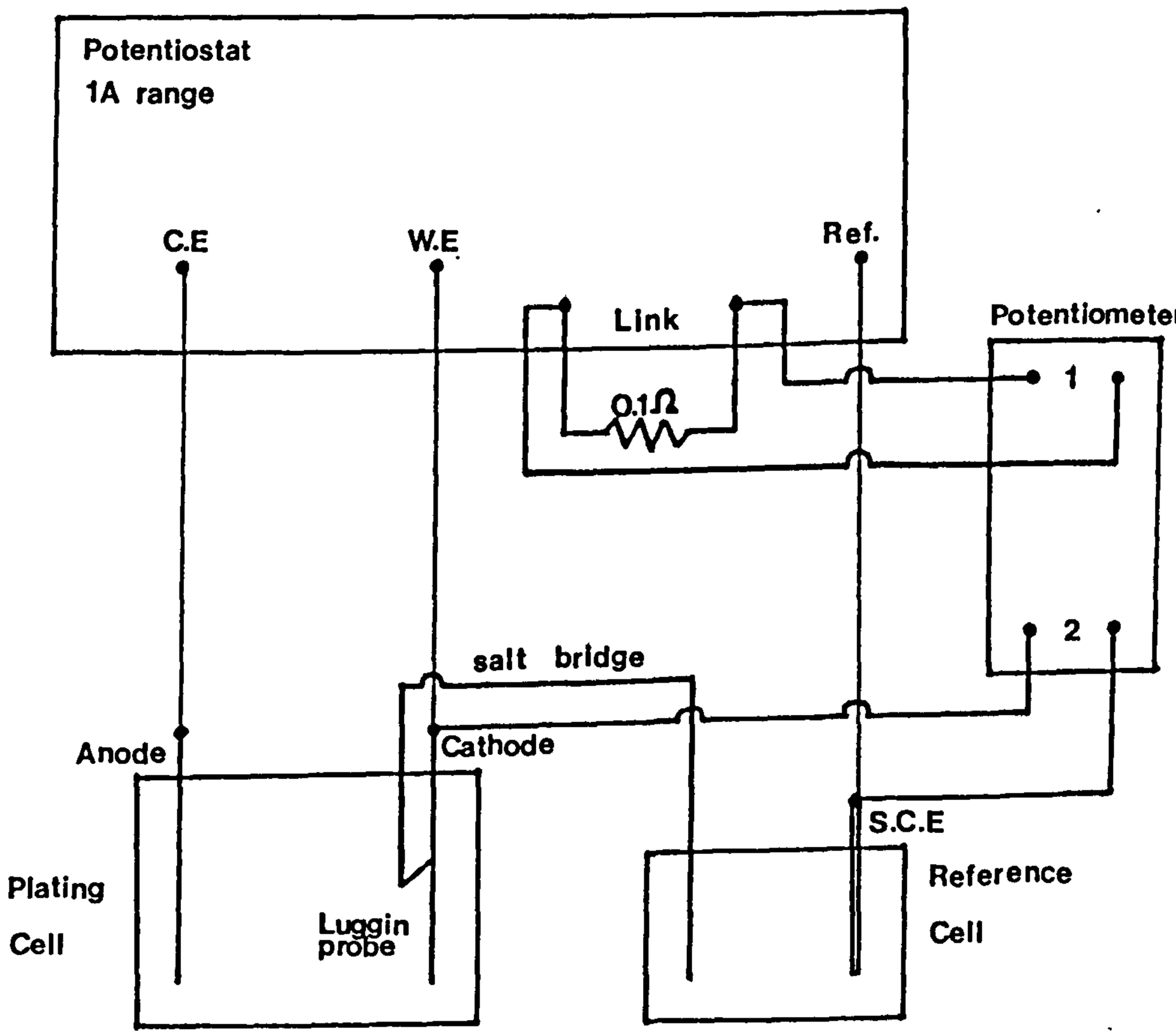
Potentiostat
1A range
C.E
W.E
Ref.
Link
0.1Ω
Potentiometer
1
2
salt bridge
Anode
Cathode
S.C.E
Reference
Cell
Plating
Cell
Luggin
probe

FIGURE 12.

Potentiostat arranged as a source of stable direct current (for use in the measurement of current efficiencies).

FIGURE 13.

Schematic diagram of the apparatus employed in the measurement of cathode current efficiencies.

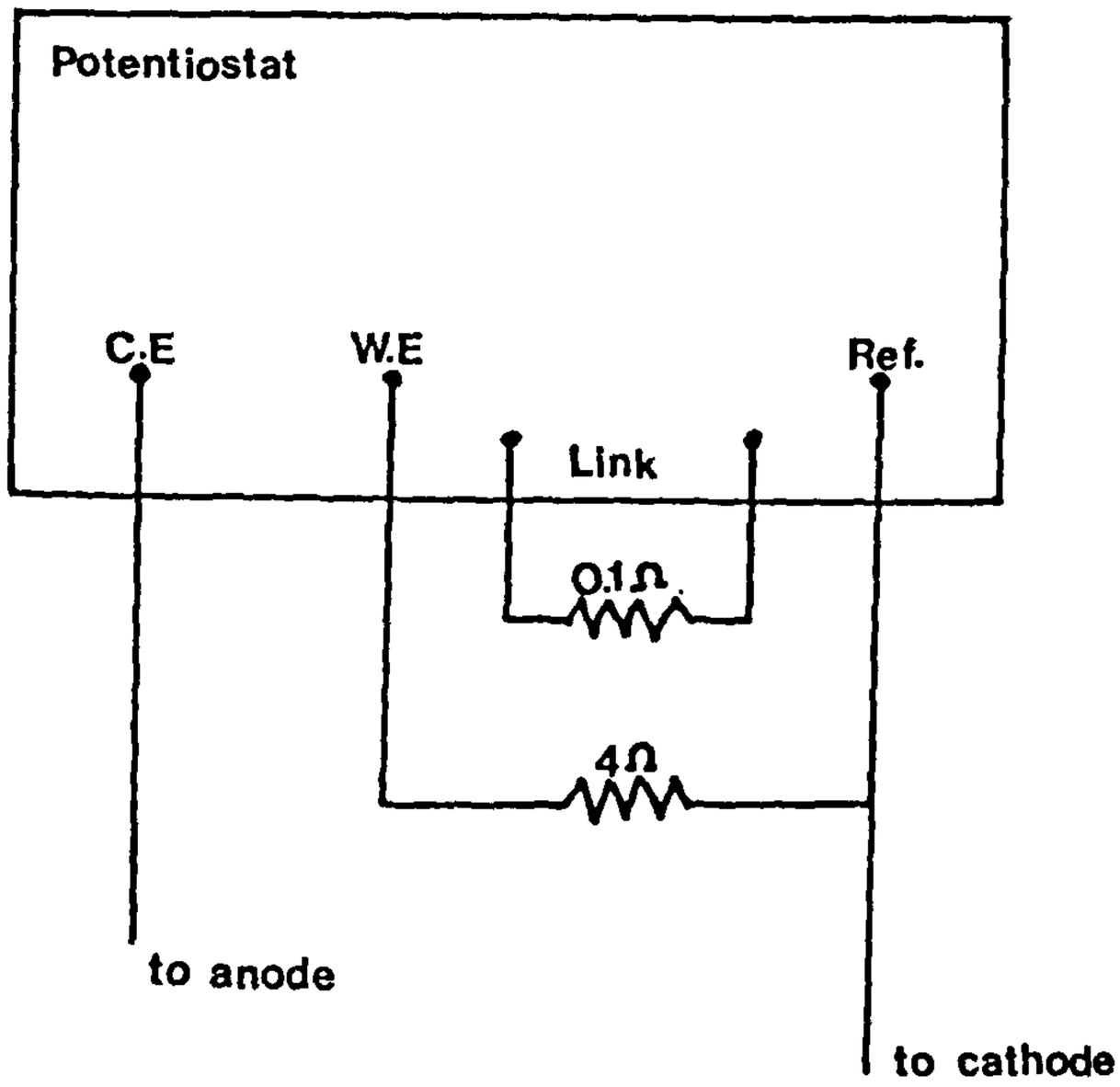
Potentiostat
C.E
W.E
Ref.
Link
0.1Ω
4Ω
to anode
to cathode

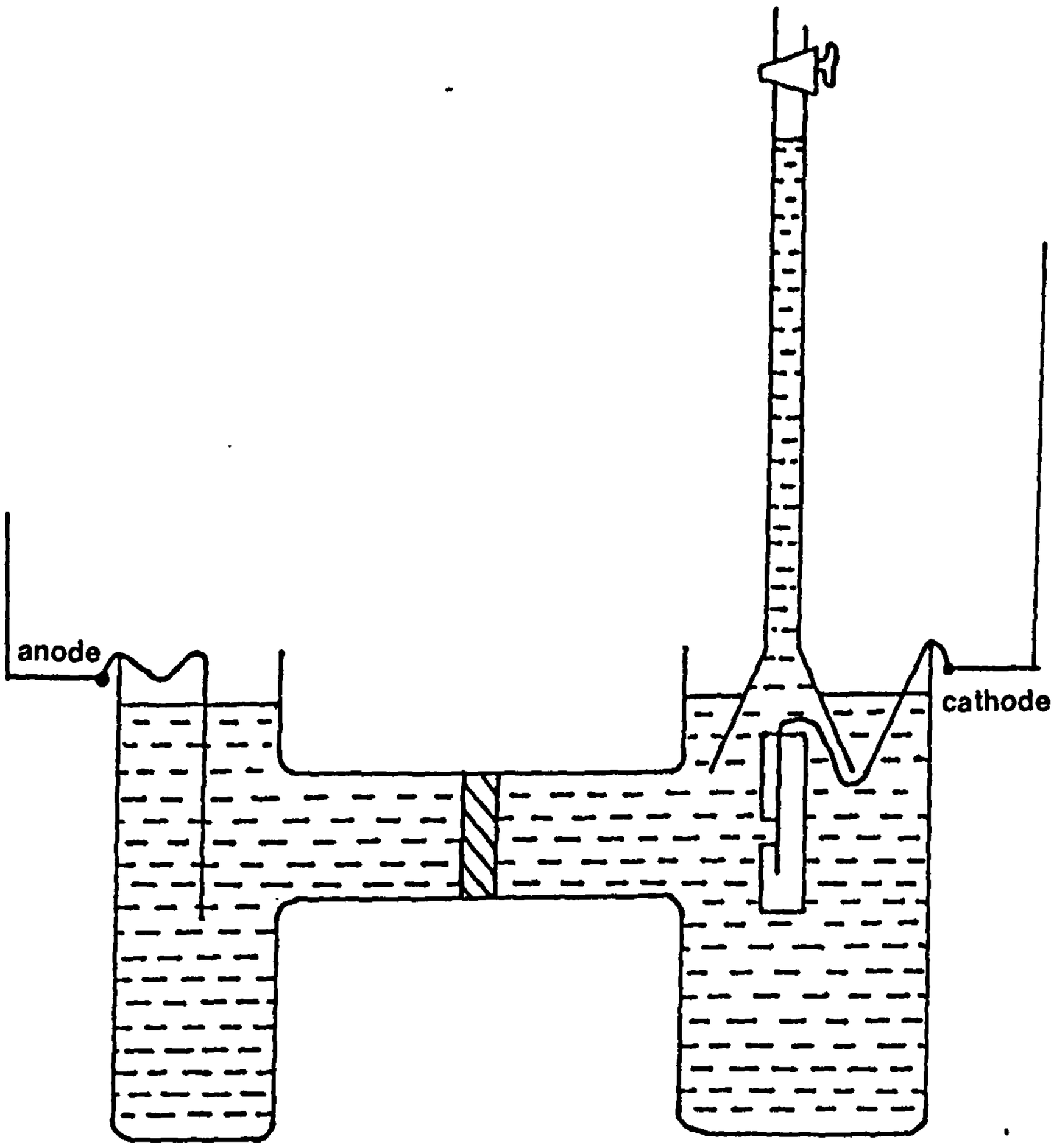
anode
cathode

FIGURE 14.

Schematic diagram of the apparatus employed in the determination of solution throwing power.

FIGURE 15.

Positioning (across $1cm^2$ sample of chromium plate) of diamond impressions used in the evaluation of Table 2.

$$P = \frac{5z}{z} = 5$$

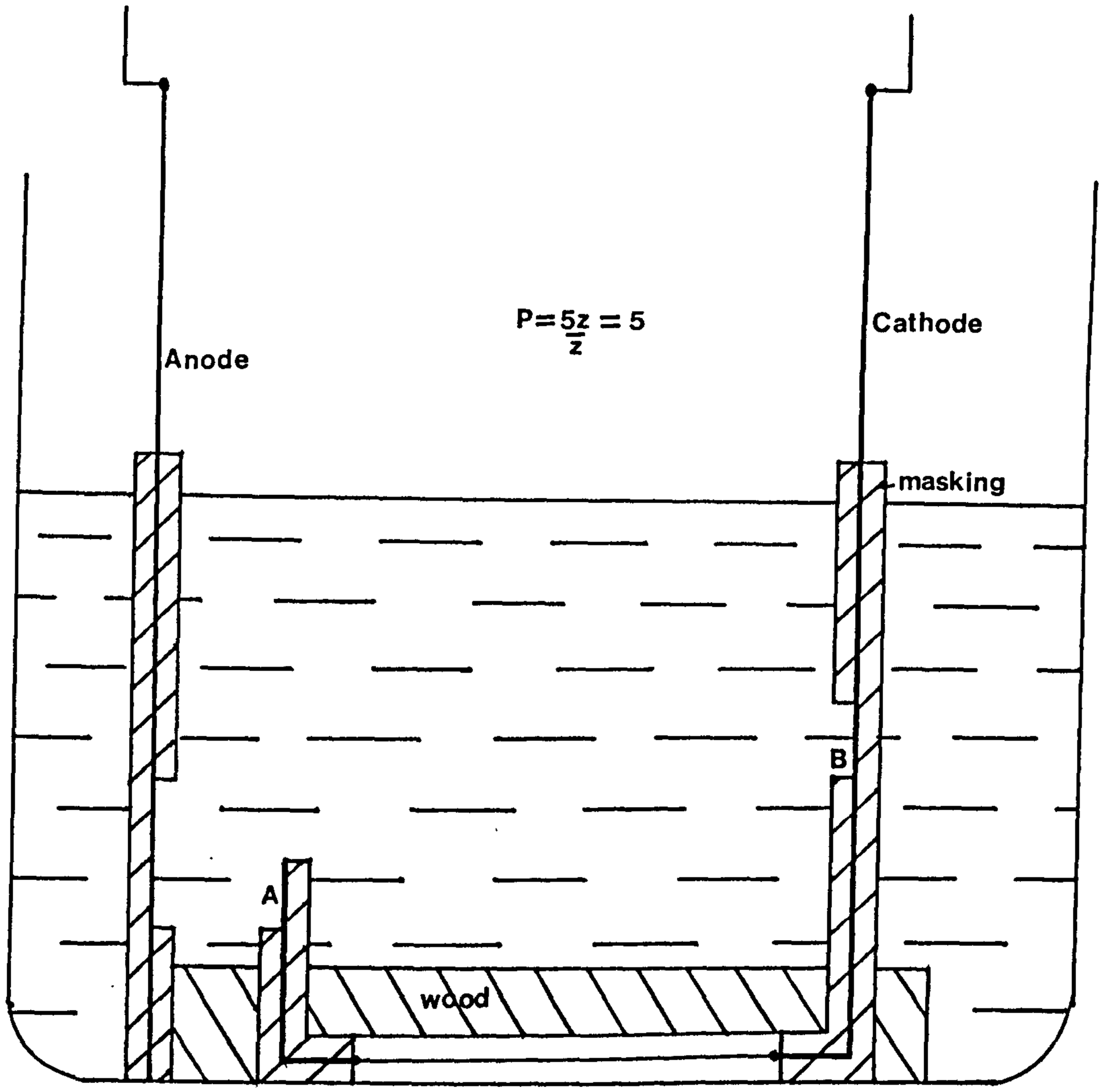

z

5z

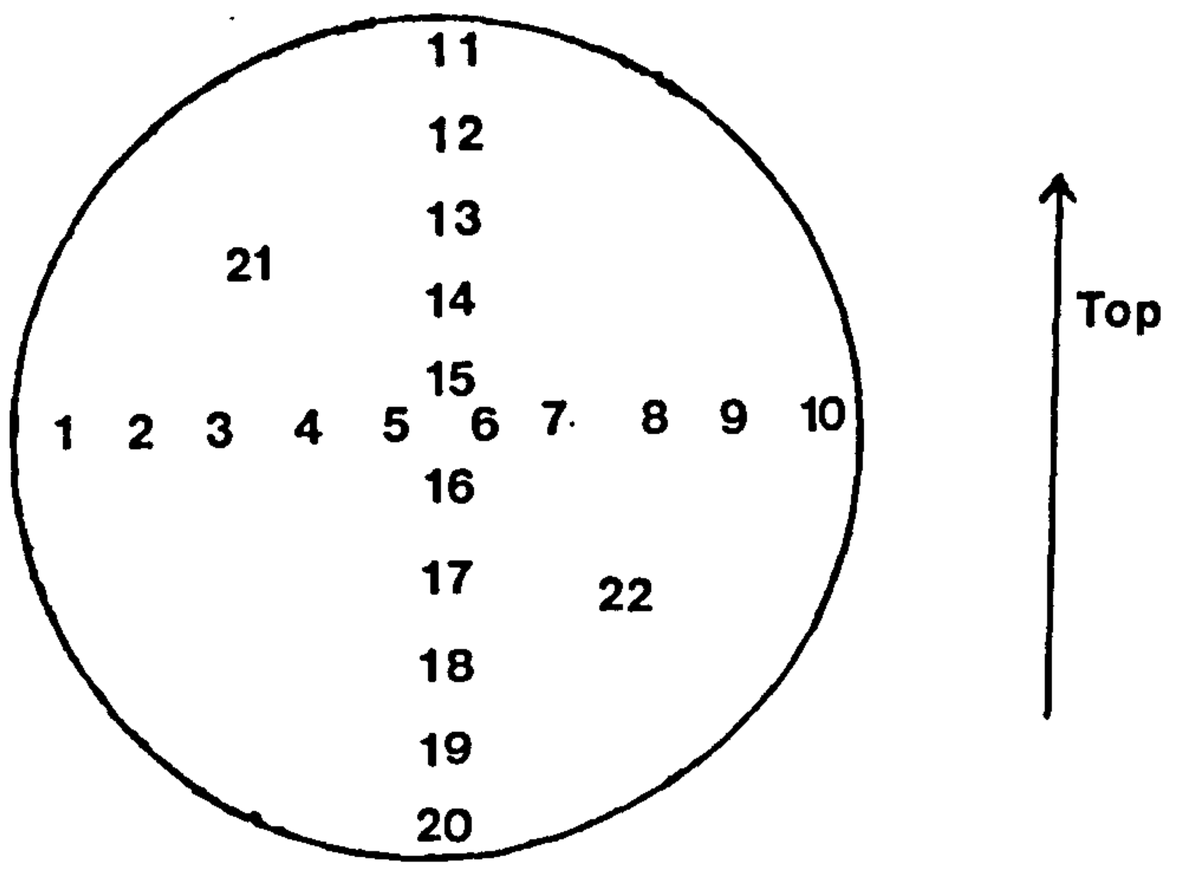

FIGURE 16.

Overall, potentiodynamically determined, cathode polarization curves from a (55°C) Standard Solution alone and with 10g/l additions of A, B and C.

Sweep rate = 30 mV/s.

Each curve averaged from 3.

Maximum observed error in current density = ± 8%

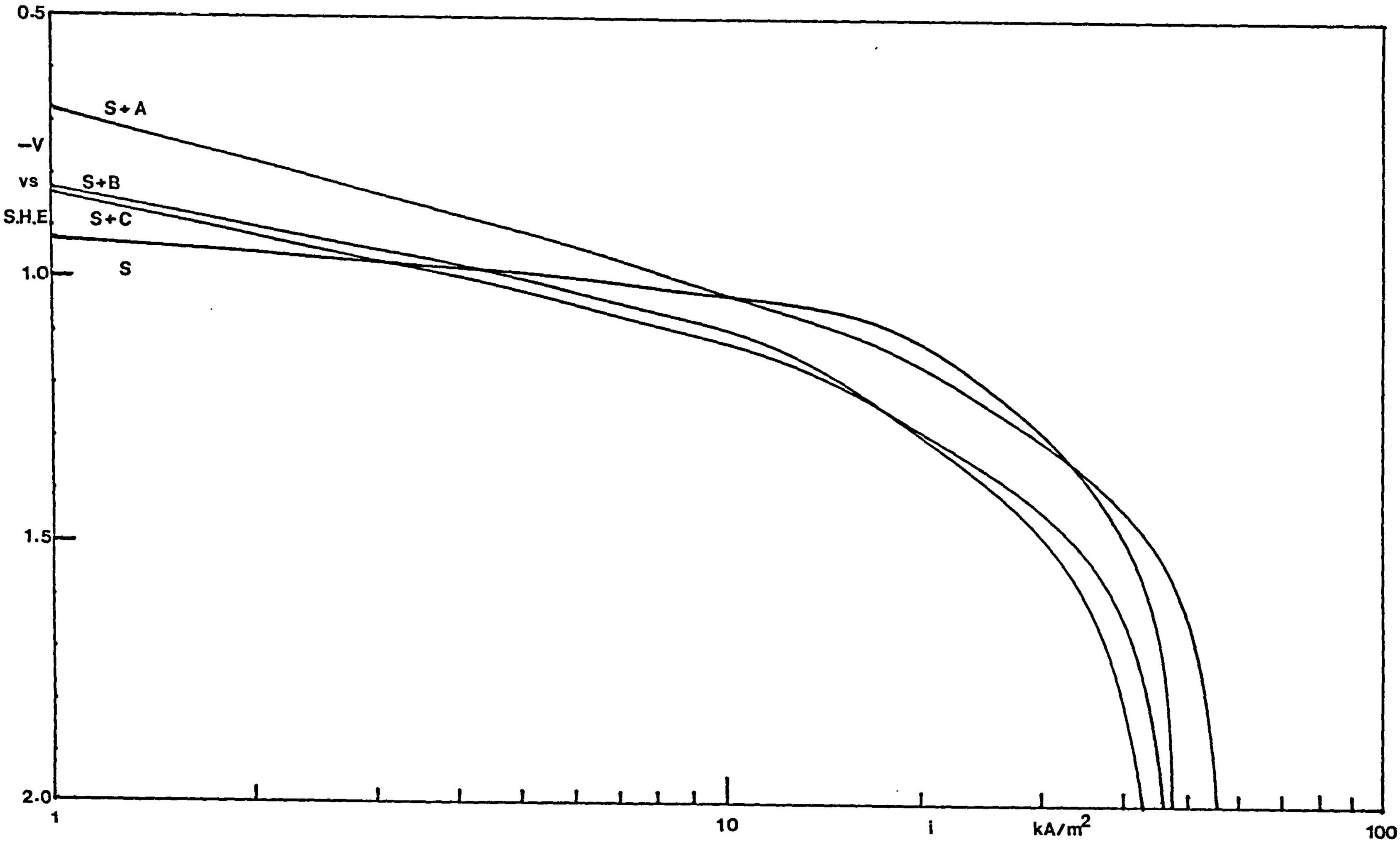
0.5
S+A
-V
vs
S+B
S.H.E
S+C
1.0
S
1.5
2.0
1
10
i
kA/m2
100

FIGURE 17.

Evidence of hysteresis in potentiodynamically determined cathode polarization curve from Standard Solution at 55°C.

Sweep rate = 100mV/s.

Points plotted were averaged from 3 runs.

It was noted that hysteresis during individual reversals (at 100mV/s using a sweep ratio of 3:2 - see Experimental) was unaffected by the presence of 10g/l $KClO_4$, but decreased in the presence of 10g/l $KBrO_3$ or $K_2B_2O_4$.

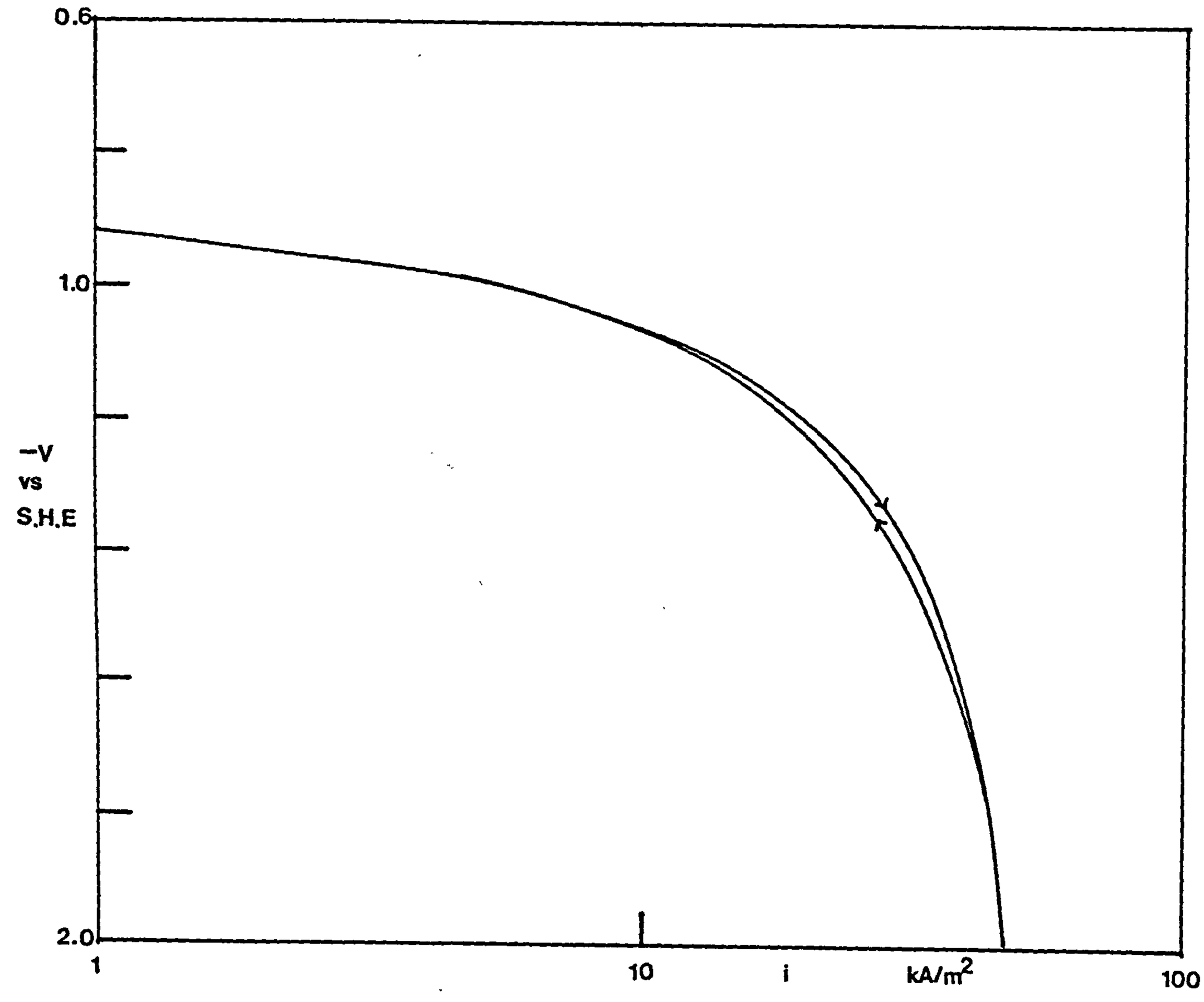
0.6
1.0
2.0
−V
vs
S.H.E
1
10
100
i
kA/m2

17a

Nett 100 mV / s , 3 : 2

One loop from each curve

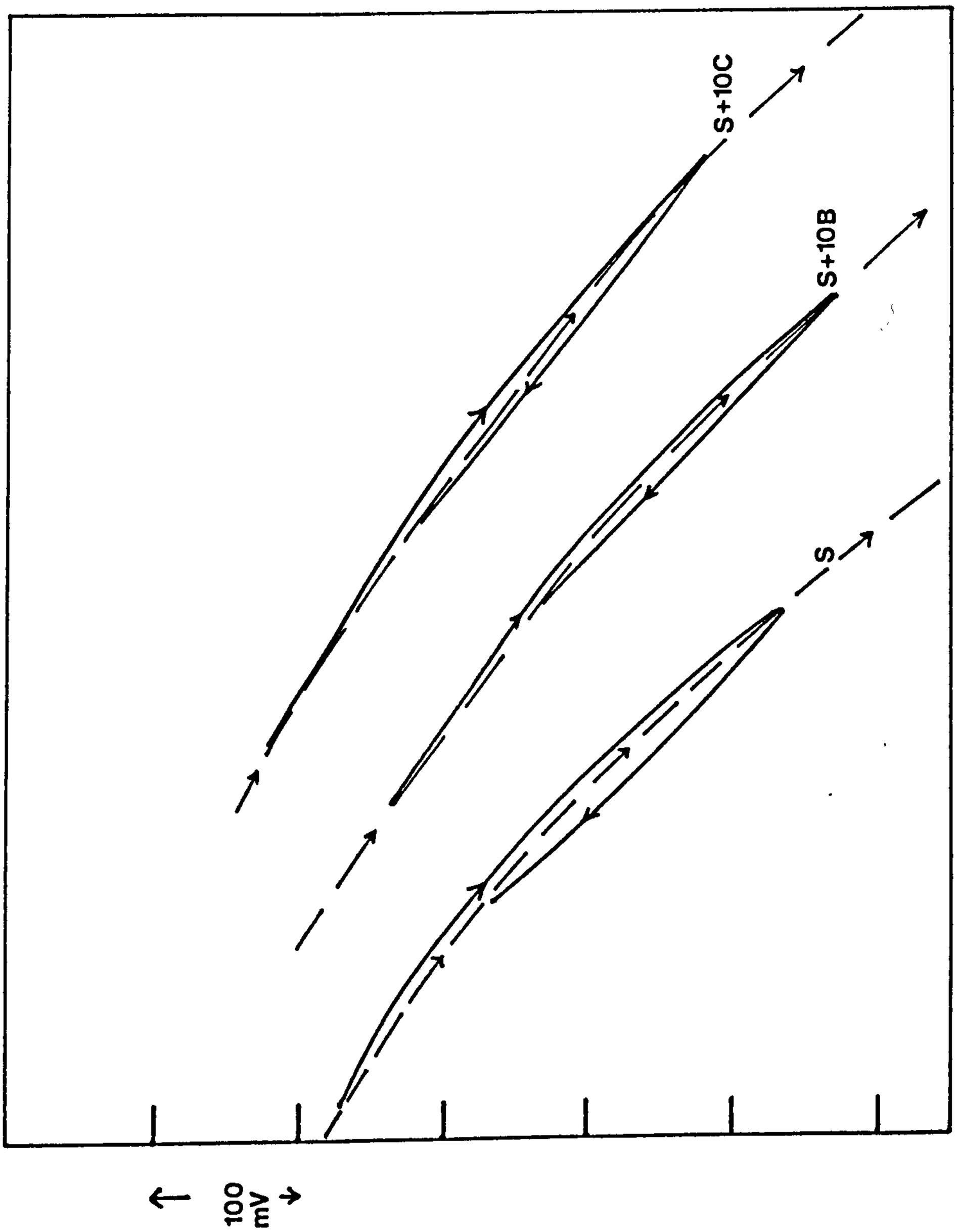

FIGURE 18.

Potentiodynamically determined cathode polarization curves from a Standard Solution at 55°C, showing the effect of sweep rate upon the curve shape.

Each curve averaged from 3.

At a sweep rate of 1mV/s,

maximum observed error in current density = $\pm$ 6%

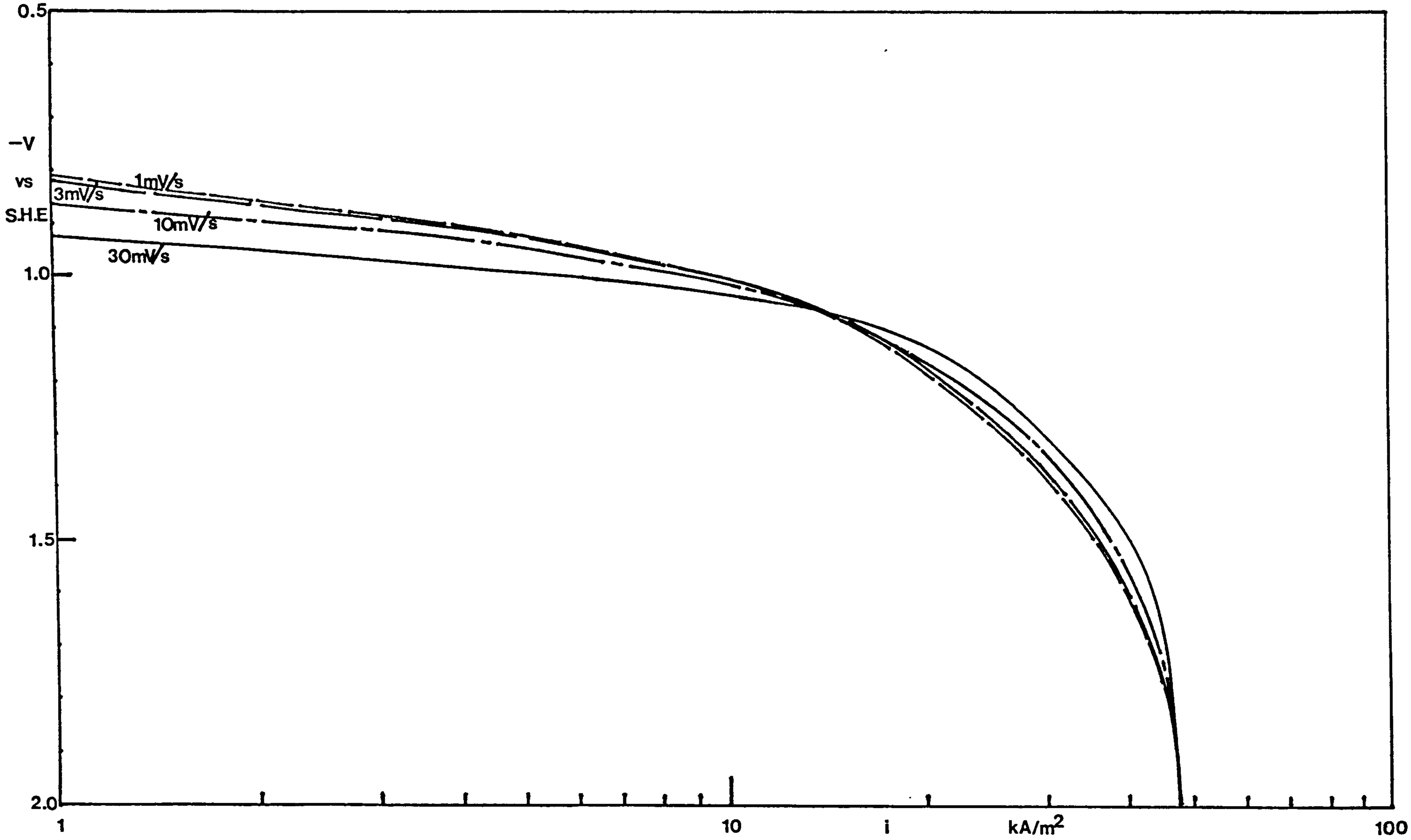
0.5
−V
vs
S.H.E
1.0
1.5
2.0
1mV/s
3mV/s
10mV/s
30mV/s
1
10
i
kA/m2
100

FIGURE 19.

Potentiostatically (step-wise) determined cathode polarization curves from a Standard Solution at 55°C, illustrating the effect of relaxation time (between potential variations of 10 mV) upon the shape of the curve.
Probe tip to cathode distance of 1 mm.

Each curve averaged from 5.

1 minute relaxation time

Maximum error in observed current density = ± 3.5%

5 minute relaxation time

Maximum error in observed current density = ± 1.5%

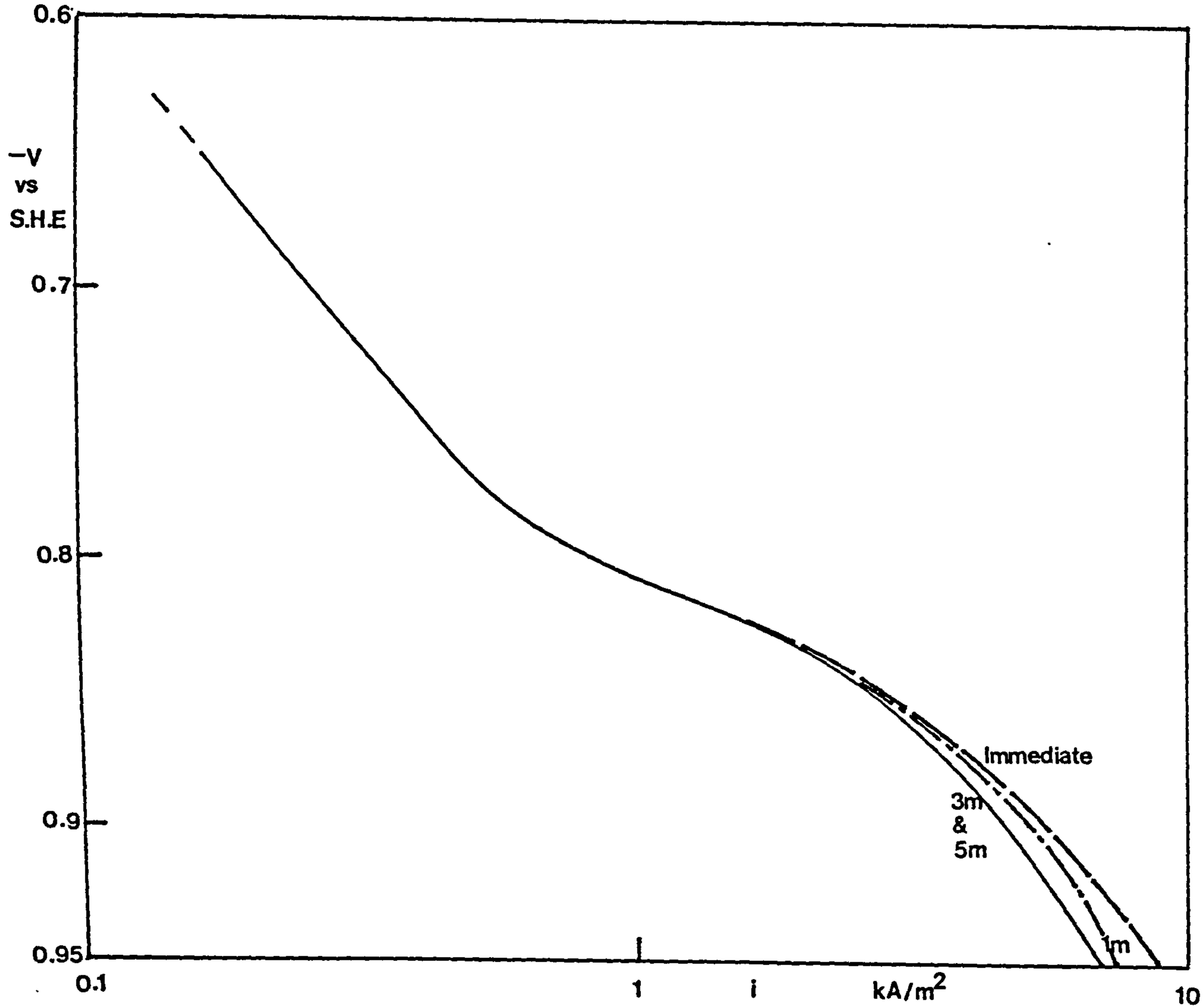
0.6
−V
vs
S.H.E
0.7
0.8
0.9
0.95
0.1
1
i
kA/m2
10
Immediate
3m
&
5m
1m

FIGURE 20.

Potentiostatically (step-wise) determined cathode polarization curves from a Standard Solution at 55°C, illustrating the effect of probe-tip to cathode distance upon the curve shape.

10 mV potential increments. 5 minute relaxation time.

Each curve averaged from 3.

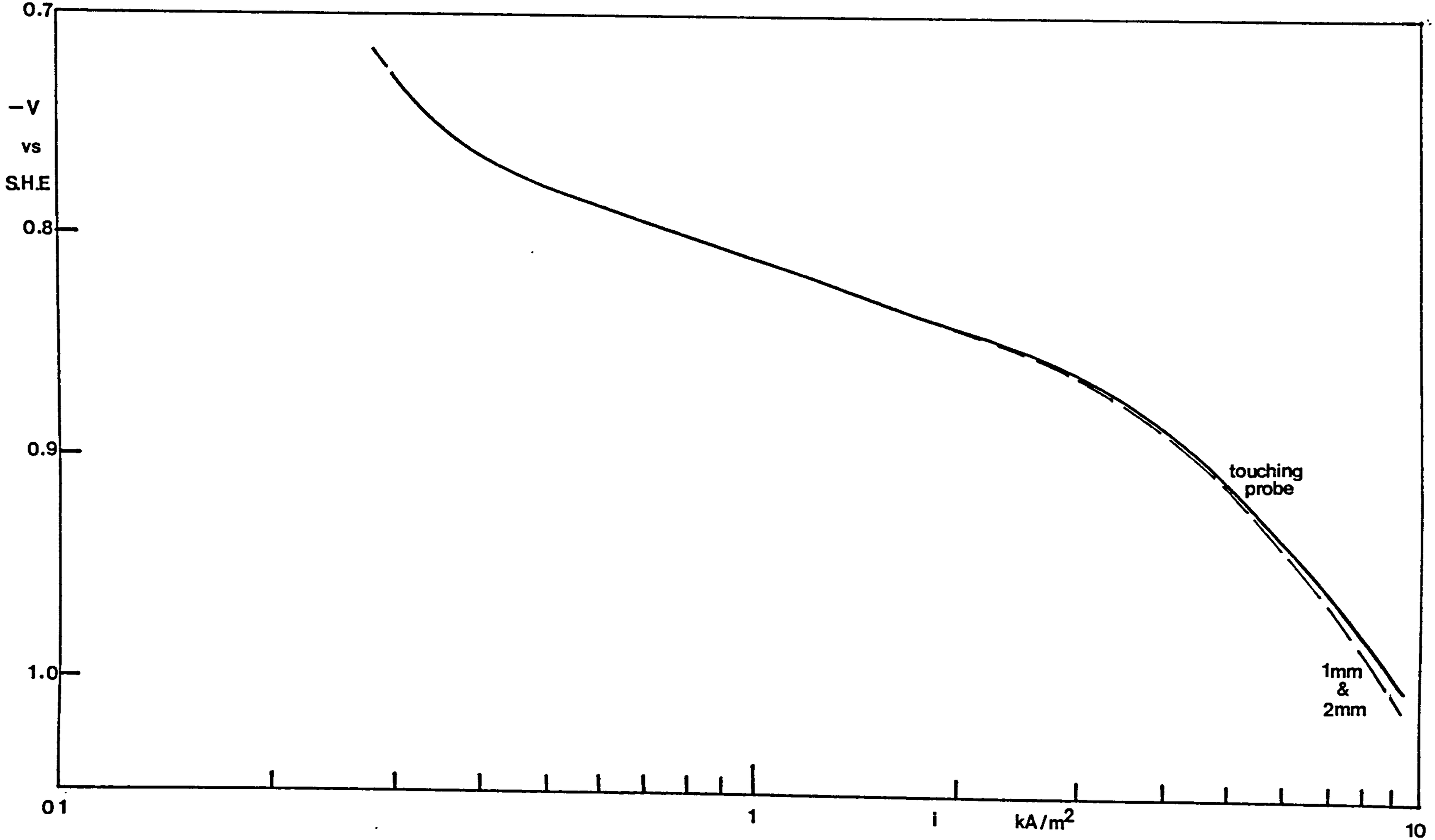
0.7
−V
vs
S.H.E
0.8
0.9
1.0
touching
probe
1mm
&
2mm
0 1
1
i
kA/m2
10

FIGURE 21.

As FIGURE 20 but magnified.

The potential drop due to probe position at current densities corresponding to apparent Tafel behaviour.

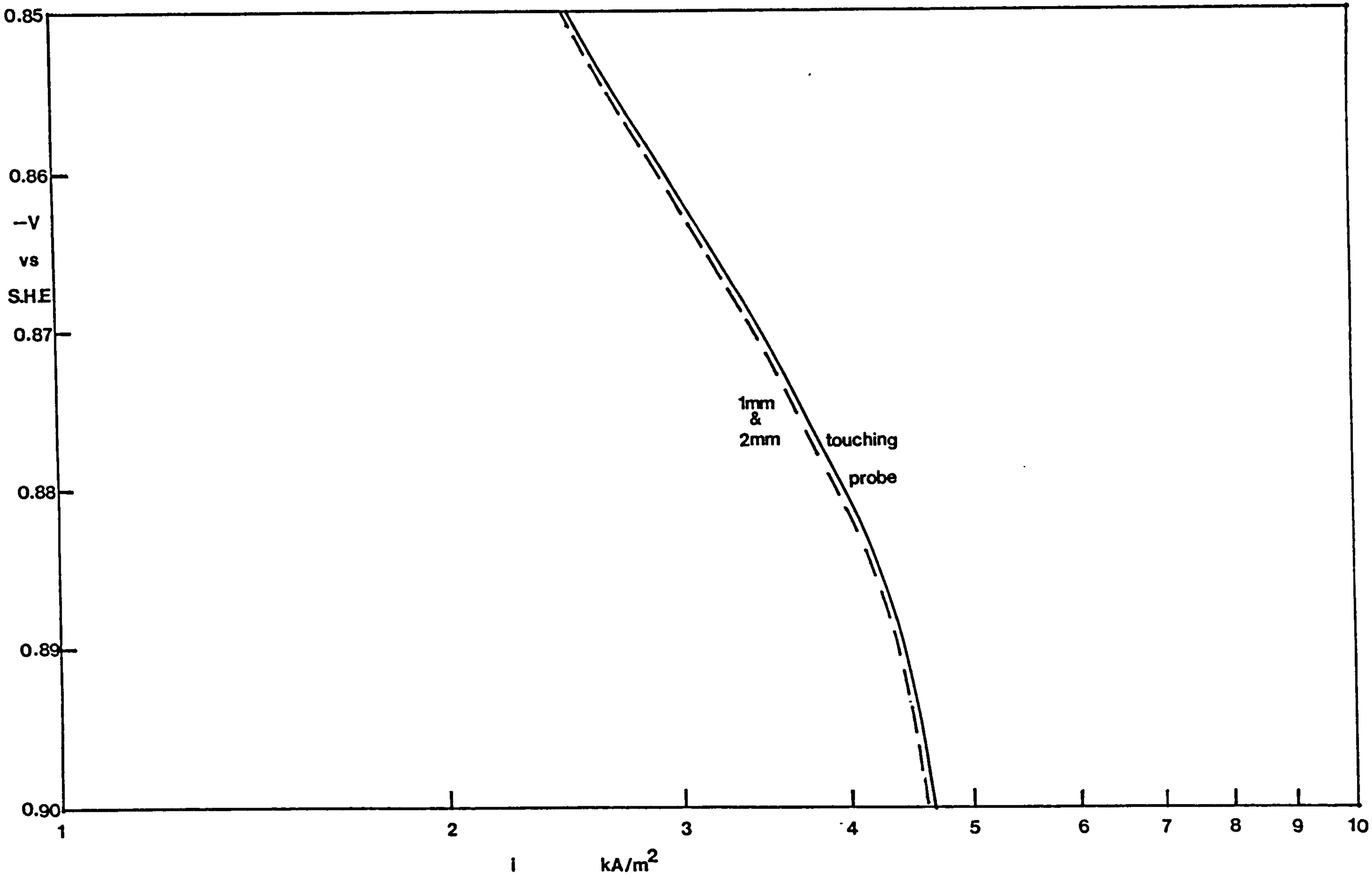
0.85
0.86
-V
vs
S.H.E
0.87
0.88
0.89
0.90
1mm
&
2mm
touching
probe
1
2
3
4
5
6
7
8
9
10
i kA/m2

FIGURE 22.

Overall potentiostatic cathode polarization curve from a Standard Solution at 55°C.

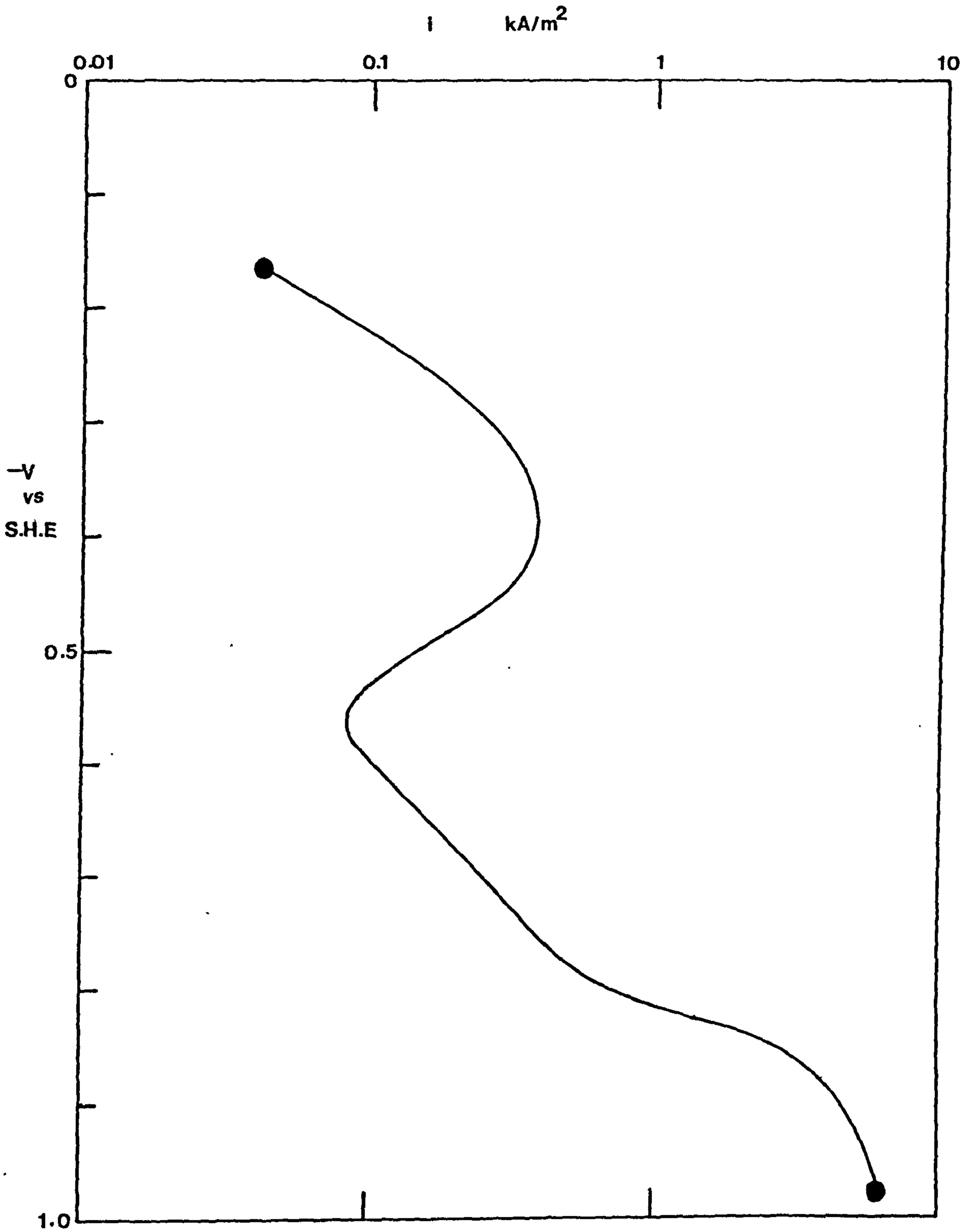
i kA/m2
0.01
0.1
1
10
0
—V
vs
S.H.E
0.5
1.0

FIGURE 23.

The variation of plating current efficiency with cathode current density in the apparent Tafel range.

The effect of $KClO_4$ presence.

FIGURE 24.

The variation of plating current efficiency with cathode current density at higher current densities.

The effect of $KClO_4$ presence.

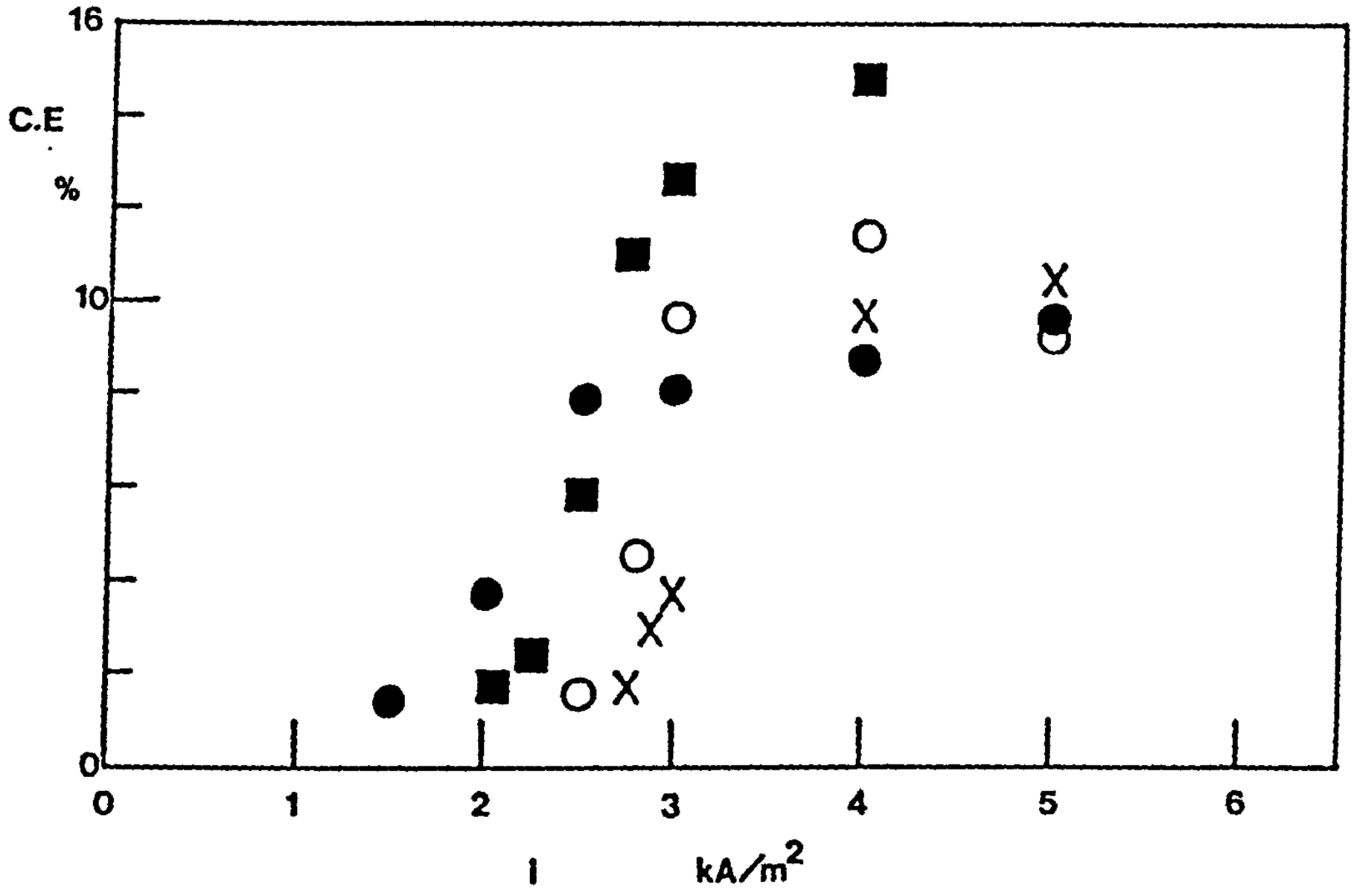
16
C.E
%
10
0
0
1
2
3
4
5
6
I
kA/m2

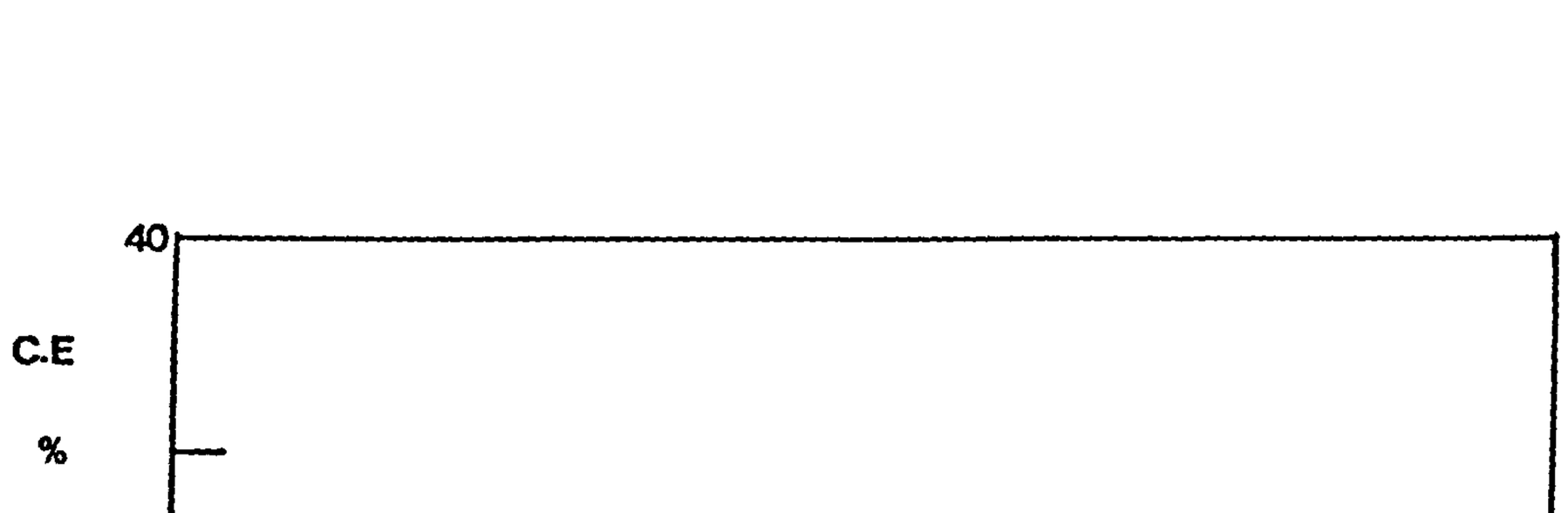
40
C.E
%
20
0
0
25
50
I
kA/m2

FIGURE 25.

The variation of hydrogen evolution current efficiency with cathode current density in the apparent Tafel range.

The effect of $KClO_4$ presence.

FIGURE 26.

The variation of hydrogen evolution current efficiency with cathode current density at higher current densities.

The effect of $KClO_4$ presence.

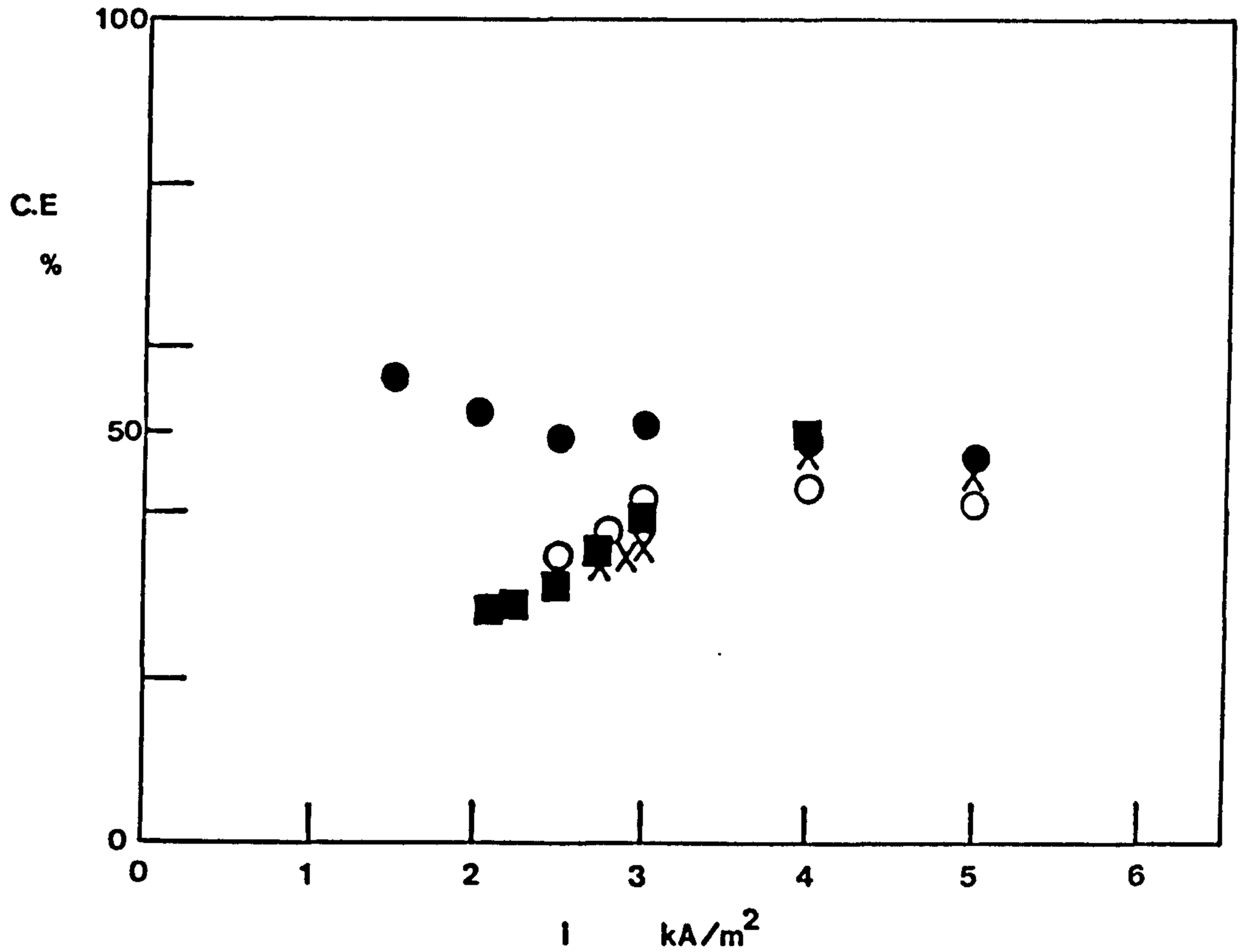
100
C.E
%
50
0
0
1
2
3
4
5
6
I kA/m2

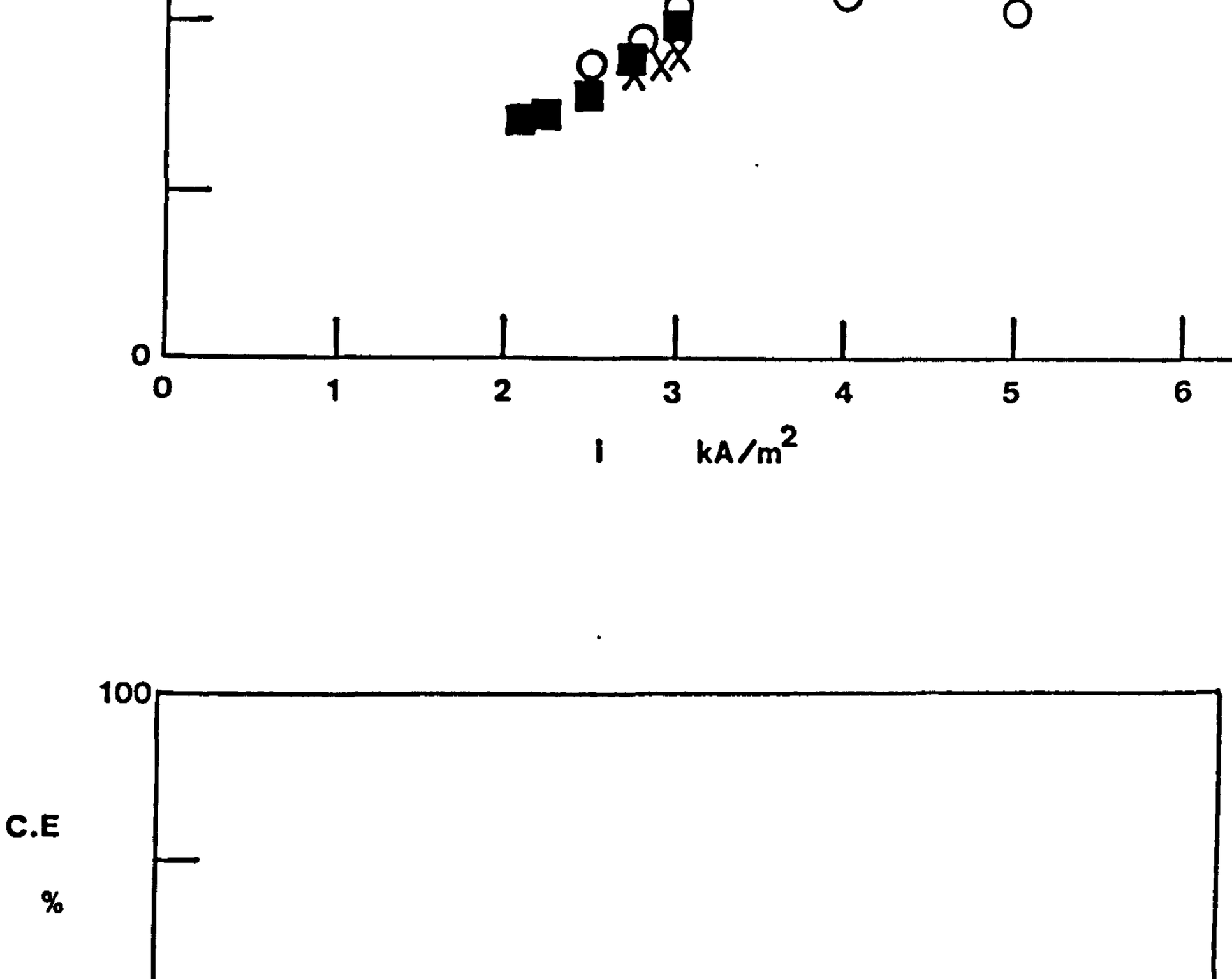
100
C.E
%
50
0
0
25
50
I kA/m2

FIGURE 27.

The variation of partial (CrVI to CrIII) reduction current efficiency with cathode current density in the apparent Tafel range. The effect of $KClO_4$ presence.

FIGURE 28.

The variation of partial (CrVI to CrIII) reduction current efficiency with cathode current density at higher current densities. The effect of $KClO_4$ presence.

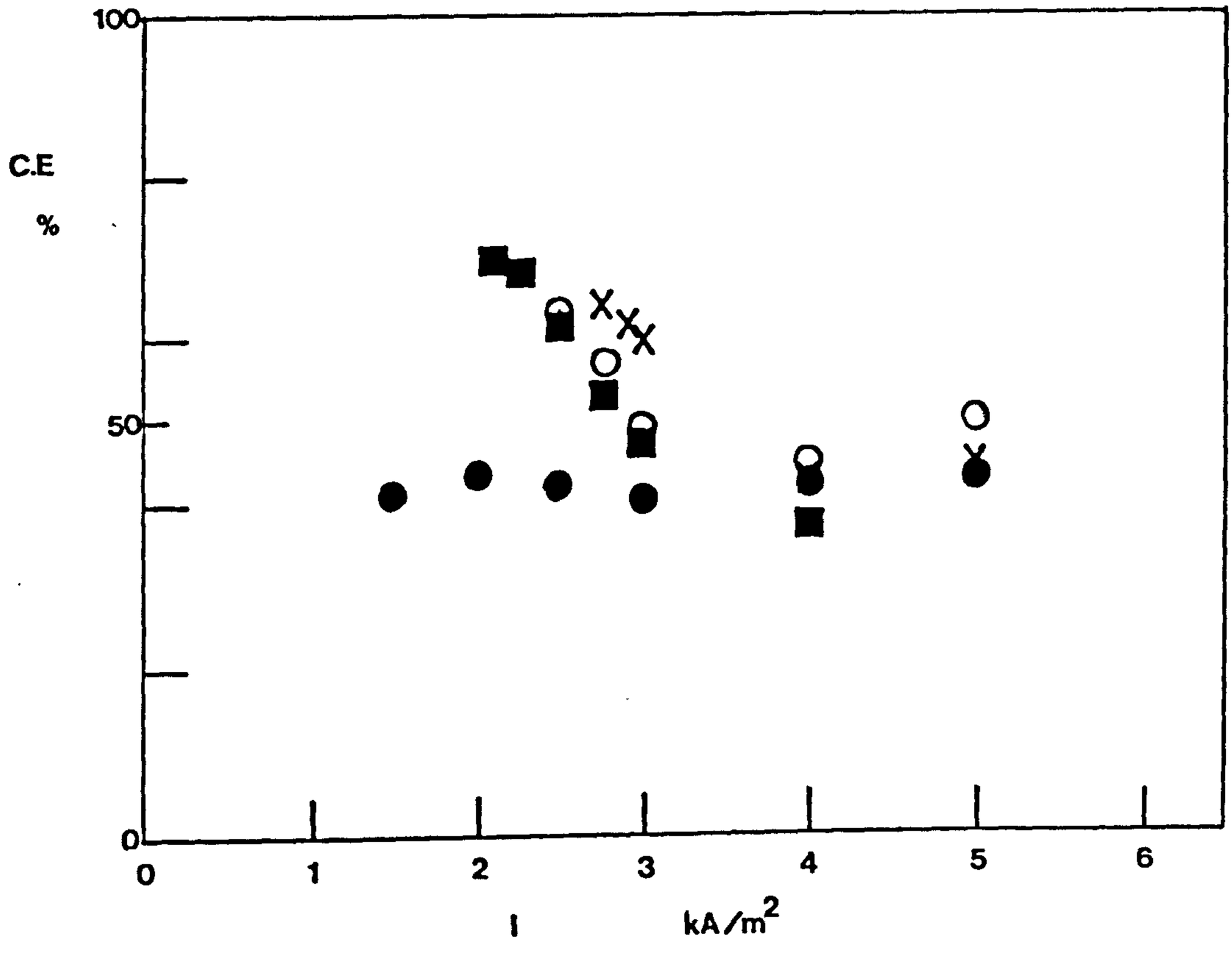
100
C.E
%
50
0
0
1
2
3
4
5
6
I
kA/m2

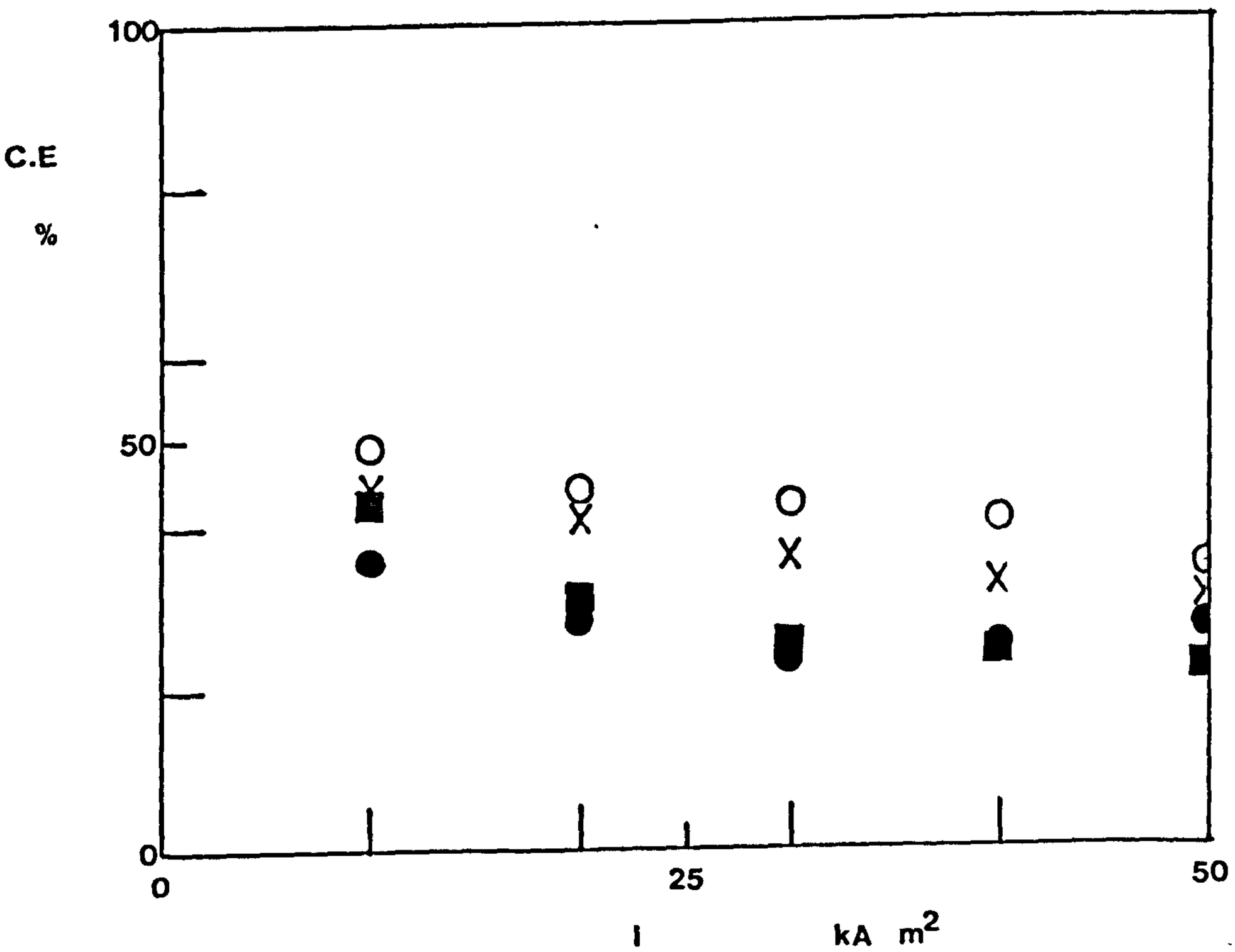
100
C.E
%
50
0
0
25
50
I
kA m2

FIGURE 29.

The apparent Tafel region of the overall cathode polarization curve (potentiostatic).

The effect of $KClO_4$ presence.

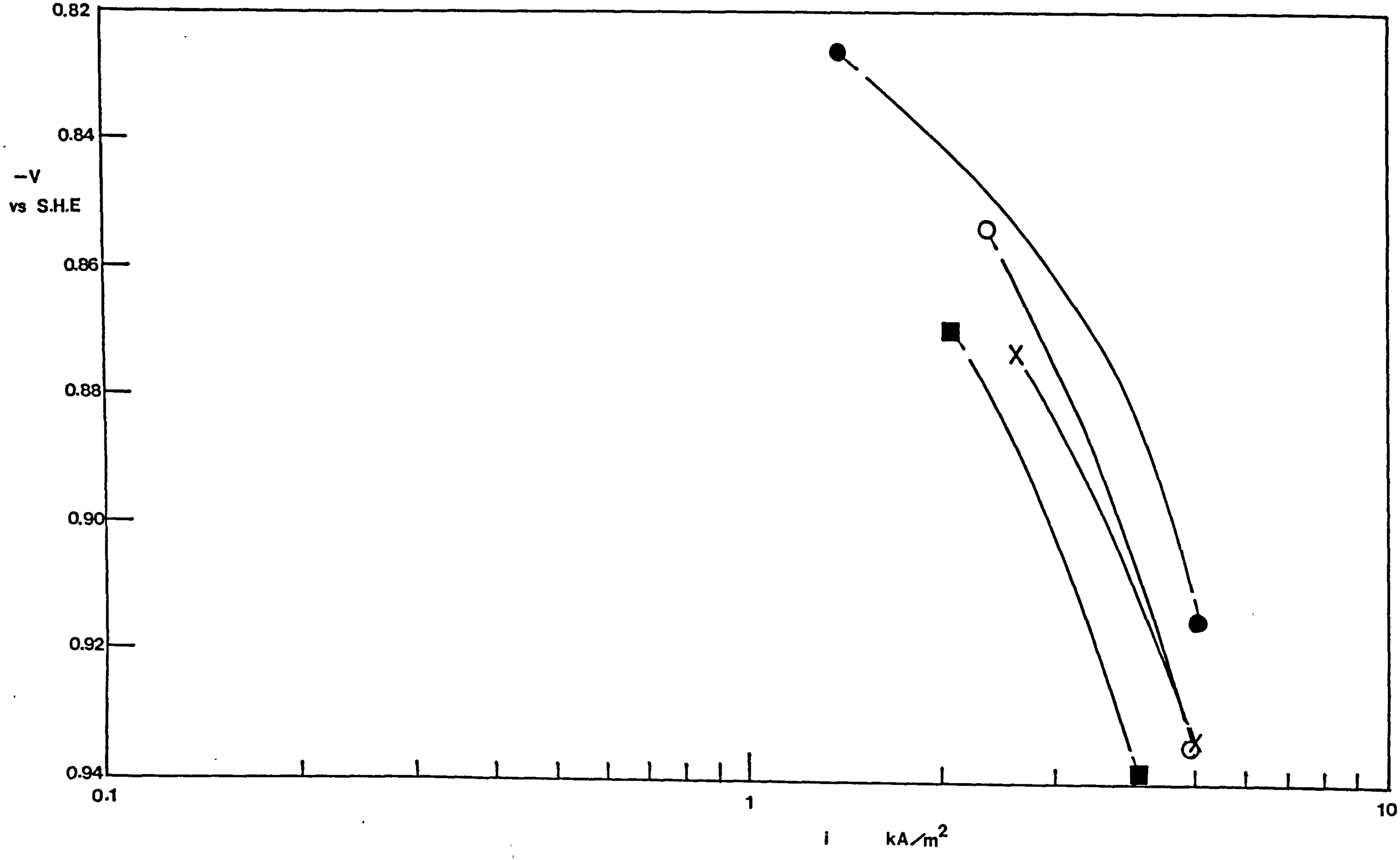
0.82
0.84
−V
vs S.H.E
0.86
0.88
0.90
0.92
0.94
0.1
1
10
i kA/m²

FIGURE 30.

Partial cathode polarization curve for the plating reaction.

The effect of $KClO_4$ presence.

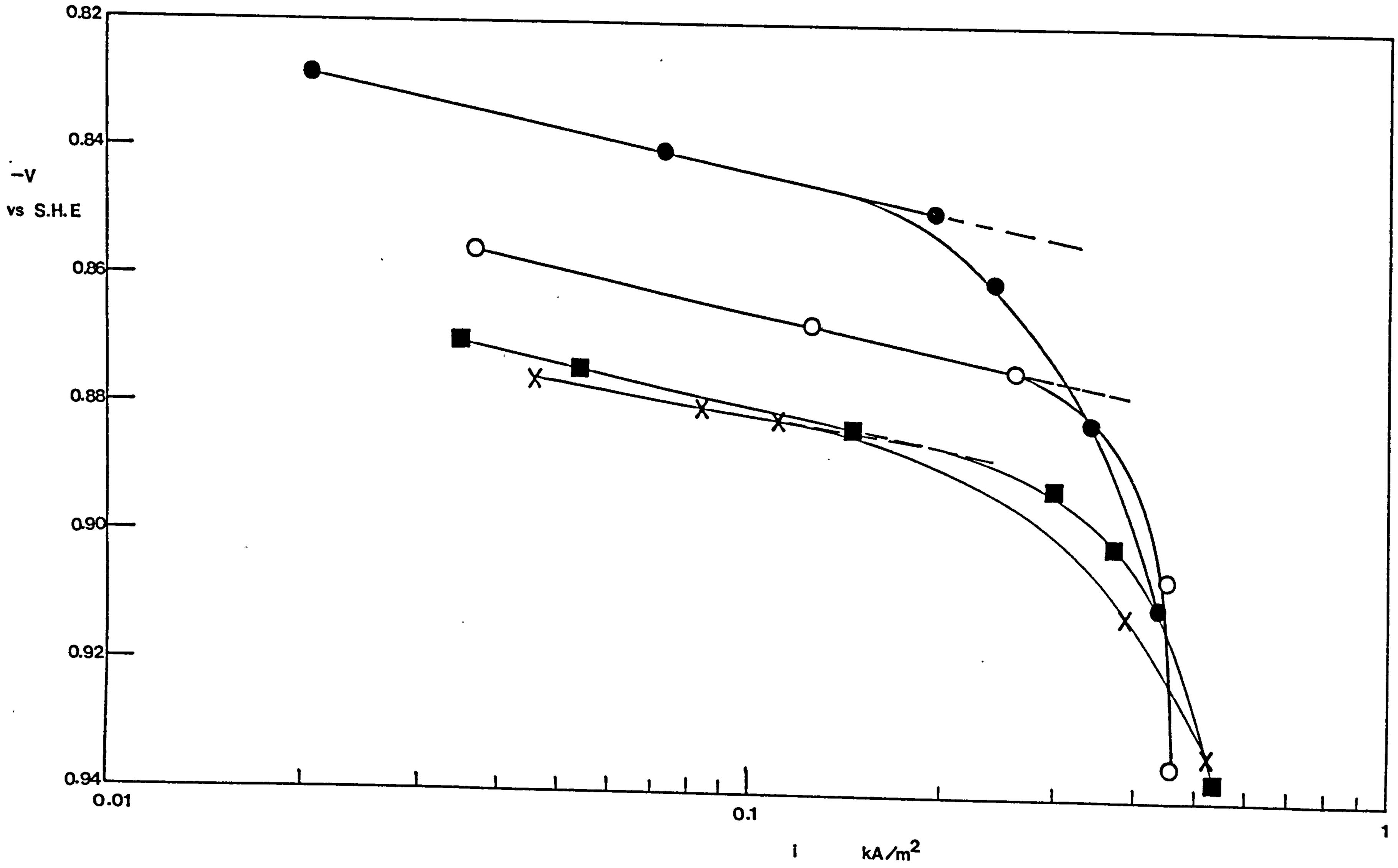
0.82
0.84
0.86
0.88
0.90
0.92
0.94
−V
vs S.H.E
0.01
0.1
1
i kA/m²

FIGURE 31.

Partial cathode polarization curve for the hydrogen evolution reaction.

The effect of $KClO_4$ presence.

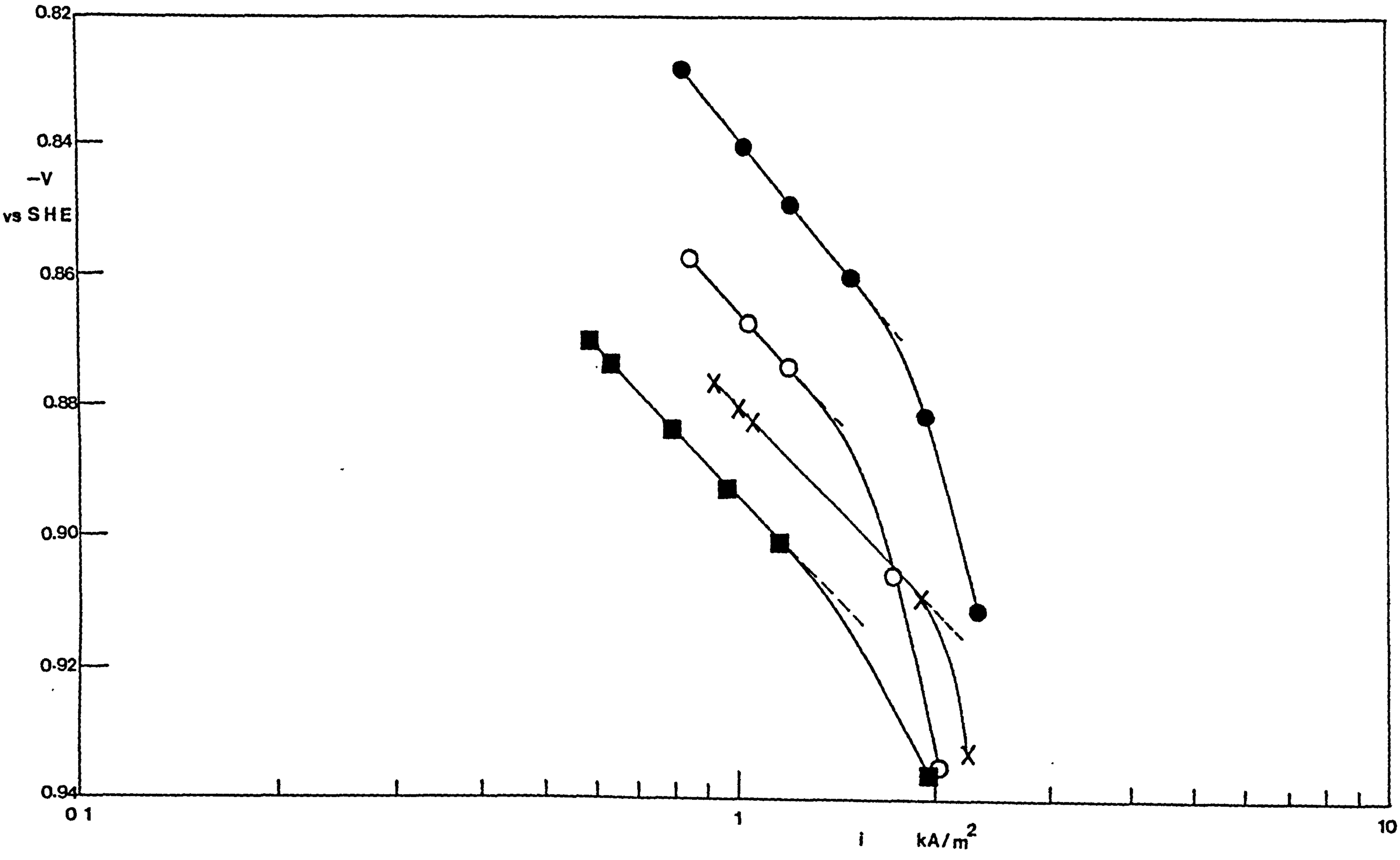
0.82
0.84
−V
vs S H E
0.86
0.88
0.90
0.92
0.94
0 1
1
10
i kA/m²

FIGURE 32.

Partial cathode polarization curve for the partial (CrVI to CrIII) reduction reaction. The effect of $KClO_4$ presence.

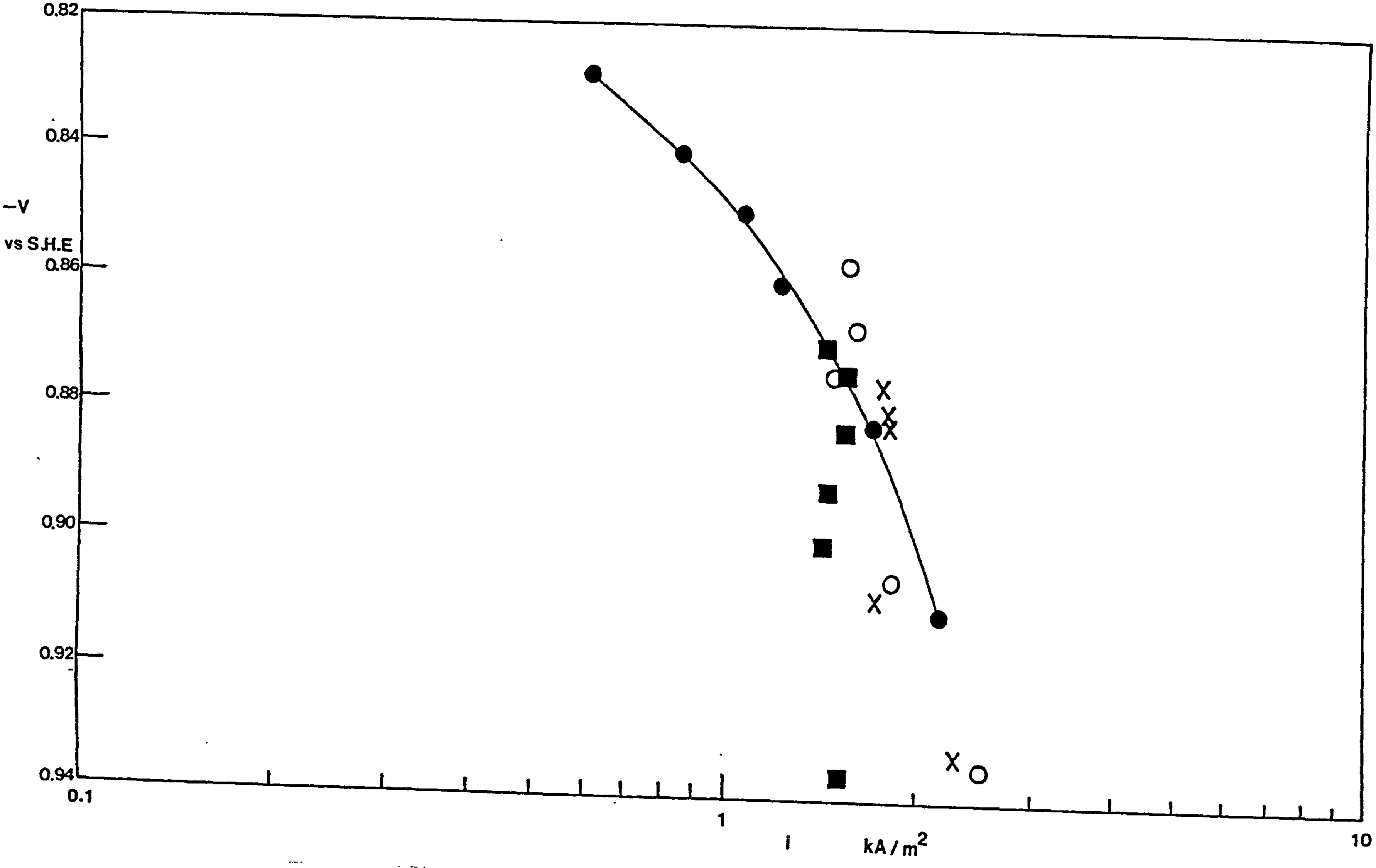
0.82
0.84
-V
vs S.H.E
0.86
0.88
0.90
0.92
0.94
0.1
1
10
i
kA / m2

FIGURE 33.

Arrhenius-type plots for the plating reaction in a Standard Solution at constant cathode potentials of

a) - 0.83V

b) - 0.84V

c) - 0.85V

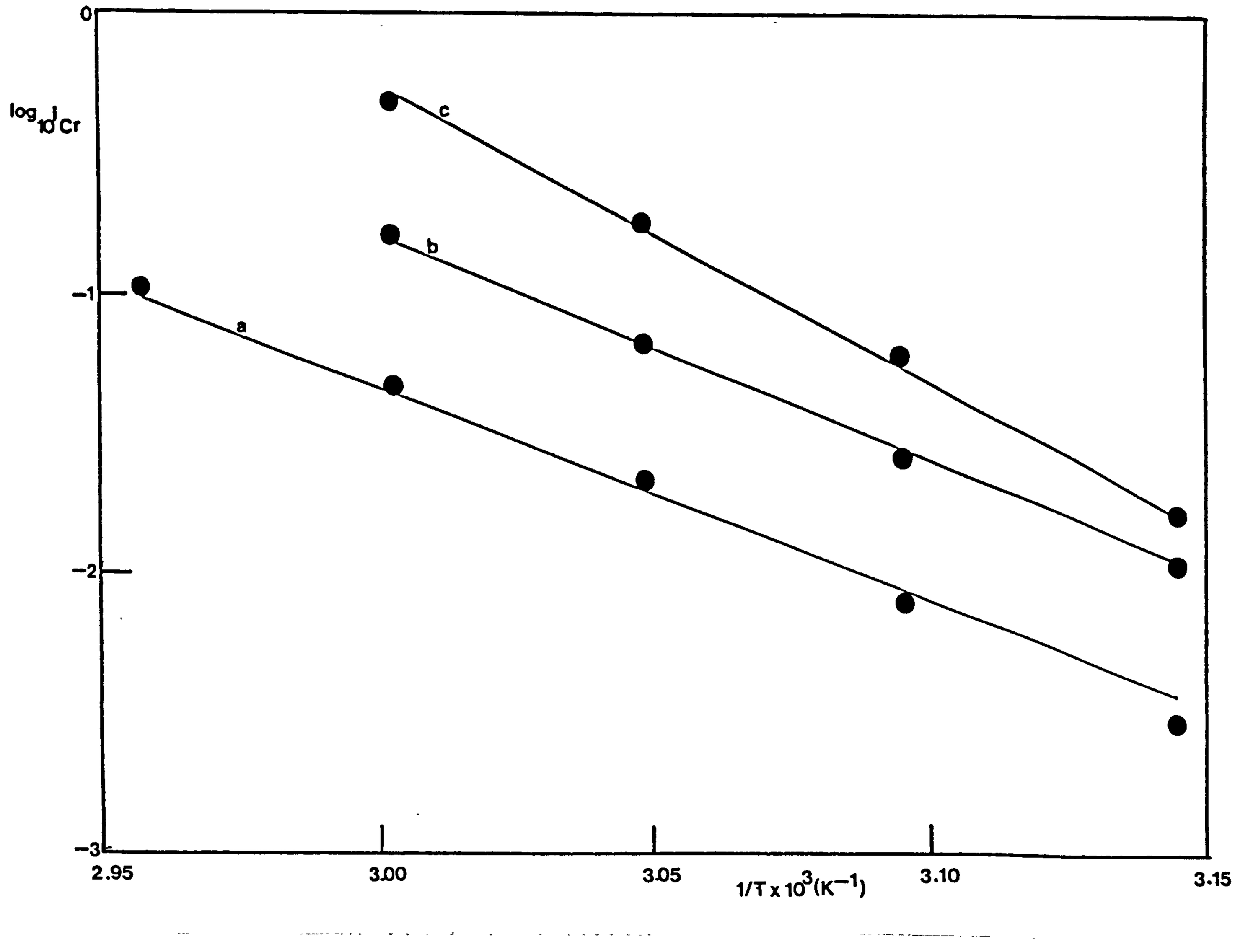
0
log10 Cr
−1
−2
−3
a
b
c
2.95
3.00
3.05
3.10
3.15
1/T x 10^3(K^−1)

FIGURE 34.

Overall potentiostatic cathode polarization curves at 55°C.

The effect of $KClO_4$ presence.

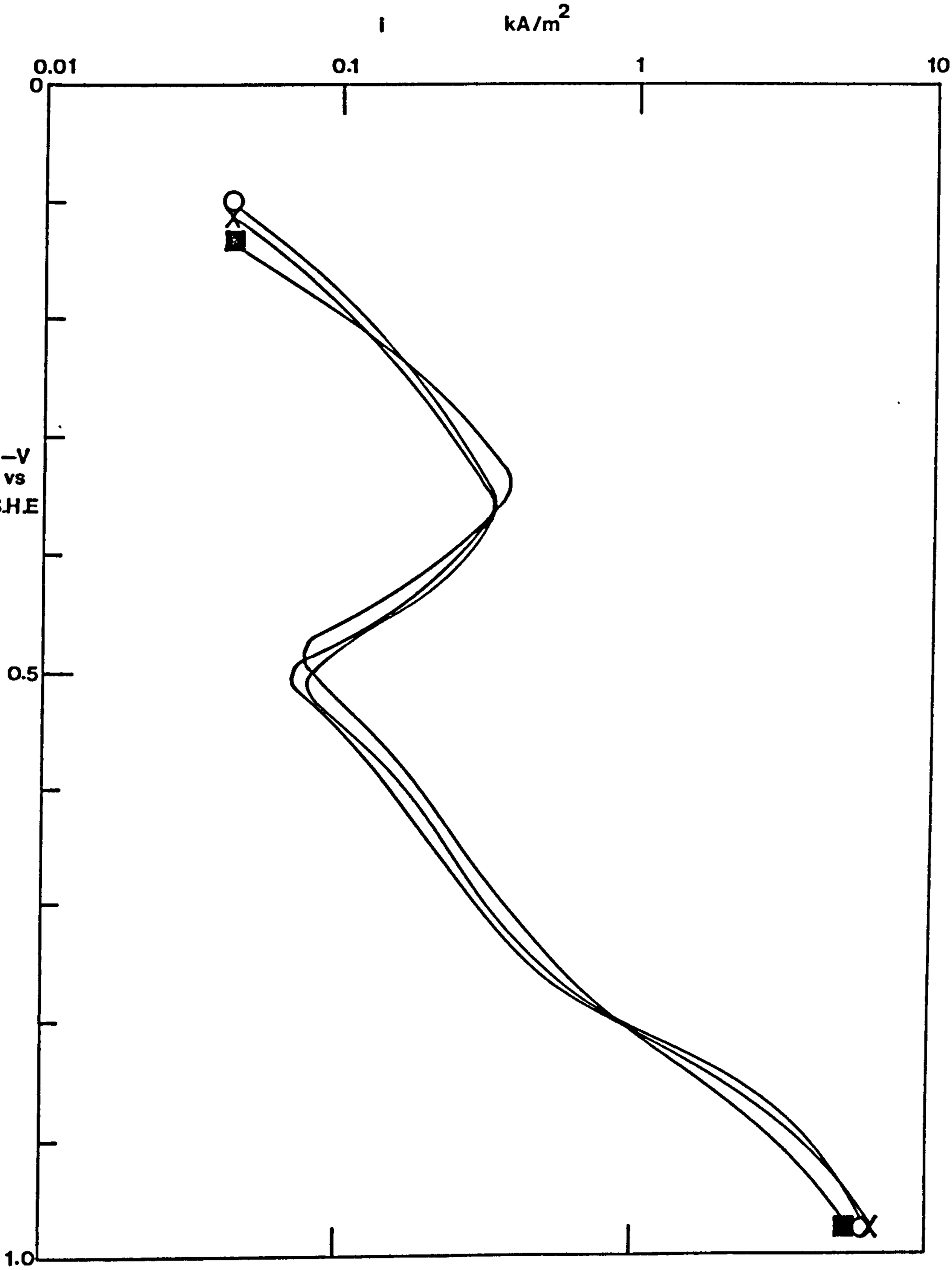
i kA/m2
0.01
0.1
1
10
0
-V
vs
S.H.E
0.5
1.0

FIGURE 35.

Overall potentiostatic cathode polarization curves at 55°C.

The effect of $KBrO_3$ presence.

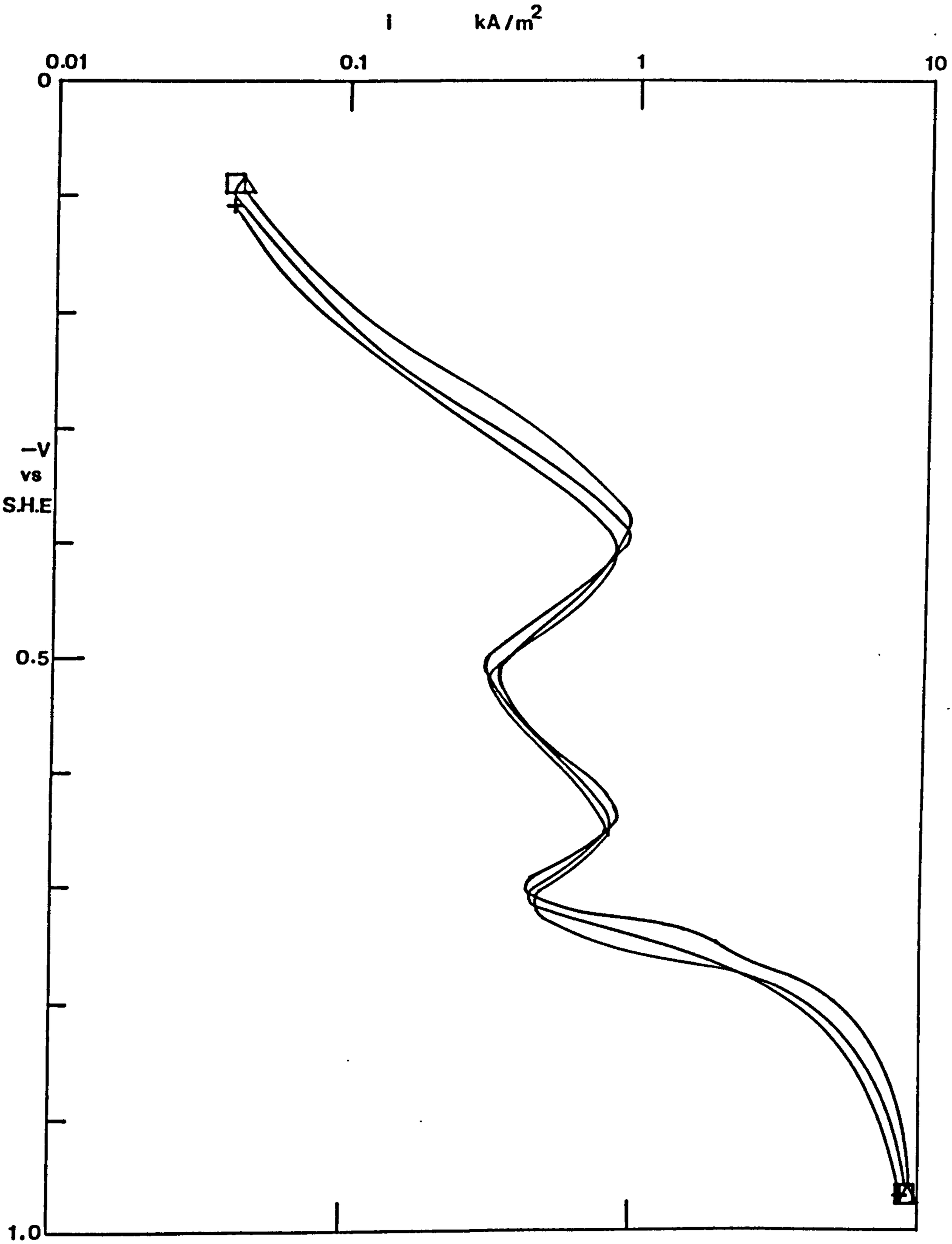
i kA/m²
0.01
0.1
1
10
0
−V
vs
S.H.E
0.5
1.0

FIGURE 36.

Overall potentiostatic cathode polarization curves at 55°C.

The effect of $K_2B_2O_4$ presence.

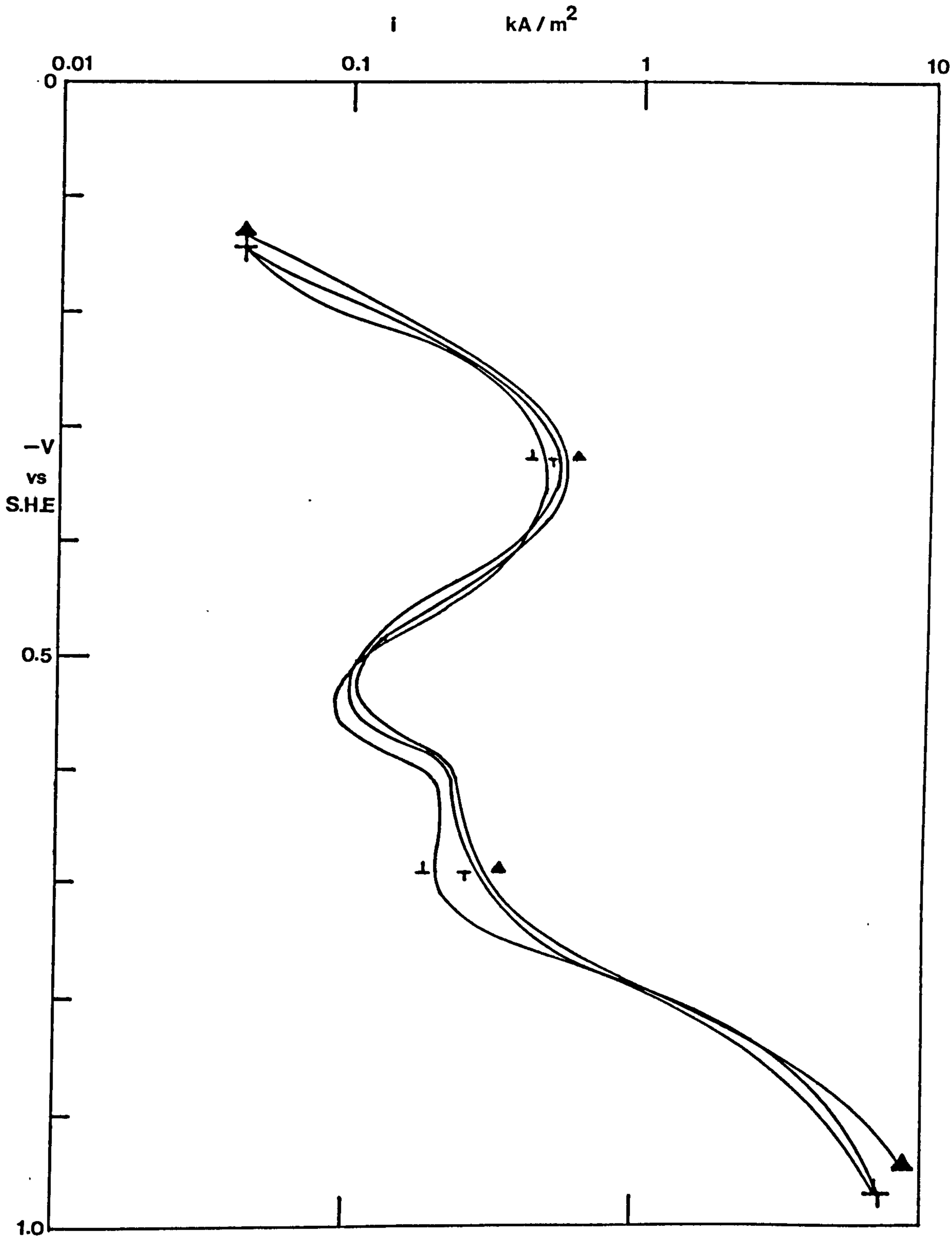
i
kA / m2
0.01
0.1
1
10
0
−V
vs
S.H.E
0.5
1.0

FIGURE 37.

The apparent Tafel region of the overall cathode polarization curve (potentiostatic). The effect of $KBrO_3$ presence.

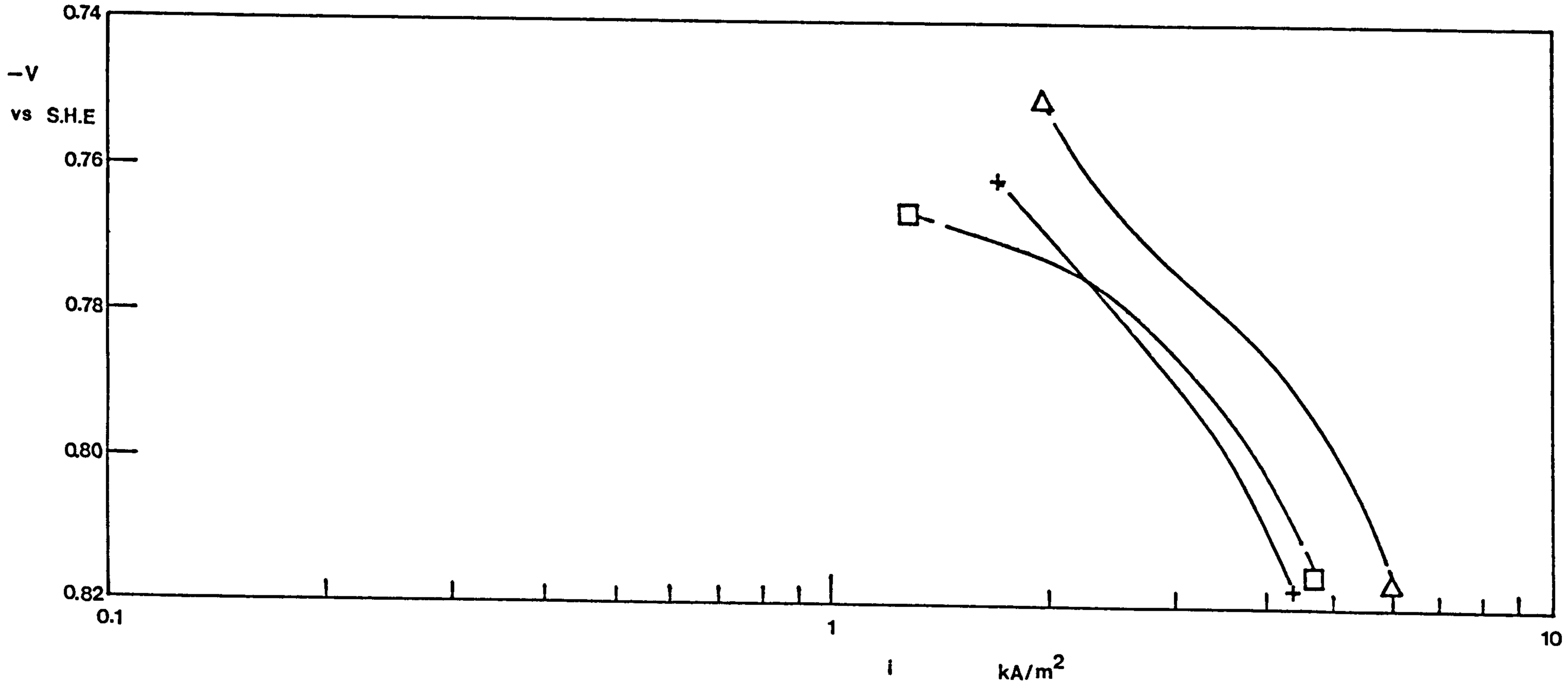
0.74
−V
vs S.H.E
0.76
0.78
0.80
0.82
0.1
1
10
i
kA/m2

FIGURE 38.

The apparent Tafel region of the overall cathode polarization curve (potentiostatic). The effect of $K_2B_2O_4$ presence.

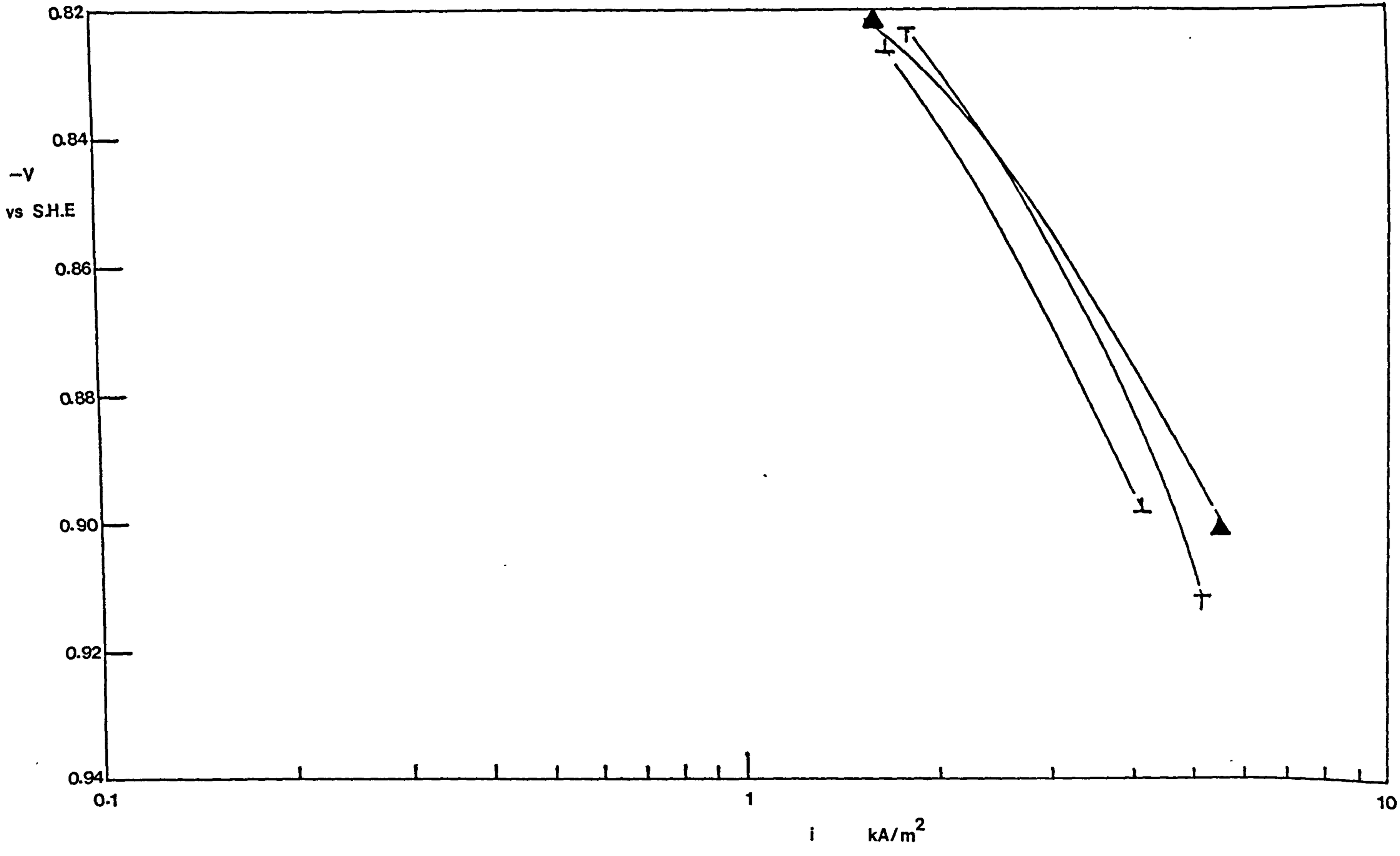
0.82
0.84
0.86
0.88
0.90
0.92
0.94
−V
vs S.H.E
T
I
I
T
0.1
1
10
i kA/m²

FIGURE 39.

The variation of plating current efficiency with cathode density in the apparent Tafel range.

The effect of $KBrO_3$ presence.

FIGURE 40.

The variation of plating current efficiency with cathode current density at higher current densities.

The effect of $KBrO_3$ presence.

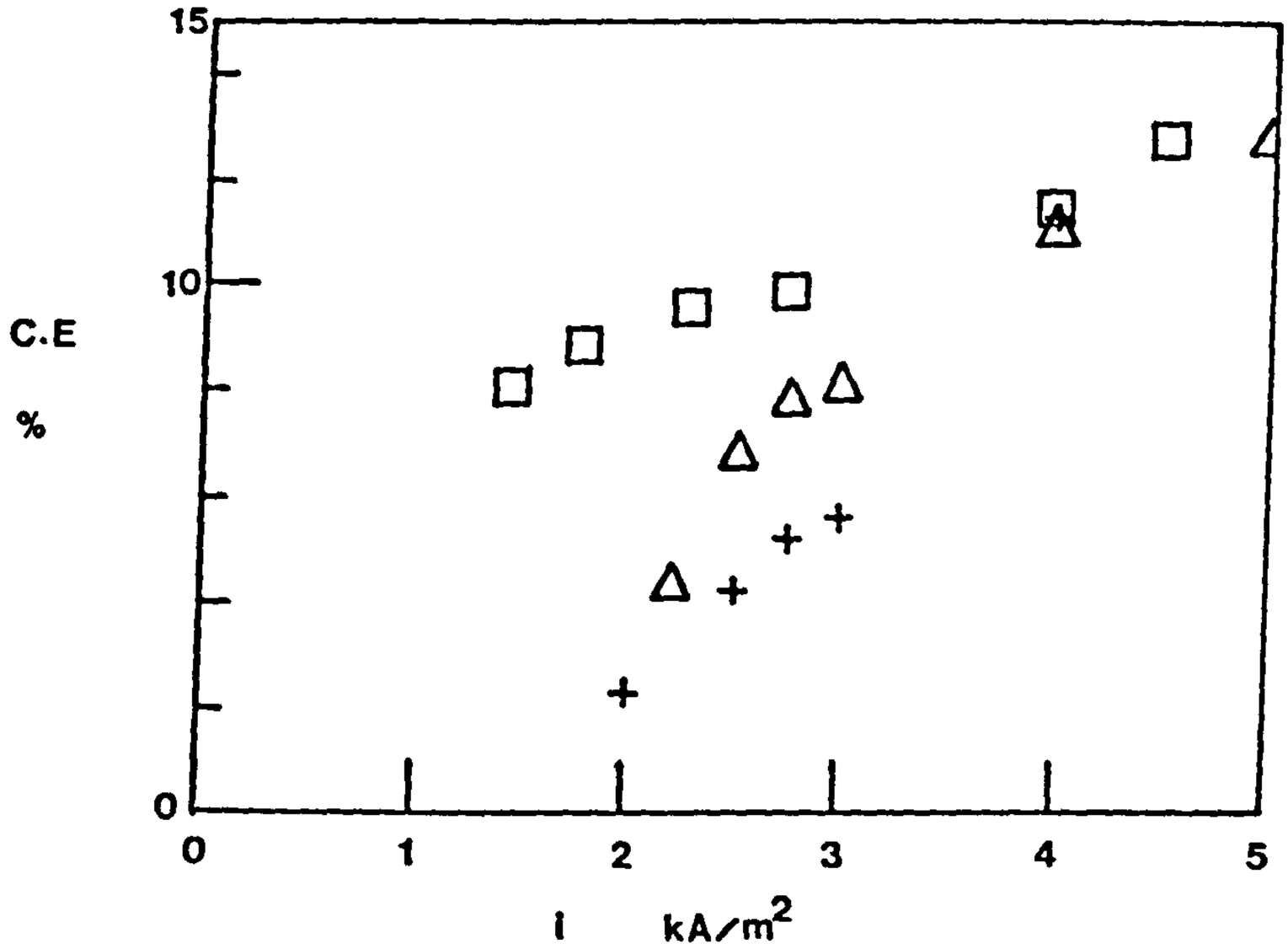
15
10
C.E
%
0
0
1
2
3
4
5
I kA/m²

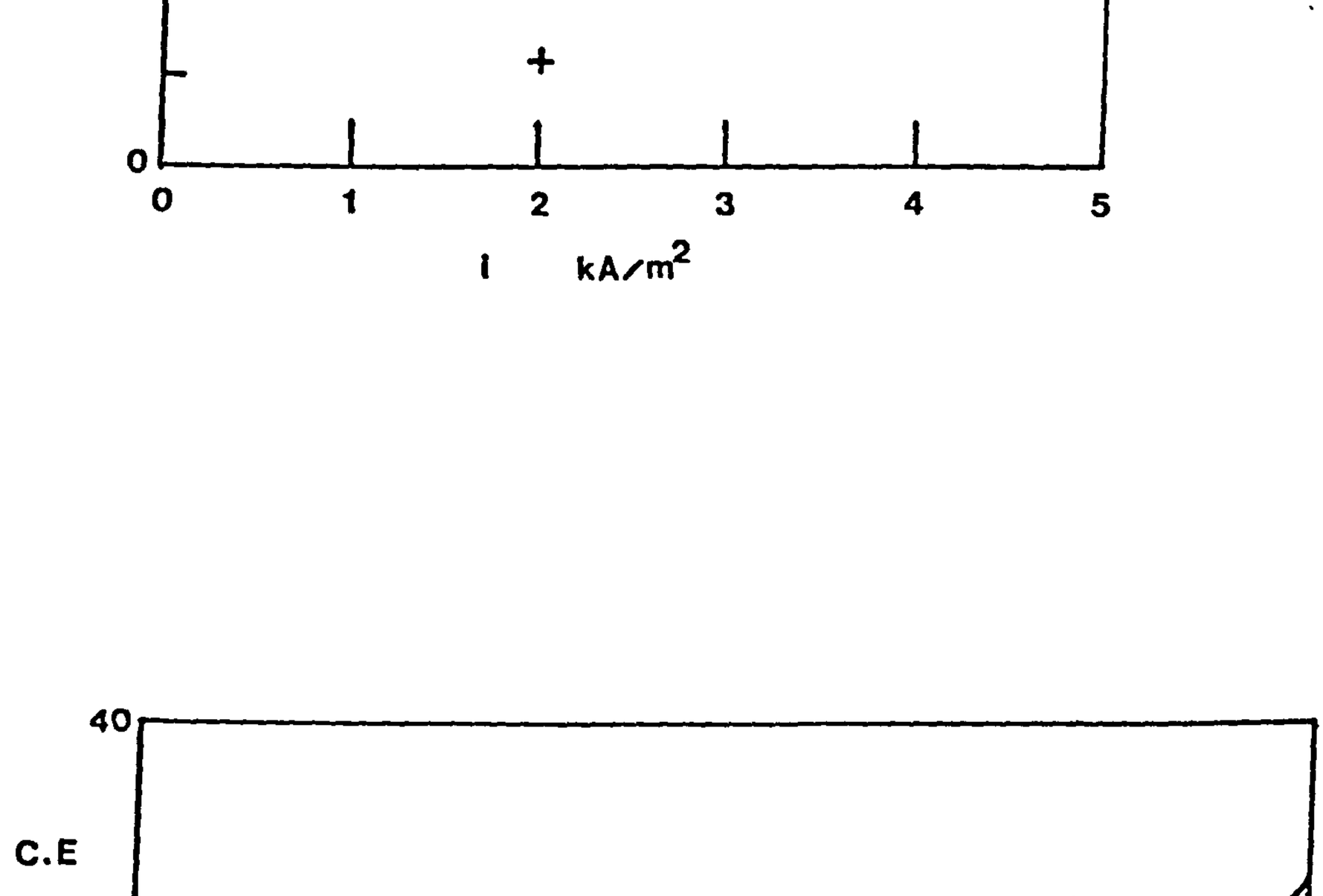
40
C.E
%
20
0
0
25
50
I kA/m²

FIGURE 41.

The variation of hydrogen evolution current efficiency with cathode current density in the apparent Tafel range.
The effect of $KBrO_3$ presence.

FIGURE 42.

The variation of hydrogen evolution current efficiency with cathode current density at higher current densities.
The effect of $KBrO_3$ presence.

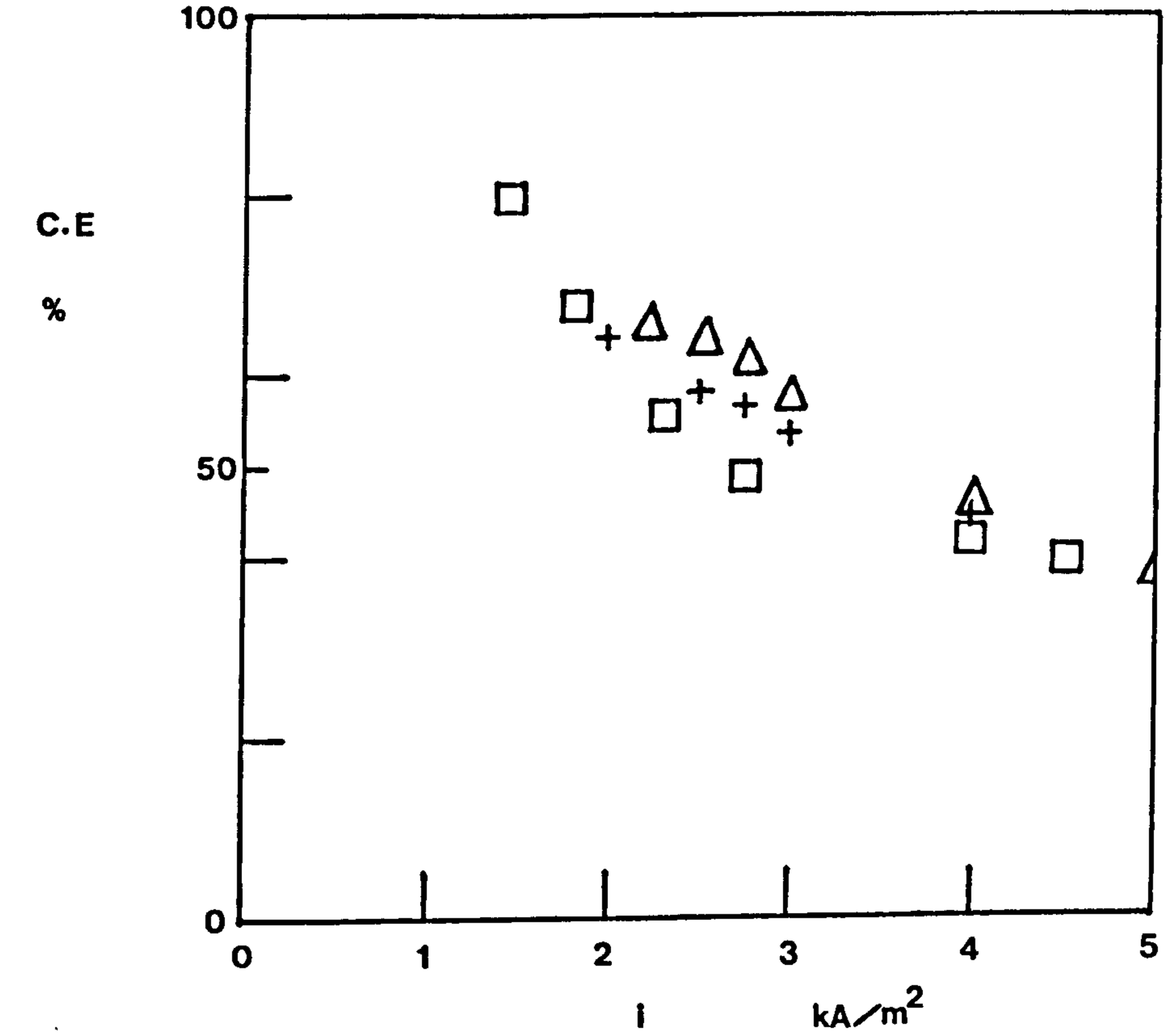
100
C.E
%
50
0
0
1
2
3
4
5
I
kA/m2

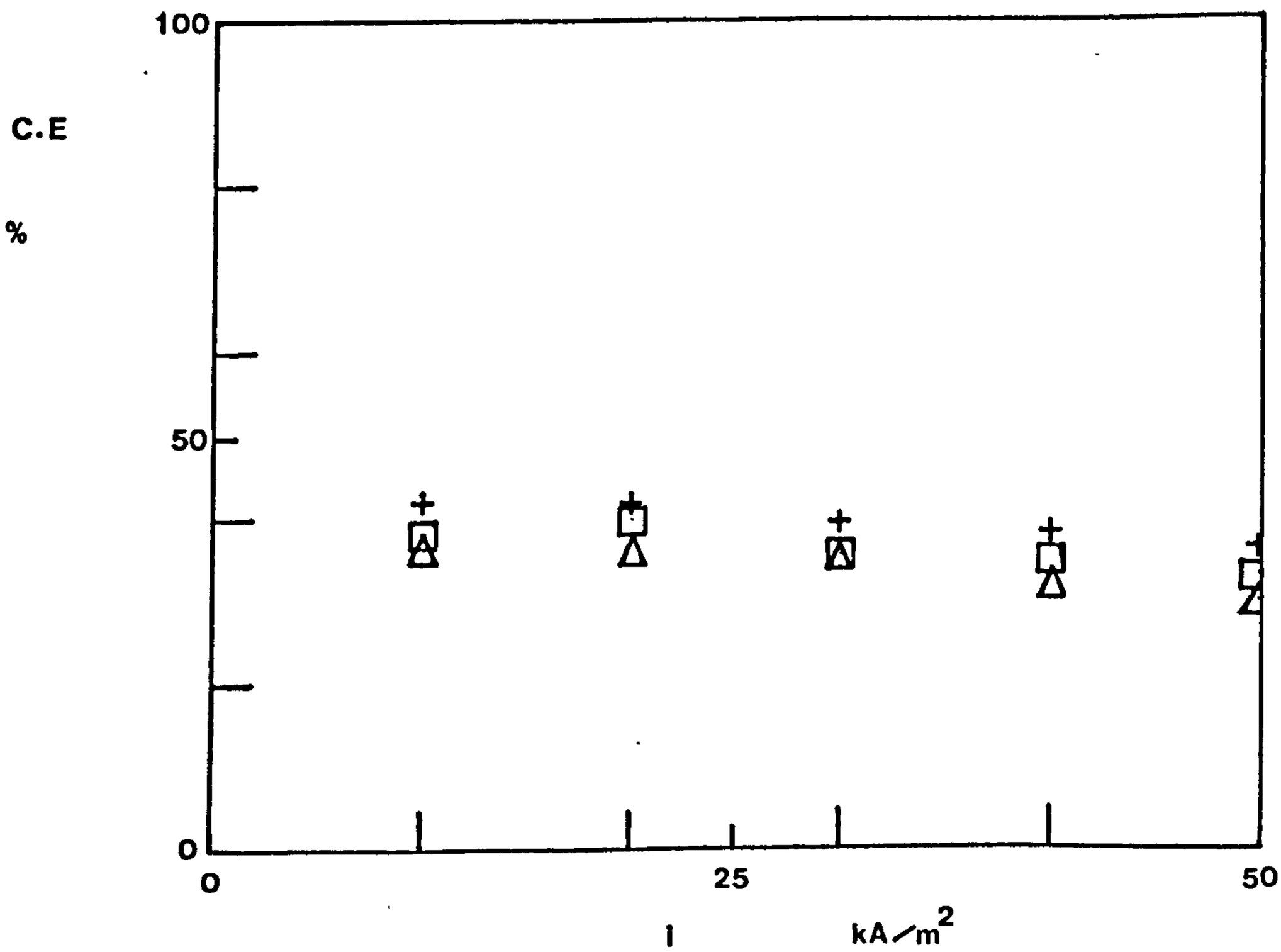
100
C.E
%
50
0
0
25
50
I
kA/m2

FIGURE 43.

The variation of partial (CrVI to CrIII) reduction current efficiency with cathode current density in the apparent Tafel range. The effect of $KBrO_3$ presence.

FIGURE 44.

The variation of partial (CrVI to CrIII) reduction current efficiency with cathode current density at higher current densities. The effect of $KBrO_3$ presence.

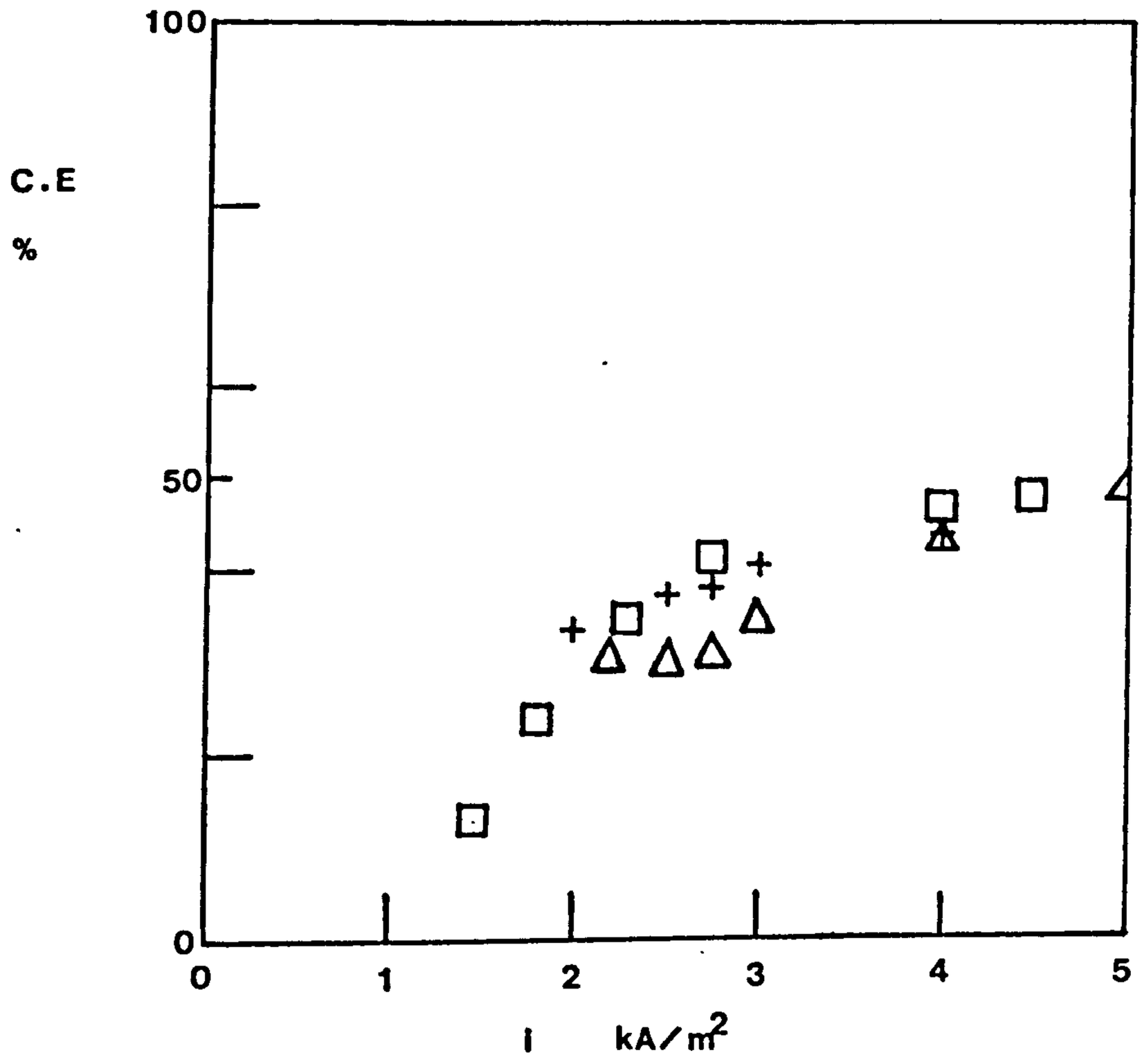
100
C.E
%
50
0
0
1
2
3
4
5
I kA/m2

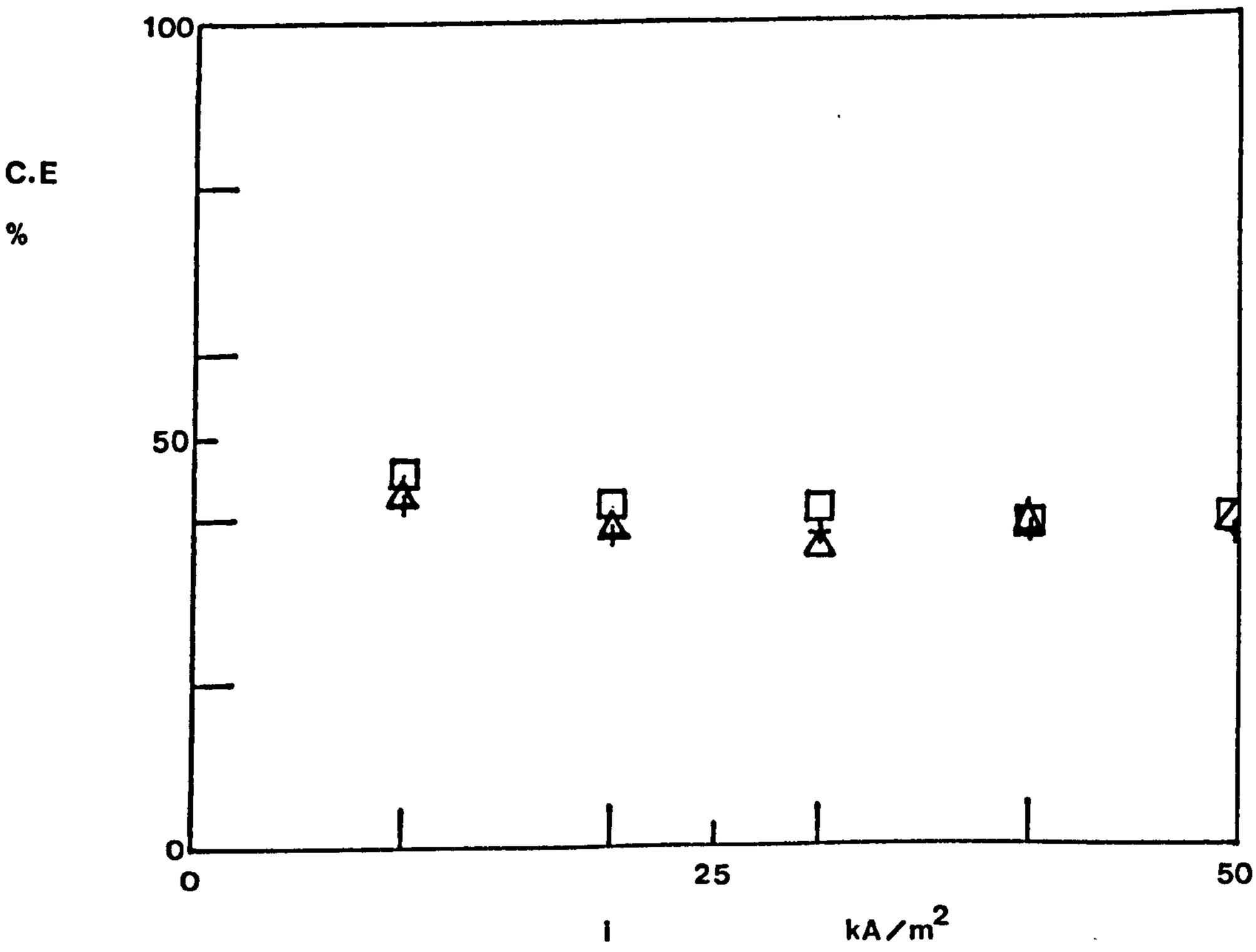
100
C.E
%
50
0
0
25
50
I kA/m2

FIGURE 45.

The variation of plating current efficiency with cathode current density in the apparent Tafel range.

The effect of $K_2B_2O_4$ presence.

FIGURE 46.

The variation of plating current efficiency with cathode current density at higher current densities.

The effect of $K_2B_2O_4$ presence.

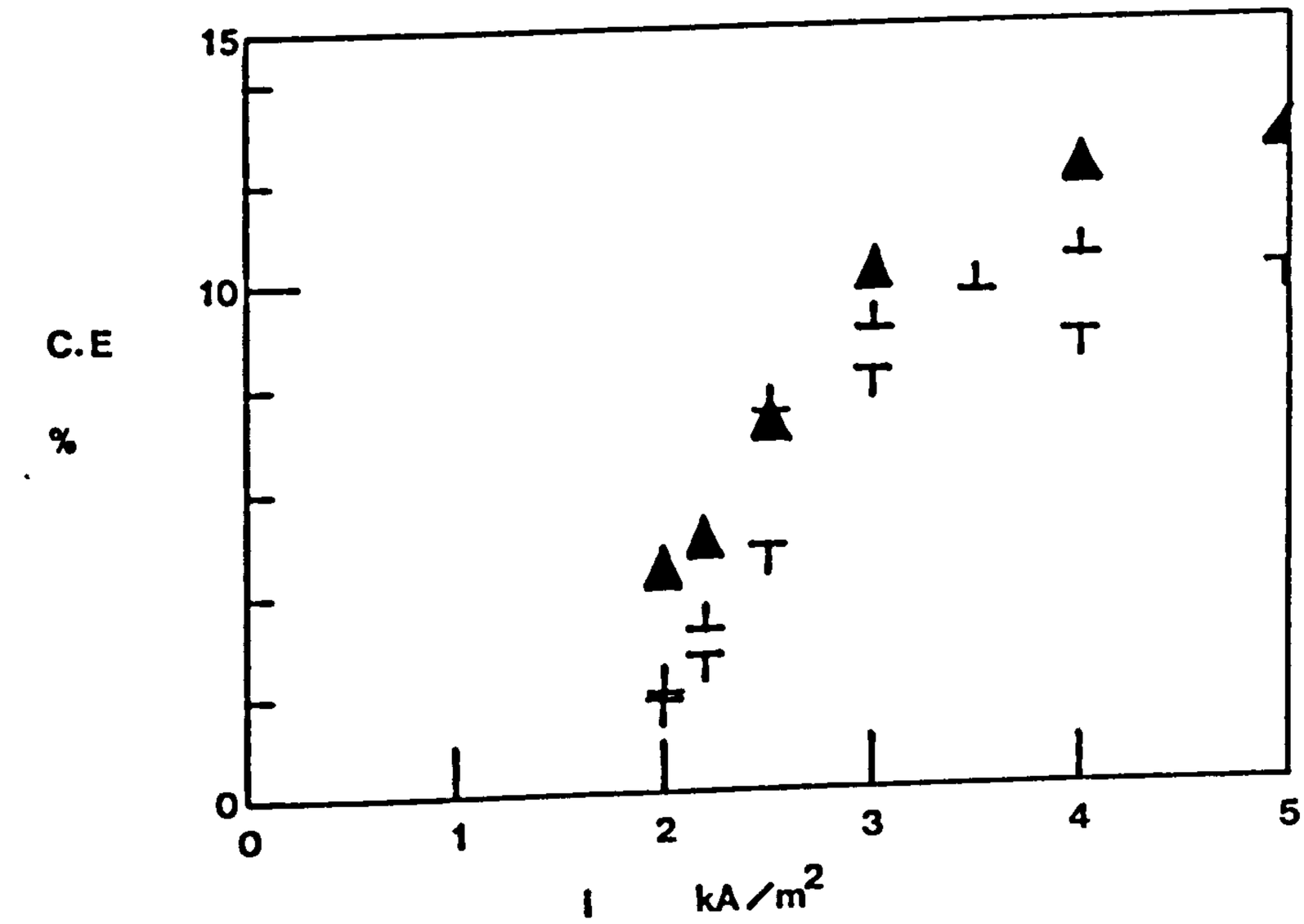
C.E
%
15
10
0
0
1
2
3
4
5
I
kA/m2

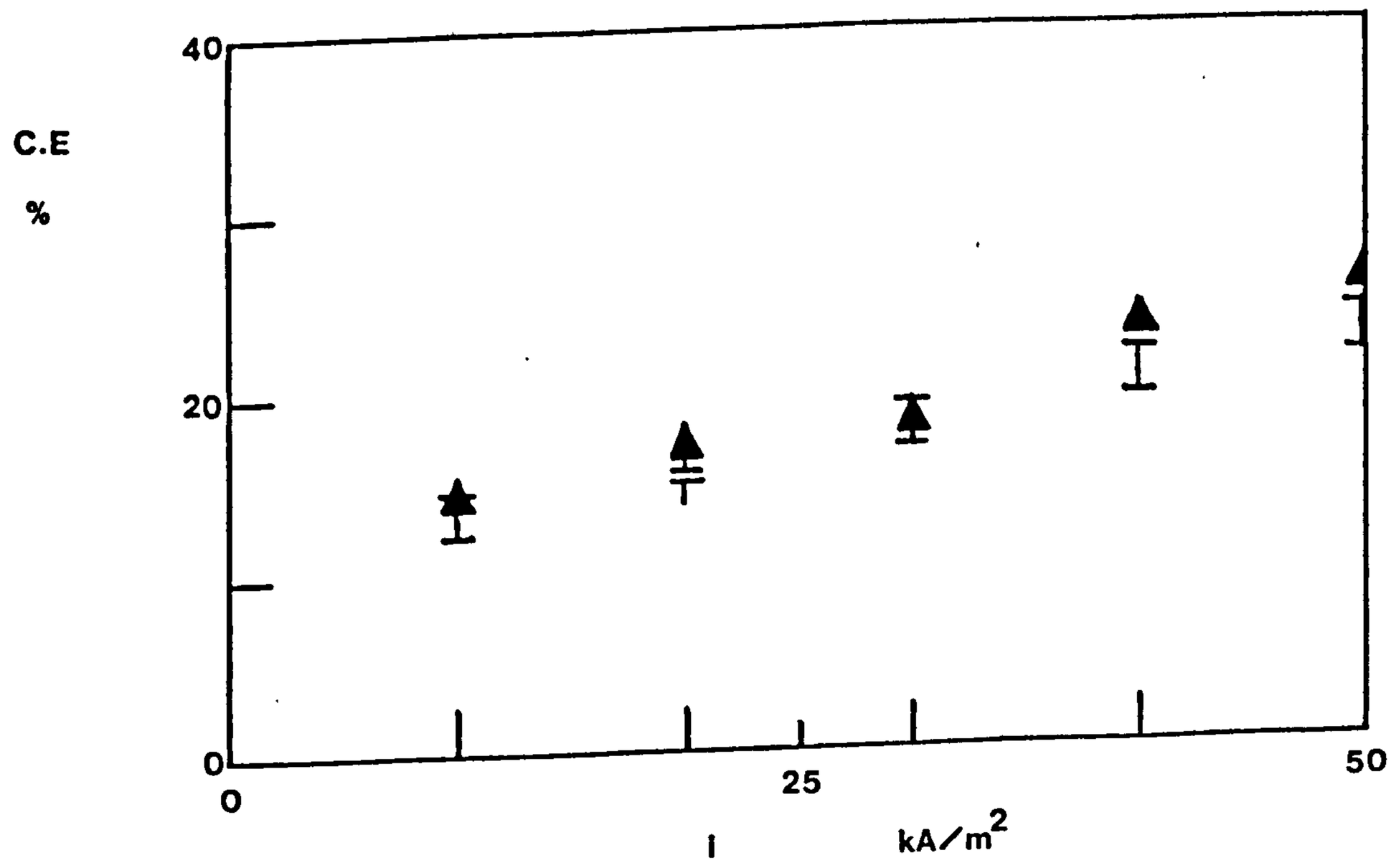
C.E
%
40
20
0
0
25
50
I
kA/m2

FIGURE 47.

The variation of hydrogen evolution current efficiency with cathode current density in the apparent Tafel range.

The effect of $K_2B_2O_4$ presence.

FIGURE 48.

The variation of hydrogen evolution current efficiency with cathode current density at higher current densities.

The effect of $K_2B_2O_4$ presence.

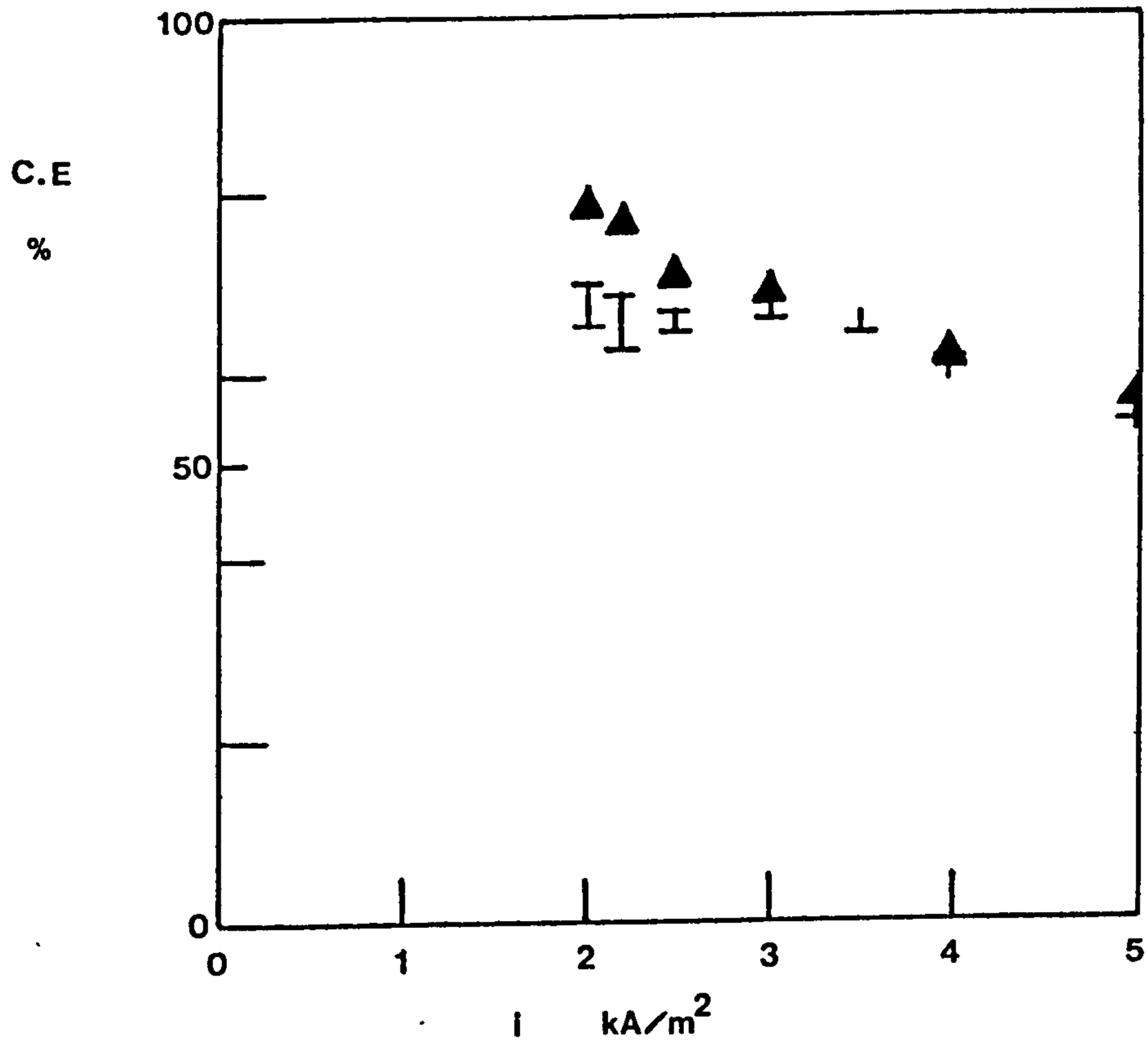
100
C.E
%
50
0
0
1
2
3
4
5
i kA/m2

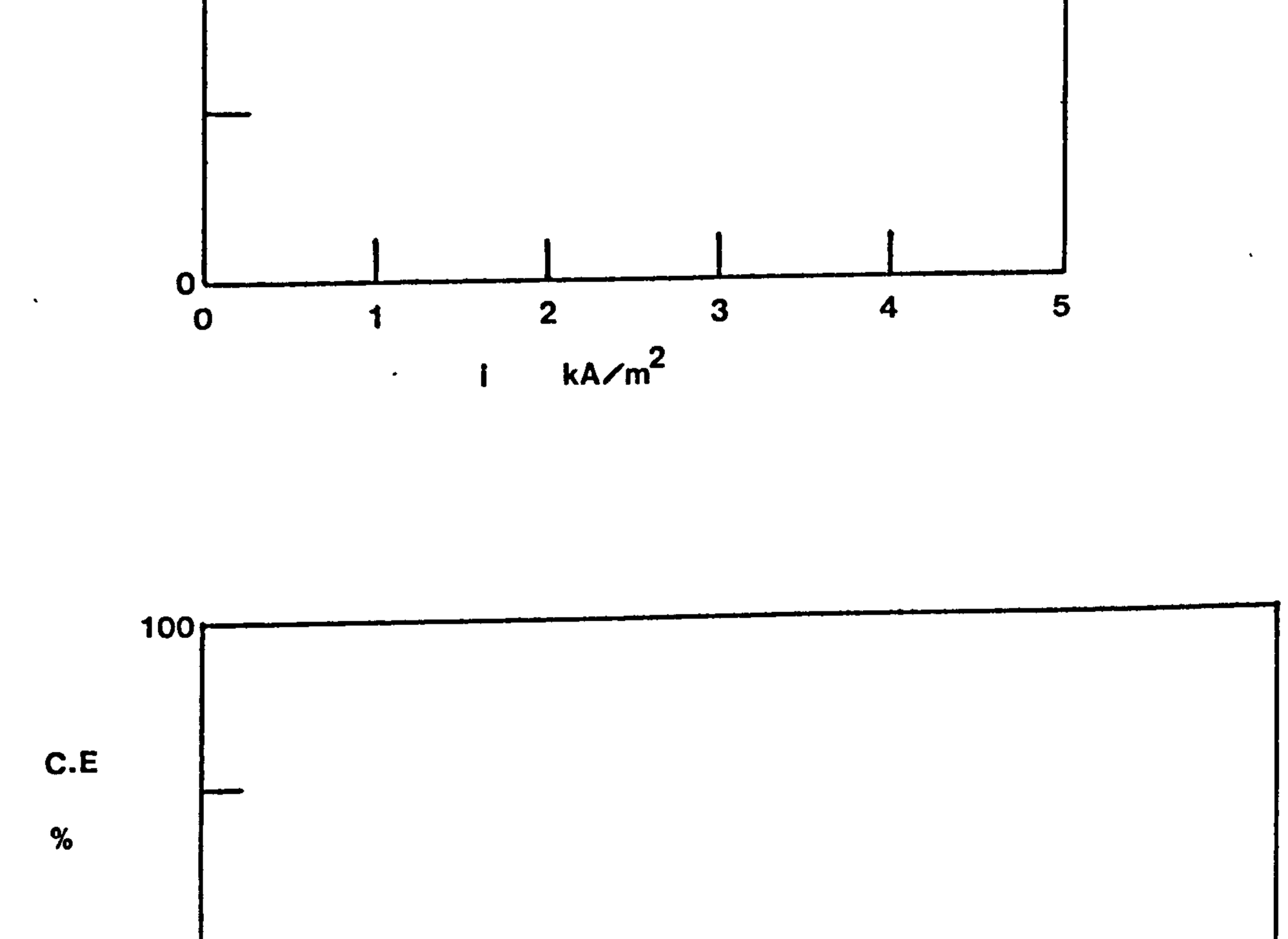
100
C.E
%
50
0
0
25
50
i kA/m2

FIGURE 49.

The variation of partial (CrVI to CrIII) reduction current efficiency with cathode current density in the apparent Tafel range. The effect of $K_2B_2O_4$ presence.

FIGURE 50.

The variation of partial (CrVI to CrIII) reduction current efficiency with cathode current density at higher current densities. The effect of $K_2B_2O_4$ presence.

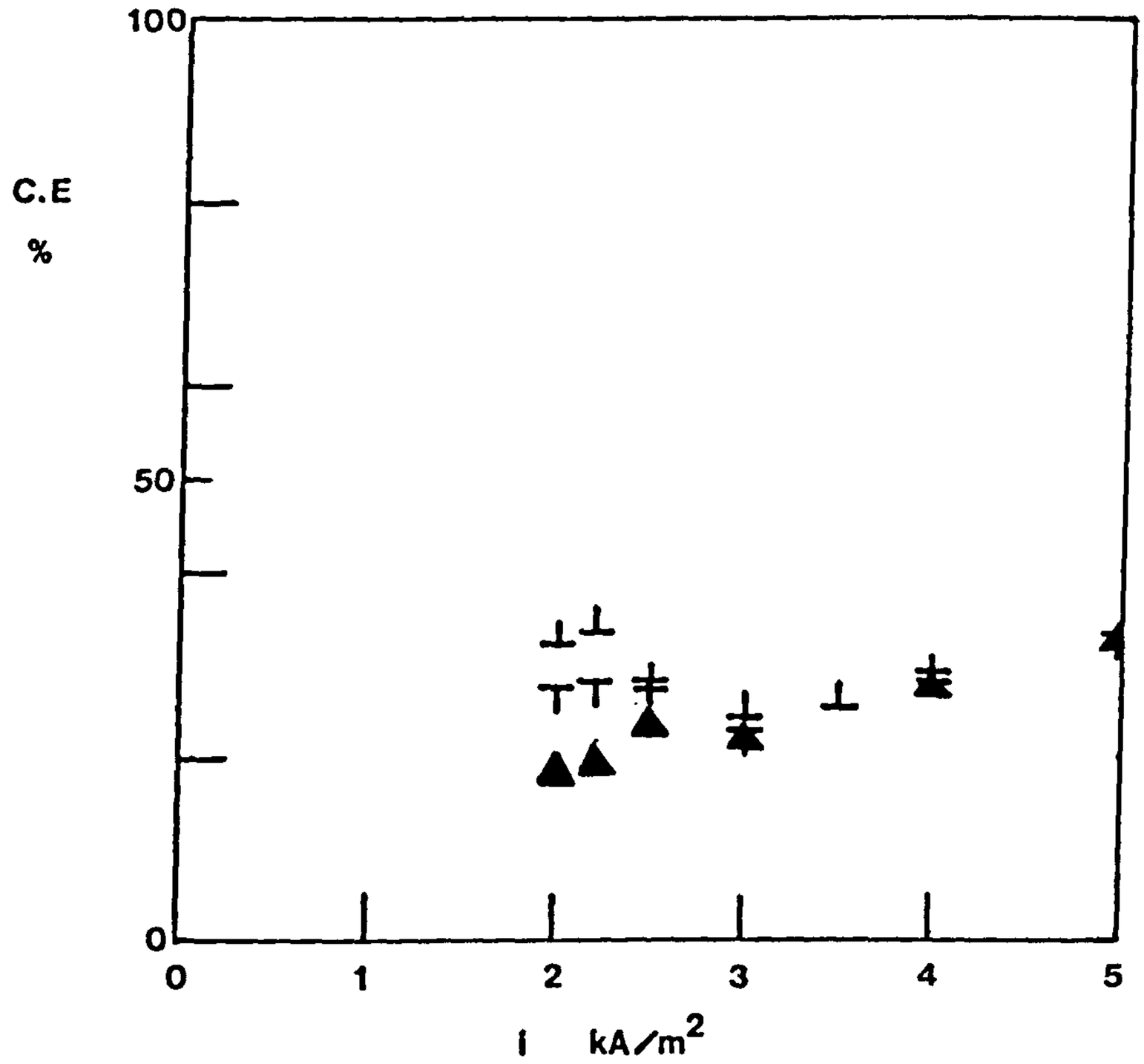
100
C.E
%
50
0
0
1
2
3
4
5
I kA/m2

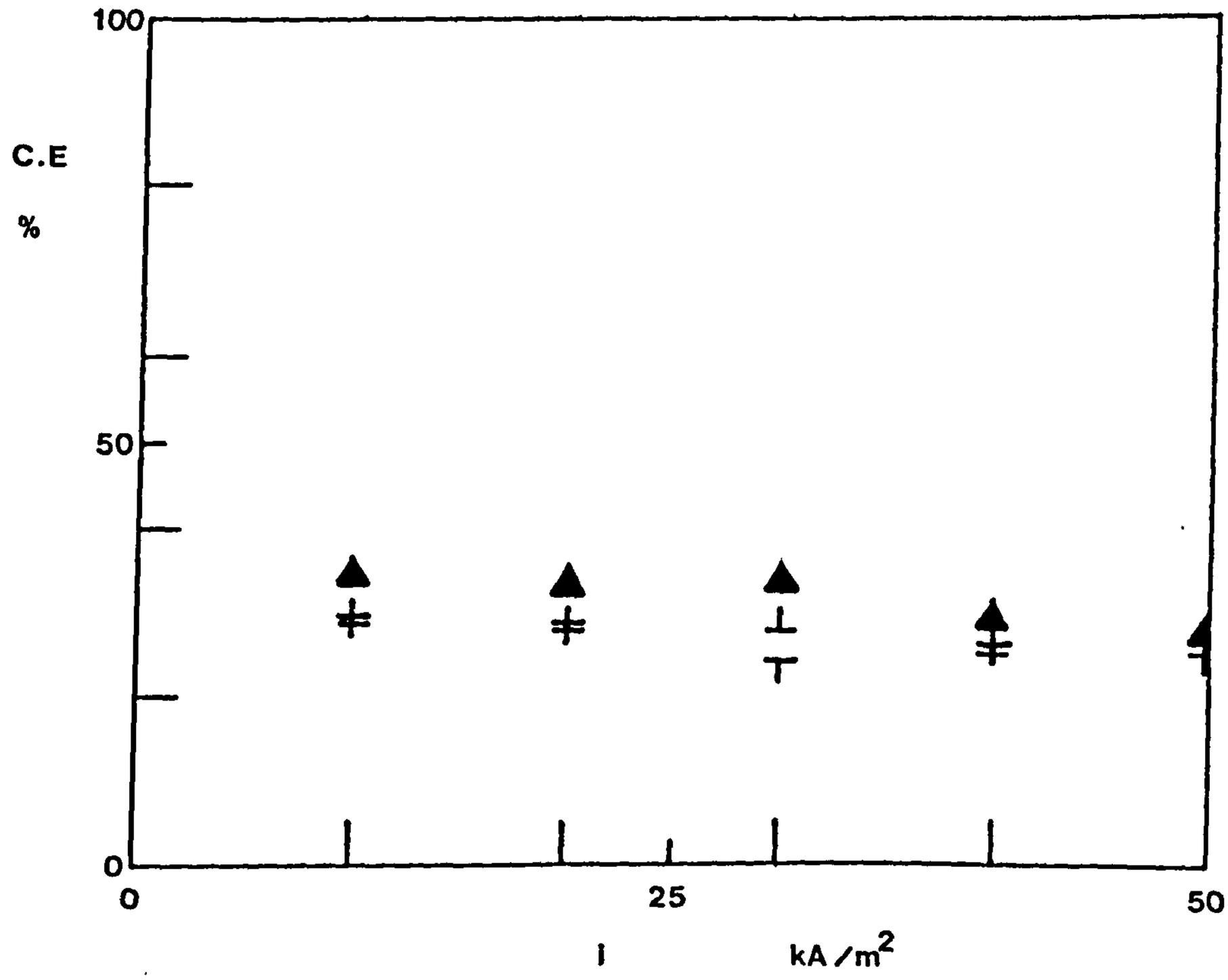
100
C.E
%
50
0
0
25
50
I kA/m2

FIGURE 51.

Partial cathode polarization curve for the plating reaction.

The effect of $KBrO_3$ presence.

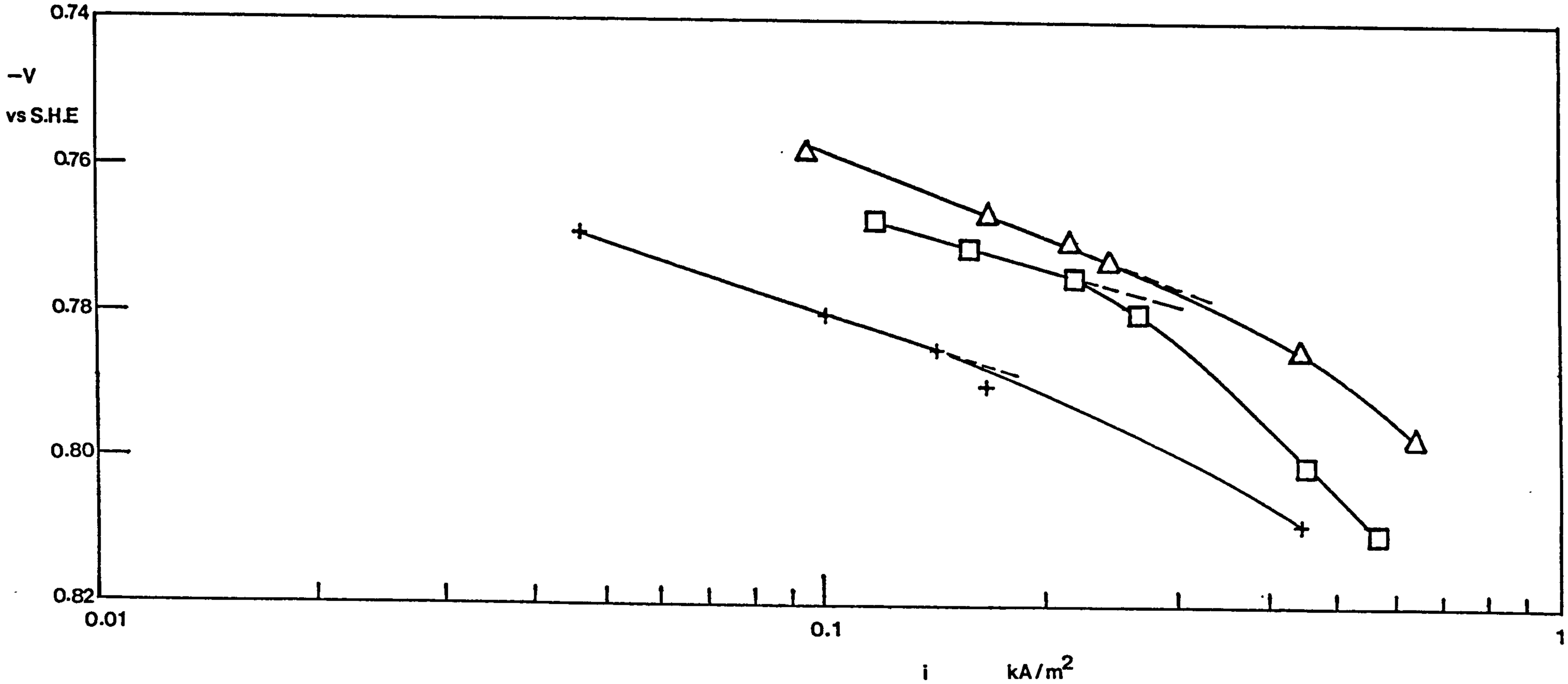
0.74
−V
vs S.H.E
0.76
0.78
0.80
0.82
0.01
0.1
1
i kA/m²

FIGURE 52.

Partial cathode polarization curve for the hydrogen evolution reaction.

The effect of $KBrO_3$ presence.

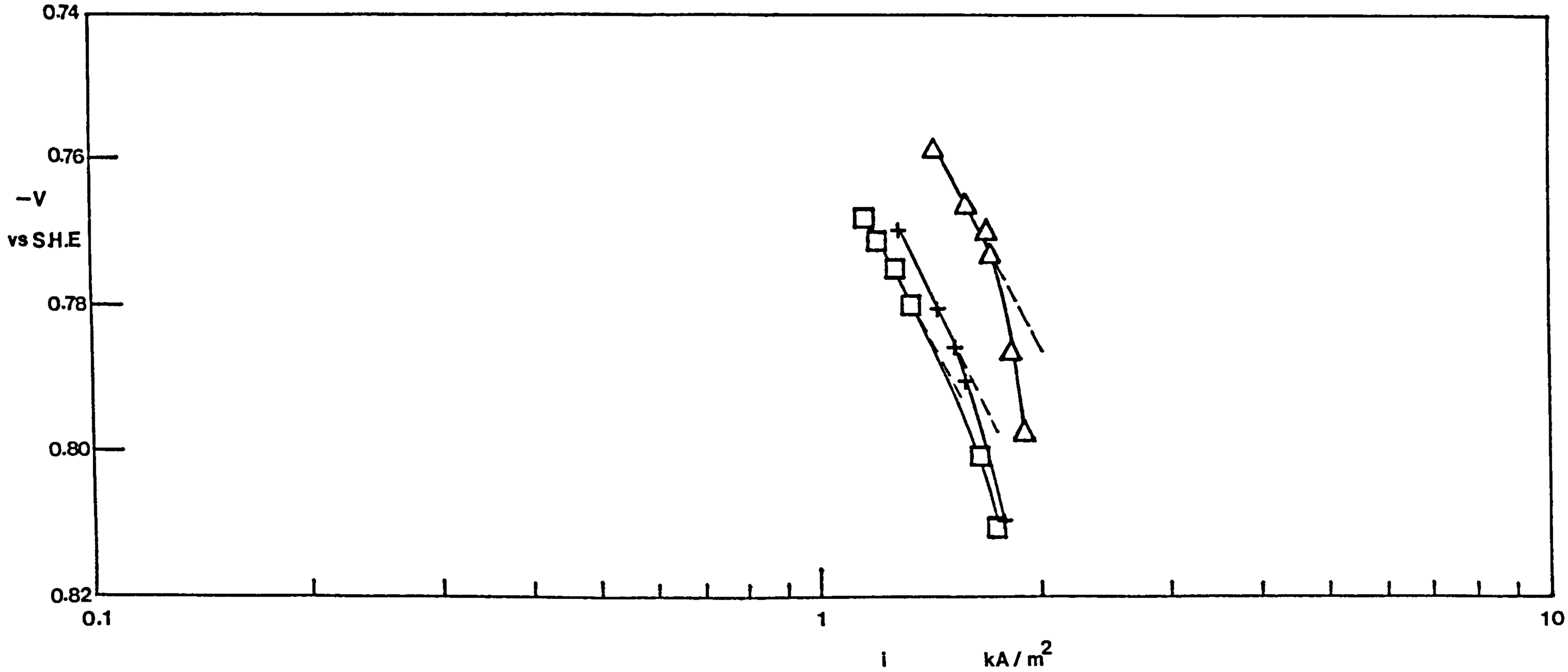
0.74
0.76
−V
vs S.H.E
0.78
0.80
0.82
0.1
1
10
i
kA / m2

FIGURE 53.

Partial cathode polarization curve for the partial (CrVI to CrIII) reduction reaction. The effect of $KBrO_3$ presence.

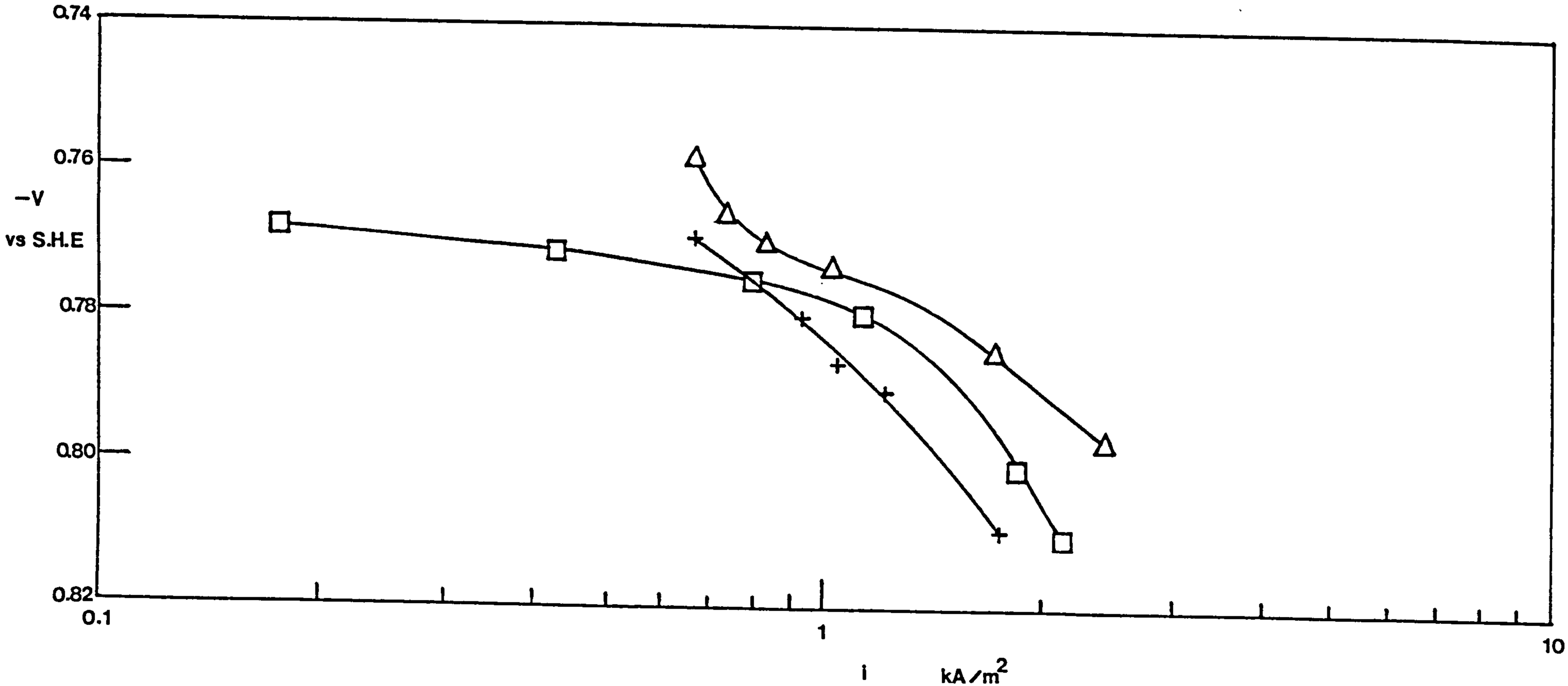
0.74
0.76
-V
vs S.H.E
0.78
0.80
0.82
0.1
1
10
i
kA/m²

FIGURE 54.

Partial cathode polarization curve for the plating reaction.

The effect of $K_2B_2O_4$ presence.

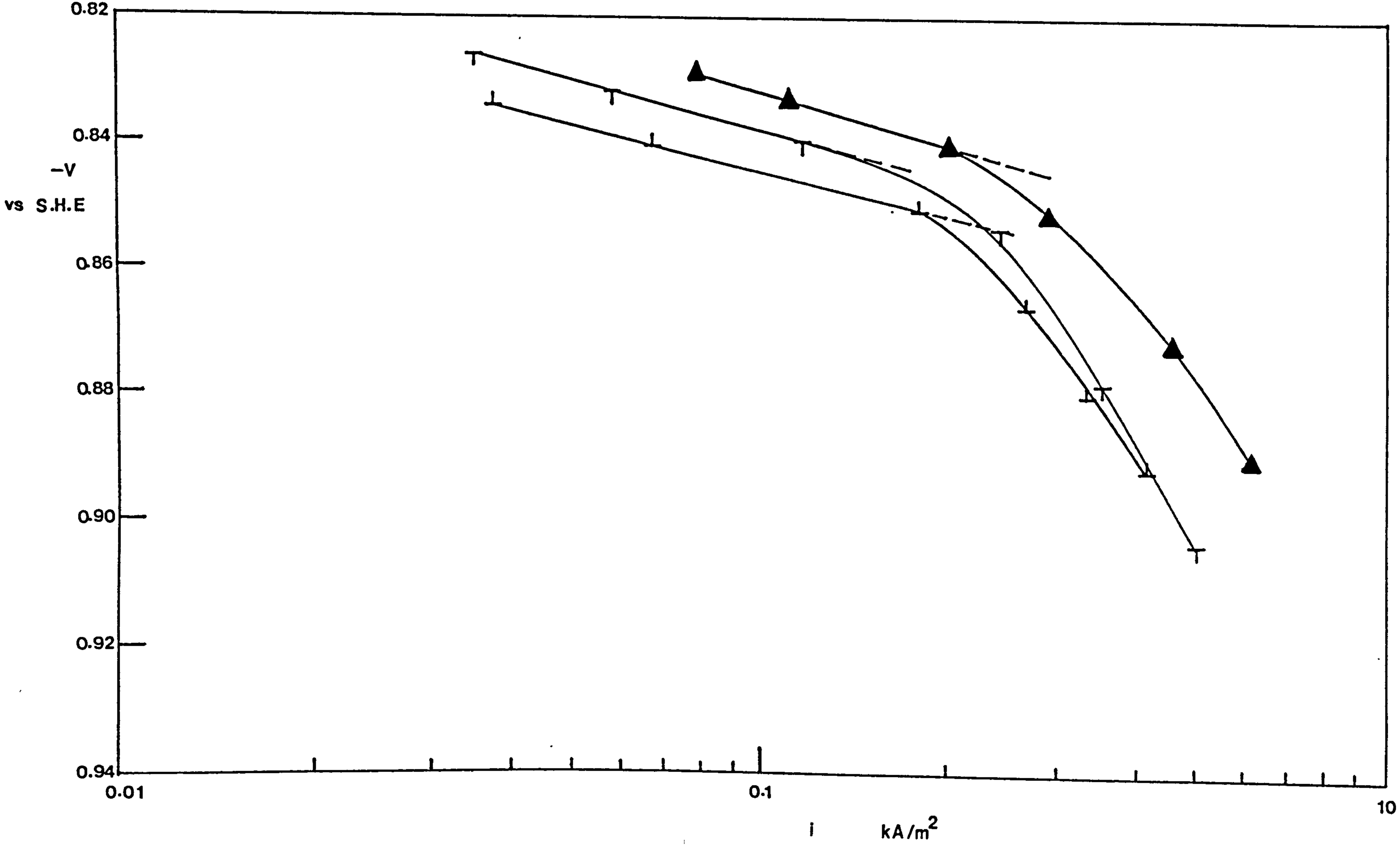
0.82
0.84
-V
vs S.H.E
0.86
0.88
0.90
0.92
0.94
0.01
0.1
10
i kA/m2

FIGURE 55.

Partial cathode polarization curve for the hydrogen evolution reaction.

The effect of $K_2B_2O_4$ presence.

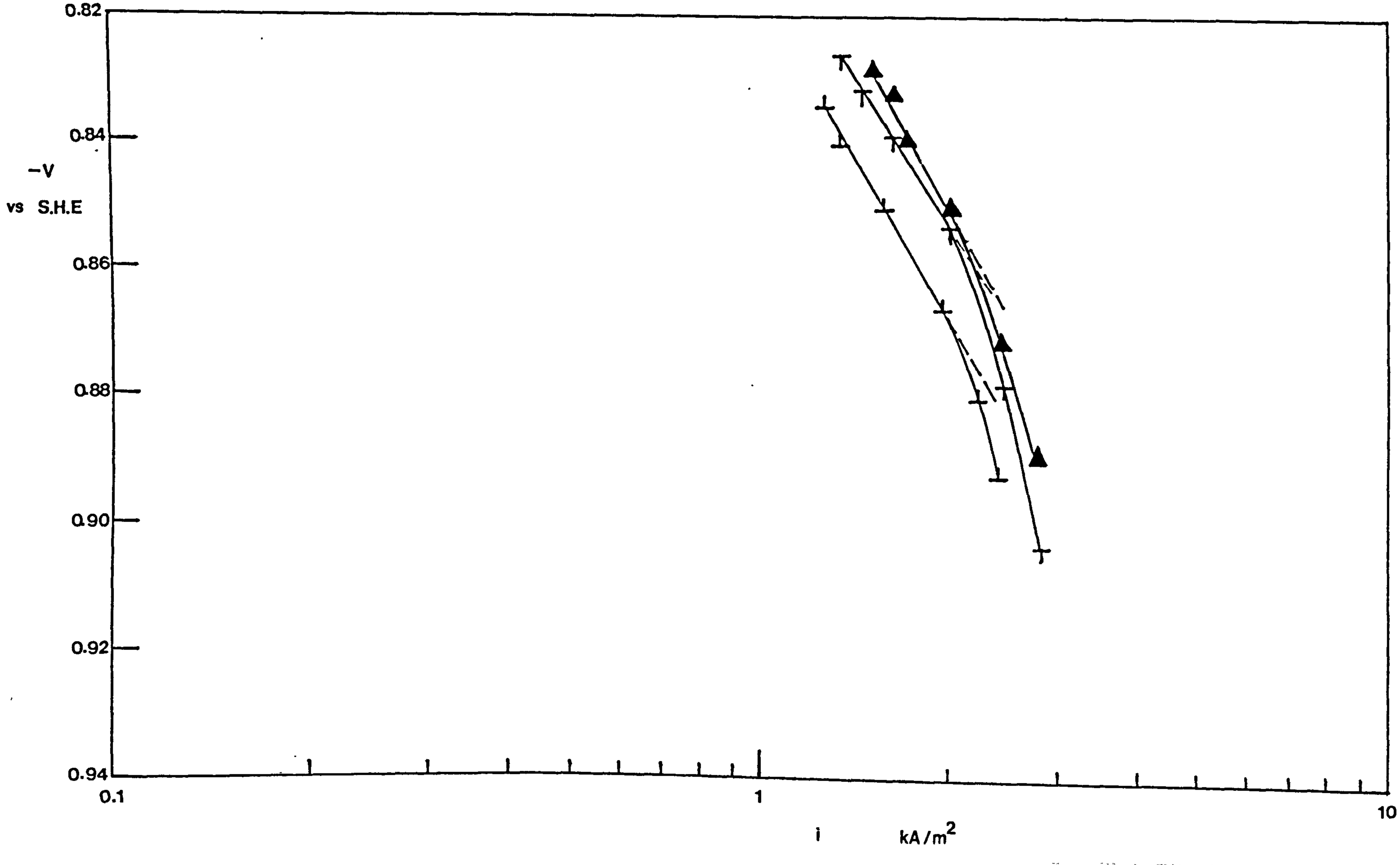
0.82
0.84
0.86
0.88
0.90
0.92
0.94
−V
vs S.H.E
0.1
1
10
i
kA/m²

FIGURE 56.

Partial cathode polarization curve for the partial (CrVI to CrIII) reduction reaction. The effect of $K_2B_2O_4$ presence.

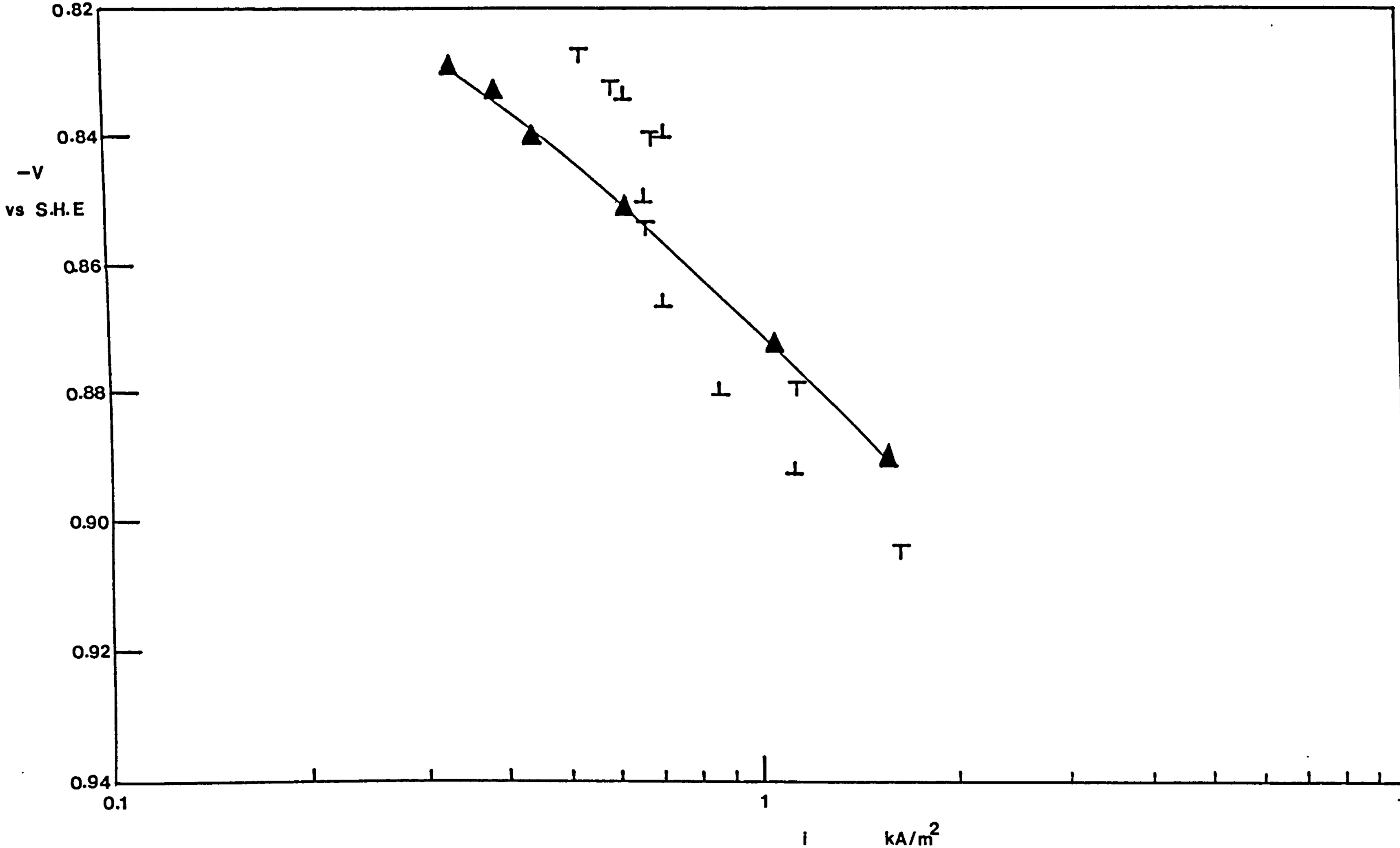
0.82
0.84
0.86
0.88
0.90
0.92
0.94
-V
vs S.H.E
0.1
1
10
i
kA/m2

FIGURE 57.

Arrhenius-type plots for the plating reaction in Standard Solutions containing $KClO_4$ at constant cathode potentials of

S + 5A

a) - 0.86V

b) - 0.87V

S + 10A

a) - 0.88V

b) - 0.885V

S + 15A

a) - 0.88V

b) - 0.89V

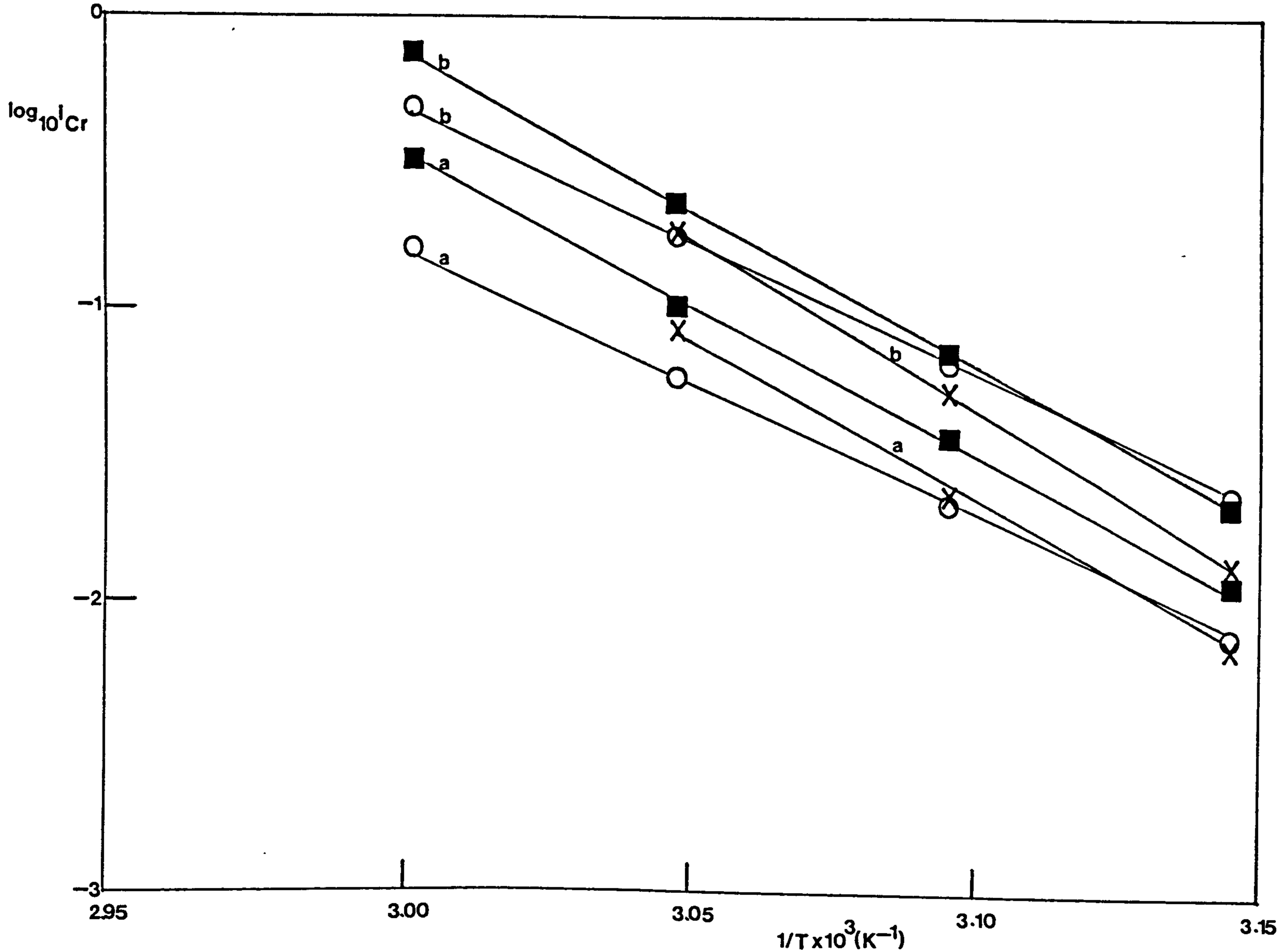
0
−1
−2
−3
$\log_{10} I_{Cr}$
b
b
a
a
b
a
2.95
3.00
3.05
3.10
3.15
$1/T \times 10^3 (K^{-1})$

FIGURE 58.

Arrhenius-type plots for the plating reaction in Standard Solutions containing $KBrO_3$ at constant cathode potentials of

S + 5B

a) - 0.78V

b) - 0.79V

S + 10B

a) 0.77V

b) 0.78V

S + 15B

a) 0.76V

b) 0.77V

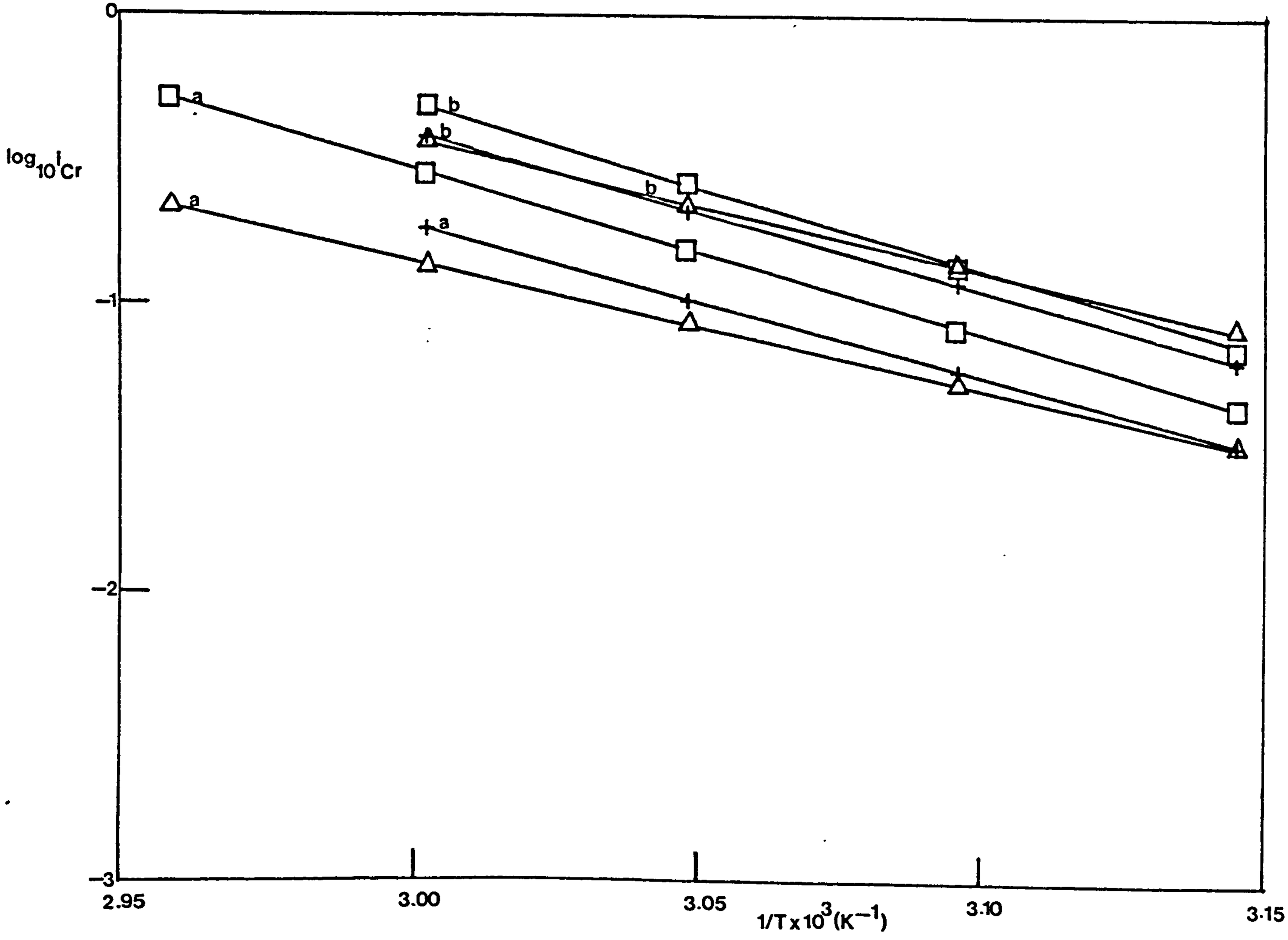
0
−1
−2
−3
$\log_{10} i_{Cr}$
a
b
2.95
3.00
3.05
3.10
3.15
$1/T \times 10^3 (K^{-1})$

FIGURE 59.

Arrhenius-type plots for the plating reaction in Standard Solutions containing $K_2B_2O_4$ at constant cathode potentials of

S + 5C

a) - 0.84V

b) - 0.85V

S + 10C

a) - 0.83V

b) - 0.84V

S + 15C

a) - 0.83V

b) - 0.84V

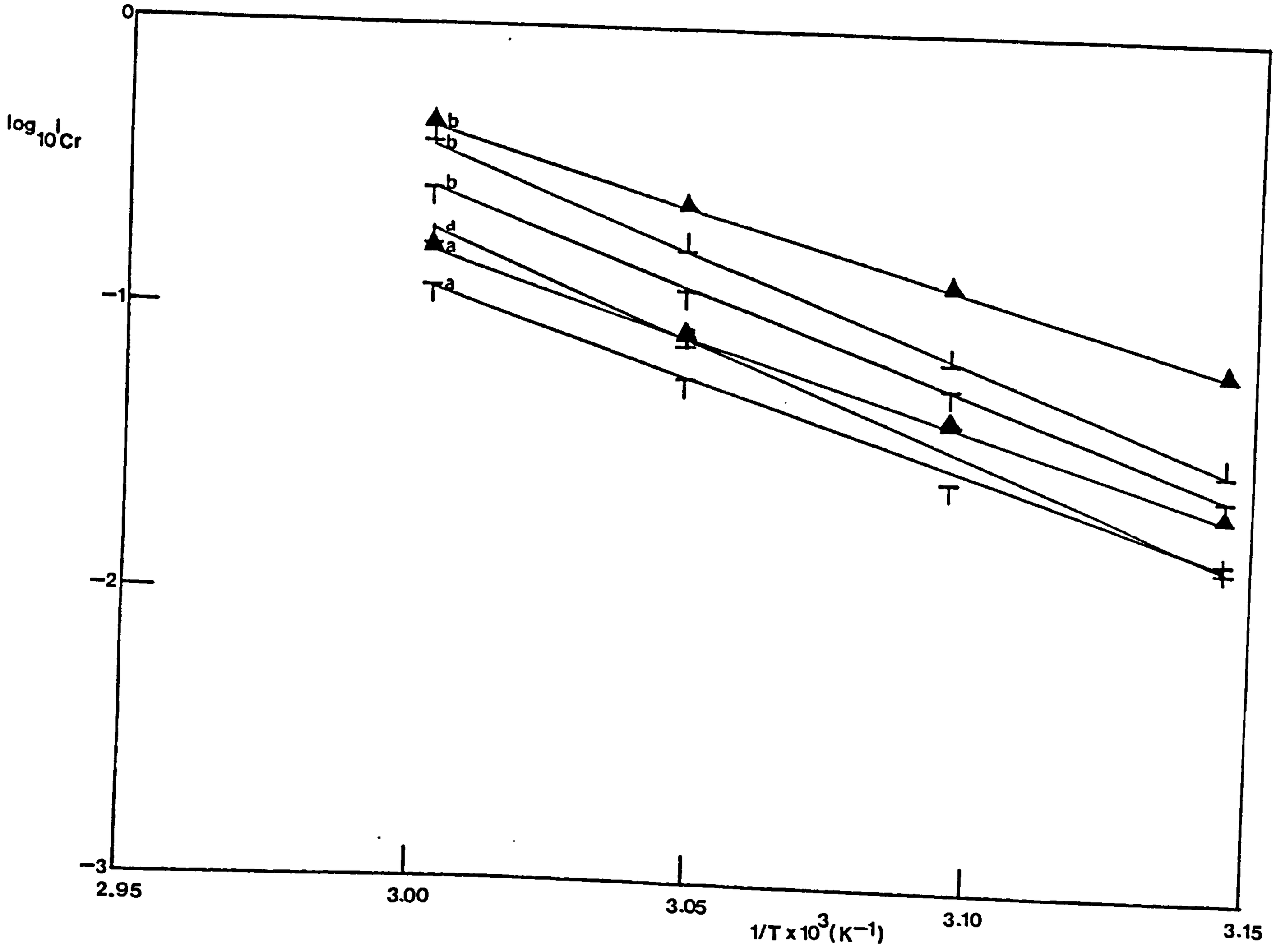
0
−1
−2
−3
log10 ICr
b
b
b
d
a
a
2.95
3.00
3.05
3.10
3.15
1/T x 10^3 (K^−1)

FIGURE 60.

The variation of anode current efficiency with current density for the oxygen evolution reaction in a Standard Solution at 55°C.

The effect of $KClO_4$ presence.

FIGURE 61.

The variation of anode current efficiency with current density for the (CrIII to CrVI) re-oxidation reaction in a Standard Solution at 55°C.

The effect of $KClO_4$ presence.

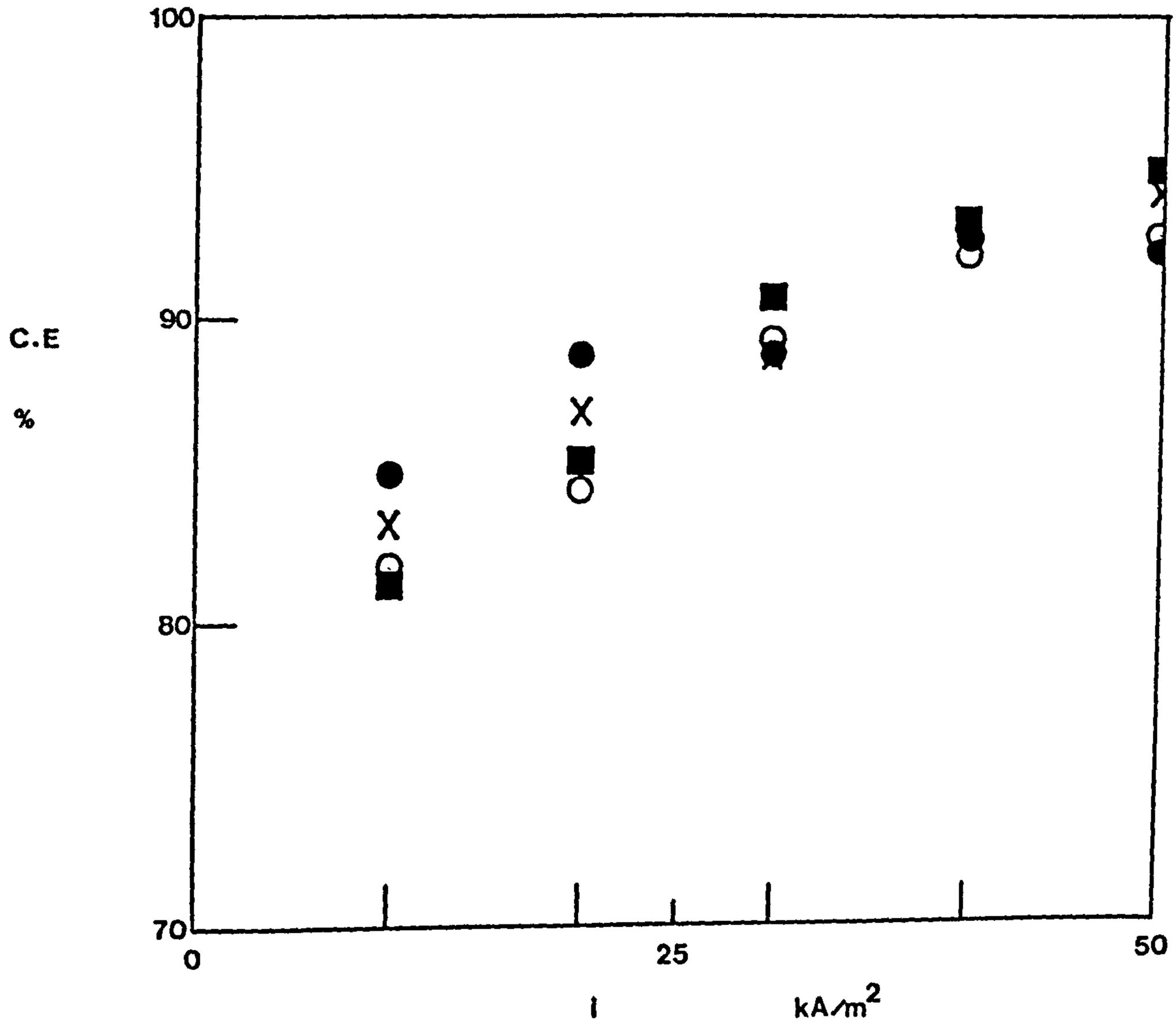
100
90
80
70
C.E
%
0
25
50
i
kA/m2

30
20
10
0
C.E
%
0
25
50
i
kA/m2

FIGURE 62.

The variation of anode current efficiency with current density for the oxygen evolution reaction at 55°C.
The effect of $KBrO_3$ presence.

FIGURE 63.

The variation of anode current efficiency with current density for the (CrIII to CrVI) re-oxidation reaction at 55°C.
The effect of $KBrO_3$ presence.

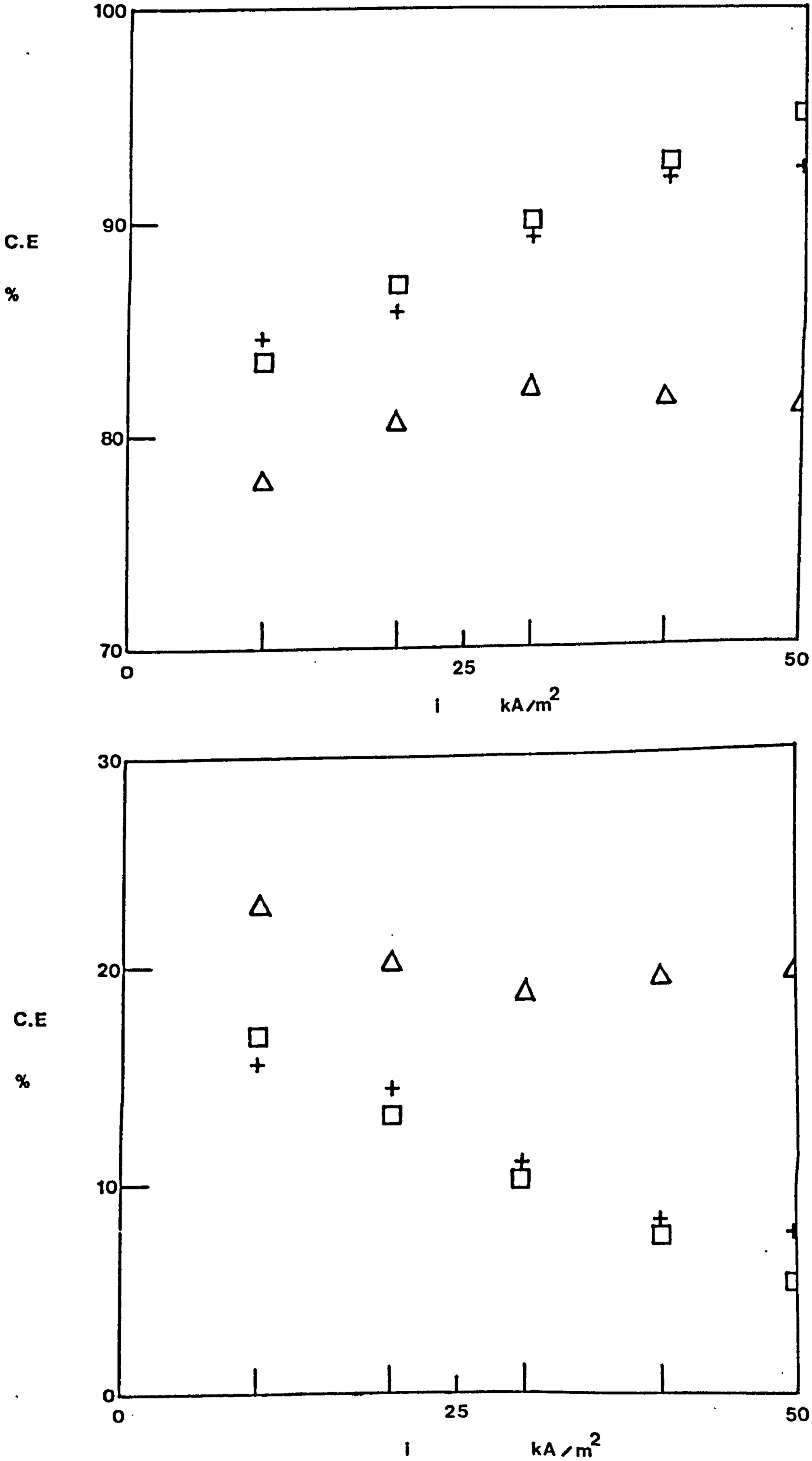
100
90
80
70
C.E
%
0
25
50
i
kA/m2
30
20
10
0
C.E
%
0
25
50
i
kA/m2

FIGURE 64.

The variation of anode current efficiency with current density for the oxygen evolution reaction at 55°C.

The effect of $K_2B_2O_4$ presence.

FIGURE 65.

The variation of anode current efficiency with current density for the (CrIII to CrVI) re-oxidation reaction at 55°C.

The effect of $K_2B_2O_4$ presence.

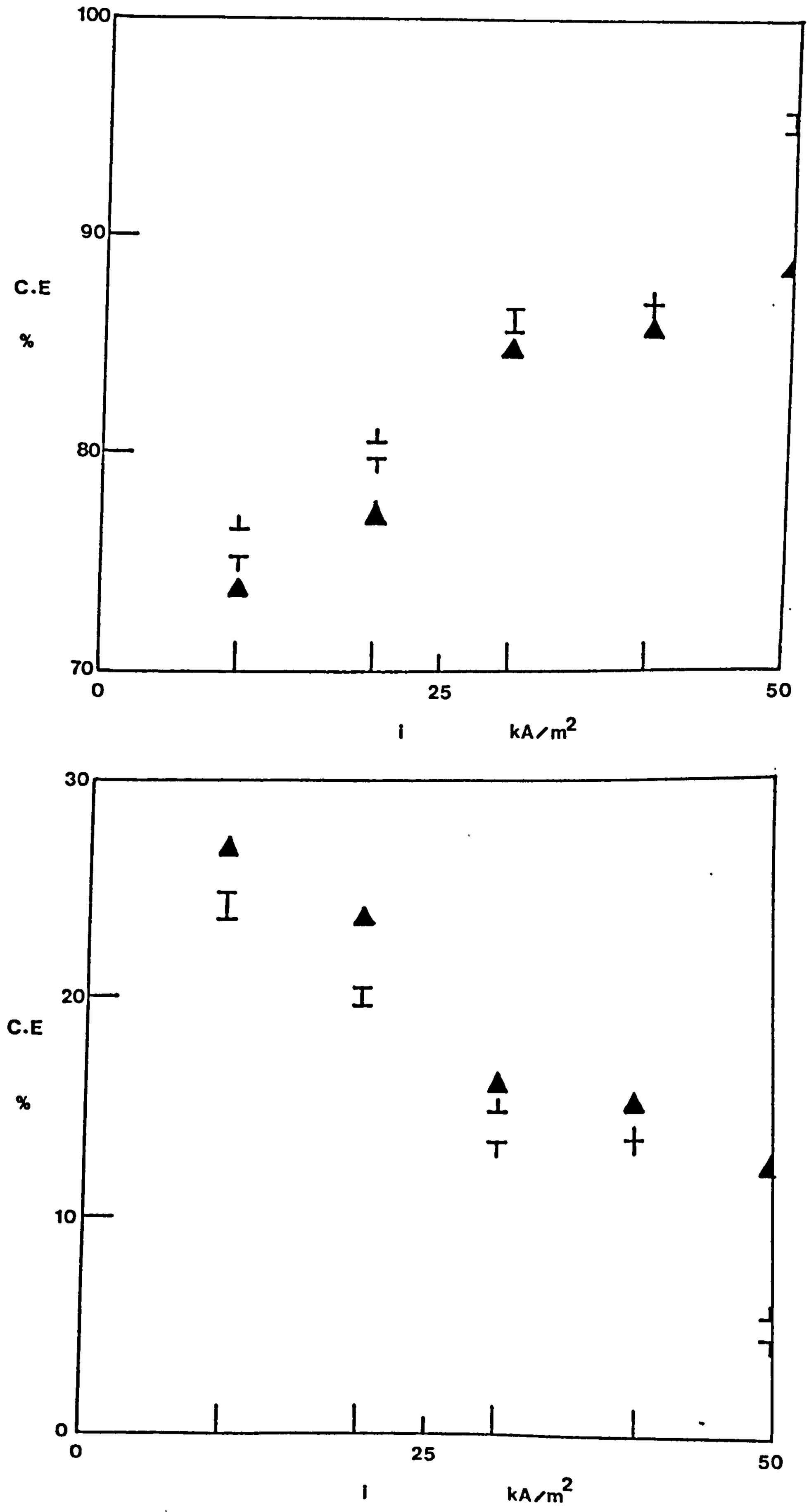
100
90
80
70
C.E
%
0
25
50
I
kA/m2
30
20
10
C.E
%
0
25
50
I
kA/m2

Steady state potentiostatic cathode polarization curves during the electrolysis of chromic acid plating solutions.

FIGURE 66.

After Okada and Yamamoto (156).

FIGURE 67.

After Hoare (118).

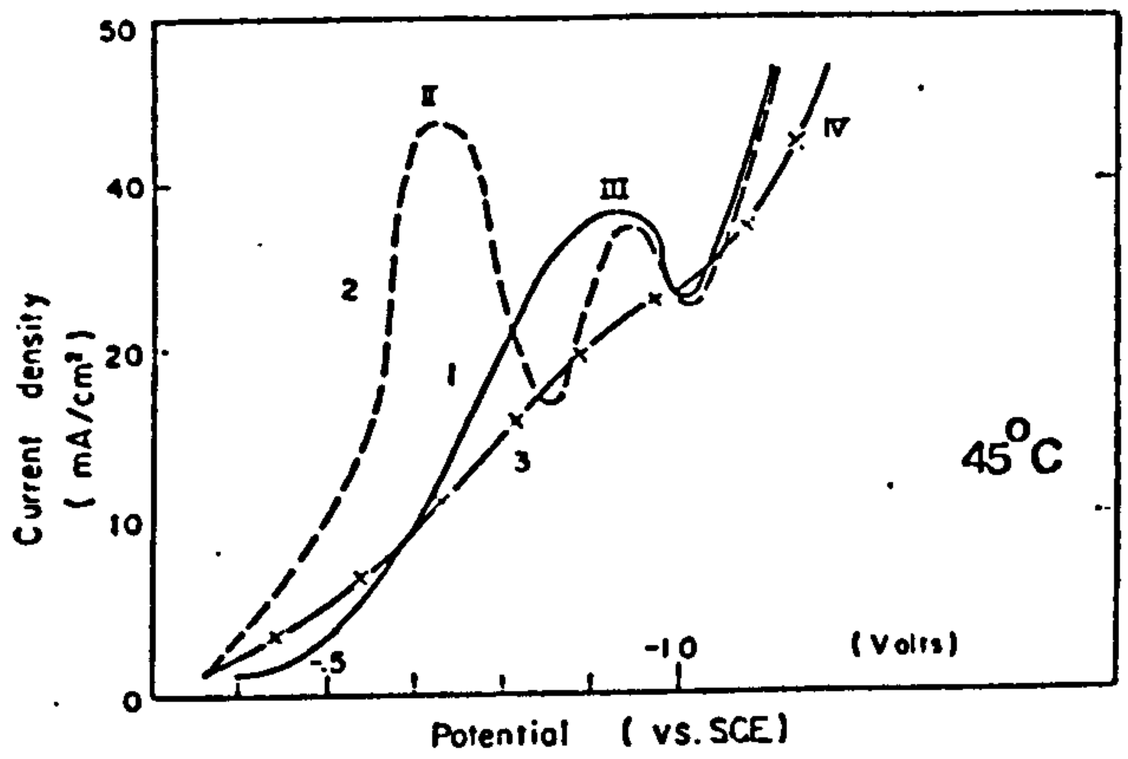

Fig. 3. Potentiostatic polarization curves of mild steel: 1—CrO_3 50 g/liter, 2—CrO_3 50 g/liter + H_2SO_4 0.3-1.0 g/liter, 3—CrO_3 10 g/liter + H_2SO_4 0.3 g/liter.

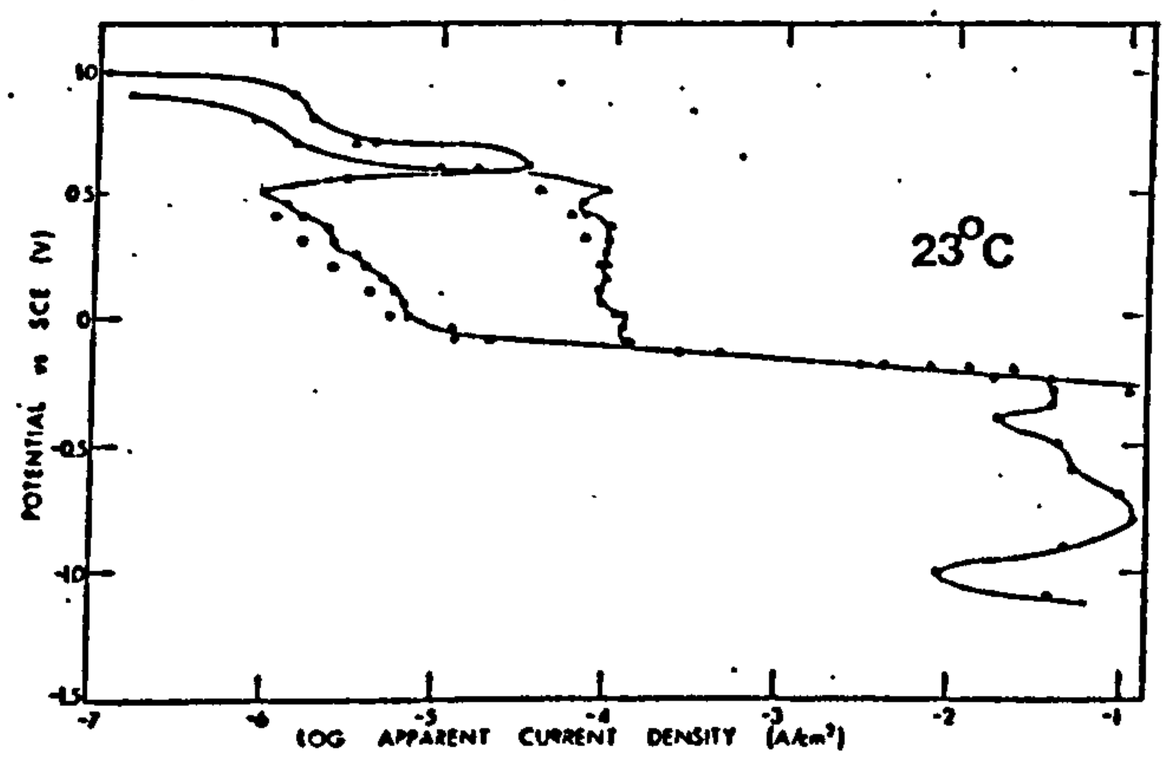

Fig. 13. Steady-state potentiostatic polarization curves obtained on a Pt bead cathode in N_2-stirred 1M $H_2Cr_3O_{10}$ solutions containing 0.01M (circles), and 0.1M (triangles), H_2SO_4; open symbols for increasing and filled symbols for decreasing cathodic current density.

PLATES

PLATE 1.

Scanning electron photomicrograph of chromium plate deposited from a Standard Solution at 55°C and a current density of 3kA/m^2. x800

PLATE 2.

As PLATE 1 but x 3200.

PLATE 3.

Scanning electron photomicrograph of chromium plate deposited from a Standard Solution at 55°C and a current density of 10kA/m^2. x 1600

PLATE 4.

Scanning electron photomicrograph of chromium plate deposited from a Standard Solution at 55°C and a current density of 30kA/m^2. x800

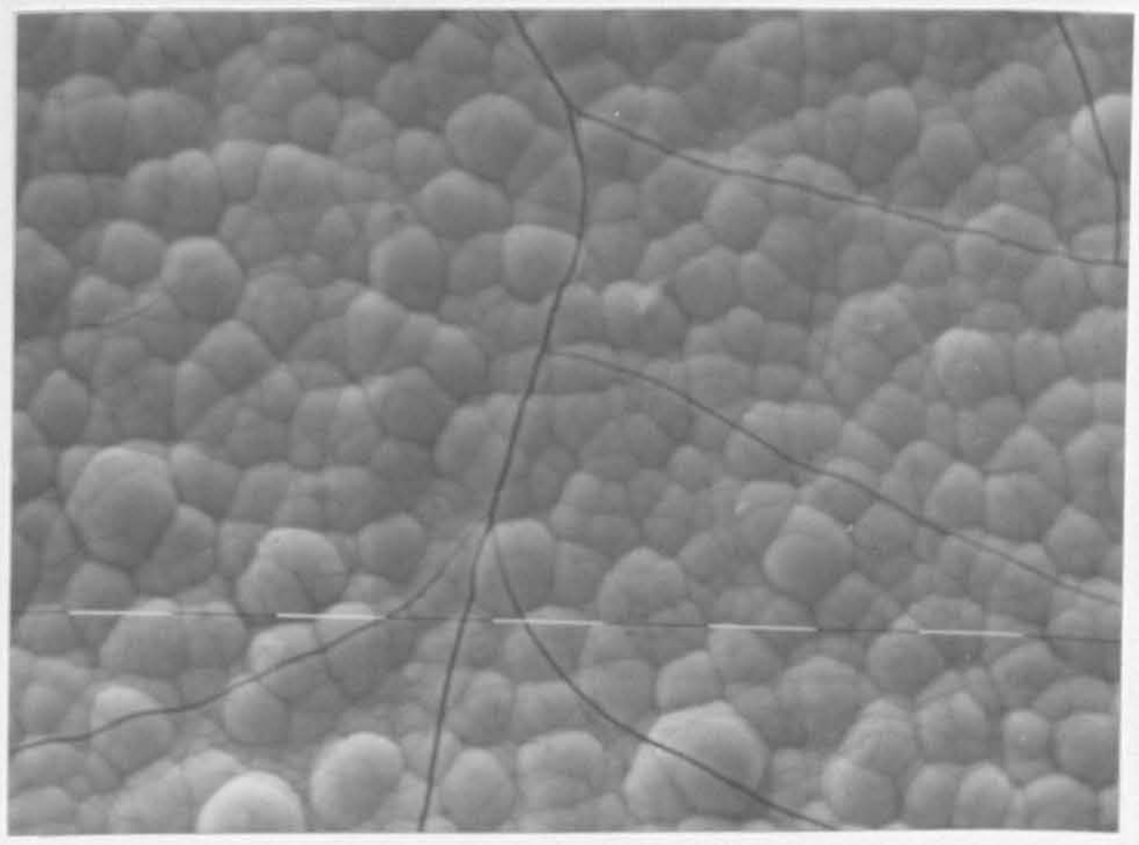

10μm

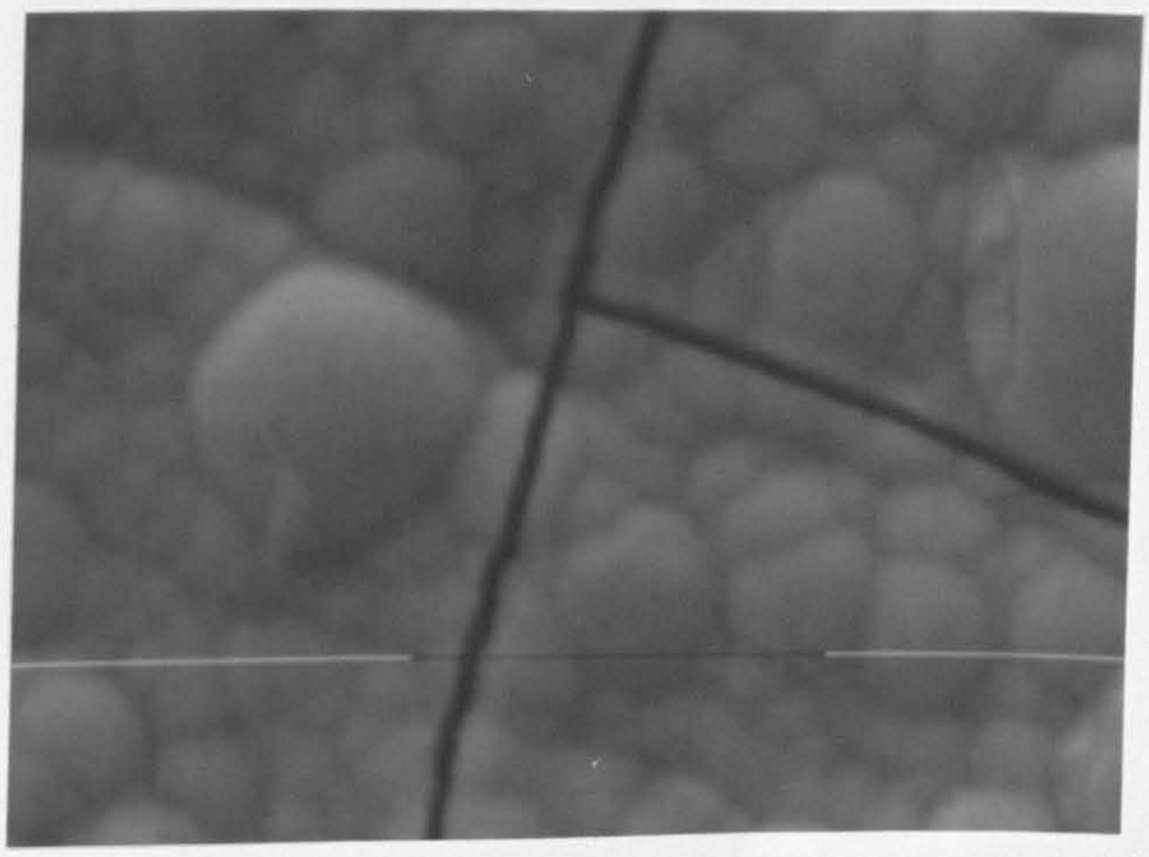

10μm

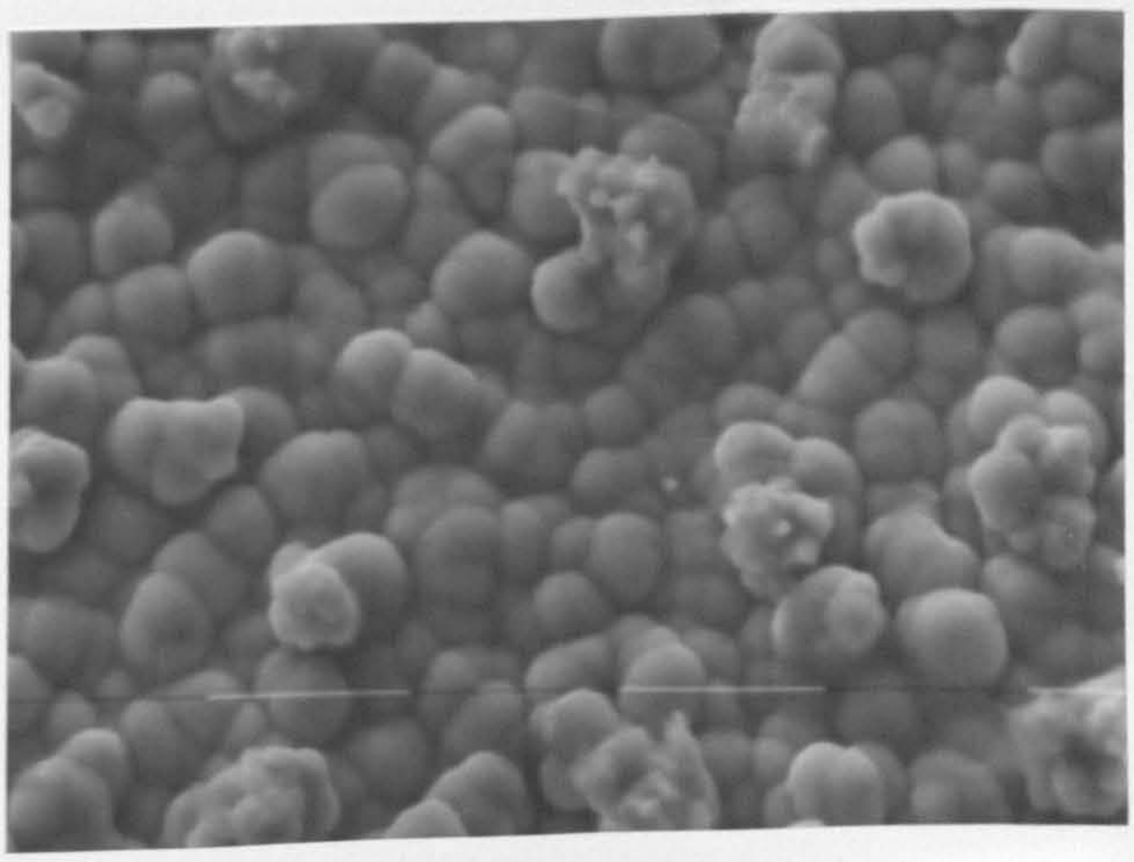

10μm

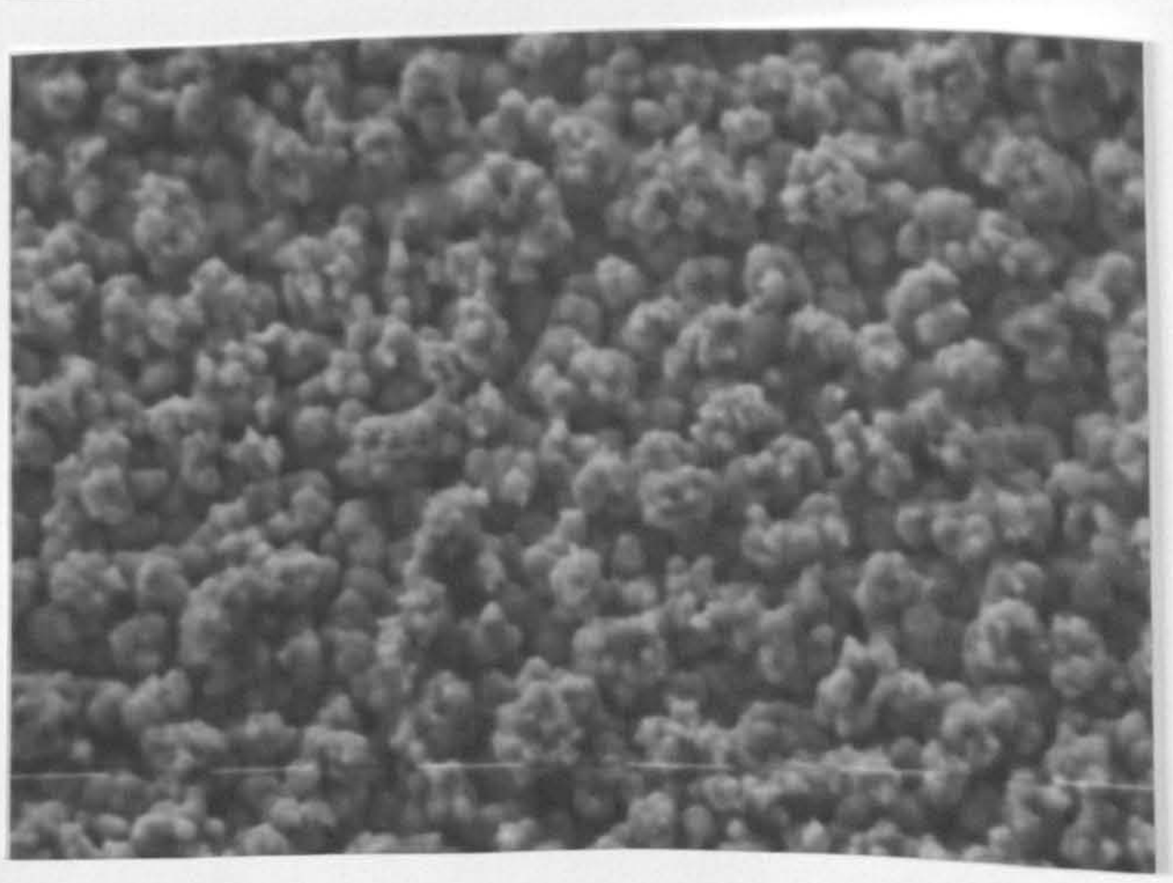

10μm

PLATE 5.

Scanning electron photomicrograph of chromium plate deposited from a Standard Solution containing 10 g/l $KClO_4$ at 55°C and a current density of 3kA/m^2.
x 800

PLATE 6.

As PLATE 5 but x 1600.

PLATE 7.

Scanning electron photomicrograph of chromium plate deposited from a Standard Solution containing 10 g/l $KClO_4$ at 55°C and current density of 10kA/m^2.
x 800

PLATE 8.

As PLATE 7 but x 3000.

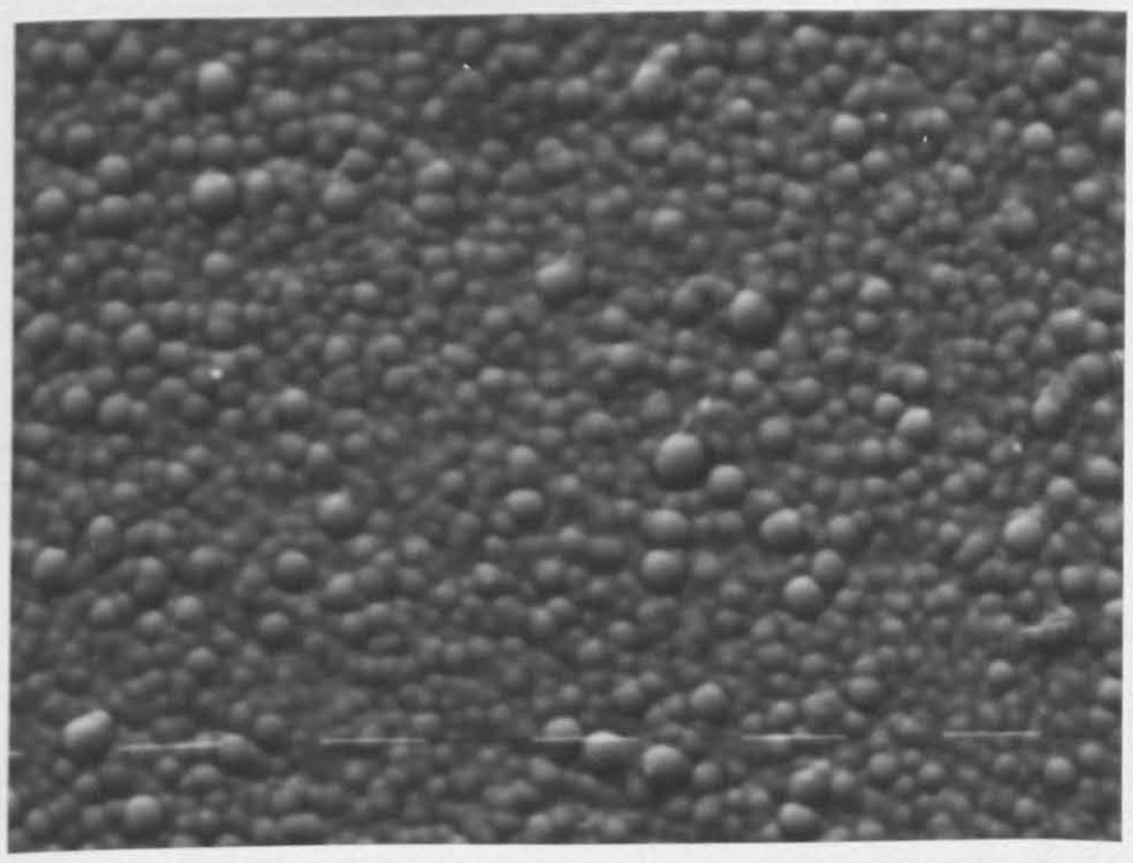

10 μm

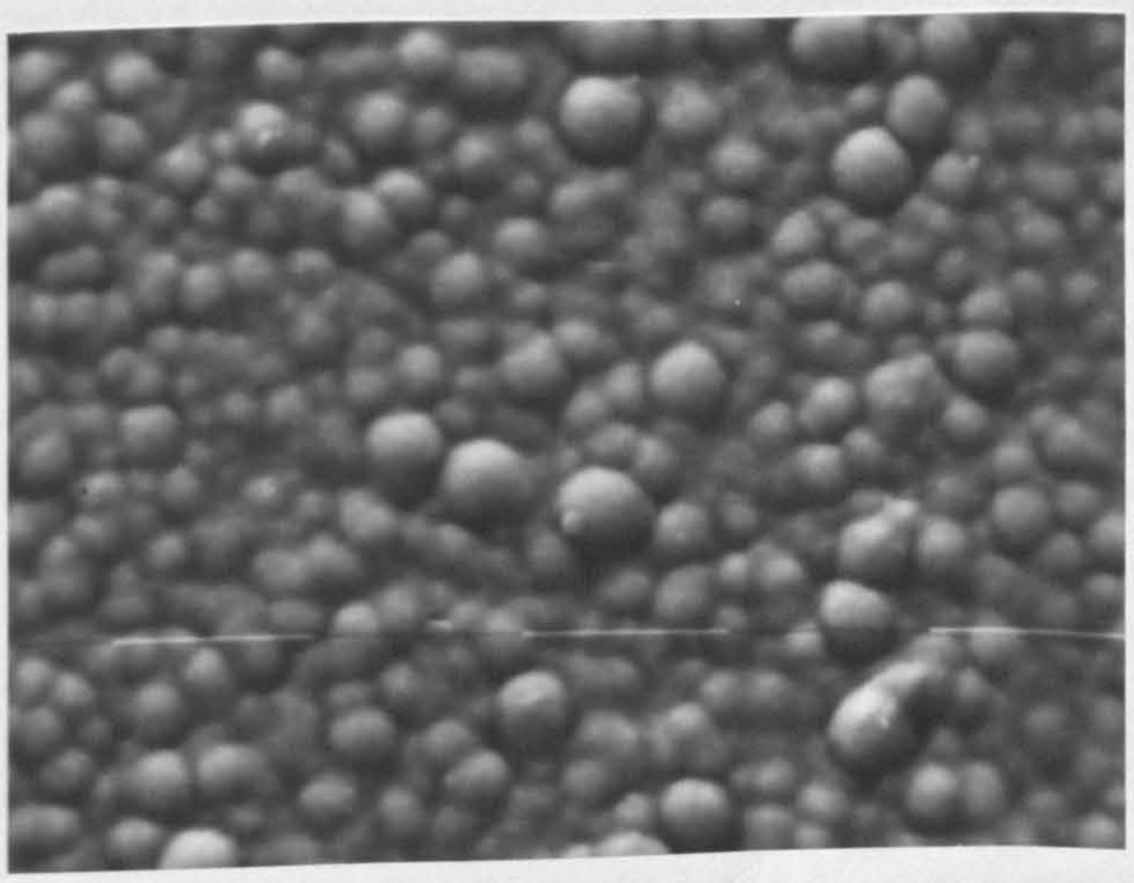

10 μm

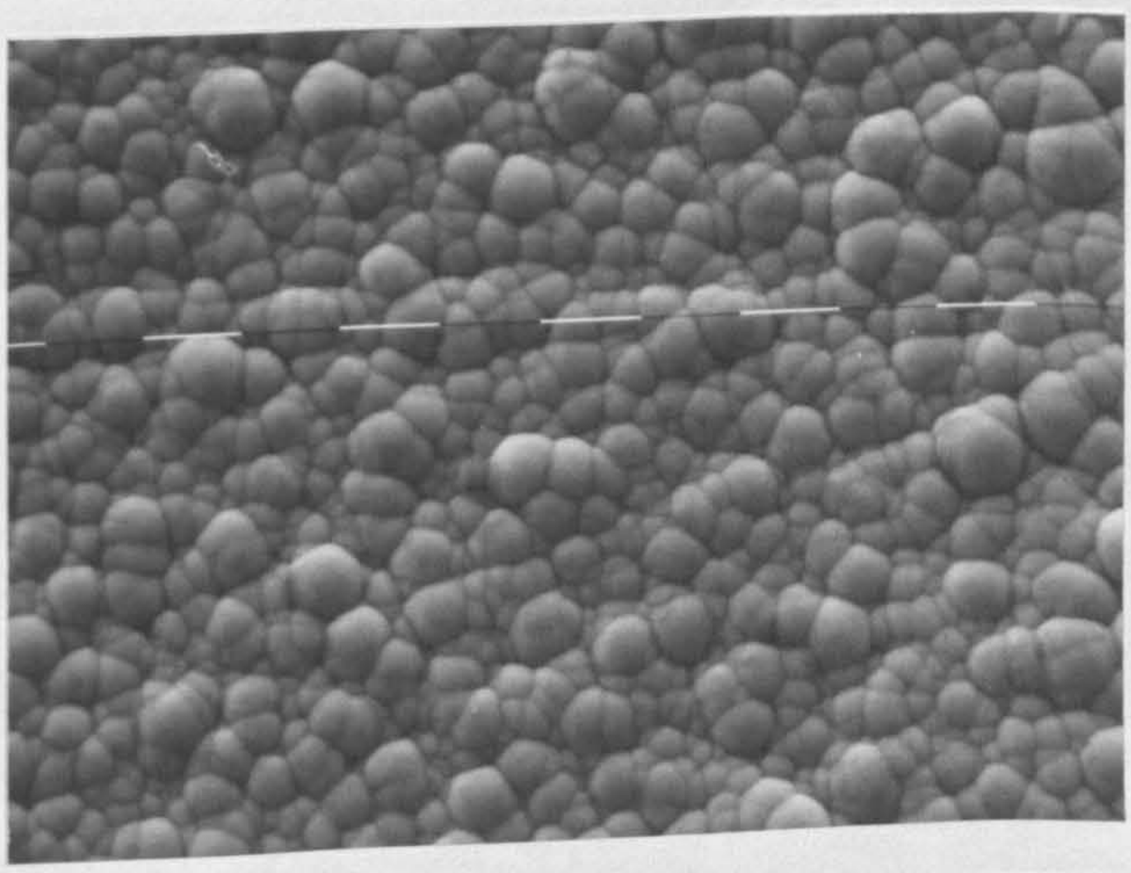

10 μm

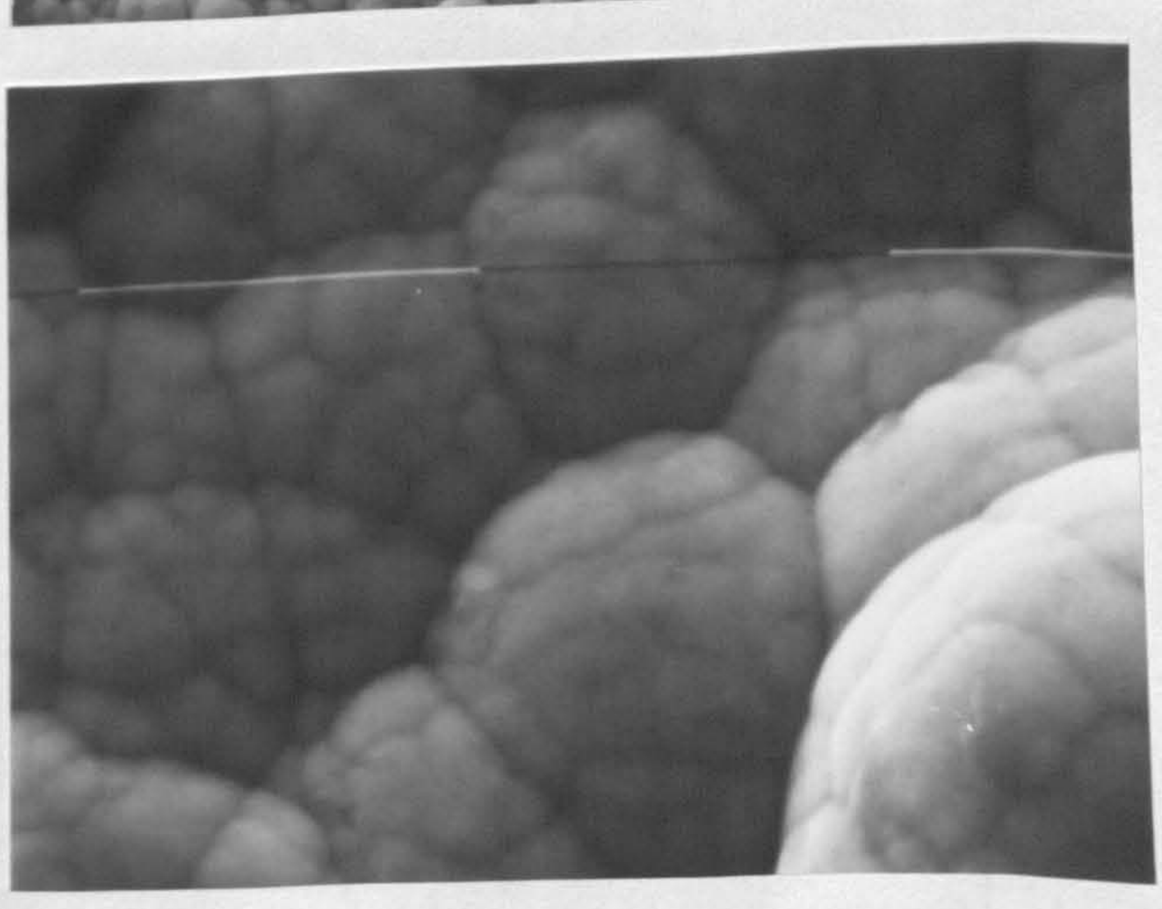

10 μm

PLATE 9.

Scanning electron photomicrograph of chromium plate deposited from a Standard Solution containing 10 g/l $KBrO_3$ at 55°C and a current density of 3kA/m^2.
x 800.

PLATE 10.

As PLATE 9 but x 3200.

PLATE 11.

Scanning electron photomicrograph of chromium plate deposited from a Standard Solution containing 10 g/l $KBrO_3$ at 55°C and a current density of 10kA/m^2.
x 800.

PLATE 12.

As PLATE 11 but x 3000.

10/Hm

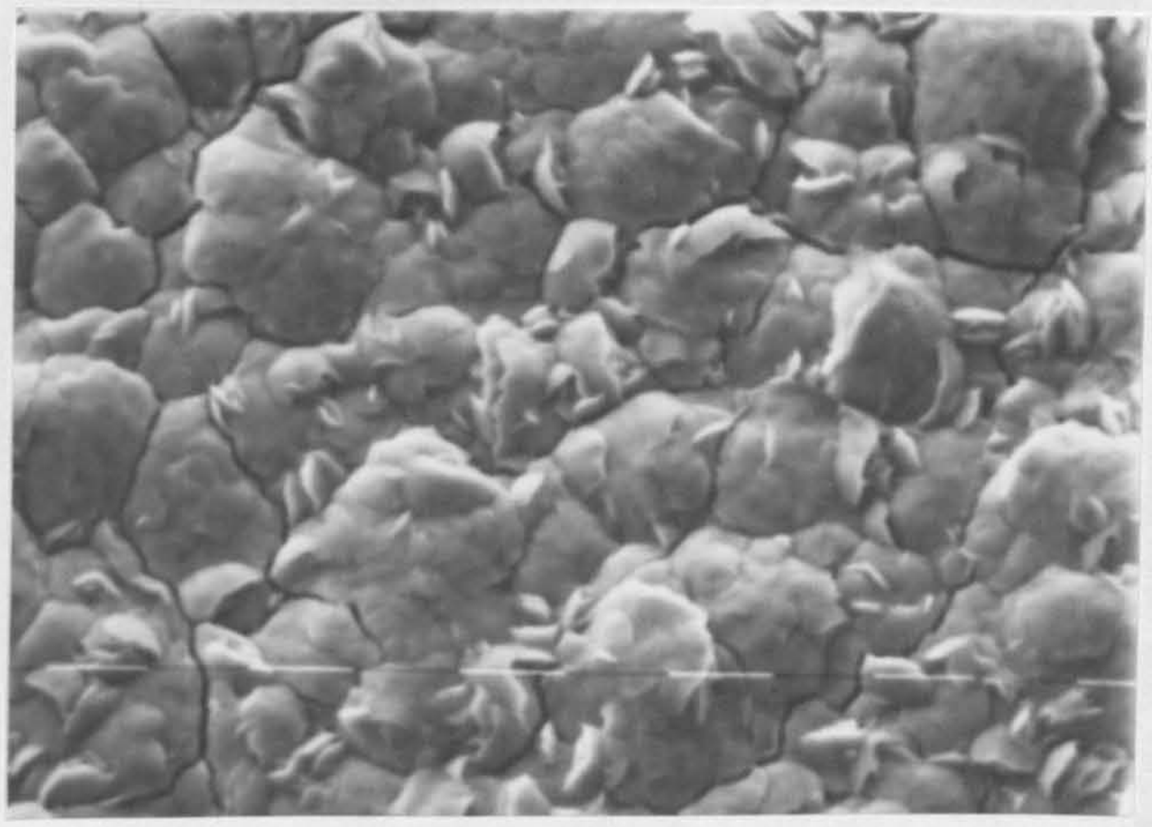

10/Hm

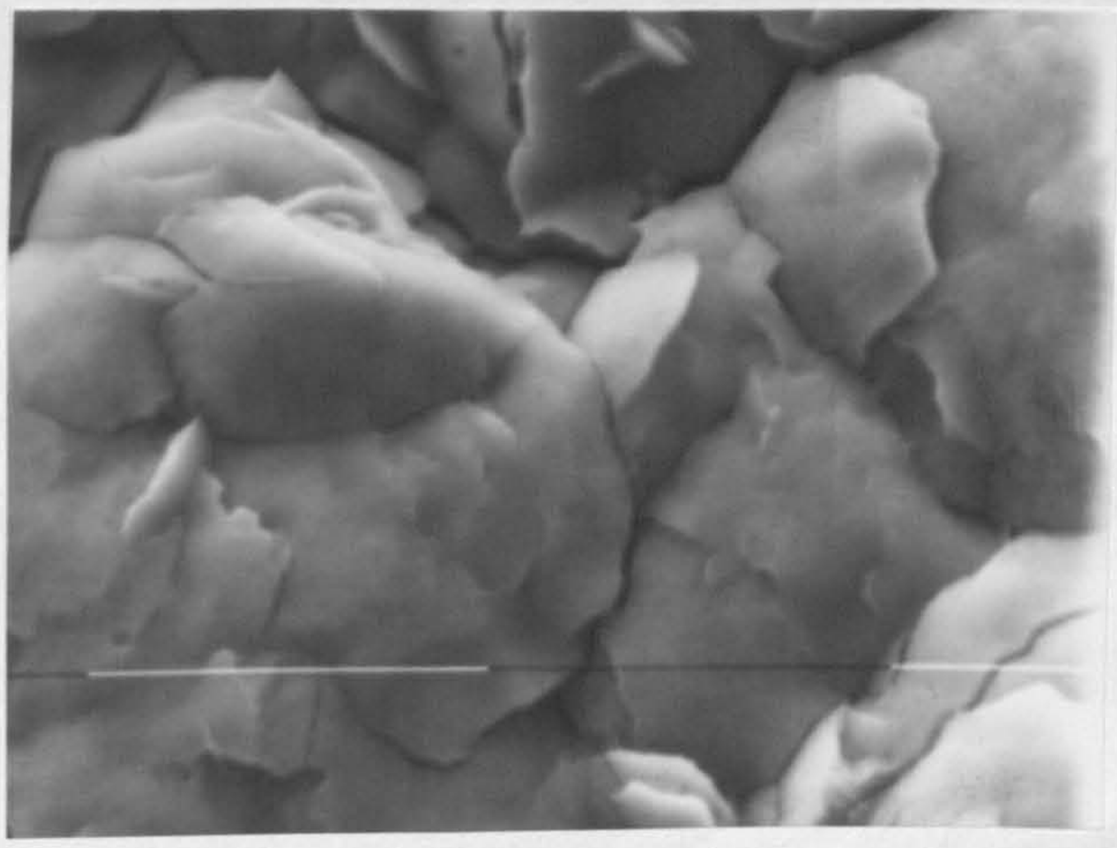

10/Hm

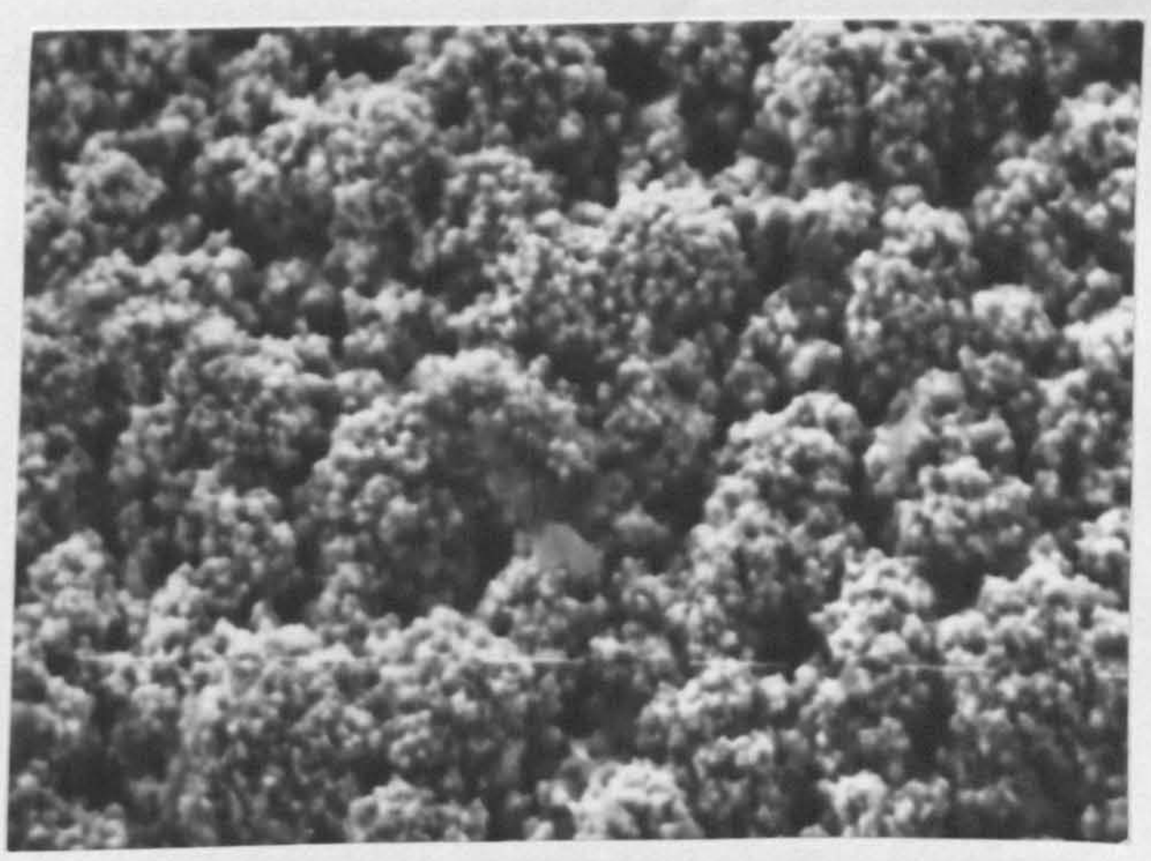

10/Hm

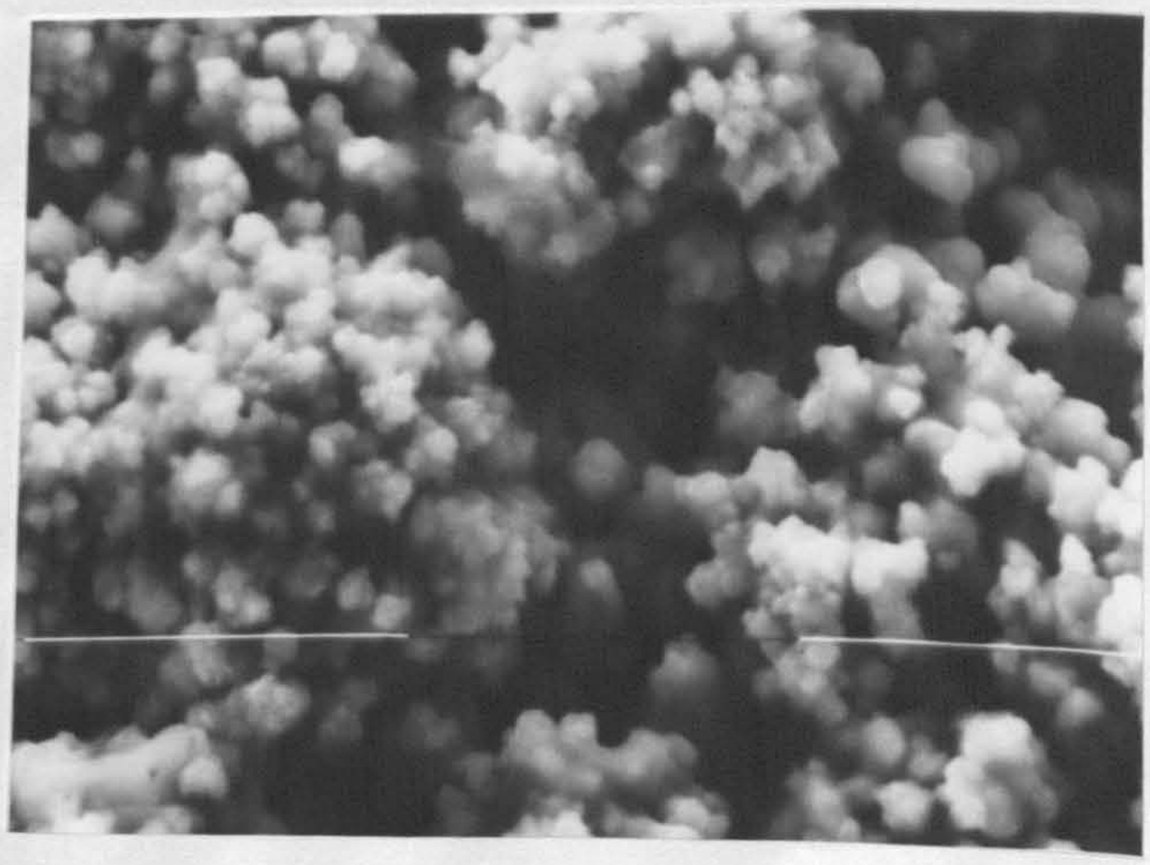

PLATE 13.

Scanning electron photomicrograph of chromium plate deposited from a Standard Solution containing 10 g/l $K_2B_2O_4$ at 55°C and a current density of 3kA/m^2.
x 800.

PLATE 14.

As PLATE 13 but x 1500.

PLATE 15.

Scanning electron photomicrograph of chromium plate deposited from a Standard Solution containing 10 g/l $K_2B_2O_4$ at 55°C and a current density of 10kA/m^2.
x 2000.

PLATE 16.

As PLATE 15 but x 7500.

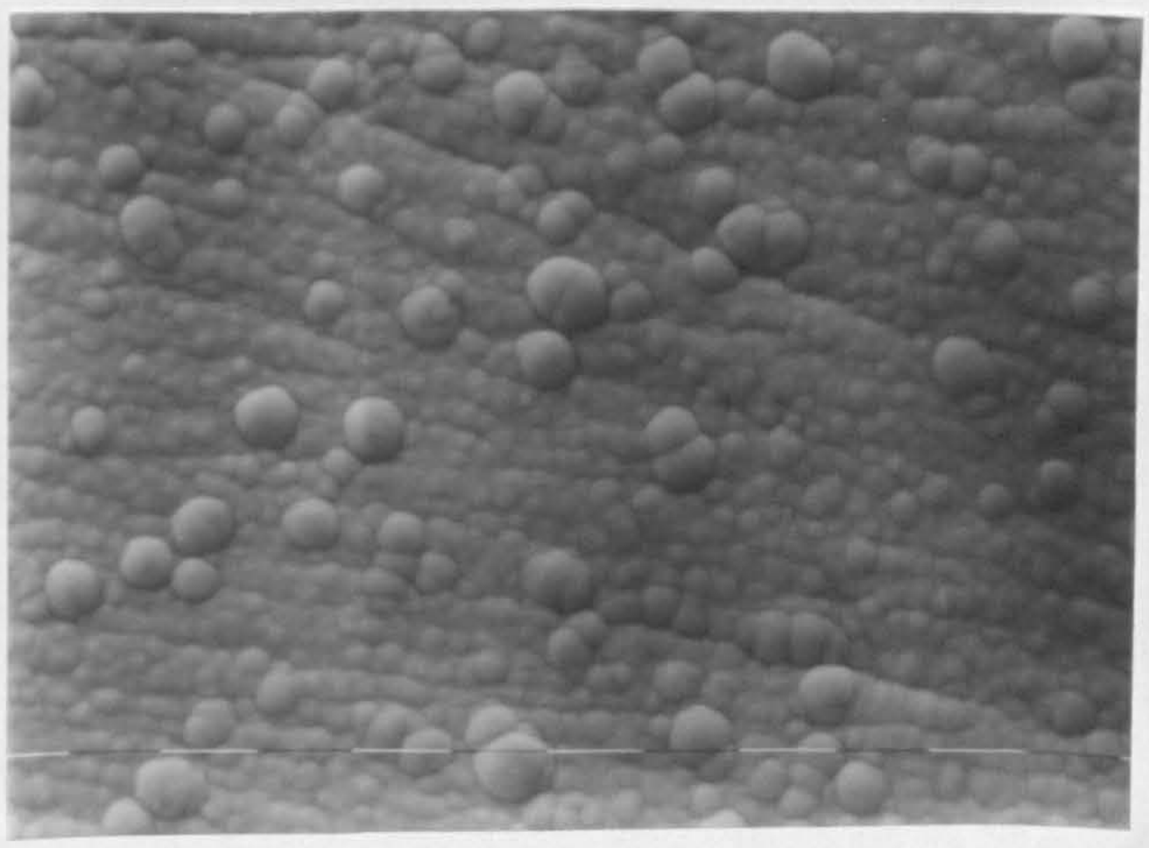

10μm

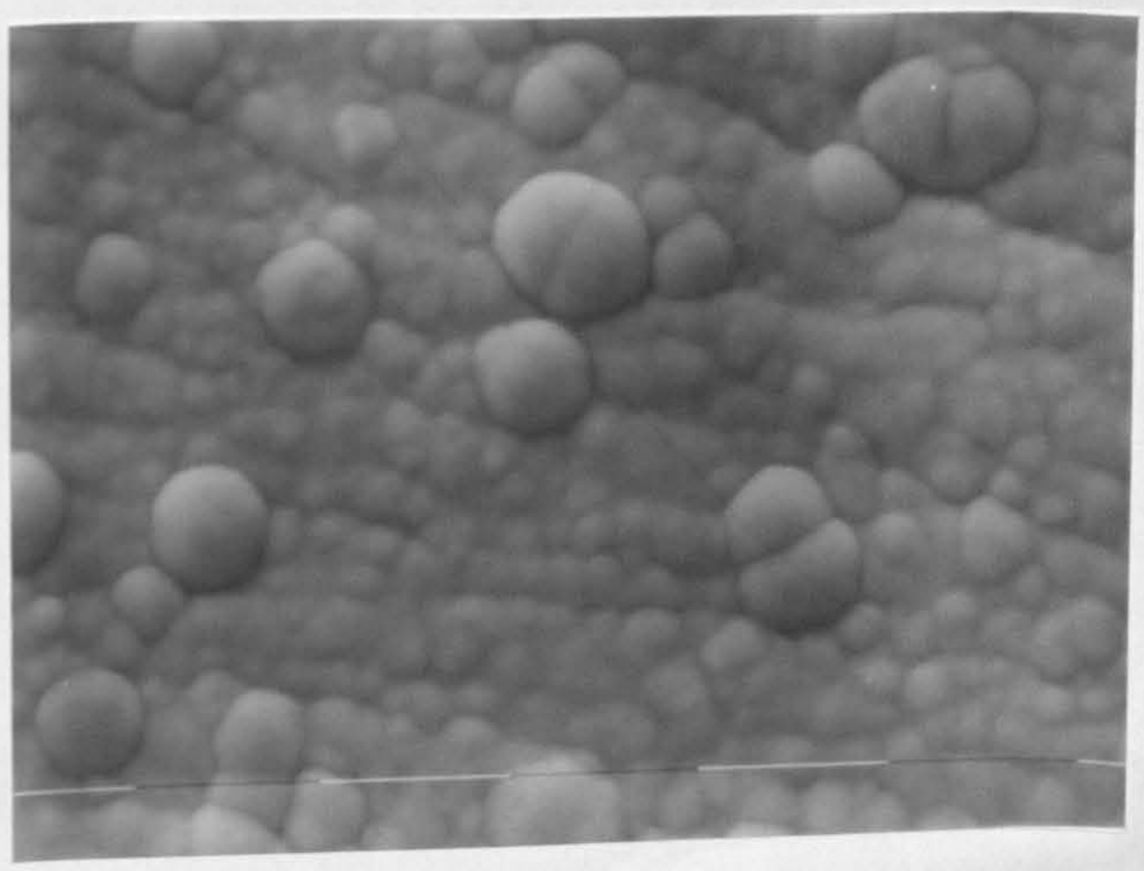

10μm

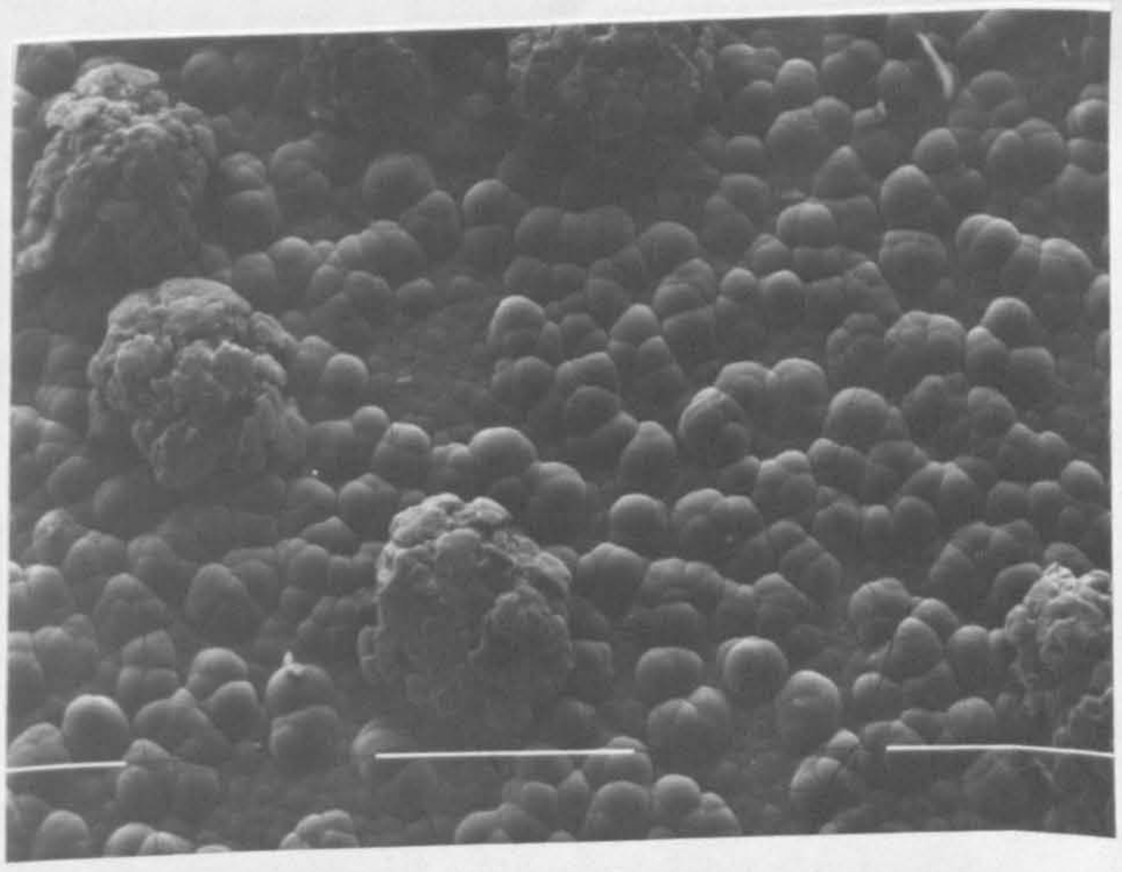

10μm

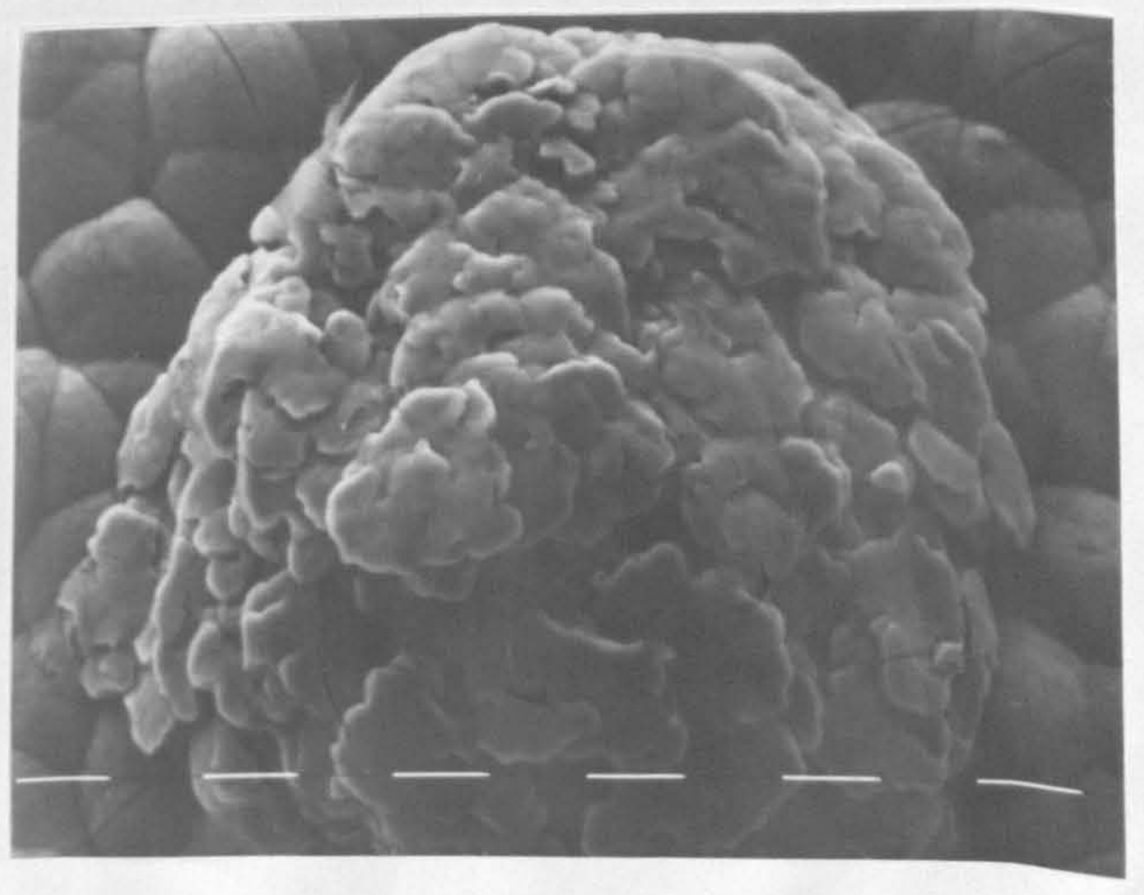

1μm

PLATE 17.

Scanning electron photomicrograph showing severe cracking and flaking in chromium plate deposited from a Standard Solution containing 10 g/l $K_2B_2O_4$ at 55°C and a current density of 3kA/m^2.

x 320.

PLATE 18.

As PLATE 17 but x 2500.

Illustrating an apparent microcellular structure in growth nodules.

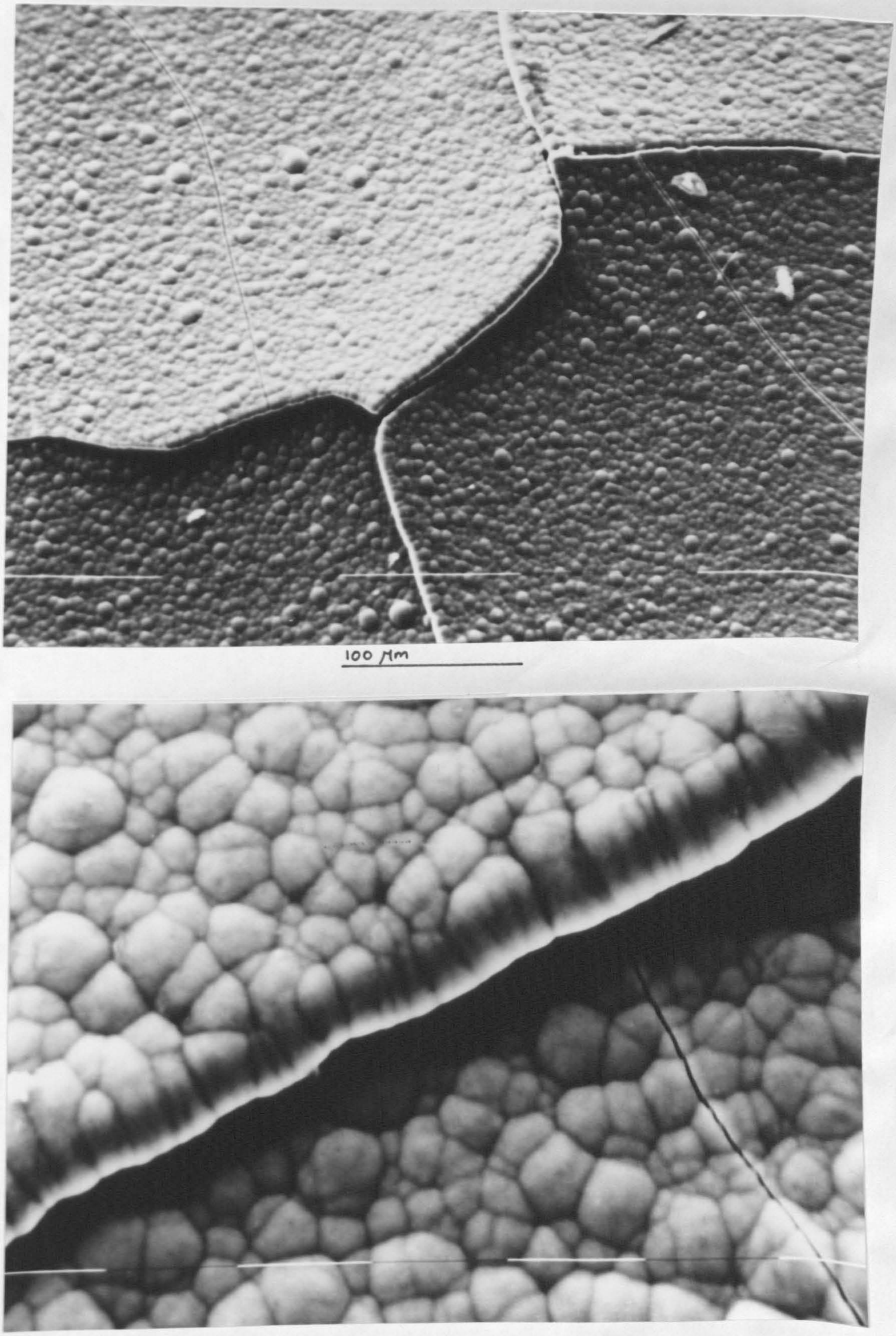

100 μm

10 μm